

A Flow Calorimetric Study of Adsorption of Dibenzothiophene, Naphthalene and Quinoline on Zeolites

by

J Keir Thomas

A thesis

presented to the University of Waterloo

in fulfillment of the

thesis requirement for the degree of

Master of Applied Science

in

Chemical Engineering

Waterloo, Ontario, Canada, 2008

© J Keir Thomas 2008

AUTHOR'S DECLARATION

I hereby declare that I am the sole author of this thesis. This is a true copy of the thesis, including any required final revisions, as accepted by my examiners.

I understand that my thesis may be made electronically available to the public.

Abstract

The purpose of this work is to develop a reliable procedure for determination of liquid phase heats of adsorption via a flow calorimetric technique. The second objective is to study heats of adsorption of target sulfur compounds on potential desulfurization sorbents. Thirdly, we strive to relate the data obtained to the properties of both the sorbent and sorbates studied. Finally, the ultimate goal of this research is to use the data obtained to develop a high capacity selective adsorbent for the desulfurization of diesel fuel.

Liquid phase flow adsorption experiments were conducted on sodium-Y zeolite (NaY), nickel exchanged NaY zeolite (NiY) and cesium-exchanged NaY zeolite (CsY). The solutions used in calorimetric experiments included naphthalene in n-hexadecane (C16), dibenzothiophene (DBT) in C16, and quinoline in C16. These solutions were used to model the adsorption of aromatic, sulphur-containing and nitrogen-containing compounds in diesel fuel, respectively. Additional experiments were conducted using equimolar concentrations of all three species in C16 to examine competitive adsorption behaviour of the mixture. During heat flow experiments, effluent samples were collected and analysed to obtain breakthrough curves for the systems.

Heat of adsorption data were obtained via flow microcalorimetry using a novel procedure developed by this group. In this study, some experiments were conducted to examine the repeatability and utility of this new method.

Characterization experiments were also conducted including BET surface area analysis, X-Ray diffraction (XRD) analysis and Inductively Coupled Plasma – Optical Emission Spectroscopy (ICP-OES) analysis to determine the properties of the sorbents. These properties were then related to data obtained in flow adsorption calorimeter experiments.

A detailed discussion on the development of a novel method for determination of liquid phase heats of adsorption is presented. Analysis of calculation results using this new method show good repeatability relative to the previous method used.

Equilibrium adsorption relationships are developed using the Langmuir adsorption model, and these results are compared to flow adsorption results obtained from the calorimeter.

Results indicate that in terms of desulfurization capability, NaY appeared to be the best sorbent. Heats of adsorption were only moderate on NaY, indicating that regeneration of the sorbent would not be difficult, and NaY had the highest sulfur capacity of the sorbents studied. This result

was not in agreement with literature results, and it is proposed that the discrepancy is the result of disruption of the crystalline structure of our sorbents during the modification process.

Recommendations are presented for ongoing work, including important calorimeter experiments, modifications for improvement of experimental procedure and apparatus, additional sorbent characterization for elucidation of adsorption mechanisms, and finally experiments for verification and further validation of our innovative experimental technique.

Acknowledgements

First and foremost, I would like to thank my supervisor, Dr. Flora Ng, for her guidance and advice throughout my study. This difficult and sometimes frustrating work would not have been possible without her patience when it appeared that despite repeated efforts, little progress was being made.

I was lucky to have a diverse group of people to work with. Though most were not directly involved with my particular project, all were extremely helpful and their advice was priceless and their assistance was always available when called upon. I would like to thank Dr. Ming Jiang, Dr. Deepyaman Seth, Dr. Donghua Zuo, Dr. Prem Pal, Dr. Zhiwen Qi, Bill O'Keefe, Amir Iravani, Tina Liu, Chris Choy, Viral Patel and Jennifer Moll. Special thanks are in order for Dr. Kamalakar Gupta for preparation and characterization of the zeolites, and to Peter Rehbein for the preparation of adsorption isotherms.

The assistance of the chemical engineering support staff, including Bert Habicher, Rick Hecktus, Ron Neill, Ralph Dickhout, Ravindra Singh, Dennis Herman, Liz Bevan, Ingrid Scherrer and Pat Anderson is gratefully acknowledged.

Finally, I would like to thank my family for their support. My parents, John and Ann Thomas, encouraged me to achieve my goals and were always available for advice, financial assistance, and possibly their most trying contribution of all, dog-sitting. Over the course of my academic career countless other family members have supported me in my life as a nomadic co-op student, either taking care of things I was forced to leave behind or making strange cities feel like home, and I will be forever grateful.

Dedication

This work is dedicated to my parents, who have been behind me since the start, and to Jennifer. She wasn't around from the get-go, but she certainly put up with a lot on the home stretch. My love to all of you.

Table of Contents

Acronyms.....	xvii
Symbols.....	xix
Subscripts.....	xx
1 Introduction.....	1
1.1 The Sulfur Cycle.....	1
1.2 Crude Oil.....	3
1.3 Desulfurization.....	4
1.4 Desulfurization Technologies.....	5
1.4.1 Biodesulfurization.....	5
1.4.2 Charge Transfer Complex Formation.....	6
1.4.3 Oxidative Desulfurization.....	7
1.4.4 Ionic Liquids.....	8
1.4.5 Photochemical Desulfurization.....	8
1.4.6 Adsorption.....	9
1.5 Objectives.....	10
2 Literature Review.....	11
2.1 Adsorbents and Properties.....	11
2.2 Adsorbents for Desulfurization.....	19
2.3 Calorimetry.....	26
3 Proposed Work.....	28

4	Experimental Methods.....	31
4.1	Reagents and Standards	31
4.2	Modification of NaY Zeolite.....	31
4.3	Calcination	31
4.4	Sorbent Characterization.....	31
4.4.1	Elemental Analysis	31
4.4.2	Surface Area	32
4.4.3	Structure.....	32
4.5	GC Analysis	32
4.6	Equilibrium Adsorption and Adsorption Rate Experiments	32
4.7	Heat of Adsorption Experiments.....	33
4.8	Competitive Adsorption Experiments.....	36
5	Results and Discussion.....	37
5.1	New Method Development	37
5.1.1	Breakthrough Curve Calculations.....	38
5.1.2	Heat Flow Curve Analysis.....	44
5.2	Method Verification.....	55
5.2.1	Effect of Feed Concentration.....	57
5.2.2	Causes of Variability	59
5.3	Zeolite Characterization.....	60
5.4	Equilibrium Adsorption Experiments	62

5.4.1	DBT Equilibrium Isotherms	63
5.4.2	Quinoline Equilibrium Isotherms	64
5.4.3	Naphthalene Equilibrium Isotherms	65
5.5	Adsorption on NaY Zeolite.....	66
5.6	Adsorption on NiY Zeolite	69
5.7	Adsorption on CsY Zeolite	73
5.8	Elucidation of Adsorption Mechanisms.....	76
5.9	Competitive Adsorption Experiments.....	77
5.10	Adsorption Kinetics	81
5.11	Comparison of Sorbents.....	87
6	Conclusions	89
7	Recommendations	91
8	References	95
9	Appendix A – Calibration Curves	105
9.1	Perkin Elmer GC.....	105
9.2	Varian GC	106
10	Appendix B – Sample Calculations.....	109
11	Appendix C – Proposed Method for In-Situ Calcination	113
12	Appendix D – Breakthrough Curve Data	117
12.1	DBT/C16 on NaY	117
12.2	DBT/C16 on NiY	118

12.3	DBT/C16 on CsY.....	119
12.4	Quinoline/C16 on NaY	120
12.5	Quinoline/C16 on NiY.....	121
12.6	Quinoline/C16 on CsY.....	122
12.7	Competitive Adsorption on NaY	123
12.8	Competitive Adsorption on NiY	125
12.9	Competitive Adsorption on CsY.....	127
13	Appendix E – Calorimeter Experiment Summaries	129
14	Appendix F – Equilibrium Isotherm Calculation Data.....	161
14.1	DBT Experiments	161
14.2	Quinoline Adsorption Experiments.....	164
14.3	Naphthalene Adsorption Experiments	167

List of Tables

Table 1. Chemical sources and their function in zeolite synthesis.....	17
Table 2. Heats of adsorption from vapour phase equilibrium isotherms.....	20
Table 3. Summary of predicted heats of adsorption on CuY zeolite.....	23
Table 4. Selected properties of sorbate molecules	29
Table 5. Summary of Early Adsorption Experiments – 1800ppmw S DBT/C ₁₆ on NaY at 30°C.	40
Table 6. Comparison of heat of adsorption results between methods	56
Table 7. Comparison of amount adsorbed results between methods.....	57
Table 8. Summary of heats of adsorption measured at different feed concentrations.....	58
Table 9. Sorbent characterization results.....	61
Table 10. DBT isotherm data	63
Table 11. Quinoline isotherm data	64
Table 12. Naphthalene isotherm data	65
Table 13. Adsorption results on NaY zeolite	67
Table 14. Adsorption results on NiY zeolite	69
Table 15. Summary of NiY preparation procedures found in literature.....	72
Table 16. Adsorption results on CsY zeolite.....	73
Table 17. Summary of competitive adsorption results	77
Table 18. Relative ranking of sorbents studied	87
Table 19. Breakthrough Data – RUNID#9.....	117
Table 20. Breakthrough Data – RUNID#13	117

Table 21. Breakthrough Data – RUNID#11	118
Table 22. Breakthrough Data – RUNID#12	118
Table 23. Breakthrough Data – RUNID#8	119
Table 24. Breakthrough Data – RUNID#10	119
Table 25. Breakthrough Data – RUNID#1	120
Table 26. Breakthrough Data – RUNID#2	120
Table 27. Breakthrough Data – RUNID#4	121
Table 28. Breakthrough Data – RUNID#5	121
Table 29. Breakthrough Data – RUNID#6	122
Table 30. Breakthrough Data – RUNID#7	122
Table 31. Breakthrough Data – RUNID#21	123
Table 32. Breakthrough Data – RUNID#22	124
Table 33. Breakthrough Data – RUNID#23	125
Table 34. Breakthrough Data – RUNID#24	126
Table 35. Breakthrough Data – RUNID#25	127
Table 36. Breakthrough Data – RUNID#26	128
Table 37. Raw Data for DBT/C ₁₆ Isotherm on NaY Zeolite	161
Table 38. Raw Data for DBT/C ₁₆ Isotherm on NiY Zeolite	162
Table 39. Raw Data for DBT/C ₁₆ Isotherm on CsY Zeolite	163
Table 40. Raw Data for Quinoline/C ₁₆ Isotherm on NaY Zeolite	164
Table 41. Raw Data for Quinoline/C ₁₆ Isotherm on NiY Zeolite	165

Table 42. Raw Data for Quinoline/C ₁₆ Isotherm on CsY Zeolite.....	166
Table 43. Raw Data for Naphthalene/C ₁₆ Isotherm on NaY Zeolite.....	167
Table 44. Raw Data for Naphthalene/C ₁₆ Isotherm on NiY Zeolite.....	168
Table 45. Raw Data for Naphthalene/C ₁₆ Isotherm on CsY Zeolite	169

Table of Figures

Figure 1. Average composition of crude oils (Adapted from Hughley et al, 2004)	3
Figure 2. Schematic representation of experimental apparatus	33
Figure 3. Summary of experimental procedure	35
Figure 4. Adsorption of 1800ppmw S DBT/C ₁₆ on NaY at 30°C, 7.6mL/h (RUNID#28)	38
Figure 5. Schematic representation of breakthrough curve for calculations	39
Figure 6. Baseline shift for adsorption of 1800ppmw S (DBT/C ₁₆) on NaY at 4.00ml/h	51
Figure 7. General heat flow curve exhibiting five distinct adsorption phases.....	45
Figure 8. Effect of varying the ‘T’ parameter in the general breakthrough model.....	49
Figure 9. Adsorption of 21.8 mM DBT on NaY at 30°C and 4.00 mL/h.	53
Figure 10. Effect of concentration of DBT in C ₁₆ at 30°C and 4.00mL/h	58
Figure 11. Comparison of heat flow curves for 21.8mM DBT/C ₁₆ on NaY (Run ID# 9,13)	59
Figure 12. X-Ray diffraction patterns for Y-type zeolites.....	62
Figure 13. Equilibrium isotherms for DBT in C ₁₆	63
Figure 14. Equilibrium isotherms for quinoline in C ₁₆	64
Figure 15. Equilibrium isotherms for naphthalene in C ₁₆	66
Figure 16. Adsorption Results on NaY zeolite.....	67
Figure 17. Adsorption results on NiY zeolite.....	70
Figure 18. Adsorption results on CsY zeolite.....	73
Figure 19. Relationship between surface area and equilibrium sorption capacity	77
Figure 20. Competitive adsorption results on NaY zeolite	78

Figure 21. Competitive adsorption results on NiY zeolite	79
Figure 22. Competitive adsorption results on CsY zeolite	80
Figure 23. Sample of adsorption kinetics calculations based on heat flow curve	82
Figure 24. Schematic representation of calorimeter cell	83
Figure 25. Adsorption kinetics curve for quinoline adsorption on NiY	84
Figure 26. Adsorption kinetics curve for quinoline adsorption on CsY	84
Figure 27. Sample calibration curve for DBT/C16 in Perkin Elmer GC.....	105
Figure 28. Sample calibration curve for quinoline/C16 on Perkin Elmer GC.....	105
Figure 29. Sample calibration curve for naphthalene/C16 on Perkin Elmer GC	106
Figure 30. Calibration curve for DBT/C16 in the Varian GC	106
Figure 31. Calibration curve for naphthalene/C16 in the Varian GC.....	107
Figure 32. Calibration curve for quinoline/C16 in the Varian GC	107
Figure 33. Experiment ID#4 – Quinoline/C16 on NiY	110
Figure 34. Schematic of in-situ calcinations apparatus	113
Figure 35. Linear isotherm for DBT adsorption on NaY zeolite.....	161
Figure 36. Linear isotherm for DBT adsorption on NiY zeolite	162
Figure 37. Linear isotherm for DBT adsorption on CsY zeolite	163
Figure 38. Linear isotherm for quinoline adsorption on NaY zeolite.....	164
Figure 39. Linear isotherm for quinoline adsorption on NiY zeolite	165
Figure 40. Linear isotherm for quinoline adsorption on CsY zeolite	166
Figure 41. Linear isotherm for naphthalene adsorption on NaY Zeolite.....	167

Figure 42. Linear isotherm for naphthalene adsorption on NiY zeolite.....	168
Figure 43. Linear isotherm for naphthalene adsorption on CsY zeolite.....	169

Acronyms

AC – Activated Carbon

AMIM – alkyl -3-methylimidazolium

BET – Brunauer, Emmett and Teller’s isotherm for determining specific surface area

BMIM – butyl-3-methylimidazolium

BMS – Benzyl Methyl Sulfate

BT – Benzothiophene

C16 – n-hexadecane

CN – Carbon Number

CSTR – Continuous Stirred Tank Reactor

CTC – Charge Transfer Complex

DBT – Dibenzothiophene

DEDBT – Diethyl Dibenzothiophene

DFT – Density Functional Theory

DMDBT – Dimethyl Dibenzothiophene

EMIM – ethyl-3-methylimidazolium

FID – Flame Ionization Detector

FCC – Fluid Catalytic Cracking

GC – Gas Chromatograph

HBP – 2-hydroxybiphenyl

HDM – Hydrodemetallation

HDN – Hydrodenitrogenation

HDS – Hydrodesulfurization

HY – Hydrogen Type-Y zeolite

ICP – Inductively Coupled Plasma

KL – Potassium Type-L zeolite
MBT – Methyl Benzothiophene
MDBT – Methyl Dibenzothiophene
NaA – Sodium Type-A zeolite
Naph – Naphthalene
ODS – Oxidative Desulfurization
OES – Optical Emission Spectroscopy
PFPD – Pulsed Flame Photometric Detector
PFR – Plug Flow Reactor
Quin – Quinoline
SRGO – Straight Run Gas Oil
SSIE – Solid State Ion Exchange
TEM – Transmission Electron Microscopy
TMBT – Trimethyl-Benzothiophene
TPA – Organic Template for Zeolite Synthesis
TPD – Temperature Programmed Desorption
TSD – Thermionic Specific Detector
USY – Ultra Stable Y-Type Zeolite
XRD – X-Ray Diffraction

Symbols

Φ = interaction potential (J)

ΔH = heat (J/g or kJ/mol)

B = growth rate of breakthrough curve (s^{-1})

C = concentration (mmol/L)

CN = Carbon Number

D_{crit} = critical diameter (nm)

F = feed flow rate (mL/h)

G = proportionality constant (J/mmol)

K = equilibrium constant (L/mmol)

m = fluid mass flow rate (g/s)

M = time of maximum growth (s)

MW = molecular weight (g/mol)

N_s = Number of sodium ions per unit cell in NaY zeolite

P = pressure (atm)

Q = rate of heat flow (mW)

q = adsorbed amount (mmol/g)

R = ideal gas constant (J/mol K)

r = adsorption rate (mmol/s)

T = temperature ($^{\circ}C$)

T = parameter affecting when maximum growth occurs in breakthrough curve (dimensionless)

t = time (s)

x = axial direction (m)

Subscripts

a = adsorption

e = equilibrium

f = final

i = component i

m = maximum

o = initial

s = sulfur

1 Introduction

There has been a great interest in recent years for research into the desulfurization of transportation fuels. Sulfur limits for diesel fuel and gasoline have decreased substantially in recent years culminating in the United States Environmental Protection Agency (USEPA) directive for sulfur content of no more than 30 ppmw S in gasoline and 15 ppmw S in on-road diesel fuel by June 2006 (Ma et al, 2002). Transportation fuels are also promising for use in fuel cells, although ultra-low S fuels (<1 ppmw S) are required to prevent poisoning of the reforming catalyst in the fuel cell (Song, 2002).

Desulfurization is commonly carried out by a process called hydrodesulfurization (HDS). Deep-desulfurization via HDS would require either increasing reactor residence time, or carrying out reactions in harsher conditions (higher temperature, pressure). Achieving deep desulfurized transportation fuels would require improvements in HDS technology and/or alternative desulfurization processes. Recent research interest has focused on both.

1.1 Sulfur Cycle

Sulfur exists in the atmosphere naturally as part of what is known as the sulfur cycle (Baird, 1999). In nature, sulfur enters the atmosphere via volcanic emissions, dust, biogenic emissions and sea salt and is removed via dry (gaseous) and wet (aqueous) deposition on the earth surface (Schnoor, 1996).

With the advent of the industrial revolution in the 19th century, anthropogenic sulfur emissions increased to the extent that they now surpass natural ones (Stern, 2005). Annual global anthropogenic sulfur emissions peaked in 1989 with 74.1 Teragrams (1 Tg = 10¹² g) S (Smith et al, 2005) released into the atmosphere compared with a global average of 52 Tg S from natural sources (Schnoor, 1996).

Combustion of fossil fuels (such as coal and petroleum) is the largest anthropogenic sulfur source due to extensive use and high sulphur content (Smith et al, 2005). The largest source of this sulfur is stationary sources such as utilities and industry. Sulfur from stationary sources in the US amounted to 19.94 Tg S in 1989, compared with 1.35 Tg S from transportation sources (Cooper and Alley, 2002). An additional 1.02 Tg S was added from stationary non combustion sources such as metal processing and waste disposal (Cooper and Alley, 2002).

Sulfur generated by combustion appears mostly in the form of sulfur dioxide (SO₂) and sulfur trioxide (SO₃), collectively called SO_x. Sulfur dioxide pollution can cause damage to plants by chlorosis (the loss of chlorophyll) and plasmolysis (tissue collapse in leaf cells) (Cooper and Alley, 2002). Effects on humans begin at concentrations above 1 ppm, and at 10 ppm effects on the eyes, nose and throat are observed (Cooper and Alley, 2002).

In general, sulfur dioxide is of little concern in the atmosphere for two reasons. One reason is that it is usually present in the atmosphere in concentrations too low to observe effects on humans. Concentrations in urban areas are generally between 0.02 and 0.5 ppm, compared with 0.005 to 0.05 ppm in rural areas (Harrison and Perry, 1986). Li et al. (1996) studied variations in SO₂ concentration over a year at three Canadian sites and found that the concentration did not rise above 0.017 ppm.

Another reason the sulfur dioxide is not a large concern is that it is quickly oxidized in the atmosphere to sulfite and sulfate (Seinfeld, 2004). This oxidation occurs both in the gaseous and aqueous phase. In the gaseous phase, the majority of sulfur molecules react with hydroxyl radicals via the scheme below (Seinfeld, 2004):



This reaction occurs relatively quickly with a time constant of about 12 days (Warneck, 2000), although it is not enough to account for all of the conversion of sulfur dioxide to sulfate. The above mechanism accounts for about 15% of sulfur oxidation (Liao et al, 2003). The remainder occurs in the aqueous phase in water droplets in clouds, predominantly by the following mechanism (Seinfeld, 2004):



The progress of the aqueous oxidation of sulfur is strongly dependent on the pH of the solution (Seinfeld, 2004).

The amount of sulfur in the atmosphere remains relatively constant at about 4.6 Tg S, because high reaction rates allow it to be quickly removed via wet and dry deposition on the earth surface (Schnoor, 1996).

Wet deposition, known as acid rain has the most pronounced effect in areas with granite or quartz bedrock, such as Scandinavia and Canada (Baird, 1999). Quartz and granite bedrock do not have the ability to neutralize the acid as do limestone and chalk (Baird, 1999).

Acid deposition is also a problem for humans. Sulfate forms fine respirable particles of less than 2.5 μm ($\text{PM}_{2.5}$) which can enter the respiratory tract and cause adverse health effects (Reid et al, 2001).

Over the last twenty years, anthropogenic sulfur emissions have decreased. Industrialized nations in North America and Europe which have been historically responsible for most sulfur emissions have made significant progress through legislative measures and technological advancements, allowing lower sulfur content fuels to be used.

1.2 Crude Oil

Crude oil is a complex mixture whose composition is dependent on, among other things, its age and location of origin (Teravainen et al., 2007). The average composition of crude oils from a variety of reserves is presented in Figure 1.

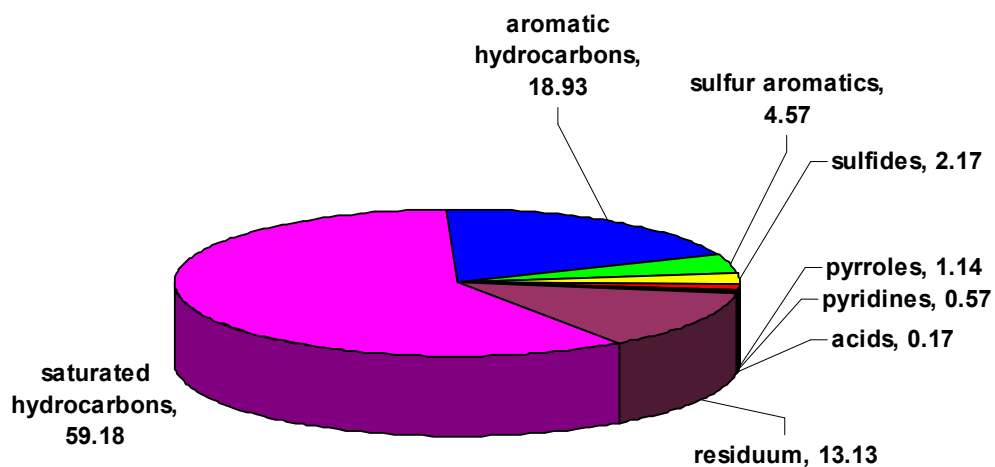


Figure 1. Average composition of crude oils (Adapted from Hughley et al, 2004)

The main components are straight chain hydrocarbons, aromatics and heteroatom containing molecules. Heteroatom compounds are those compounds containing atoms other than hydrogen and carbon, such as sulfur, nitrogen, oxygen or metal atoms. Typically crude contains about 10 wt% heteroatom species (Teravainen et al., 2007) and 1 wt% sulfur (Macaud et al., 2000). More than 20,000 heteroatom species have been identified in crude oil (Teravainen et al., 2007). As crude oil reservoirs have been further exploited, the portions left for recovery are heavier (i.e. higher sulfur content).

Heteroatom species are a concern for many reasons. In the catalytic reforming of petroleum, they poison catalysts and cause coke deposition (Teravainen et al., 2007). Since many of these compounds are poisonous and/or carcinogenic (Teravainen et al., 2007), they present a danger in the handling and use of the refined fuels. Combustion products of sulfur and nitrogen containing compounds include SO_x and NO_x which are precursors to acid rain and smog.

These species are removed from crude oil during the refining process by hydrodemetallation (HDM), hydrodenitrogenization (HDN) and HDS.

1.3 Desulfurization

Desulfurization is traditionally carried out via HDS, where sulfur is catalytically converted to H_2S (Ma et al., 1994). Typical catalysts used are $\text{CoMo}/\text{Al}_2\text{O}_3$ or $\text{NiMo}/\text{Al}_2\text{O}_3$ (Ho, 2004a) and reactions are carried out at elevated temperatures (300-340°C) and pressures between 20 and 100 atm (Xue et al., 2005).

HDS occurs via direct interaction between the sulfur atom and the catalyst surface and is therefore effective at removing sulfides, thiols and some lighter thiophenic compounds (Liu et al., 2007) in which the sulphur atom is not protected by alkyl groups on the molecule. Liang et al. (2006) found that in a low sulfur diesel fuel (433 ppmw S), the sulfur species present in the highest concentrations in order, were 4-MDBT>DBT>4,6-DMDBT>2,3,7-TMBT>2,3,5-TMBT. These refractory compounds are generally heavier thiophenic compounds such as dibenzothiophene, benzothiophene and their alkylated derivatives. They remain after HDS because steric hindrance prevents (or greatly inhibits) direct interaction between the sulfur atom and the catalyst surface. Ma et al. (1994) studied the reactivity of the refractory sulfur compounds in HDS and found a 35-fold decrease in HDS rate constants between alkylated BTs and 4,6-DMDBT due to steric hindrance on the sulphur molecule.

Song (2003a) used these rate constants to calculate the size of the catalyst bed required to achieve desulfurization down to 15 ppmw S. He determined the volume of the catalyst bed required to reach 15 ppmw S would have to be three times larger than the bed required to achieve the previous requirement of 500 ppmw S. Other possibilities to achieve deep desulfurized fuel via HDS include increasing the hydrogen pressure fed to the reactor or increasing the reaction temperature. Reactions under these harsher conditions hydrogenate olefins in the fuels, decreasing their energy content (Ng et al., 2005).

Other technologies have thus received increased attention in recent years for desulfurization.

1.4 Desulfurization Technologies

Several technologies exist in various stages of development for the desulfurization of transportation fuels. An excellent review is presented by Song (2003a) in which he describes many new or proposed technologies for desulfurization. New technologies focus on desulfurizing fuels both before and after fluid catalytic cracking (FCC). The different desulfurization technologies are described below.

1.4.1 Biodesulfurization

Several microorganisms have been found with the ability to metabolize thiophenic sulfur species and their use for desulfurization has been of significant scientific interest. Specific organisms such as *pseudomonas delafieldii* (Luo et al, 2003 and Li et al, 2006), *Rhodococcus sp.* (Oldfield et al., 1997), *Brevibacterium sp.* and *pseudomonas aeruginosa* (van Afferden et al., 1993) have been studied.

Oldfield et al. (1997) showed that *Rhodococcus sp.* converted DBT to 2-hydroxybiphenyl (HBP) and sulfite through oxidation of the DBT molecule with three DBT desulfurization operons, named DszA, DszB and DszC.

Van Afferden et al. (1993) focused on desulfurization of organic sulfur species found in coal, including DBT and benzyl methyl sulfone (BMS). While BMS is not of concern for the deep desulfurization of transportation fuels, the results for DBT desulfurization are important. *Brevibacterium sp.* metabolized only DBT through a mechanism similar to that of *Rhodococcus sp.* On the other hand, *pseudomonas aeruginosa* metabolized only BMS and thus was not a suitable micro-organism for desulfurization of transportation fuels.

It was found that DBT desulfurization by *pseudomonas delafieldii* was influenced heavily by the oil-to-water ratio and the concentrations of both DBT and *p. delafieldii* (Luo et al., 2003). They found an optimum oil-to-water volume ratio of about 0.4 with desulfurization rate falling off sharply at higher and lower ratios. The ratio of oil-to-water is significant because it determines the contact between the organic phase sulfur compounds and the aqueous phase micro organisms. The maximum rate of DBT desulfurization was found to be 11.4 mmol S kg⁻¹ dry cells h⁻¹.

Work has also been conducted studying the use of micro-organisms for indirect applications to desulfurization. An example is the use of *pseudomonas delafieldii* for the regeneration of desulfurization sorbents (Li et al., 2006). Their work involved adsorption of DBT in n-octane on transition metal-exchanged Y-type zeolites (NaY, CeY, CuY and CoY and NiY). CuY was studied for bioregeneration in a suspension of the sorbent, n-octane and the cells. CuY was found to retain 85% of its sorption capacity after regeneration, although some of the DBT adsorbed was reported to first desorb by the addition of n-octane to the regeneration suspension. It was unclear how much of the DBT metabolism occurred in the adsorbed phase compared with the dissolved phase, making the utility of these results unclear.

1.4.2 Charge Transfer Complex Formation

Refractory sulfur species have an electron-rich structure (Milenkovic et al., 1999), and thus the possibility exists to form charge transfer complexes (CTCs) between the electrons in the sulphur species and π -electron acceptors. CTCs are promising for desulfurization, selectively removing the more refractory sulfur species because of their higher electron density (Milenkovic et al., 2004). Additionally, they are insoluble in the organic phase so upon complex formation with the sulfur species, they precipitate out of solution and are easily removed (Milenkovic et al., 1999).

A preliminary study by Milenkovic et al. (1999) showed 2,4,5,7-tetranitro-9-fluorenone (TNF) as the most promising complexing agent, and has been followed by a significant amount of research on CTC formation. The interest in CTCs for desulfurization is not simply as an additional desulfurization treatment after HDS to obtain ultra-low S fuel. Research into indirect desulfurization applications has also been conducted.

Koltai et al. (2002) found that pre-treating HDS feeds with complexing agents greatly improved desulfurization efficiency. The CTC formation enhanced desulfurization of the refractory species, increased the rate of desulfurization, particularly at deep HDS conditions (i.e. lower sulfur concentrations). The reasons for this were not described, although it was noted that preferential CTC formation with the refractory sulfur species could prevent them from inhibiting HDS of the less refractory species, such as BT.

Further work by this group (Macaud et al., 2004) sought to support desulfurization by removing competitive species from solution before the HDS process. It was found that HDS capability could be increased by preliminary denitrogenation of feed. Denitrogenation was carried out via a combination of charge transfer and ion exchange processes.

1.4.3 Oxidative Desulfurization

Oxidation is a promising technology for desulfurization. Like adsorption, it operates under relatively mild conditions (Sampanthar et al., 2006). In general, thiophenes are oxidized to form highly polar sulfones which can easily be removed from the fuels by techniques such as solvent extraction.

A summary of oxidants and catalysts used in oxidative desulfurization is presented by Sampanthar et al. (2006). Oxidants used include H_2O_2 , NO_2 , O_3 , *tert*-butylperoxides and air. Catalysts such as acetic acid, formic acid, heteropolyacids, inorganic solid acids, cobalt catalysts and heterogeneous catalysts have been employed.

Sampanthar et al. (2006) used simple air as an oxidant and several different transition metal (Co, Mn) loaded γ - Al_2O_3 catalysts. One interesting result of their work was the finding that the conversion of the less reactive HDS compounds (4-MDBT, 4,6-DMDBT and 4,6-DEDBT) was higher initially than that of the less refractory sulfur species (3-MBT, DBT). It was proposed that in the ODS process, the increased electron density on the S atom in the substituted and disubstituted DBTs overcomes the increased steric hindrance caused by those groups. Thus, ODS is a promising technique for removal of these refractory sulfur species.

Chica et al. (2006) also found ODS to be a promising technique for removal of the refractory sulfur species. They used catalysts such as Ti-MCM-41 and *tert*-butyl

hydroperoxide as an oxidant. They found conversion of DBTs was generally higher than smaller BTs and thiophenes as reaction times increased.

Greater than 99% yield of oil with a sulfur concentration of less than 1ppm was obtained by Gao et al. (2006) in the desulfurization of straight run gasoline with an amphiphilic catalyst in an oil-water emulsion

ODS is thus a promising technique for desulfurization and so significant resources are being devoted to advancement in the field.

1.4.4 Ionic Liquids

One important difference between aromatic and aliphatic compounds is polarizability. Due to the delocalised nature of the electrons in aromatic molecules, they are easily polarized (Zhang et al., 2004) by interaction with other polar species, such as ionic liquids. Thus, extraction with ionic liquids is a technique which has garnered some interest for desulfurization in recent years.

Work by Zhang et al. (2004) showed that absorption capacities of ionic liquids decreased as the number of alkyl groups on the absorbed molecules increased. For example, absorption capacity of thiophene was found to be much greater (by a factor of about 3) than that of 2-methylthiophene.

Ionic liquids employed in their work were based on 3-methylimidazolium (MIM), including 1-alkyl 3-methylimidazolium (AMIM), butyl 3-methylimidazolium (BMIM) and ethyl 3-methylimidazolium (EMIM). The liquids used were either of the tetrafluoroborate type (i.e. EMIMBF₄) or the hexafluorophosphate type (i.e. BMIMPF₆).

The benefit of the ionic liquids is that they are immiscible in both aqueous and organic phases and can be regenerated. A potential issue to be addressed in further work is the pronounced effect of steric hindrance

1.4.5 Photochemical Desulfurization

Photochemical desulfurization is the process of removing polar organosulfur species from fuels via liquid extraction with a polar solvent (water, acetonitrile), followed by photochemical oxidation in the solvent phase (Shiraishi et al., 1999a). The resulting sulfoxides and sulfones accumulate in the polar phase.

Work into this area was conducted mostly in the latter half of the 1990's (Harai et al., 1996, 1997; Shirashi et al., 1998, 1999b). No research in more recent years could be found in the literature.

1.4.6 Adsorption

Adsorption is a mass transfer process wherein molecules in a free phase become bound to a surface by intermolecular forces (Hines and Maddox, 1985). It is often employed to remove trace impurities, such as the removal of trace amounts of aromatics from aliphatics (Takahashi et al., 2002).

From a theoretical point of view, adsorption is an attractive process for desulfurization of transportation fuels for several reasons:

- i. Adsorption is effective in separation processes involving low sorbate concentrations, and thus potential exists for removal of refractory sulfur compounds in transportation fuels.
- ii. Adsorption can occur at lower temperatures and pressures than many other processes (particularly HDS), resulting in lower operating costs.
- iii. Adsorbents may be regenerated by simple engineering means, such as increasing temperature, decreasing pressure or washing with a solvent. The use of these regenerable sorbents may decrease the costs associated with the fuel processing.
- iv. The properties of sorbents, including their capacity and selectivity, are strong functions of their structure and composition (Smith et al., 2001). Furthermore, these properties can be readily modified via preparation procedures or post preparation modification procedures. Thus, the properties can potentially be optimized to maximize both sulfur capacity and sulfur selectivity.

Takahashi et al., (2002) found the adsorption energy, calculated via molecular orbital theory, was higher for thiophene than benzene on model Y-type zeolite surfaces. Similarly, Ma et al. (2002) reported obtaining ultra-low sulphur (<1 ppmw S) gasoline, diesel and jet fuel by adsorption on a transition metal supported on silica gel. Results showed little octane penalty from adsorption, representing an important benefit over HDS. Promising results obtained by these groups led to significant recent research into desulfurization of model fuels and transportation fuels; however,

to date little work has been reported on experimental determination of liquid phase heats of adsorption.

Work by this group has shown that zeolites, and more specifically sodium-Y type zeolite (NaY) showed promise for removal of thiophenic sulphur compounds from both n-octane and n-hexadecane under flow conditions (Ng et al., 2005). This work introduced the use of a flow calorimetric technique and was followed by a more detailed study of adsorption of thiophenic sulphur compounds on NaY using thermal gravimetry and flow calorimetry (Jiang et al., 2005). Finally Jiang and Ng (2006) showed higher heats of adsorption for benzothiophene in n-octane on NiY and CuY over NaY, indicating the potential of transition metal exchanged Y-type zeolites for desulfurization. This work is discussed in more detail in Sections 2.2 and 2.3.

1.5 Objectives

Adsorption appears to be a promising technique for desulfurization. The objectives of this work are as follows:

- i. To develop an improved method for determination of liquid phase heats of adsorption via flow calorimetry. Primarily, a method for simultaneous determination of heats of adsorption and adsorbed amounts would represent a significant advance in this work.
- ii. To investigate the heat of adsorption of dibenzothiophene, quinoline and naphthalene in model diesel fuel on zeolites at 30°C.
- iii. To determine the adsorption capacity of dibenzothiophene, quinoline and naphthalene on different zeolites, both at equilibrium and under flow conditions at 30°C.
- iv. Determine the selectivity of different zeolites for dibenzothiophene adsorption relative to quinoline and naphthalene adsorption.

2 Literature Review

2.1 Adsorbents and Properties

Adsorption is a mass transfer process wherein molecules in a free phase become bound to a surface by intermolecular forces (Hines and Maddox, 1985). The adsorbed molecule is called the adsorbate and the surface to which it is adsorbed is called the adsorbent. Adsorption is important as both a separation process and a step in catalytic reactions (Smith et al., 2001). Since adsorption relies on interactions between molecules and surfaces, the most effective adsorbents are generally porous, high surface area solids such as activated carbon, aluminas, silicas, and zeolites (Smith et al., 2001).

Adsorption may be classified as either physical (physisorption) or chemical (chemisorption) based on the nature of the adsorbent-sorbate interaction (Smith et al., 2001). Physisorption involves weak attractive forces including van der Waals' forces (Hines and Maddox, 1985) and electrostatic induction/dispersion forces (Smith et al., 2001). Since physisorption does not rely on direct sorbent-sorbate interaction, it may occur in multiple layers on the surface (Hines and Maddox, 1985). Chemisorption, on the other hand, is characterized by the sharing of electrons between the sorbate and sorbent molecules (Hines and Maddox, 1985). This direct interaction means that in the case of chemisorption, adsorption only occurs in a single monolayer where sorbate molecules are fixed to the surface (Smith et al., 2001).

The three most important properties in the design of a sorbent are capacity, selectivity and adsorption strength (measured as heat of adsorption).

2.1.1 Capacity

Adsorption capacity is defined as the number of moles (or the mass) adsorbed per unit mass (or surface area) of the sorbent. In this work, a sorbent is desired with a very high capacity for sulfur. High sulfur removal capacities are desired to minimize the bed volume (and mass) required, as well as to maximize the operation time before the bed becomes saturated.

Adsorption capacity is traditionally determined with equilibrium adsorption isotherms. An adsorption isotherm is a plot of the adsorbed amount as a function of the concentration of the solution (or pressure of gas) with which it is in equilibrium.

Many types of adsorption isotherms exist, but the most common is the Langmuir isotherm which is derived based on the reaction



where :

A = adsorbate

S = surface site

$A-S$ = sorbate – surface site complex

The full derivation was presented by Hines and Maddox (1985), based on four assumptions:

- i. All adsorption sites are energetically equal.
- ii. There is no interaction between adsorbed molecules.
- iii. Adsorption occurs only in a monolayer.
- iv. All sorbate-sorbent complexes are identical.

The resulting equilibrium relationship is:

$$q_e = \frac{q_m K_a C_e}{1 + K_a C_e} \quad (4)$$

where :

q_e = adsorbed amount (mmol / g)

q_m = adsorption capacity (mmol / g)

K_a = adsorption equilibrium constant

C_e = solution concentration of adsorbate in equilibrium with q_e (mmol / L)

Rearranging (4) gives

$$\frac{C_e}{q_e} = \frac{1}{q_m} C_e + \frac{1}{K_a q_m} \quad (5)$$

which is in the form of a straight line relationship. Plotting C_e/q_e vs C_e should result in a straight line with a slope of q_m^{-1} and an intercept of $1/q_m K_a$ (Ho, 2004b). Thus, from an

equilibrium isotherm, both the equilibrium sorption capacity and adsorption equilibrium constant may be obtained.

Other (generally empirical) equilibrium relationships exist, including the Freundlich, Volmer and Hill de Boer Isotherms (Hines and Maddox, 1985). Some isotherms combine properties of the different models. The Langmuir-Freundlich Isotherm, for example, combines the theoretically based Langmuir Isotherm with correction factors based on the empirical Freundlich Isotherm (Hines and Maddox, 1985).

Since the Langmuir isotherm is based on the assumption that the system is in equilibrium, its use for prediction in transient systems may be limited. Under flow conditions such as in the flow microcalorimeter, either this assumption must be verified or a different method must be employed.

Other methods for determination of the adsorbed amount exist which do not rely on equilibrium being reached. They include calculations based on breakthrough curves and the novel method developed in this work. Both methods are discussed later.

2.1.2 Selectivity

Transportation fuels are complex mixtures containing alkanes, aromatic compounds and heteroatom containing species (Figure 1). In a complex mixture, there are many species potentially competing for the same adsorption sites. It is desired to develop a sorbent which adsorbs the sulfur species preferentially over all those species present in the fuel.

Selectivity is influenced by several factors. Properties of the sorbent as well as properties of the sorbate contribute to the properties of the sorbate-sorbent system. For a given sorbent, sorbate molecules with different sizes and shapes have different interaction potentials and therefore adsorb in different amounts and with different strengths. Likewise, for a given set of sorbate molecules, pore size and shape influence the different sorbate molecules differently. For example, consider a system of two sorbate species with different molecular diameters, D_1 and D_2 . For a sorbent with pore size $D_p > D_1, D_2$ both sorbate species would enter the pores and likely be adsorbed in some amounts. If the diameter of the pore were to decrease to some value where $D_1 < D_p < D_2$ then species 1 would be able to enter the pores to be adsorbed, but species 2 would not be able to fit inside the pores.

Selectivity is determined by conducting adsorption in competitive conditions and measuring the relative amounts of the different species adsorbed. Several definitions of selectivity exist and are useful in different applications. Since this work focuses on desulfurization, a useful definition of selectivity is the amount of a substance adsorbed relative to the amount of sulfur adsorbed during an experiment. That is:

$$Selectivity(S) = \frac{q_s}{q_i} \quad (6)$$

where :

Selectivity(S) = selectivity of sulfur relative to component i

q_i = amount of i adsorbed (mmol / g)

q_s = amount of sulfur adsorbed (mmol / g)

Thus, a high value (>1) of selectivity indicates that sulfur is adsorbed preferentially. A low value (<1) indicates that species *i* is adsorbed preferentially. In our work, therefore, we desire to maximize the selectivity value such that sulfur is adsorbed preferentially over all other species.

Selectivity can be predicted based on the single component isotherms. For example, Yang (2003) presented the hybrid Langmuir-Freundlich equation for an *n*-component mixture:

$$q_i = \frac{q_{mi} K_i C_i^{1/\eta_i}}{1 + \sum_{j=1}^n K_j C_j^{1/\eta_j}} \quad (7)$$

where η_i is an empirical parameter from the Freundlich equation and K_i is the equilibrium constant in the single component isotherm. The above equation relies on several simplifying assumptions which reduce its accuracy, although it remains useful for practical design (Yang, 2003).

Additionally, it is a hypothesis of this work that at equilibrium, selectivity may be predicted qualitatively based on the strength of adsorption of different sorbates, measured as the heat of adsorption. A more strongly adsorbed species would likely be adsorbed in a greater amount than a less strongly adsorbed species at equilibrium. This hypothesis will be examined in this work.

2.1.3 Heat of Adsorption

For adsorption to be thermodynamically favourable, the interaction potential must be equal to the energy required to bring a molecule into the adsorbed phase (Yang, 2003). Thus, adsorption occurs when

$$\phi = RT \ln \frac{P}{P_o} \quad (8)$$

where :

ϕ = interaction potential

R = ideal gas constant

T = Temperature

P = Pressure

P_o = saturated vapour pressure

Further, the heat of adsorption is defined as

$$\Delta H = \phi - RT + F(T) \quad (9)$$

where $F(T)$ is a function of the translational and vibrational energies of the sorbate (Yang, 2003).

Heat of adsorption is important for two reasons; it has significance in both relative and absolute terms. A sorbent is desired with a high heat of adsorption for sulfur compounds relative to others in the fuels (nitrogen containing compounds, aromatics, etc). Higher heats of adsorption indicate a more thermodynamically favourable adsorption process and thus a higher amount adsorbed at equilibrium relative to that of other compounds in a competitive situation. Conversely, a lower heat of adsorption is desirable for regeneration of the sorbent. It has been stated that one benefit of adsorption is its reversibility (that is, desorption of all adsorbed molecules). The energy required for desorption is equal to the energy released during adsorption. Thus, higher heats of adsorption translate to higher energy requirements for regeneration, resulting in higher operating costs.

The ideal adsorbent has a high capacity for sulfur, with a heat of sulphur adsorption on the sorbent that is low, but still higher than that for the other compounds.

Heats of adsorption can be determined in several different ways. One method is the prediction of heats of adsorption based on molecular orbital calculations (Takahashi et al., 2002). Computer simulations are used to predict the energies of interaction between specific sorbate molecules and a model of the sorbent structure. This method is useful for sorbents with regular structures having adsorption sites which are, in general, energetically equal. On other sorbents with heterogeneous sites of different energies (such as activated carbon), prediction of heats of adsorption is less reliable.

Another method for determining heats of adsorption involves calculations based on equilibrium isotherms. Determination of isotherms in the vapour phase at different temperatures allows for calculation of the heat of adsorption via the Clausius-Clapeyron equation (Takahashi et al., 2002).

Direct measurement of heats of adsorption is possible using calorimetry. Calorimetry is simply the direct measurement of the heat evolved (or absorbed) during a process such as adsorption, a chemical reaction or a physical change of state. Calorimetry is discussed in Section 2.3.

Commercially successful sorbents are generally high surface area porous solids. Some common types of adsorbents are activated carbon (AC), silica gel, activated alumina and zeolites (Yang, 2003).

Based on the observation that zeolite ZSM-5 selectively removed thiophene from benzene (Takahashi et al., 2002), interest in zeolites as desulfurization sorbents increased in the 1990s. Further studies, discussed in Section 2.2, have shown zeolites to be extremely promising desulfurization sorbents.

Zeolites are composed of regularly ordered SiO_4 and AlO_4^- tetrahedra which combine to form, depending on the type of zeolite, pores of between 0.2 and 1.0nm (Weitkamp, 2000). Zeolites are aluminosilicates with uniform pore sizes on the order of molecular dimensions (Maesen et al., 2001). These pores can thus prevent passage of some molecules while allowing others to go through. This creates an exciting possibility in the field of catalysis (Oxtoby et al., 1999). Excluding some molecules from pores may prevent the formation of unwanted products, resulting in increased selectivity.

Zeolites are comprised of AlO_4^- and SiO_4 tetrahedra. The SiO_4 gives the zeolite its stability, where the AlO_4^- provides a charge for the addition of cations to the framework (Milton, 1959a). These tetrahedra combine to produce a variety of shapes and configurations, such as sodalite and pentasil units. A very thorough discussion on different types of building units and some structures resulting from them is given by van Koningsveld (2001).

Zeolites have been known to humans for about 250 years (Flanigen, 2001). Natural zeolites have been of little use in catalysis due to irregularities in structure and impurities in composition. Synthetic zeolites have been available since the 1940's (Flanigen, 2001).

Zeolites are used today as adsorbents, catalysts and ion exchange resins, with a wide range of uses within each category. For example, zeolites are finding use in the detergent industry as ion exchange resins. The Na^+ ion is exchanged for Mg^{2+} and Ca^{2+} ions in the water, and therefore acts as a softening agent (Weitkamp, 2000).

Due to the wide range of applications for zeolites, a variety of zeolite preparation techniques exist to allow for the synthesis of zeolites to meet specific needs. Even so, there is still a basic 'recipe' for the preparation of zeolites.

There are five main ingredients in the synthesis of zeolites (Jansen, 2001). They are summarised in Table 1.

Table 1. Chemical sources and their function in zeolite synthesis

Sources	Function(s)
SiO_2	Primary building unit(s) of the framework
AlO_2^-	Origin of the framework charge
OH^-	Mineralizer, guest ion
Alkali cation, template	Counter ion of AlO_2^- , guest molecule
Water	Solvent, guest molecule

From Jansen (2001)

The above components are obtained from a variety of specific sources.

SiO₂

Silica may be obtained in a variety of forms, the properties of which affect the properties of the resulting zeolite (Jansen, 2001). Differences in solubility and impurity levels can affect the crystallization of the zeolite (Jansen, 2001). For example, in the preparation of zeolite A, silica

sources can include silica gel, silicic acid or sodium silicate (Milton, 1959a). Zeolite X may be made from any of these sources as well as colloidal silica (Milton, 1959b).

Al₂O₃

The choice of the alumina source is affected by the same considerations as for the silica source. Extremely pure alumina is available; however it is not very soluble (Jansen, 2001). Examples of alumina sources for the manufacture of zeolite A are activated alumina, γ -alumina, α -alumina, alumina trihydrate or sodium aluminate (Milton, 1959a). Zeolite X may use any of the above except for α -alumina (Milton, 1959b).

OH and Alkali Cation

OH⁻ is the counter ion of the alkali cation. In solution it is used to control the pH of the reaction mixture. This makes the reaction mixture basic, which is desirable for zeolite synthesis (Jansen, 2001). For example, the pH of the reaction mixture for zeolite A, X and L should be between 9 and 12 (Milton, 1959a,b, Breck et al., 1965).

An organic template (denoted as TPA) is a carrier for the alkali cation. As stated in Table 1, the cation balances the charge of the aluminate ion.

It is often useful to use the OH⁻ ion as the organic template. This is done in the synthesis of NaA (Milton, 1959a), NaX (Milton, 1959b) and KL (Breck et al., 1965). NaOH is used to produce sodium types, while KOH is used to generate the potassium type. Using the hydroxide ion has three main benefits (Milton, 1959a):

- i. one reactant can provide both the cation and the pH control.
- ii. metal hydroxides are readily soluble in water.
- iii. sodium ion may be easily exchanged with other cations after synthesis if required (not applicable for KL).

The basic procedure for zeolite synthesis is as follows (Milton, 1959a): The reactant mixture is heated and left for a period of time to cool and crystallize. After crystallization, the zeolite is filtered out of the liquor and rinsed. Then, the zeolite is calcined and ready to use. In some cases, the zeolite may be subjected to secondary synthesis or ion exchange before calcination.

The reaction temperature can vary from as low as room temperature (Milton, 1959a) to as high as 300°C (Jansen, 2001). The reaction rate is strongly temperature dependent. For zeolite A, the reaction time is as much as 6 days at room temperature or as little as 45 minutes at 100°C (Milton, 1959a).

Jansen (2001) gives a more detailed description of the process of zeolite synthesis. It can be summarised as follows: The reactants are mixed at low temperature (below 60°C). At this temperature, the silicate is hydrolyzed, creating a molecule of the type $\text{Si}(\text{OR})_4\text{OH}$. These monomers then combine into clusters. According to Jansen (2001), as the reactant mixture is heated (<200°C), the association of the primary building units occurs. It is suggested (Jansen, 2001) that this reorganisation is driven by the lower surface energy in accordance with the Ostwald ripening principle.

The high temperature reaction process leads to (i) nucleation, (ii) crystallization and finally (iii) precipitation (Jansen, 2001). Nucleation occurs when the clusters begin to associate with cations and finally become stable. There are several theories on the identity of the building units of the crystals, including silica and alumina tetrahedra of the monomers, and the clusters formed at the lower temperature (Jansen, 2001).

The zeolite is then isolated via filtration and rinsed with distilled water. The filter residue is dried at temperatures between 25 and 150°C (Milton, 1959a), and the dried zeolite is either activated or undergoes secondary synthesis procedures or other processes such as ion exchange.

2.2 Adsorbents for Desulfurization

Y-type zeolites have been a primary focus in adsorptive desulfurization for several years. Ng et al. (2005) showed that NaY had a higher capacity for both thiophene and DBT than HY, USY and 13X zeolites. Further, equilibrium adsorption experiments indicated high capacities of NaY for thiophene, benzothiophene, DBT and 4,6-DMDBT.

Y-type zeolites have a faujasite type structure, with a unit cell composition of $\text{M}_x\text{Al}_x\text{Si}_{192-x}\text{O}_{384}$, where $0 \leq x \leq 77$ (Calero et al., 2004). They are composed of sodalite units and with 1.3 nm cages accessed through 0.74 nm windows (Weitkamp, 2000).

Early work by Yang et al. (2001) showed that heats of adsorption (based on molecular orbital calculations) for thiophene were higher than for benzene on metal ion exchanged zeolites CuY and AgY. The proposed explanation was the back donation of d-electron density by the

transition metal for formation of relatively strong π -complexes. Thus, π -complexation adsorption has been of significant interest in recent years.

Further work (Takahashi et al., 2002) determined heats of adsorption on several adsorbents via adsorption isotherms and the Clausius-Clapeyron equation. Results are presented in Table 2. Heats of adsorption are given as a range of values covering a range of surface coverages. In all cases, the highest heat in each range represents the lowest fractional coverage.

Table 2. Heats of adsorption from vapour phase equilibrium isotherms

	ΔH_{ads} (kJ/mol)	
	Benzene	Thiophene
NaY	71.2-76.2	79.9-82.0
NaY ^b		20.97
AgY	79.5-84.1	89.2-90.0
AgY ^a	84.1	89.6
CuY	80.8-91.3	87.1-93.8
CuY ^a	91.3	93.3
H-USY	27.6-54.8	33.1-46.9
NaZSM-5	69.1-74.9	77.9-80.4
AC (PCB type)	54.8-67.4	33.5-100.0
Selexsorb CDX	70.3-82.0	67.4-73.3

All data from Takahashi et al., 2002, except

^aYang et al., 2001

^bNg et al., 2005

The technique for prediction of heats of adsorption based on molecular orbital calculations was verified by comparison of the predicted results with experimental results of Yang et al. (2001), as denoted in Table 2 with superscript ‘a’.

The heat of adsorption of thiophene on NaY measured by Ng et al. (2005) was based on measurements using liquid phase flow microcalorimetry. A solution of thiophene (1800 ppmw S) in n-hexadecane was prepared, and adsorption occurred on a sorbent which had already been saturated with pure n-hexadecane. Results reported in this work therefore represent liquid phase heats of displacement, rather than heats of adsorption. They are understandably lower than those estimated by Takahashi et al. (2002), since they include both the endothermic desorption of n-hexadecane molecules and the adsorption of thiophene molecules.

From the work of Takahashi et al. (2002), it was noted that in zeolites the heats of adsorption tended to be higher for thiophene than for benzene, indicating potential as desulfurization sorbents. Further, the metal exchanged Y-type zeolites (NiY, AgY and CuY) had the highest heats of adsorption of all zeolites studied.

These sorbents were the basis for future work in which liquid phase adsorption experiments were carried out using model fuels on CuY and AgY zeolite (Hernandez-Maldonado and Yang, 2003a) followed by commercial fuels on CuY zeolite (Hernandez-Maldonado and Yang, 2003b). Studies of adsorption of thiophene (2000 ppmw S) from n-octane showed that CuY had a higher saturation loading (2.55 mmol/g) than AgY (0.90 mmol/g) and NaY (1.05 mmol/g). In the adsorption experiments using commercial fuels, CuY with an activated carbon guard bed (15% of the bed weight) had saturation loadings of 0.50 and 0.59 mmol/g for gasoline and diesel fuel, respectively.

Hernandez-Maldonado et al (2004a) also studied desulfurization of commercial diesel fuel containing 297 ppmw S on NiY and NiX zeolites. Findings indicated higher sulfur removal capacities for NiX (0.251 mmol/g) than NiY, (0.204 mmol/g), though neither had removal capacities as high as CuY (0.374 mmol/g) (Hernandez-Maldonado and Yang, 2004c). The higher capacity of X-type zeolite relative to that of Y-type zeolite was the opposite of that found by Ng et al (2005) using NaY and 13X zeolites. Their work found NaY had a higher capacity for both benzothiophene and dibenzothiophene than 13X zeolite. No published results on Cu-exchanged X zeolite could be located for comparison. Work with ZnY (0.116 mmol/g) zeolite (Hernandez-Maldonado et al., 2005) showed a lower sulfur removal capacity than CuY (0.723 mmol/g) from commercial jet fuel.

Several ion exchanged HY zeolites were studied for sulfur removal capacity from jet fuel in batch experiments (Velu et al., 2003), indicating that sulfur removal capacity increased in the order ZnY<HCuY<HNiY<HY<HCeY<HPdY. No information was provided regarding preparation of sorbents however. Since sorbents were calcined in air, it is unlikely that reduction of copper from Cu(II) to Cu(I) occurred, making comparison with desulfurization results from Hernandez-Maldonado and Yang's research impossible.

Guard beds have been used in desulfurization (Hernandez-Maldonado et al., 2004a; 2004b; 2004d), and shown to increase sulfur removal capacity per unit mass of sorbent bed. The guard beds (~25% of total bed weight) removed competitive compounds found in diesel fuel, allowing more of the desulfurization sorbent capacity to be used for sulfur adsorption. For example, Hernandez-Maldonado and Yang (2004c) reported an improvement in desulfurization capacity from 0.374 mmol/g to 0.59 mmol/g for commercial diesel fuel with CuY zeolite when 15% of the CuY was replaced with activated carbon in the form of a guard bed (Hernandez-Maldonado and Yang, 2003b).

Jiang and Ng (2006) found that the heats of adsorption of benzothiophene in n-octane obtained via flow calorimetry increase in the order $USY \sim NaY < NiY \ll CuY$, indicating that the metal exchanged Y-type zeolites show great promise for use in desulfurization of fuels due to their high heats of adsorption for organosulfur compounds. No work was presented on similar experiments with organonitrogen compounds or aromatics.

Jiang et al. (2005) studied the use of flow calorimetry for desulfurization of model diesel fuels and the effect of adsorption parameters such as the feed concentration and flow rate on the adsorption process. They found that the adsorption capacity increases as the carbon number of the solvent decreases. Also, the apparent heat of adsorption decreases with increasing carbon number of the alkane solvent.

This result can be explained, at least in part, by the observation that the liquid phase calorimetry method employed measures *apparent* heat of adsorption, not the actual heat of adsorption (Ng et al., 2005). That is, the method measures the heat evolved when a solvent molecule in the adsorbed phase is replaced by a sorbate molecule. In short, it is the heat of *displacement* of solvent molecules by sorbate molecules that is being measured. It is known that for alkane solvents, the heat of adsorption increases as the carbon number increases. Indeed, Calero et al (2004) provided the following relationship between heat of adsorption of alkanes on Na – faujasite zeolites and the carbon number of the alkane:

$$-\Delta H_0 (kJ/mol) = \frac{2}{T} [(144.1N_s + 27438.4)CN - 49567.3] + (4.37N_s + 432.8)CN + 1111.13 \quad (10)$$

where :

CN = carbon number of solvent

N_s = number of sodium cations per unit cell

T = Temperature (K)

Since the longer chain alkanes have higher heats of adsorption, more energy is required to desorb them. Thus, as the length of the alkane molecule displaced by a sorbate molecule increases, the net heat change (the apparent heat of adsorption as measured in this work) decreases.

Further expanding on the promising adsorption results with CuY, additional molecular orbital calculations were conducted to estimate heats of adsorption of some important compounds in diesel fuel on the zeolite. These results are summarized in Table 3.

One interesting result of these predictions is that the heats of adsorption of sulfur compounds tend to increase as the size of the molecule increases, indicating that the less reactive species in HDS may be preferentially removed during adsorption. Flow adsorption experiments by Ng et al.(2005) were in agreement with this prediction.

Table 3. Summary of predicted heats of adsorption on CuY zeolite

Compound	ΔH_{ads} (kJ/mol)
Thiophene ^a	89.6
2-methylthiophene ^a	94.2
Benzothiophene ^a	95.9
Dibenzothiophene ^a	98.8
4,6-dimethyl Dibenzothiophene ^a	98.4
Benzene ^a	85.8
Toluene ^a	90.0
Fluorene ^b	89.2
Naphthalene ^b	91.3
Phenanthrene ^b	92.5
Quinoline ^b	105.5
Carbazole ^b	115.1
MTBE ^c	129.8
Ethanol ^c	174.1

^aYang et al, 2004

^bJayaraman et al, 2006

^cLi et al, 2006

The data in Table 3 also suggest that sulfur adsorption should, in general, be slightly preferred over adsorption of aromatics on CuY zeolite, although nitrogen-containing compounds and oxygenates would likely be adsorbed preferentially over sulphur compounds. Ma et al. (2002) have found thiophenic sulfur compounds to be adsorbed preferentially over aromatics using a model diesel fuel on an unidentified porous support loaded with an unidentified transition metal. Preferential adsorption of quinoline over DBT and anthracene has also been confirmed by Ng et al. (2005).

Studying the desulfurization of jet fuel (1172 ppmw S), Wang et al. (2006) found that PdCl₂ was a promising desulfurization sorbent. Supported on activated carbon, PdCl₂/AC exhibited a saturation capacity of 0.616 mmol S/g. For various thiophenic sulphur compounds, the

selectivity over benzene was one to three orders of magnitude higher on PdCl₂/AC than on CuY, indicating potential for the use of palladium-based sorbents in desulfurization. This finding agrees with those of Velu et al. (2003), who found HPdY zeolite had a higher desulfurization capacity than other metal-exchanged zeolites on a model jet fuel.

Recent research by Ma and Yang (2007a, 2007b) has focused on relating heats of adsorption from the vapour phase with heats from liquid solution. This promising work may present an opportunity to overcome one of the limitations of the liquid phase technique, wherein only heats of solvent displacement are measured rather than actual heats of adsorption.

Indeed, this group (2007b) compared their liquid phase heats of adsorption based on isotherms and the Clausius-Clapeyron equation with the results of Ng et al. (2005) and Jiang and Ng (2005), and found good agreement for adsorption of T, BT and DBT in hexadecane on NaY. They further related the liquid phase heats of adsorption to the vapour phase heats based on their new proposed method (2007a), although no basis for comparison exists with experimental vapour phase heats of adsorption. An interesting comparison would be to extend their previous work based on vapour phase heats of adsorption, or predicted vapour phase heats of adsorption (obtained from molecular orbital calculations) on CuY zeolite with the predicted vapour phase heats based on the Clausius-Clapeyron equation and liquid solution heats of adsorption.

The basicity of the nitrogen compounds is thought to play a role in their preferential adsorption over sulfur species (Ng et al., 2005). Decreasing the acidity of the zeolite was thought to possibly reduce the selectivity for nitrogen. Promising results were obtained by Laborde-Boutet et al. (2006) who found that increasing electropositivity of the zeolite by changing the framework cation increased selectivity for thiophene adsorption relative to toluene due to interactions between the nucleophilic S atom and the framework cation. They found that the ion exchanged Y zeolites, in order of increasing thiophene selectivity were LiY<NaY<KY<RbY<CsY, following the trend for increasing basicity of zeolites. More work is required to determine if such zeolite modifications could improve sulfur selectivity relative to nitrogen selectivity.

Although π -complexation adsorption using zeolites has attracted significant attention for sulphur removal, other types of desulfurization sorbents have been receiving attention in research as well. Kim et al. (2006) recently studied desulfurization and denitrogenation of a model diesel fuel using activated carbon, activated alumina and Ni/SiO₂-Al₂O₃. They found

activated carbon to have an extremely high adsorption capacity (0.508 mmol/g) from a feed solution containing 686.7 ppmw S and 303.0 ppmw N, although it showed little selectivity for sulfur compounds. The activated alumina was found to be a superior sorbent for denitrogenation due to acid-base interactions between the sorbent and quinoline molecules. Ni/SiO₂-Al₂O₃ was found to be a promising sorbent for desulfurization due to direct interaction between the surface nickel and the sulphur atoms.

The high capacity of activated carbon found by Kim et al. (2006) indicated the potential for use of activated carbon as a desulfurization sorbent. Zhou et al. (2006) studied adsorption of organosulfur compounds on three different types of activated carbon and reported that the desulfurization ability of the sorbent varies significantly with the type of carbon used. Thus, further studies to understand the effect of different properties and to determine the optimum activated carbon type to use are underway.

Yang et al. (2007) examined adsorption on micrometer sized mesoporous silica spheres, finding a capacity of up to about 0.64 mmol S per gram sorbent via fixed bed adsorption experiments with 500 ppmw S DBT in C8. The capacity was found to be significantly reduced when aromatics in the form of 5 wt% of 2-methylnaphthalene were added. It was also found that due to the mesoporous nature of the adsorbent, mass transfer limitations were minimal and the breakthrough curve was extremely sharp, indicating that breakthrough does not occur until the sorbent is nearly saturated. This result is promising because it implies that a large portion of the adsorption capacity can be used to produce deep desulfurized fuel before regeneration is required.

Richardeau et al. (2004) showed that thiophene could react catalytically at low temperatures after adsorption on H-USY zeolite. Huntley et al. (1996) studied the scission of C-S bonds in thiophenic compounds adsorbed on Ni(111). Carbon aerogels have also been shown as promising desulfurization sorbents (Haji and Erkey, 2003) due to their high sulfur capacity and significant selectivity over naphthalene.

Adsorption has also been studied for multi-stage processing in order to achieve maximum desulfurization. For example, Sano et al. (2005) proposed a two-stage adsorption process for diesel desulfurization coupled with HDS. In their process, hydrotreated straight run gas oil (SRGO) is passed over a bed of fresh activated carbon (AC) to remove the refractory species. Once this adsorption bed is spent, it is used as a pre-treatment adsorption bed, in order to

desulfurize and denitrogenate the HDS feed, while a new fresh AC bed is placed downstream from the HDS reactor. Thus, their process involves adsorption both before and after HDS, in order to remove HDS inhibiting compounds and refractory compounds, respectively.

2.3 Calorimetry

Calorimetry is the measurement of the heat released (or absorbed) during a change of state (physical or chemical). It can therefore be used to measure the heat released during adsorption.

Calorimetry is primarily carried out for vapour phase processes, although it may also be conducted on liquid phases. Liquid phase flow calorimetry is difficult compared to calorimetry in the vapour phase. The main reason for this is that in vapour phase calorimetry pure sorbate can be fed to the calorimeter in small amounts whereas in the liquid phase the only way to feed small amounts of sorbate is in a dilute solution. Adding another species (the solvent) necessarily complicates the system, and in many cases makes it difficult to separate the solvent adsorption effects from adsorption of the target species being studied.

Liquid phase calorimetry does have unique advantages however, making it extremely useful for some purposes:

- i. Some systems of interest (such as desulfurization of fuels, for example) occur naturally in the liquid phase. Thus, liquid phase calorimetry yields results more representative of the physical system of interest.
- ii. Some species, such as 4,6-DMDBT are difficult to vapourize, and the temperature and pressures required to do so would yield results which would not be useful for comparison to the actual adsorption process.

Thus, liquid phase flow calorimetry was chosen as the most suitable technique for our purposes. Work was carried out for the development of a reliable method for determination of heats of displacement, with an eventual goal of determination of heats of adsorption.

A unique benefit of flow calorimetry is that the output of the calorimeter is a real time measurement of the heat flow as a function of time. This real time data provides information regarding rates of adsorption, allowing for calculation of kinetic parameters in addition to the thermodynamic parameters obtained using other calorimetric techniques. Additionally, some thermodynamic parameters not available in standard calorimetry become available during flow

calorimetry. Standard techniques, for example, measure integral heat of adsorption. Flow calorimetry, in addition to integral heat of adsorption could potentially be used to measure differential heats of adsorption.

Flow calorimetry is a technique which can be employed to obtain data on a wide array of thermodynamic, kinetic and physical properties, from which much can be learned about adsorption systems. The data obtained can be used to determine:

- Heats of displacement
- Molar heats of displacement
- Adsorbed amounts
- Adsorption rates, rate constants
- Adsorption equilibrium constants
- Equilibrium adsorption capacity

As a pioneer in the field of flow microcalorimetry, A.J. Groszek (1998) provides a review of flow adsorption microcalorimetry, including its history and applications. He describes methods for determining the heat of adsorption and adsorbed amounts simultaneously. Ultraviolet spectrometry or measurement of refractive indices are employed downstream of the calorimeter to measure the effluent concentration of the sorbate in real time. The instantaneous amount adsorbed may be inferred by subtracting the effluent concentration from the known feed concentration. This method is adapted for this work through the collection of discrete effluent samples which are subsequently analyzed in a gas chromatograph (GC). Results are presented by Groszek (1998) illustrating the technique for the reversible adsorption of 10 g/L butanol in water on graphitized carbon black at 25°C and a flow rate of 3mL/h. Groszek accounts for axial diffusion within his system by conducting a control experiment in which his solution is passed over an inert bed of PTFE powder and measuring the effluent concentration as a function of time. Adsorption is then conducted with the desired sorbent and the effluent curve is subtracted from the control curve.

Groszek (1998) further explains methods such as the flow injection adsorption technique (FIAT) for determination of differential heat of adsorption as a function of surface coverage. Using FIAT, small amounts of solution are injected into a stream of flowing carrier liquid and the heat of adsorption is determined for each injection. A downstream detector is again employed to determine the amount of sorbate in the effluent. The amount adsorbed in each

injection is thus calculated allowing the molar heat of adsorption to be determined. Injections are continued until all injected sorbate has passed through the measurement cell. An example of this method is presented by Groszek (1998) for potassium chloroplatinate (K_2PtCl_6) adsorption on graphitized carbon black. Four injections of $0.2 \mu\text{mol } K_2PtCl_6$ resulted in heats of adsorption of 128, 58, 36 and 31 kJ/mol, respectively. Some of his more recent work has focused on determining heats of displacement (Groszek et al., 2005) and the assessment of active surface sites on activated carbon, based on inferences made from flow calorimetry data (Lagerge et al., 1999).

Liquid phase heats of adsorption of thiophenic sulphur compounds on zeolites were first reported by Ng et al. (2005). This work represented a significant advance in the field of both calorimetry and desulfurization, as it introduced a method for verifying predicted heats of adsorption from molecular orbital calculations. This pioneering work was followed by a study of the effect of the parameters of the adsorption system (particularly flow rate and solvent species) on measured heats of adsorption (Jiang and Ng, 2005). One limitation of the work was that molar heats of adsorption were calculated based on equilibrium adsorption capacities; no reliable method existed for simultaneous determination of heat of adsorption and amounts adsorbed.

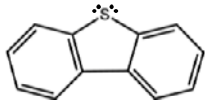
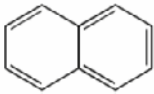
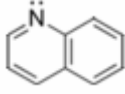
This thesis includes both adaptation of the methods of Groszek (1998) and the development of a new method for simultaneous determination of heats of adsorption and amounts adsorbed.

3 Proposed Work

This study proposes to expand on the results presented by Ng et al (2005) to determine the heat of displacement of refractory sulphur compounds using flow calorimetry. A model solution is used in our experiments in order to simplify the adsorption process so that the relevant information can be obtained. The model solvent was chosen as n-hexadecane (C16), representative of the alkane fraction of diesel fuel. Sorbate molecules were chosen in order to represent sulfur species, aromatics, and nitrogen-containing species to study competitive adsorption behaviour. The specific sulfur, aromatic and nitrogen compounds chosen were DBT, naphthalene and quinoline, respectively. Data on the sorbate molecules are presented in Table 4.

DBT was chosen as the model sulphur containing compound due to its presence as a refractory sulphur compound in diesel fuel. In searching for a sorbent that preferentially adsorbs sulphur-containing compounds, the nature of the heteroatom was expected to play an important role. As such, it was desired to study the adsorption of molecules which were structurally identical to DBT with the exception of the nature of the heteroatom. The ideal model aromatic and nitrogen containing analogues to DBT would thus be fluorene and carbazole. Fluorene and carbazole are identical in structure to DBT, with a CH₂ and N-H group in place of the S atom, respectively. Use of these sorbates was not possible in practice however because some of the properties of fluorene and carbazole (such as solubility) were unsuitable for our purposes. Therefore, discussion of results will consider structural effects on adsorption in addition to effects of the heteroatom.

Table 4. Selected properties of sorbate molecules

	DBT	Naph	Quin
Structure			
Formula	C ₁₂ H ₈ S	C ₁₀ H ₈	C ₉ H ₇ N
MW	184.26	128.17	129.16
D_{crit} (nm)	0.8 ^a	0.719 ^b	0.711 ^c
Relative Acidity	Moderately High	Highest	Lowest

^aJayne et al, 2005

^bSong et al, 1999

^cCorma, 1993

In Table 4, acidity of the sorbate molecules is described in a qualitative manner. Since no pK_a values for DBT could be found in the literature, relative acidity/basicity was used and should therefore be explained.

Naphthalene is the most acidic molecule. This is because the carbanion formed upon proton donation is stabilized by the aromatic nature of the molecule. DBT is slightly less acidic than naphthalene because the presence of the sulphur atom in the thiophenic ring destabilizes the aromatic structure slightly relative to naphthalene. Quinoline is much less acidic than naphthalene due to the presence of the electronegative nitrogen atom in the ring. The electronegative nitrogen atom is a proton acceptor, making it more basic (and therefore less acidic) than naphthalene.

The sorbents chosen for this study were NaY, NiY, and CsY. NaY was chosen as a sorbent for study because it is commercially available and has proven effective for desulfurization of model fuels (Ng et al., 2005 and Hernandez-Maldonado and Yang, 2003a).

To study π -complexation adsorption, NiY zeolite was chosen. Both NiY and Cu(I)Y zeolites have shown promise as desulfurization sorbents in previous work (Jiang and Ng, 2006), NiY is easier to use with the present experimental equipment. Since Cu(I)Y is quickly oxidized in air to form Cu(II)Y which is not capable of forming π -complexes, it is necessary to calcine the sorbent in-situ. Since our apparatus currently does not support in-situ calcination, NiY zeolite was chosen.

Recent work has shown that exchanging the framework sodium ion with an alkali metal cation increases the selectivity for thiophene over toluene (Laborde-Boutet et al., 2006). It is also proposed that using the more basic alkali cations will increase selectivity for sulphur species over nitrogen containing species due to acid-base interactions. It was decided to use CsY which has the highest sulphur selectivity determined by Laborde-Boutet et al. (2006) for our experiments.

4 Experimental Methods

4.1 Reagents and Standards

DBT and quinoline were obtained from Aldrich, and naphthalene was obtained from BDH Laboratories. Hexadecane (anhydrous, 99+%) was obtained from Aldrich. All were used without further purification.

4.2 Modification of NaY Zeolite

NaY zeolite was obtained from STREM Chemicals. Nickel nitrate and cesium nitrate were obtained from Fisher Scientific and Aldrich Chemicals, respectively. Before modification, NaY zeolite was dehydrated in air at 400°C for two hours in an oven. 100 g of 0.1 M solution of the nitrate salt of either Ni or Cs were prepared by dissolving the corresponding salt in deionized water. 3 g of NaY was added to the metal nitrate solution immediately upon removal from the oven. The resulting mixture was stirred at 80°C for 12 h, and then cooled to room temperature. It was then filtered, and the filtrate washed with large amounts (3-4 L) of distilled water. The ion-exchange process was repeated two more times. The filtered solid paste was dried in an oven at 70°C overnight. Finally the powder was pressed, ground and sieved to between 250 and 500 µm particle size.

4.3 Calcination

A zeolite sample was prepared in a clean ceramic crucible with the amount required for the experiment plus about 30% to account for water mass loss, and placed in a furnace set to 400°C. Samples were left in the furnace in an air atmosphere for 90 minutes and removed. Upon removal from the furnace, the sample was placed in the pre-weighed proper vessel (calorimeter cell, vial for shaker bath) as quickly as possible to minimize exposure to humidity in the air. The vessel was weighed again to determine the mass of the zeolite.

4.4 Sorbent Characterization

4.4.1 Elemental Analysis

Samples were sent to Galbraith Laboratories, Inc. in Knoxville, Tennessee for elemental analysis via Inductively Coupled Plasma – Optical Emission Spectroscopy (ICP-OES).

4.4.2 Surface Area

Surface area of the adsorbents was determined by BET nitrogen adsorption. Samples were pretreated at 400°C in a flowing helium atmosphere for three hours. They were cooled to room temperature for analysis in a Micromeritics Gemini instrument.

4.4.3 Structure

XRD analysis was carried out using a Phillips XRD instrument with Ni filtered CuK α radiation. A step size of 0.01 was used from 2 θ angle of 5-40°. Samples were analysed in powder state with no pre-treatment.

4.5 GC Analysis

GC analysis was carried out in a Varian CP-3800 equipped with an autosampler, a VF-5MS column (30 m x 0.32 mm) with a film thickness of 1.0 mm and three detectors: Flame Ionization Detector (FID), Thermionic Specific Detector (TSD) and Pulsed Flame Photometric Detector (PFPD). The FID was kept at a temperature of 300°C, nitrogen specific TSD at 300°C, and sulfur specific PFPD at 200°C.

The initial temperature of the GC oven was 80°C, and after injection it was immediately increased to 250°C at a rate of 10°C/min. It was held at 250°C for 8 min.

Early GC analysis was carried out using a Perkin-Elmer Autosystem GC equipped with FID. The GC was fitted with an HP-5 column (30 m x 0.32 mm). The general method used was an initial oven temperature of 100°C, which was increased at a rate of 10°C/min to 250°C and held there for 2 minutes. When attempting to increase precision, parameters of this method were slightly varied. In addition to changing the GC method, the split ratio and column were also varied at times.

4.6 Equilibrium Adsorption and Adsorption Rate Experiments

Equilibrium adsorption experiments were carried out in a New Brunswick Scientific Gyrotory Water Bath Shaker (Model G 76). About 50 mg of calcined sorbent was loaded into a 20 mL vial containing 10 g of solution. The exact mass of solution and zeolite was measured on a Sartorius balance to 0.0001 g and recorded for subsequent calculations. As a control, an equal amount of solution was placed in another 20 mL vial with no sorbent.

The vials were placed in a shaker bath filled with water at 30°C. The shaker bath was covered and left for 24 h. Sample concentrations were then determined via GC analysis (generally in the Perkin Elmer GC), from which the amount adsorbed was calculated.

In order to increase the precision of the concentrations measured in the Perkin Elmer GC, separate calibrations were run each day the GC was used. Sample calibration curves are presented in Appendix A.

4.7 Heat of Adsorption Experiments

The experimental apparatus for determination of heats of adsorption are presented in Figure 2.

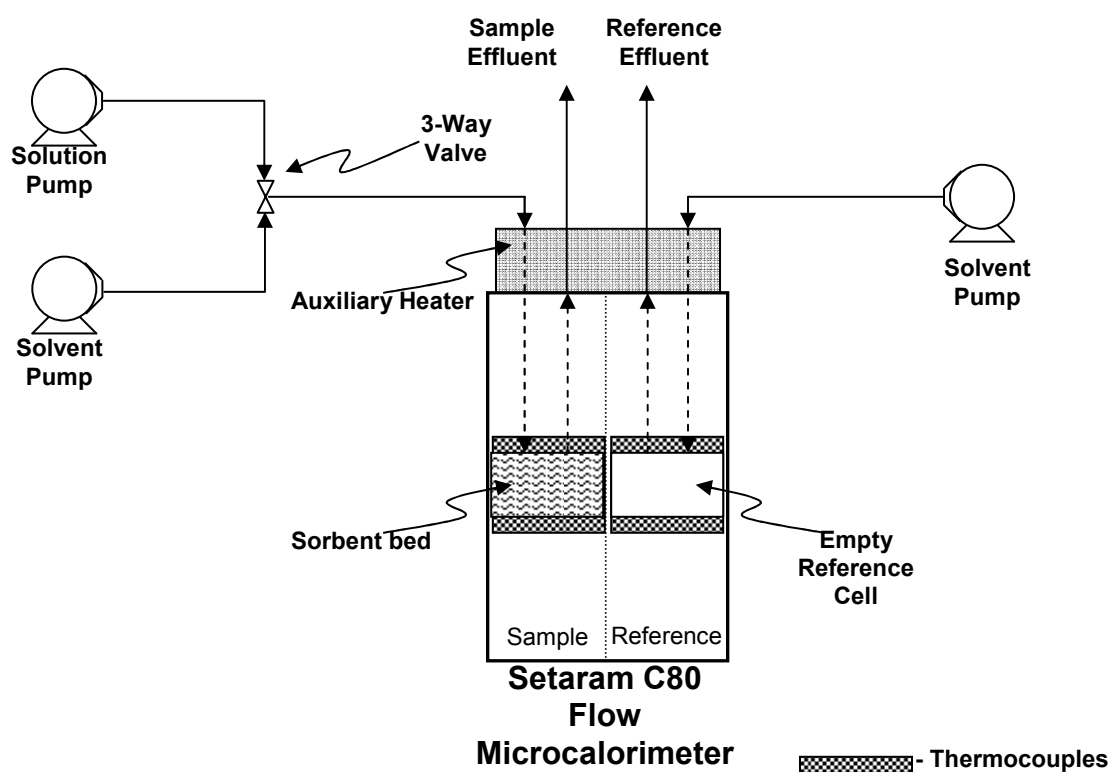


Figure 2. Schematic representation of experimental apparatus

This work was carried out using a Setaram C80 Flow Microcalorimeter with a resolution of 0.10 μW and noise (RMS) of 0.10 μW . The calorimeter was fitted with an auxiliary thermostat for improved temperature control and two 12.5 cm^3 measurement cells; one functioning as a reference and the other as a sample measurement cell. Three Teledyne ISCO D-Series syringe pumps were employed to control solvent flow to the reference side, and solution and solvent flow to the sample side separated by a three way valve.

In flow calorimetry, a solution is passed over a sorbent bed in a measurement cell, and the heat evolved during the adsorption is measured. The calorimeter measures the heat flow based on the Calvet Principle, wherein the sample and reference cells are both surrounded by blocks containing many thermocouples to precisely measure the temperature difference between the cell and the block (Le Parloeur and Mathonat, date unknown). The heat flow is then calculated by the resident software using an electrical calibration which relates the heat flow to the temperature difference based on the Joule effect (Le Parloeur and Mathonat, date unknown).

250 mg of calcined sorbent was loaded into the sample cell, which was placed in the calorimeter. Pure solvent ($n\text{-C}_{16}$) was passed both through the empty reference cell and over the adsorbent bed in the sample cell at a rate of 4.00 mL/h. The calorimeter and auxiliary heater were both set to 30°C to preheat the feed. No sorbent is added to the reference cell to ensure the baseline heat flow is not a function of the sorbent used.

Pure solvent was then passed through the calorimeter until equilibrium was reached. While the system is equilibrating, two separate processes are occurring. First, the sample cell is being heated from room temperature to the experiment temperature (30°C in this work), absorbing large quantities of heat and inducing a large negative heat flow. Simultaneously, solvent molecules are being adsorbed on the zeolite, resulting in a positive heat flow as the exothermic adsorption takes place. When both processes are complete, the heat flow is constant at a value of 0 mW (in theory, but usually slightly above in practice) indicating that a steady state has been reached and the experiment may commence. This process is illustrated in a sample heat flow curve provided in Figure 3. The exothermic heat of adsorption of the pure solvent is not visible in Figure 3 because it is occurring at the same time as the endothermic temperature equilibration within the cell which is much greater in magnitude.

The feed to the sample cell in the calorimeter was then switched to the adsorption solution at the same flow rate via the three way valve, while pure solvent continued to flow through the reference cell at the same flow rate. The standard adsorption solutions used in this work contained 21.8 mmol/L of sorbate in $n\text{-C}_{16}$.

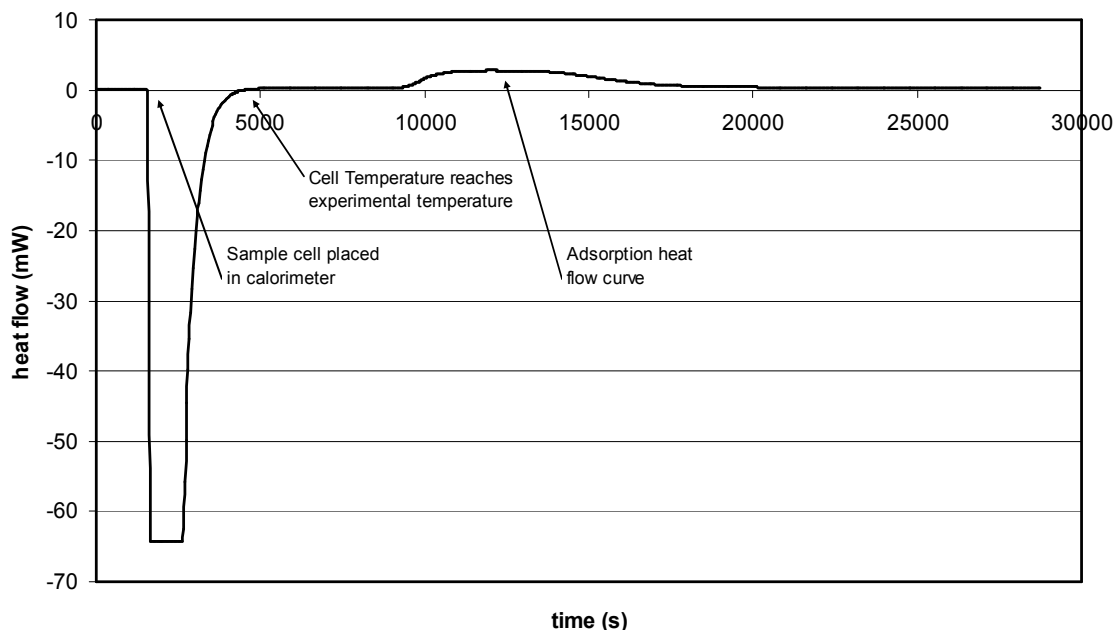


Figure 3. Summary of experimental procedure

As the adsorption solution passed over the sorbent bed, the heat evolved (or absorbed) from the displacement of solvent molecules by solute molecules was measured by the calorimeter.

Samples of the effluent of the calorimeter were collected every 10 to 20 minutes, with the actual time of the sample being recorded. Their concentration was determined via GC analysis as discussed previously, and the breakthrough curve was constructed from these results. Sample calibration curves for the Varian GC are presented in Appendix A. Breakthrough curves were constructed based on effluent samples collected at the calorimeter outlet some time after they have passed through the sample cell. Thus, the breakthrough curve must be shifted in order to compare simultaneous events, i.e., the point on the breakthrough curve coincides with the heat evolved (or absorbed) by that same volume element when it passed through the calorimeter. The breakthrough curve should be shifted backwards by the length of time required for a volume element to travel from the adsorbent bed to the system outlet.

Shifting of the breakthrough curve is done using a simple calculation. The total time required for the liquid to travel from the three-way valve to the system outlet is measured as the time between the start of the experiment and when the first liquid element exits the calorimeter (based on visual observation – typically about 2 h). The length of time for a volume element to travel from the three way valve to the adsorbent bed is the difference between the time that the heat flow curve begins to rise (when the first sorbate molecules begin reaching the bed) and the

time at which the three way valve was switched from pure solvent to the experimental solution (typically about 26 to 30 min). Finally, the time by which the breakthrough curve should be shifted back is the difference between the two times calculated above:

$$t_{shift} = t_{bed\ to\ outlet} - t_{valve\ to\ outlet} + t_{valve\ to\ bed} \quad (11)$$

An example of this calculation may be found in Appendix B.

4.8 Competitive Adsorption Experiments

Competitive adsorption experiments were conducted in much the same manner as described in Section 4.7. In this case, feed solutions were prepared so that the total concentration of the three sorbates (quinoline, DBT and naphthalene) was the specified 21.8 mmol/L.

These solutions were prepared by combining three separate solutions. The solutions contained 21.8 mmol/L DBT, naphthalene and quinoline, respectively. The three solutions were then mixed in a 1:1:1 mass ratio, resulting in a solution with 7.24 mmol/L of each species.

During the experiment, effluent samples were again collected and analysed in the Varian GC. Separate breakthrough curves were generated for each species. Since the heat flow curve in this case was a function of the adsorption of all three species, adsorbed amounts could not be calculated based on the heat flow curve via our new method. Instead, in the case of competitive adsorption experiments, adsorbed amounts were calculated from the breakthrough curves, as discussed in Section 5.1.1.

5 Results and Discussion

5.1 New Method Development

Initially, experiments were carried out using the Setaram C80 flow microcalorimeter and a single peristaltic pump. The reference cell in the calorimeter contained pure solvent and was kept stationary during experiments. A calcined sorbent sample was placed in the calorimeter and pure solvent was passed over it. The following times were noted on a stopwatch for use in later calculations:

- The time at which the pure solvent entered the calorimeter
- The time at which the pure solvent exited the calorimeter
- The time at which the pure solvent reached the outlet of the tubing (the point at which samples were collected)

After baseline heat flow was reached, the inlet end of the tubing was moved from a bottle containing pure solvent to a bottle containing the adsorption solution (generally 1800 ppmw N or S, or the molar equivalent concentration of naphthalene). In doing this, a small air bubble was introduced into the transparent tubing, which allowed tracking of the solvent/solution interface until it reached the calorimeter. The time was recorded at this point. Once the bubble entered the calorimeter, it could no longer be seen and thus the time at which the solution reached the sample point at the outlet had to be calculated based upon the times recorded above.

The heat flow curve for adsorption was then recorded (Figure 4), and the breakthrough curve obtained from effluent samples. Heat of displacement was obtained in J/g, and the heat in kJ/mol was calculated based on the heat per gram of sorbent, and the adsorption capacity from equilibrium isotherms.

Several challenges were initially identified:

- There was no evidence that saturation of the sorbent was achieved within the calorimeter, meaning that the heat of displacement in kJ/mol could not be calculated based on the assumption that the amount adsorbed was equal to the adsorption capacity measured from equilibrium sorption experiments.

- Breakthrough curves were obtained from experiments, but not utilized. Calculation of adsorbed amounts based on the breakthrough curve would eliminate the assumption of equilibrium within the calorimeter.

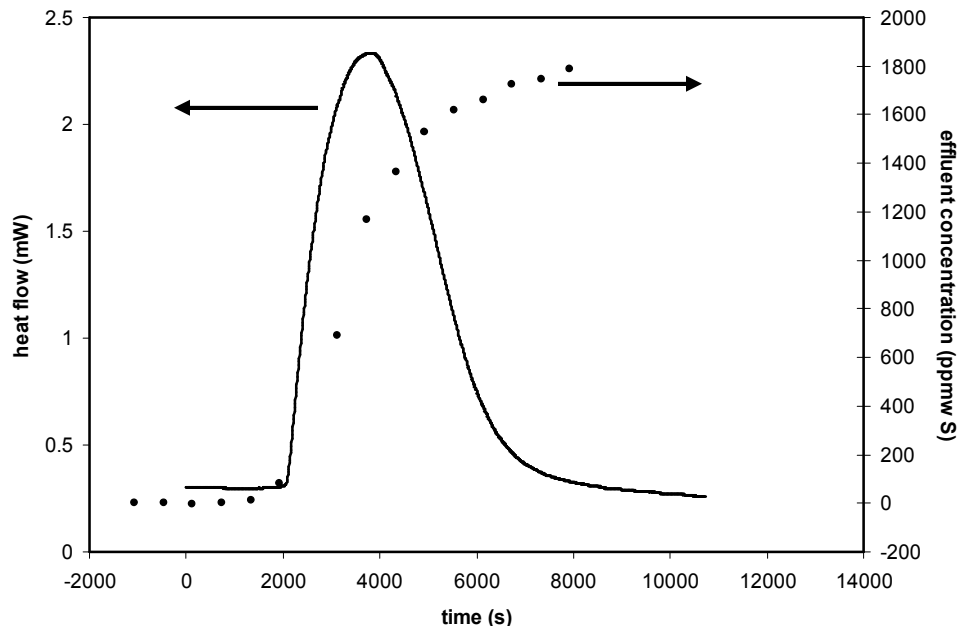


Figure 4. Adsorption of 1800 ppmw S DBT/C16 on NaY at 30°C, 7.6 mL/h (RUNID#28)

A method was subsequently developed to calculate the amount adsorbed from the breakthrough curves.

5.1.1 Breakthrough Curve Calculations

In addition to the heat flow curve, effluent samples are collected from the calorimeter and the sorbate concentration is determined in the GC. The resulting breakthrough curve (effluent concentration as a function of time) is plotted with the heat flow curve. A schematic breakthrough curve is presented in Figure 5.

With a constant flow rate, the amount adsorbed may be calculated from the breakthrough curve by the equation

$$M_{ads} = \frac{\rho F}{MW} \left[C_0 \Delta t_{feed} - \sum C_i \Delta t_i \right] \quad (12)$$

Where :

ρ = solution density ($g mL^{-1}$)

F = flow rate ($mL \cdot h^{-1}$)

MW = species molecular mass

C_o = feed concentration ($mmol L^{-1}$)

Δt_{feed} = length of time feed flows over sorbent bed

C_i = mixing cup concentration over period i ($mmol L^{-1}$)

Δt_i = length of period i

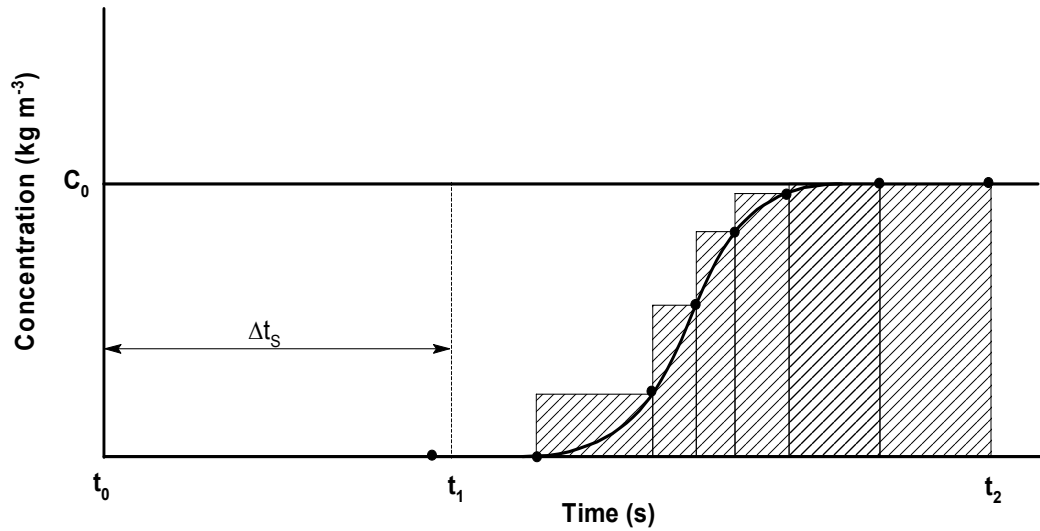


Figure 5. Schematic representation of breakthrough curve for calculations

The term $C_i \Delta t_i$ represents the shaded areas as shown in Figure 5. The sum of the areas of the shaded regions are used rather than integration under the smooth breakthrough curve because the concentration of each effluent sample represents the average concentration over the previous interval rather than an instantaneous effluent concentration.

Since the breakthrough curve presents the effluent concentration (*ie.* The amount *not* adsorbed) as a function of time, it can be used to calculate the rate of adsorption:

$$r(mm\text{ol} / s) = \frac{C_{in}(mm\text{ol} / mL) - C_{out}(mm\text{ol} / mL)}{\Delta t(s)} \quad (13)$$

This relationship is limited in that it can only provide the average adsorption rate over the time period Δt , which is usually relatively large (10-30 min). Instantaneous adsorption

rates may be calculated based on the instantaneous effluent concentration estimated by fitting a breakthrough curve to the data points although no work has been conducted by this group to assess the reliability of this method. One additional limitation of calculations based on this formula is that they do not account for axial diffusion within the calorimeter. Between the time when a volume element reaches the sorbent bed and when it exits the calorimeter, its concentration may change due to diffusion within the tubing in addition to adsorption onto zeolite. This would mean that the concentration exiting the calorimeter is not necessarily equivalent to the concentration of that volume element when it was passing through the sorbent bed.

Based on this new calculation method, amounts adsorbed could be calculated from breakthrough curves. It was no longer necessary to assume that equilibrium was reached within the calorimeter to estimate the amount adsorbed. Further, this independent method of calculating the amount adsorbed could be compared with equilibrium isotherms to determine if, in fact, equilibrium was being reached within the calorimeter. Table 5 provides a summary of the experimental data obtained from Figure 4, as well as three additional experiments studying the same system.

Table 5. Summary of Early Adsorption Experiments – 1800ppmw S DBT/C₁₆ on NaY at 30°C

Date	Run ID#	Flow Rate (mL/h)	Capacity (mmol/g)	Heat of Adsorption	
				(J/g)	(kJ/mol)
6/20/2005	28	7.6	0.9	23.24	25.86
6/22/2005	29	5.8	1.04	26.12	25.03
6/23/2005	30	5.9	1.33	26.84	20.17
6/24/2005	31	6	1.03	26.15	25.36
Average		6.33	1.08	25.59	24.11
Std. Dev		0.85	0.18	1.60	2.65

Experimental data sheets used to generate Figure 4 and Table 5 may be found in Appendix E.

There were several other problems with the experimental procedure:

- Amounts obtained via the breakthrough curve appeared to be highly variable (See Table 5). The average amount adsorbed over several experiments seemed to be roughly equal to the adsorption capacity as determined by equilibrium isotherms, although the variation between experiments was in some cases up to 50%.
- Calculation of the exit time of the solvent/solution interface was based on the assumption that the flow rate remained constant over the course of an experiment. Occasional flow

rate measurements showed that this was not the case. The silicone tubing used in the peristaltic pump swelled over the course of an experiment, resulting in a progressive increase in flow rate. A reliable flow rate was required in order to calculate adsorbed amounts using the breakthrough curve.

- In order to study adsorption at elevated temperatures, control of the temperature of the feed solution was required.
- Experiments should be conducted with the respective liquids flowing through both the sample and reference side of the calorimeter in order to eliminate any possible effects of flow on the heat flow curve.

In order to study the effect of temperature on adsorption, an auxiliary pre-heater accessory for the calorimeter was purchased from Setaram. This pre-heater allowed for experiments at temperatures up to 270°C, although it was not used in this study.

New tubing for the peristaltic pump was purchased. Investigations revealed that the choices of tubing which was resistant to the chemicals used, but pliable enough to operate in our peristaltic pump were limited. Fluran tubing was eventually chosen since it had the highest resistance to the sulfur species. Flow measurements were extremely promising. Although the flow rate changed from day to day due to slight differences in length of tubing cut for the pump, the flow rate was extremely stable over the course of a single experiment.

Since it was not possible to set a precise flow rate, it was not possible to provide flow in both the sample and reference sides of the calorimeter. In order for this to work, flow rates had to be both *constant* and *equal*.

Over the course of several experiments, more issues became apparent:

- Although flow rate was kept constant, adsorbed amounts obtained via the breakthrough curve remained highly variable. The average amount adsorbed over several experiments seemed to be roughly equal to the adsorption capacity as determined by equilibrium isotherms, although the variability between experiments was in some cases greater than 20%.
- The air bubble introduced into the system was not an ideal method of tracking the solvent/solution interface between the feed bottle and the calorimeter. Upon reaching the

sorbent bed, moisture in the air would be strongly adsorbed potentially affecting results. Additionally, provided a reliable flow rate was maintained, the air bubble would be unnecessary for predicting the location of the interface. The experimental set-up made it nearly impossible to eliminate the bubble since the feed tubing had to be physically moved from one bottle to another.

- Solutions being fed to the calorimeter were still exposed to the atmosphere. Two major concerns were the possibility of evaporation changing the solution concentration over time, and absorption of moisture by the solution over time. It was hypothesized that the former may be, at least in part, responsible for the variability in adsorbed amount calculations.
- Experiments at elevated temperatures exhibited a pronounced shift in baseline heat flow before and after adsorption took place. The cause of this baseline shift was initially unknown.
- A method of matching flow between reference and sample sides of the calorimeter was still required

In order to address several issues at one time, three high precision Teledyne ISCO syringe pumps were purchased. These pumps provided the following benefits over the peristaltic pumps:

- Flow rates could be matched, so that flow could be provided on both the sample and reference sides of the calorimeter at equal flow rates
- The pumps were fully enclosed meaning that the solutions were not exposed to the atmosphere, and thus would not absorb moisture from the atmosphere.
- A valve was purchased to switch between the solvent pump and the solution pump, preventing air from being introduced when switching during experiments.
- The pumps provided a wide range of flow rates, so that experiments could be conducted at both higher and lower rates than possible with the peristaltic pumps

With the ability to provide precise flow in the reference cell, work was done to determine the optimal reference cell configuration. This included matters such as whether the reference cell

should contain any sorbent, whether it should be stationary or provide flow and whether it should contain pure solvent or the analyte solution were examined.

With the addition of the high precision syringe pumps to our experimental apparatus, our group was given the opportunity to provide flow in both the reference and sample cells. It was found that matching flow rates in both cells lowered the equilibrium baseline heat flow slightly compared to a stationary reference cell. This was because the reference cell could better mimic heat flow characteristics due to both flow and heating of feed solution.

Initially, it was believed that the reference cell should contain a 250 mg sorbent sample similar to the sample cell, although the zeolite in the reference cell should not be changed daily. This would allow the flow conditions in the sample cell to be mimicked by the reference cell without any adsorption taking place (since it would contain already saturated sorbent). Initially, this method seemed to work, resulting in a flat baseline slightly above 0 mW before the adsorption took place. Gradually, over the course of several experiments, it was found that this baseline decreased to a negative value. Examination of the sorbent showed that over time, the sorbent was degrading into fine particles, which was affecting the flow through the bed relative to that of fresh sorbent. It was therefore decided that placing sorbent in the reference cell was not advantageous.

Based on the above observations, it was decided that the optimum configuration of the reference cell would be an empty cell with a flow rate equal to that of the sample cell. The liquid flowing through the reference side of the calorimeter should be pure solvent. Pure solvent was chosen over analyte solution simply for ease of use. Since the same solvent was used in all experiments, it was not necessary to clean the reference pump (a time consuming exercise) whenever the analyte solution was changed.

Although the syringe pumps provided several improvements over the peristaltic pumps, it was found that variability in the calculated adsorbed amount still existed. The heats measured per unit mass of sorbent were relatively constant, suggesting that the variability was due to our estimation of the amount adsorbed and not necessarily indicative of the actual variability in the quantity.

Calculation of the amount adsorbed (Equation 12) depends mostly on the length of each sampling period and the concentration measured therein. Since the lengths of the sample periods were measured to within 1-2 seconds over an interval of over 10 minutes, it seemed likely that variability was due to the measured effluent concentrations.

Initial work was carried out using a Perkin Elmer Autosystem Gas Chromatograph (GC). Investigations examining the use of our GC were conducted in an attempt to increase precision in measurements of effluent concentration. The effect of the GC components was examined, including the use of different syringes/injection volumes and GC columns. Techniques such as multiple injections, altering split ratio and increasing the number of calibration standards showed negligible improvement in precision. Similarly, different calibration techniques such as the use of internal standards made little difference. It was decided that the best method available to determine the amount adsorbed was to perform several experiments and use the average adsorbed amount estimated via the breakthrough curve.

It was decided to lower the concentration of the feed solution from 1800 ppmw S (43.5 mM) to 900 ppmw S (21.8 mM) for several reasons. First, the lower concentration would allow the split ratio of the GC to be decreased, presumably offering more precision in measured concentrations and therefore the estimate of the adsorbed amount. Second, since the heat capacity of the solution changes with the concentration, a dilute solution would have a closer heat capacity to pure solvent than a concentrated solution would, thereby reducing the observed baseline shift. Finally, the lower concentration of sulfur would be more indicative of actual fuel sulfur concentrations, which are generally about 500 ppmw S. An interesting observation followed from experiments using the lower sulfur concentration.

It was noted that when studying adsorption using low flow rates (4.00 mL/h) and low feed concentrations (21.8 mM) the heat flow curve exhibited a plateau (Figure 6). In order to understand the significance of this result, it is useful to examine the heat flow curve in detail to determine what information may be extracted.

5.1.2 Heat Flow Curve Analysis

The output of the calorimeter is the instantaneous heat flow (in mW) as a function of time. We call this instantaneous heat flow $Q(t)$. The heat flow curve can be broken into five distinct phases, as shown in Figure 6. The phases are described briefly and will be discussed in more detail, along with the relevant mathematical description later.

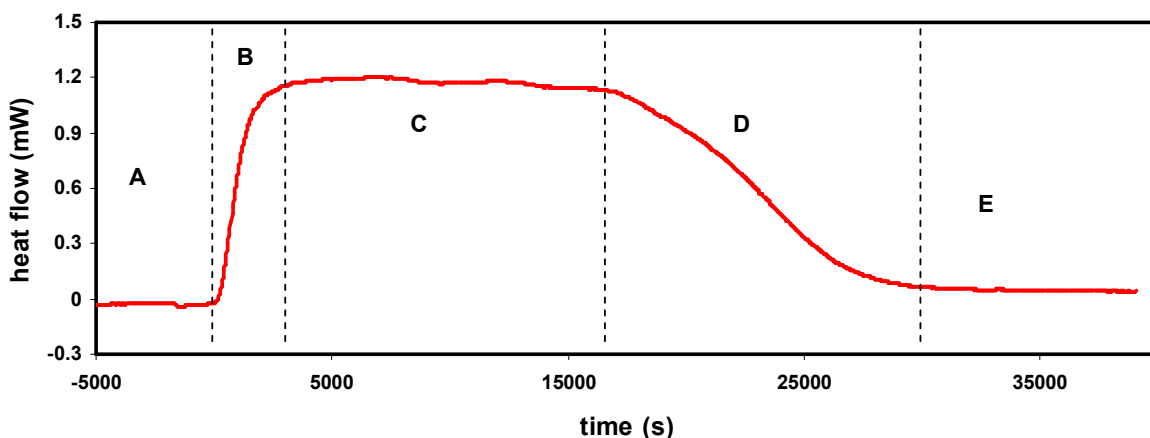


Figure 6. General heat flow curve exhibiting five distinct adsorption phases

Phase A is defined as the ‘solvent flow phase’. It is characterized by a constant heat flow of 0 mW, and represents a time when only pure solvent is flowing over the adsorbent bed.

During phase B the initial adsorption takes place. This region of the heat flow curve takes the form of a sigmoid curve. The reason for this is thought to be axial diffusion in the tubing. This will be discussed in more detail later.

Phase C is the steady state adsorption region. It occurs when the heat flow curve reaches its peak and remains relatively constant for a period of time. This plateau region corresponds to complete adsorption of the feed solution, as seen with comparison to GC data.

Phase D is the breakthrough region of the heat flow curve. During this phase, the heat flow drops as a function of time as the adsorbent bed becomes saturated and the rate of adsorption decreases. Some of the decrease in heat flow may also be attributed to decreasing differential heat of adsorption due to increasing surface coverage.

Finally, phase E is called the equilibrium phase. During this phase, the heat flow curve has returned to its initial value and remains constant as adsorption no longer occurs. The equilibrium phase is indicative of a saturated sorbent.

General Heat Flow Curve Equations

The basis for our adsorption experiments is that the integral heat flow is proportional to the amount adsorbed, i.e.,

$$\Delta H = G \cdot q \quad (14)$$

where :

ΔH = heat evolved (J / g)

G = proportionality constant (J / mmol)

q = zeolite loading (mmol / g)

In actuality, this proportionality constant G is the heat per mole adsorbed, but it is left as G in this derivation for simplicity. The heat evolved is calculated by integrating the heat flow curve.

$$\Delta H(J / g) = \frac{1}{M_z} \int_0^t Q(t) dt = G \cdot q \quad (15)$$

where :

M_z = zeolite mass (g)

By differentiating equation (15) with respect to time, we obtain

$$Q(t) = G \cdot M_z \frac{dq}{dt} \quad (16)$$

Equation 16 indicates that the instantaneous heat flow at any point on the heat flow curve is proportional to the rate of adsorption at that point.

It is assumed in equation (16) that G (the heat evolved per mole adsorbed) is constant. It is known that in some cases this heat varies as a function of coverage. Equation (16) applies to most cases where we have found that differential heat of adsorption is for the most part independent of coverage. This assumption likely applies to situations such as chemisorption and π -complexation where adsorption is site specific and stronger than physical adsorption and site specific, such that interaction between surface sorbate molecules plays only a minor role.

Although little work has been done on this to date, it would seem that in cases where the heat is a function of coverage a relationship describing $G(q)$ could be determined and substituted into equations (14-16). For our purposes, however, we maintain G as a constant.

To take our derivation one step further, we will differentiate equation (16) with respect to time.

$$\frac{dQ(t)}{dt} = M_z G \frac{d^2 q}{dt^2} \quad (17)$$

This states simply that the slope of the heat flow curve is proportional to the rate of change of the adsorption *rate*.

Solvent Flow Phase

During the solvent flow phase, the heat flow curve is flat at a value of 0 mW. That is $dQ(t)/dt = 0$ and $Q(t) = 0$. Using equations 13 and 14 we can therefore infer that the rate of adsorption is constant at 0 mmol/s. This is no surprise, considering that no sorbate is being fed to the calorimeter in this phase. An important thing to note at this point is that the region is not species specific and so there is no adsorption of solute or solvent molecules. Thus, when this condition is reached, adsorption of solvent molecules is complete and the feed may be switched to the required solution.

Initial Adsorption Phase

The initial adsorption phase exhibits a sigmoidal shape before reaching the plateau value. Previous experiments in which heat flow and breakthrough curves were obtained simultaneously have shown that no sorbate molecules exit the calorimeter during this phase, and therefore all sorbate molecules fed are being adsorbed. It is believed that this sigmoidal shape is due to a concentration gradient caused by axial diffusion in the tubing between the three-way valve and the sorbent bed.

The rigorous mathematics needed to describe and model the diffusion process are beyond the scope of this thesis. The width of this axial concentration profile (region B in Figure 6) is slightly over 40 minutes, and is expected to depend on flow rate.

Steady State Phase

During the steady state phase, the heat flow curve is flat at the peak heat flow value. That is $dQ(t)/dt = 0$ and $Q(t) = Q_{\max}$. We can therefore say that the rate of adsorption is constant and equal to the rate at which adsorbate is being fed to the calorimeter. This assumption has been verified by comparison of breakthrough and heat flow curves.

During this phase, we can examine the validity of our main assumption. That assumption is that the differential heat is independent of coverage. During the steady state phase the rate of adsorption remains constant (this has been verified by comparison of heat flow and breakthrough curves – See Appendix E). Therefore, if the differential heat is independent of coverage, the heat flow curve will remain flat as surface coverage increases. If the heat flow curve gradually falls off during this phase of adsorption, it can be inferred that the differential heat is gradually decreasing as coverage is increasing. Such a phenomenon would likely be indicative of a weaker physical adsorption mechanism such as pore filling.

Breakthrough Phase

One of the most important phases in the adsorption process is the breakthrough phase. Traditionally a breakthrough curve was constructed based on the analysis of calorimeter effluent samples, however recent developments (specifically the use of equation 11) have allowed for the calculation of a pseudo-breakthrough curve based on the heat flow curve. A general model called Richards' Curve (Richards, 1959) can be fit empirically to breakthrough data to obtain some useful parameters. The equation and explanation of the physical meaning of the parameters are presented here:

$$C(t) = C_0 + \frac{C_f}{\left[1 + Te^{-B(t-2M)}\right]^{1/T}} \quad (18)$$

where :

C_0 = initial concentration

C_f = final concentration

M =time of max growth

B = growth rate

T = parameter affecting when max growth occurs

C_0 is zero since by definition there is no sorbate present in the effluent before breakthrough. C_f would be equal to the feed concentration is set by the experimenter.

The time of maximum growth is basically the ‘center’ of the breakthrough curve. It is the inflection point at which the rate of adsorption stops increasing and begins to slow. In mathematical terms, the time M is defined as the time at which $d^2C/dt^2 = 0$.

The growth rate B is the parameter which defines the ‘sharpness’ of the breakthrough curve. As B increases, the breakthrough curve sharpens. A sharper breakthrough curve is desirable in an adsorption process, because it indicates more complete bed usage. In physical terms, a sharp breakthrough curve means that saturation of the bed occurs soon after breakthrough, such that the amount of unused sorbent at breakthrough is minimized.

The physical meaning of the parameter T is more difficult to describe, although it is equally important in characterizing the breakthrough curve. Changing the value of T affects where maximum growth occurs. In other words, if T is large, the initial portion of the breakthrough curve will be elongated. This concept is easier to understand with a visual representation as shown in Figure 7.

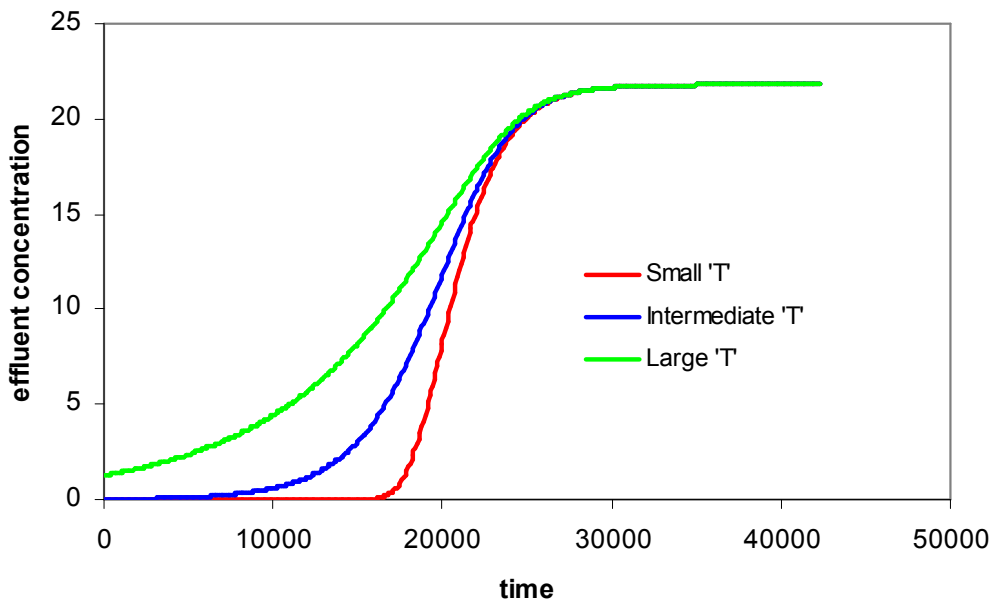


Figure 7. Effect of varying the ‘ T ’ parameter in the general breakthrough model

Figure 7 makes it easier to see the physical significance of the parameter T . The breakthrough curve with the intermediate ‘ T ’ value is roughly symmetrical. A large ‘ T ’ value leads to an elongated initial portion.

In some adsorption processes, the effluent concentration reaches a value very close to the feed concentration, indicating that the bed has become nearly saturated, but actual saturation does not occur until some time after due to diffusion resistance within the pores of the adsorbent. This has been observed in our lab in some samples where disruption of the crystalline structure affects internal diffusion (and therefore adsorption), but not adsorption on surface sites. In such cases, a small T value would be appropriate to elongate the final portion of the breakthrough curve relative to the initial portion. An example of this is shown later (Figure 22) in the case of quinoline adsorption on CsY.

Fitting equation (18) to the breakthrough data or the calculated pseudo-breakthrough data would allow for quantitative comparison of breakthrough curves. Knowledge of the physical significance of these parameters is useful for optimizing the adsorption processes.

Equilibrium Region

In the equilibrium region, as in phase A, the heat flow curve is flat and equal to zero indicating that the rate of adsorption is constant at zero. In practice, the equilibrium heat flow in this region is not quite zero (it is usually slightly negative but occasionally slightly positive). Further, experience has shown that the magnitude of the baseline shift increases with temperature. There seem to be two factors contributing to this phenomenon, one of which is easily corrected in most cases. An example is provided in Figure 8.

The first cause of the baseline shift (and the easiest to correct) is switching the calorimeter feed to the solution too soon, before solvent adsorption has reached equilibrium. This phenomenon is simple to visualize based on the following explanation. We have shown previously that if no adsorption is occurring, the heat flow will be zero (Equation 16). Thus if equilibrium is incorrectly assumed and adsorption begins, the baseline value set as zero will be in fact slightly higher than that value corresponding to no adsorption. Thus, the final baseline when the adsorption rate actually is zero will appear to be slightly below the initial baseline.

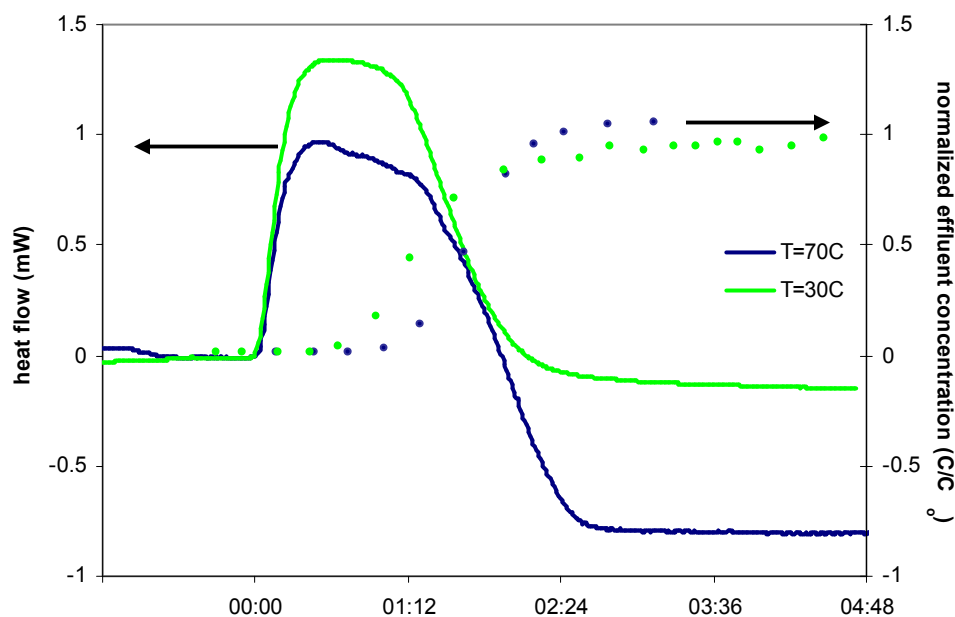


Figure 8. Baseline shift for adsorption of 1800 ppmw S (DBT/C₁₆) on NaY at 4.00 ml/h

Knowing when equilibrium is actually reached comes with experience. In order to be certain equilibrium is reached, without the benefit of experience, allowing several hours for equilibration is advised. If possible, the system should be allowed to equilibrate overnight. In some cases (with modified Y-zeolites for example), this is not a practical option. When the crystalline structure of the zeolite is altered, diffusion is severely limited and thus equilibrium is reached very slowly. Similarly, displacement of the solvent molecules occurs extremely slowly and the resultant heat flow is not easily detectable. In these cases, adsorption should be started early even though equilibrium has not been reached. In this case, the small baseline shift is considered the ‘lesser of two evils’, so to speak.

The second reason is more difficult to compensate. To understand the phenomenon, we must visualize the calorimeter in two separate parts: the pre-heater and the measurement cell. The pre-heater is a large heating block through which the solution flows. Due to its size, the pre-heater is considered to provide a constant heat flow.

The total heat absorbed by the fluid over a given time is given as

$$Q = mC_p\Delta T \quad (19)$$

Where :

Q = *heat flow rate*

m = *fluid mass flow rate*

C_p = *fluid heat capacity*

We can see that, according to equation 19, if the heat flow is constant then the change in temperature will be inversely proportional to the solution flow rate and heat capacity. Since our experiments all operate at the same flow rate (4.00 mL/h), we can say that a fluid with a lower heat capacity will be heated to a higher temperature in the pre-heater.

Looking now at the measurement cell of the calorimeter, we refer again to equation 19. This time, however, the rate of heat flow is not constant: it is proportional to the difference in temperature between the solution and the calorimeter. Thus, the solution with the lower heat capacity (and therefore the higher temperature entering the cell) will have a lower baseline heat flow than the higher heat capacity solution. Therefore, the baseline before adsorption (when pure solvent is flowing through the measurement cell) will have a different value than the baseline after adsorption (when adsorption solution is flowing through the cell). This explains why the magnitude of the baseline shift is greater at elevated temperatures, as seen in Figure 8.

It can now be seen why this is a more difficult situation to correct for than the first cause of baseline shift. This phenomenon is the result of the fundamental properties of the fluids used rather than the experimental technique. The only way to ensure that the baseline heat flow is the same before and after adsorption is to ensure that both solutions are at the same temperature when they enter the measurement cell. This can be accomplished two ways:

- i. Easing the load on the pre-heater. Using lower flow rates, for example, would increase the residence time in the pre-heater giving it more time to heat the feed solutions to the required temperature. This is not an ideal option because it would increase the length of time required to complete an experiment. Additionally, it would make it difficult to compare historical results obtained at 4.00 mL/h flow rate with newer results at the new flow rate.

- ii. Improved temperature control. Heating the solutions to the required temperature before they enter the calorimeter pre-heater eliminates reliance on the pre-heater which has proved insufficient for the task.

Since the current temperature difference between the feed and the calorimeter is small (roughly 8°C), the magnitude of the baseline shift is also small. Immediate steps to correct this shift, then, are not necessary. In the future, when adsorption at higher temperatures is to be studied, regulation of feed temperature will likely be a necessity.

A significant amount of information can be obtained from the heat flow curves. Quantitative information such as the total heat evolved per gram of sorbent, the total heat per mole of sorbate, and the amount adsorbed can be obtained. As will be discussed in the next section, heat flow is proportional to the rate of adsorption, assuming the differential heat of adsorption is constant. Thus, kinetic data may also be obtained such as the rate of adsorption allowing for calculation of the theoretical breakthrough curve. Finally, curve fitting equation 18 to this breakthrough data can allow for quantitative comparison of the parameters in that equation.

As stated in Section 5.1.2, the plateau of the heat flow curve corresponds to adsorption of all sorbate molecules fed to the calorimeter. This is supported by the breakthrough curve in Figure 9, where it can be seen that at the time when the plateau is observed, no solute is exiting the calorimeter, indicating complete adsorption.

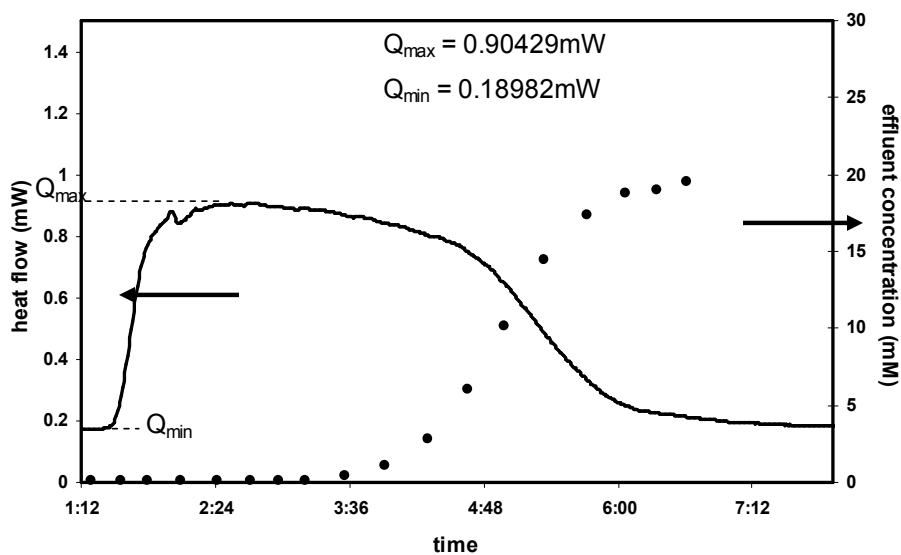


Figure 9. Adsorption of 21.8 mM DBT on NaY at 30°C and 4.00 mL/h.

In the plateau region, both the instantaneous heat flow (the height of the heat flow curve) and the instantaneous rate of adsorption (based on the rate of sorbate feed) are known. The heat per mole adsorbed can thus be calculated from the following dimensional equation:

$$\Delta H_{ADS} (mJ / mmol) = \frac{Q(mW)}{r(mmol / s)} \quad (19)$$

where :

ΔH_{ADS} = heat of adsorption

Q = rate of heat flow

r = rate of adsorption

The value of Q is determined simply as the maximum height of the heat flow curve relative to the initial heat flow. As previously stated, when complete adsorption of the feed is known to be occurring, the instantaneous rate of adsorption is equal to the rate of sorbate feed. Therefore, (19) can be rewritten as:

$$\Delta H_{ADS} \left(\frac{kJ}{mol} \right) = \frac{Q(mW)}{C \left(\frac{mmol}{L} \right) \cdot F \left(\frac{mL}{h} \right)} \left(\frac{1mJ}{mW \cdot s} \right) \left(\frac{10^3 mL}{L} \right) \left(\frac{3600s}{h} \right) \left(\frac{kJ}{10^6 mJ} \right) \left(\frac{10^3 mmol}{mol} \right) \quad (20)$$

Grouping all conversion factors gives:

$$\Delta H_{ADS} (kJ / mol) = 3600 \cdot \frac{Q(mW)}{C(mmol / L) \cdot F(mL / h)} \quad (21)$$

The integral heat of adsorption can be determined using equation (15). Integration under the heat flow curve yields the total heat of adsorption. Dividing this heat by the known sorbent mass gives the integral heat in J/g. Thus, our method allows us to determine independently the heat evolved per unit mass of sorbent, and per mole sorbate.

Since the parameters are independent, they can be used to calculate the amount adsorbed simply by taking the ratio of the two heats:

$$q(mmol / g) = \frac{\Delta H_{ads} (J / g)}{\Delta H_{ads} (kJ / mol)} \left(\frac{kJ}{10^3 J} \right) \left(\frac{10^3 mmol}{mol} \right) = \frac{\Delta H_{ads} (J / g)}{\Delta H_{ads} (kJ / mol)} \quad (22)$$

Substituting (15) into (23), we obtain:

$$q(\text{mmol} / \text{g}) = \frac{1}{M_z} \frac{\int_0^t Q(t) dt}{\Delta H_{ads} (\text{kJ} / \text{mol})} \quad (23)$$

The above formulae are based on several assumptions which must be stated:

- i. Differential heat of adsorption is independent of coverage. This assumption is believed to be reasonable since the calculation is performed at an early stage of the adsorption process corresponding to low surface coverage.
- ii. The baseline heat flow is constant, meaning no baseline shift occurs.
- iii. The peak heat flow corresponds to complete adsorption.

There are several benefits that this method has over those previously employed:

- Calculations are independent of equilibrium conditions.
- Heats of adsorption and amounts adsorbed are expected to be independent of flow rate and feed concentrations, meaning conditions can be altered in order to induce a plateau in the heat flow curve, and the results still comparable to other experiments conducted at different feed concentrations / flow rates. More data are required to verify this hypothesis.
- Results do not depend on additional instrumentation, such as a GC or other downstream concentration detectors. This reduces the cost and time required to complete experiments.

Although this method does not rely on the breakthrough curve, our work still includes collection and analysis of effluent samples. This is because our novel method is still in its infancy, and until further verification of the method is conducted, the breakthrough curves serve as an additional source of data for comparison.

5.2 Method Verification

A major benefit of this novel calculation method is that the no additional data are required. Thus, the calculations can be performed on previous experimental data sets (Appendix E) and compared

to assess the quality of the method. Such calculations were performed to give the results shown in Table 6.

In Table 6, ‘New Method’ refers to the new technique, where the molar heat of adsorption is calculated based on the height of the heat flow curve and the rate of feed of sorbate to the calorimeter (Eq. 22). ‘Old Method’ refers to the method of dividing the integral heat of adsorption (Eq. 15) by the amount adsorbed based on breakthrough curve calculations (Eq. 12).

Table 6. Comparison of heat of adsorption results between methods

		Run ID#s	ΔH_{ads} (kJ/mol)			
			New Method <i>(Average \pm St. Dev)</i>		Old Method <i>(Average \pm St. Dev)</i>	
Quin/C ₁₆	NaY	1,2,3	63.1	\pm 2.6	55.1	\pm 5.9
Quin/C ₁₆	NiY	4,5	97.3	\pm 5.2	103.2	\pm 8.3
Quin/C ₁₆	CsY	6,7	44.8	\pm 0.1	53.6	\pm 4.5
DBT/C ₁₆	NaY	9,13	29.5	\pm 0.05	31.7	\pm 4.3
DBT/C ₁₆	NiY	11,12	33.2	\pm 0.5	31.9	\pm 3.4
DBT/C ₁₆	CsY	8,10,14	25.0	\pm 0.5	46.4	\pm 29.8
Naph/C ₁₆ *	NaY	15,16	20.6	\pm 0.4	21.9	\pm -
Naph/C ₁₆ *	NiY	17,18	26.1	\pm 1.5	-	\pm -
Naph/C ₁₆ *	CsY	19,20	24.2	\pm 0.9	-	\pm -

*Calculations could not be performed utilizing the Old Method due to the lack of breakthrough curve data

The data presented in Table 6 were all calculated from either two or three experiments. In each case the numbers presented are the average heat from the experiments and the variability is the standard deviation calculated for that set. Although it is noted that a standard deviation calculated from only two values is unreliable at best, it is striking that in each of the 6 sets of experiments the standard deviation calculated from the new method is lower than that calculated from the old method.

In calculations using the breakthrough curve, the heats of adsorption for quinoline in C₁₆ were 55.1 \pm 5.9 kJ/mol on NaY and 53.6 \pm 4.5 kJ/mol on CsY. Thus, it is not possible to say whether the heat is higher on NaY or CsY. From calculations based on instantaneous heat flow, however, these values become 63.1 \pm 2.6 kJ/mol and 44.8 \pm 0.1 kJ/mol, respectively, showing that the heat of displacement on NaY is higher than that on CsY.

A similar comparison was performed on the amounts adsorbed, and is presented in Table 7.

Table 7. Comparison of amount adsorbed results between methods

		Run ID#s	q_m mmol/g					
			New Method			Old Method		
			<i>(Average \pm St. Dev)</i>			<i>(Average \pm St. Dev)</i>		
Quin/C ₁₆	NaY	1,2,3	0.93	\pm	0.07	1.06	\pm	0.09
Quin/C ₁₆	NiY	4,5	0.63	\pm	0.03	0.59	\pm	0.05
Quin/C ₁₆	CsY	6,7	0.40	\pm	0.01	0.34	\pm	0.04
DBT/C ₁₆	NaY	9,13	1.16	\pm	0.08	1.10	\pm	0.22
DBT/C ₁₆	NiY	11,12	0.94	\pm	0.003	0.98	\pm	0.12
DBT/C ₁₆	CsY	8,10,14	0.36	\pm	0.04	0.25	\pm	0.14
Naph/C ₁₆	NaY	15,16	1.86	\pm	0.01	1.77	\pm	-
Naph/C ₁₆	NiY	17,18	0.85	\pm	0.07	-	\pm	-
Naph/C ₁₆	CsY	19,20	1.26	\pm	0.04	-	\pm	-

*Calculations could not be performed utilizing the Old Method due to the lack of breakthrough curve data

In Table 7, ‘New Method’ refers to the calculation of the amount adsorbed by our new method (Eq. 24). The ‘Old Method’ Refers to the calculation of the amount adsorbed based on the breakthrough curve (Eq. 12)

Once again the results are striking. In all 6 experiment sets, the variability is lower using the new calculation than the old. These results seem to indicate that the method of calculation using the instantaneous heat flow is much more consistent and repeatable than those using the breakthrough or equilibrium loadings.

5.2.1 Effect of Feed Concentration

Experiments were carried out varying the feed concentration to assess its effect on the heat of adsorption. A summary of the experimental results is provided in Figure 10.

Upon inspection of the figure, some sources of error become immediately apparent. First, there is a pronounced downward spike in the heat flow for the 43.5 mmol/L solution. These experiments were carried out early on in the development of our experimental procedure, when the operation of all equipment was not yet completely understood. It is believed that during the cleaning of the instrumentation, an air bubble was introduced into the system which, upon reaching the measurement cell of the calorimeter, created a brief period with a reduced amount of adsorption and thus reduced measured heat. This phenomenon was eliminated in subsequent experiments through revision of pump cleaning procedures.

A summary of the heat of adsorption results from the above experiments is presented in Table 8.

Table 8. Summary of heats of adsorption measured at different feed concentrations

Concentration (mmol/L)	Height (mW)	ΔH_{ads}^* (kJ/mol)
43.5	1.23092	25.5
10.9	0.29134	24.1
6.0	0.18764	28.0

*Experiments using DBT/C₁₆ on NaY at 4.00 mL/h

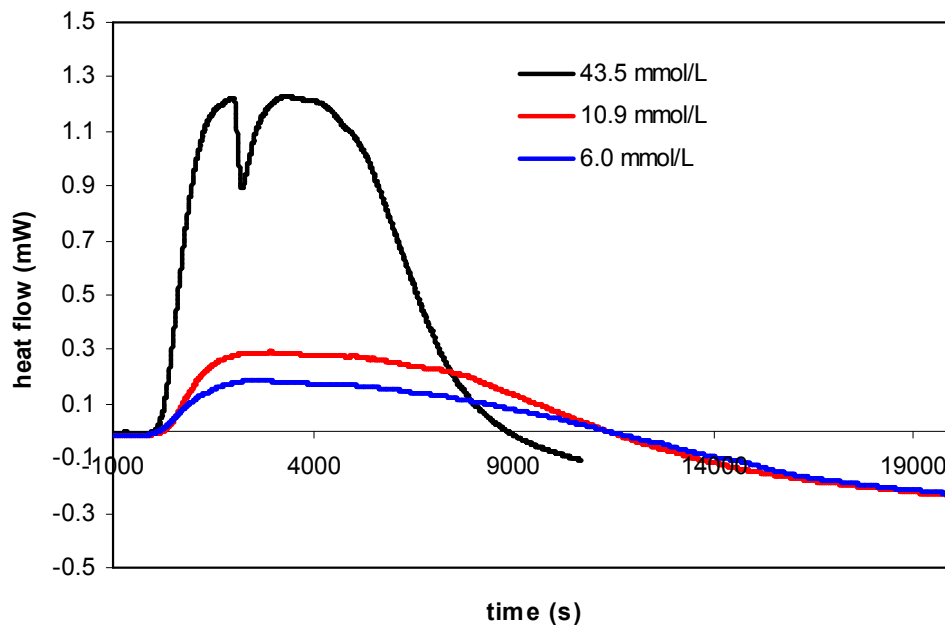


Figure 10. Effect of concentration of DBT in C₁₆ at 30°C and 4.00mL/h

The measured heats of adsorption seem to agree to within about 10% of one another. Although this result does not prove that the molar heat is independent of feed concentration, it does seem to support that hypothesis. Although the three measured heat values do not agree exactly with one another, there does not seem to be a correlation between feed concentration and heat of adsorption.

This variability in the results may simply be due to lack of experience on the part of the experimenter. As stated, these experiments were done at an early stage in the development of this method. In addition to the presence of the air bubble in the system, there appears to be a significant baseline shift for all three heat flow curves. It is possible

that the experiments were commenced before equilibrium was reached, and that this also contributed to the variability of the data.

5.2.2 Causes of Variability

It is useful to examine the source of variability of adsorption processes. Figure 11 compares two heat flow curves generated under the same conditions in order to examine one source of variability in the heat of adsorption per gram of sorbent.

Figure 11 is a typical representation of two heat flow curves obtained from duplicate experiments. The first thing to notice is that during the initial stage of adsorption (up to about 9000 s) the heat flow curves are nearly identical. The reason for this is that initially, adsorption takes place on easily accessible surface sites. The rate of transport of sorbent molecules to the surface sites is governed by the feed flow rate and concentration. Since both of these parameters can be precisely controlled there is little variation in this region between experiments.

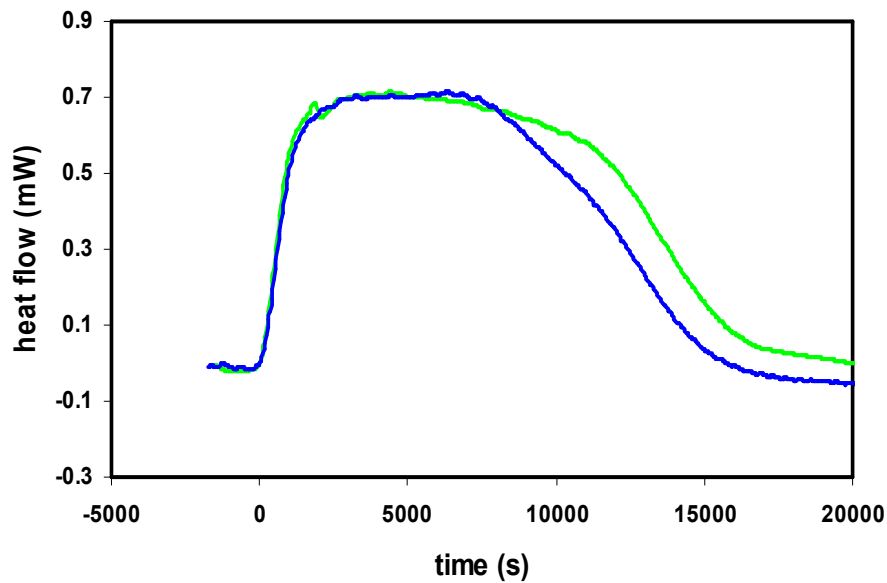


Figure 11. Comparison of heat flow curves for 21.8mM DBT/C16 on NaY (Run ID# 9,13)

Experience has shown that the point at which breakthrough of sorbate molecules occurs is equivalent to the point where the heat flow curve begins to fall. This point of breakthrough corresponds to the time when sorbate molecules reach the discharge

without being able to adsorb onto the zeolite. It can be seen in Figure 11 that this point is the point at which the two heat flow curves begin to deviate from one another. It follows that differences in the heat flow curves (and thus in the heat evolved per gram of sorbent) arise from differences in diffusion kinetics between samples. The most likely reason that diffusion limitations would differ from one experiment to another is slight differences in particle size distributions between samples.

The practical implications of this phenomenon become extremely significant in the determination of the heat evolved per mole of sorbent. Since the differences occur when the rate of adsorption is relatively small, the difference between the feed and effluent concentration is also small. As the feed and effluent concentration values approach each other, the ability of the GC to differentiate the concentrations becomes statistically insignificant. In other words, the variability in concentrations measured by the GC becomes larger than the concentration difference between the feed and effluent, and thus we cannot measure the rate of adsorption. The ability to measure slight differences in the heat per gram of sorbent, but not in the amount adsorbed affects the precision in the calculation of the heat evolved per mole adsorbed.

This may explain why adsorbed amount calculations based on breakthrough curve calculations were extremely variable, while measurements of heat evolved per gram of sorbent were relatively constant.

5.3 Zeolite Characterization

A summary of sorbent characterization experiments are presented in Table 9.

The surface area of the Y-type zeolites decreases in the order NaY>NiY>CsY. The surface area of CsY and NiY are 37% and 23% lower than the NaY from which they were prepared, respectively. This decrease in surface area appears to be the result of the ion exchange process. Other groups have found little change in surface area after ion exchange. For example, the surface area of NaY zeolite as prepared by STREM chemicals is 820 m²/g (Jiang et al., 2005). Surface areas of NiY prepared by various ion exchange procedures, including solid state ion exchange (SSIE) have resulted in sorbents with surface areas between 700 – 800 m²/g (Hernandez-Maldonado and Yang, 2004a). Similarly, the surface area of a Cu exchanged NaY zeolite was found to be 778 m²/g (Hernandez-Maldonado et al., 2004b). A comparison and discussion of ion exchange procedures used in the literature is presented in Section 5.6.

Table 9. Sorbent characterization results

	NaY	NiY	CsY
BET Surface Area (m ² /g)	677	524	429
Ionic Radius ^a (nm)	0.098	0.078	0.165
Al (wt%) ^b	8.3	8.26	6.83
Si (wt%) ^b	24.3	24.8	20.5
Na (wt%) ^b	7.44	1.87	2.09
Cation (wt%) ^b	-	5.59	22.8
Unit Cell Composition	Na ₃₃ (Si ₈₉ Al ₃₂ O ₃₈₄)	Ni ₁₀ Na ₈ (Si ₉₁ Al ₃₂ O ₃₈₄)	Cs ₂₂ Na ₁₂ (Si ₉₄ Al ₃₃ O ₃₈₄)
n _{Si} /n _{Al}	2.81	2.88	2.88

^aShackelford, 2000^bGalbraith Laboratories, Knoxville, TN

All calculations of unit cell composition were performed with a basis of 384 O atoms per unit cell. A sample of the calculation of unit cell composition may be found in Appendix B. The composition of the zeolites all show good agreement with the typical structure (Hernandez-Maldonado and Yang, 2004a). Data for NiY shows that while 25 Na⁺ ions were removed during ion exchange, only 10 Ni²⁺ ions replaced them, creating a net charge on the unit cell of -5. It is possible that this discrepancy is within the limits of precision of the ICP-OES analysis. It is also possible that discrepancy is the result of incomplete ion exchange, perhaps due to mass transfer limitations in the zeolite framework.

The silica/alumina ratio is used as a check to ensure accuracy of the ICP results as well as to verify that the general composition of the zeolite was not altered during the ion exchange process. The measured ratio of 2.81 for NaY zeolite is close to that reported by STEM (n_{Si}/n_{Al}=2.83). It can also be seen that this ratio is not significantly altered during the ion exchange process, as both NiY and CsY have a ratio of 2.88. In preparing NiY zeolite from NaY as in our work, Hernandez-Maldonado and Yang (2004a) found a decrease in the ratio Si/Al to 2.44.

XRD analysis was also performed on the adsorbents. Figure 12 presents the XRD patterns for the sorbents.

The blue data series represents the diffraction pattern for zeolite NaY. The diffraction peaks at 2θ angles of 10, 12, 16 and 21° are pronounced on the NaY pattern, but extremely small for NiY and CsY. This indicates that the crystalline structure of the zeolite is disrupted during the ion exchange process. Several other peaks (2θ = 6, 24, 32°) are also decreased in intensity after ion exchange. The diffraction pattern shows agreement with that of Dooryhee et al. (1991), most notably with peaks at 2θ=6, 16, 32°. No work could be found in the literature comparing XRD patterns of modified Y zeolites with their NaY precursor.

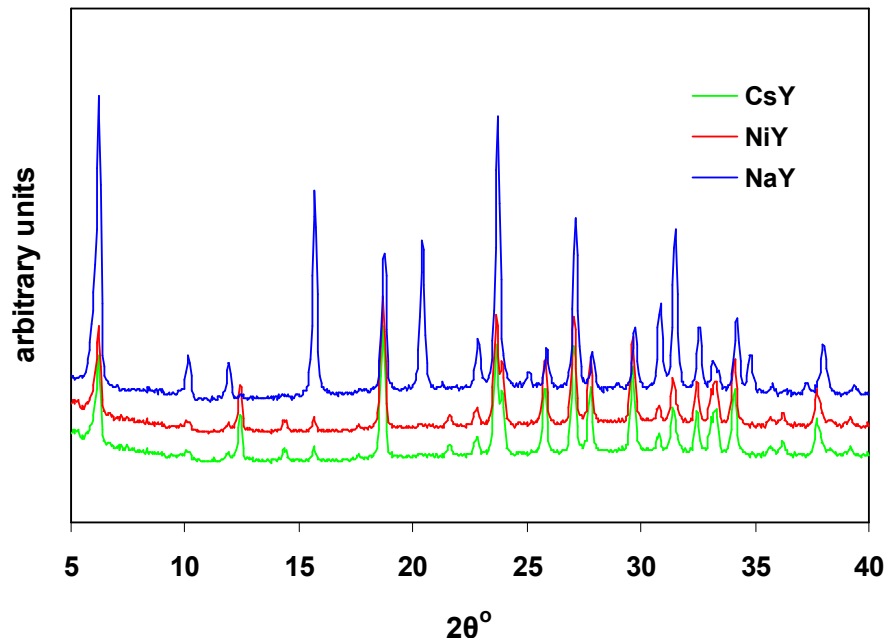


Figure 12. X-Ray diffraction patterns for Y-type zeolites

The decrease in peak intensity appears to be slightly greater for CsY than NiY, indicating a greater degree of disruption of the crystalline structure. This is likely due to the higher degree of ion exchange present in the CsY zeolite than in the NiY zeolite (Table 9). Roughly the same number of sodium ions was displaced per unit cell in both NiY and CsY. Each Ni^{2+} ion however must displace two Na^+ ions, whereas each Cs^+ ion displaces one Na^+ ion in order to maintain charge neutrality. Thus, the concentration of ions in CsY is greater than in NiY zeolite. Also, each Cs^+ ion is much larger than a Ni^{2+} ion (Table 9). The resulting CsY zeolite would thus contain much more mass per unit cell than NiY, and disruption of the crystalline structure would likely be required to accommodate it. Disruption of the crystalline structure of the zeolite may contribute to decreased surface area.

5.4 Equilibrium Adsorption Experiments

Equilibrium adsorption experiments were carried out for comparison to flow adsorption experiments. The results of these experiments are summarised in the following tables. The linear isotherms and raw data used to calculate the equilibrium capacity and equilibrium constant are shown in Appendix F.

5.4.1 DBT Equilibrium Isotherms

The results of DBT equilibrium adsorption experiments are shown in Table 10 and Figure 13.

Table 10. DBT isotherm data

Sorbent	Slope	Intercept	R ²	q _m (mmol/g)	K _a (L/mmol)
NaY	0.687	0.3605	0.9989	1.46	1.91
NiY	0.984	0.3994	0.9994	1.02	2.46
CsY	0.989	0.2092	0.9993	1.01	4.73

*Experiments performed for 24h at 30°C

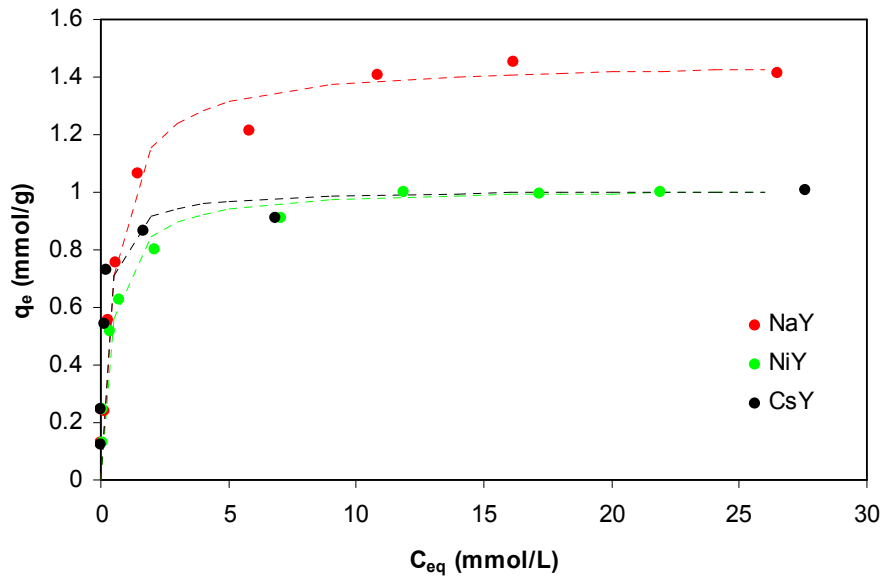


Figure 13. Equilibrium isotherms for DBT in C16

The K_a value in the last column of Table 10 is the equilibrium constant for the adsorption reaction (see equation 4). The definition of the equilibrium constant, the ratio of the forward and reverse reaction rates for adsorption, shows that the larger the value of K , the more preferred the adsorption reaction is over the reverse desorption reaction. In practical terms (using equation 4) a larger equilibrium constant means that saturation of the sorbent occurs at a lower sorbate concentration in the solution. Thus, a high equilibrium constant would indicate a sorbent capable of removing large amounts of sorbate from dilute solutions.

Equilibrium constants decrease in the order $CsY > NiY > NaY$. Although they have a lower sulphur removal capacity, the ion exchanged zeolites may be more suited for deeper

desulfurization than NaY due to their higher equilibrium constant. That is, they may be more suited to removing sulphur from fuel with already low sulphur content.

In the case of adsorption of DBT in C16, capacity decreases in the order NaY>CsY~NiY. The decrease in capacity after ion exchange is likely due to the structural deformations observed in XRD analysis.

5.4.2 Quinoline Equilibrium Isotherms

The results of quinoline equilibrium experiments are shown in Table 11 and Figure 14.

Table 11. Quinoline isotherm data

Sorbent	Slope	Intercept	R ²	q _m (mmol/g)	K _a (L/mmol)
NaY	0.516	0.0423	0.9997	1.94	12.19
NiY	1.147	0.0963	0.9985	0.87	11.91
CsY	0.821	7.728	0.3885	1.22	0.11

*Experiments performed for 24h at 30°C

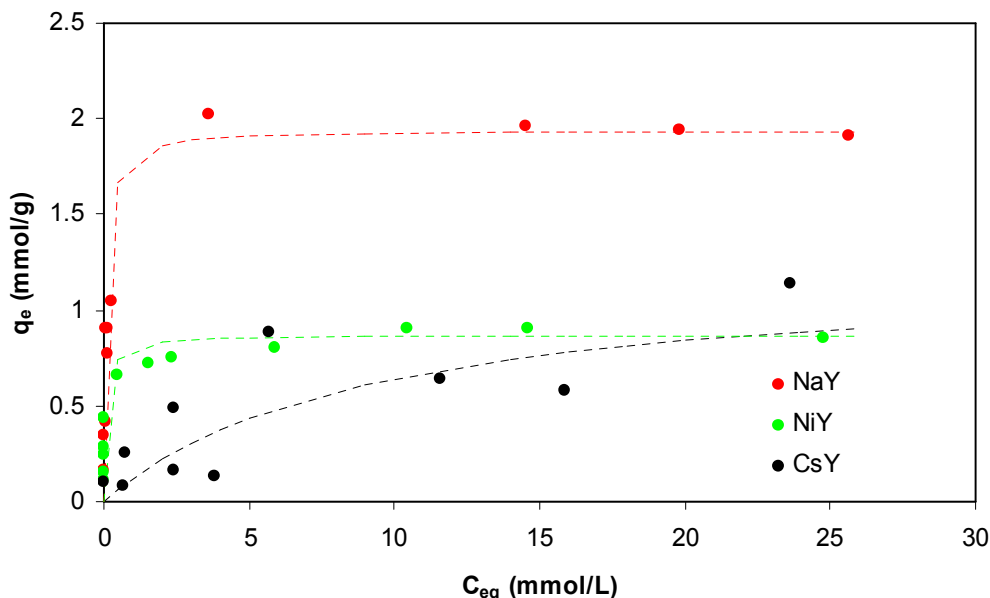


Figure 14. Equilibrium isotherms for quinoline in C16

The isotherms for NaY and NiY fit closely with the expected shape of the Langmuir isotherm. When fit to the linear approximation of the Langmuir isotherm both sorbents yield r^2 values well above 0.99. CsY zeolite on the other hand does not fit such an approximation. The r^2 value for the linear approximation is only about 0.39, and in Figure 14 it can be seen that the data exhibits significant scatter. The results presented for CsY

are the result of a second experiment, the first of which showed a similar amount of scatter. The isotherm appears to be of the Langmuir form with significant variability, rather than that of another isotherm. The reason for the scatter is unknown. Due to the apparently unreliable nature of the isotherm results for quinoline adsorption on CsY zeolite, it is excluded from the subsequent discussion.

Equilibrium adsorption capacity for quinoline decreases in the order NaY>NiY. These values follow the trend in decreasing surface area (Table 9). Surface area (and by extension pore volume) is believed to play a significant role in the adsorption capacity of the sorbents for quinoline.

Equilibrium constants apparently decrease in the order NaY>NiY. Although these constants are very close, the lower equilibrium constant for NiY than NaY suggest that NaY would be more effective at removing nitrogen from dilute solutions. In addition, NaY has a larger equilibrium sorption capacity for quinoline.

5.4.3 Naphthalene Equilibrium Isotherms

Finally, the results of naphthalene equilibrium adsorption experiments are summarised in Table 12 and Figure 15.

Table 12. Naphthalene isotherm data

Sorbent	Slope	Intercept	R²	q_m (mmol/g)	K_a (L/mmol)
NaY	0.573	0.385	0.9990	1.74	1.4899
NiY	0.797	0.493	0.9986	1.26	1.6166
CsY	0.925	0.306	0.9991	1.08	3.0193

*Experiments performed for 24h at 30°C

Capacity for naphthalene increases in the order CsY<NiY<NaY. The order of increasing capacity on the Y-type zeolites follows the order of increasing surface area, and it is likely that this property is responsible for the trend observed.

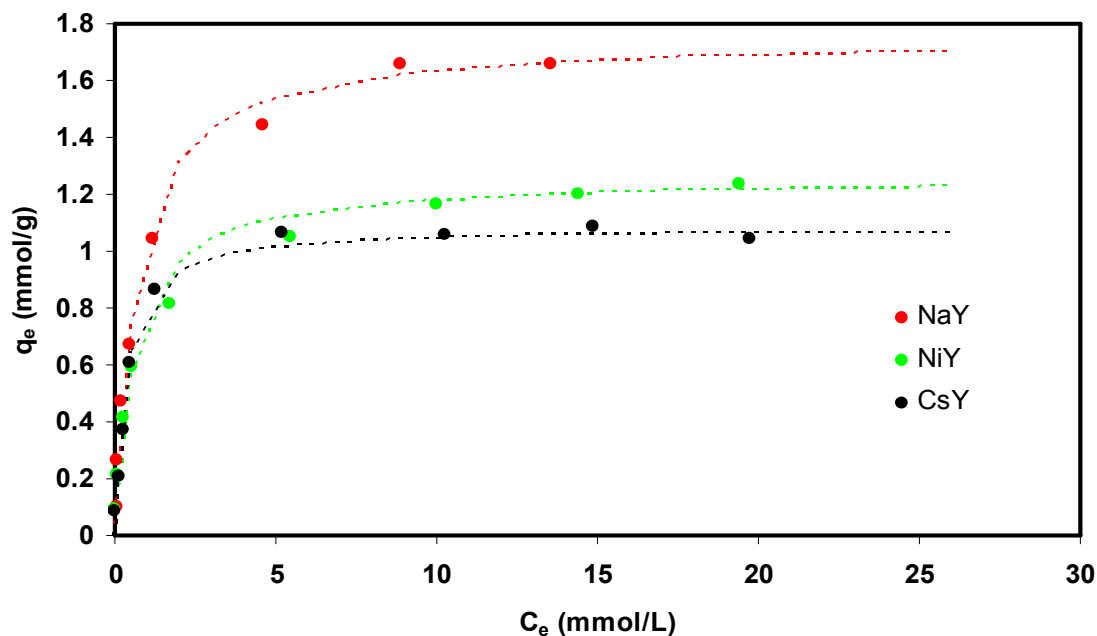


Figure 15. Equilibrium isotherms for naphthalene in C16

Equilibrium constants for adsorption of naphthalene increase in the order $\text{NaY} < \text{NiY} < \text{CsY}$. As with DBT adsorption, the equilibrium constant increases after modification of the zeolite.

Some trends can be observed from the above data. First, in general, the adsorption capacity for the three sorbates on Y-type zeolites decreases in the order $\text{NaY} > \text{NiY} > \text{CsY}$, which also follows the order of decreasing surface area (Table 9). The trend in equilibrium adsorption capacity is thus likely a result of the deformation of the crystalline zeolite structure caused by the ion exchange process.

5.5 Adsorption on NaY Zeolite

Adsorption results on NaY zeolite are shown in Table 13 and Figure 16.

Heats of adsorption decrease in the order $\text{quinoline} > \text{DBT} > \text{naphthalene}$. The three zeolites, in order of decreasing basicity are $\text{quinoline} > \text{DBT} > \text{naphthalene}$. It appears that in adsorption on NaY zeolite, acid-base interactions may play a strong role in the strength of adsorption. The results indicate that steric effects due to the size of the sorbate molecule are not significant, since DBT has a higher heat of adsorption than the much smaller naphthalene molecule.

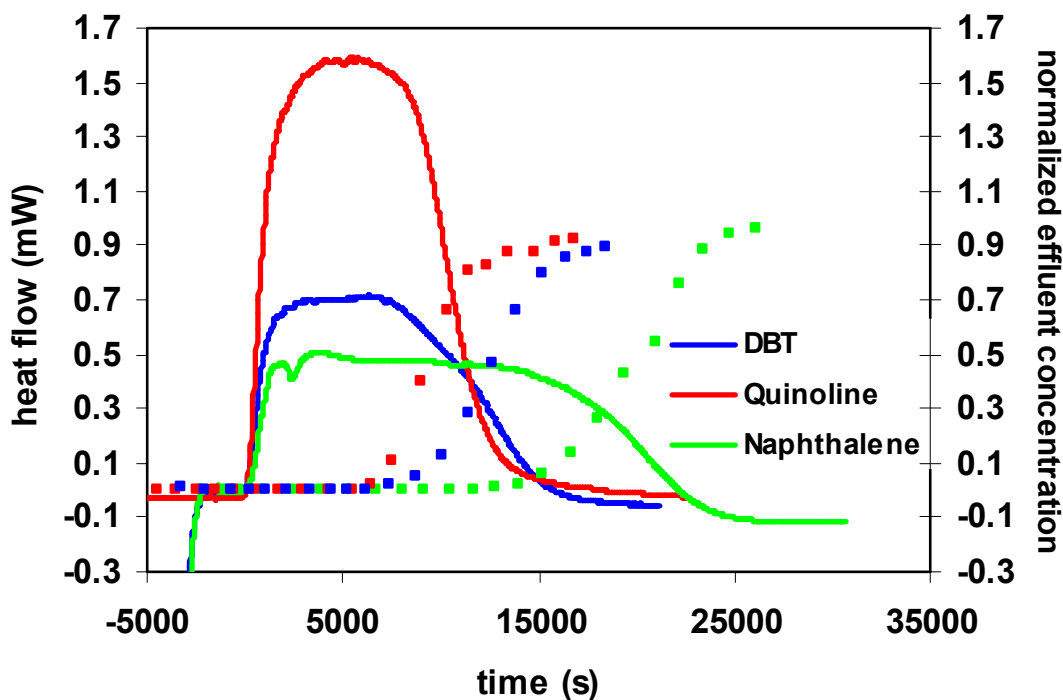
Table 13. Adsorption results on NaY zeolite

Sorbate	$-\Delta H_{\text{Ads}}$		Amount Adsorbed (mmol/g)		
	J/g	kJ/mol	Experimental	Isotherm	Breakthrough
DBT	34.3	29.5	1.16	1.43	1.10
Quinoline	60.2	63.1	0.94	1.94	1.06
Naphthalene	38.2	20.6	1.86	1.69	1.77

Experiments carried out at 21.8 mM Sorbate in n-C₁₆ at 30°C and 4.00mL/h

Amounts adsorbed in the ‘Experimental’ column are calculated using the new method developed in this work. The ‘Isotherm’ column presents the equilibrium amounts adsorbed for a solution concentration of 21.8 mM using the Langmuir isotherms developed in Section 5.4. Finally, the ‘Breakthrough’ column presents adsorbed amounts at saturation calculated from the breakthrough curves.

Curiously, adsorption capacities decrease in the opposite order of the heats of adsorption (naphthalene>DBT>quinoline). Likewise, the trend of increasing sorption capacity does not follow the order of decreasing critical diameter (Table 4). It appears that the explanation of adsorption capacity on NaY zeolite can be explained neither by the strength of adsorption nor size exclusion and/or diffusion limitations for the larger molecules alone.

**Figure 16.** Adsorption Results on NaY zeolite

DFT calculations (Hernandez-Maldonado et al., 2005) have shown that adsorption of DBT occurs via complexation between the framework cation of the sorbent and the aromatic π electron cloud of the sorbate molecules, resulting in the sorbate molecule lying relatively flat on the sorbent surface. Work by Yang et al. (2004) has predicted a similar orientation for benzene on a model of the CuY surface. Due to its similar structure, naphthalene is likely oriented in a similar manner. Quinoline on the other hand has a lone pair of electrons, which may form the bond with the cation. This would likely cause the quinoline molecule to stand on its edge rather than to lie flat in the sorbent surface. Results of Larrubia et al. (2002) have shown that when direct interaction between the heteroatom and adsorbent surface occurs, the sorbate molecules assume this type of orientation. Curiously, their results indicate that organosulfur compounds stand on edge while the organonitrogen compounds lie flat. Their experiment used different sorbents in which direct interaction between the sulfur atom and the sorbent occurred, and the π -electrons in the organonitrogen compounds interacted with the sorbent surface. Thus, we can draw reasonable comparisons between their situation and ours.

If the quinoline molecule were standing on edge as hypothesized, it may block the pores of the zeolite, significantly reducing the rate of diffusion through the zeolite, and by extension the rate of quinoline adsorption. It is possible that the rate of quinoline adsorption would be reduced to the extent that no measurable heat flow is generated, leading the experimenter to believe that steady state has been achieved. Although DFT calculations similar to those for sulfur containing species have been completed for nitrogen containing species (Jayaraman et al., 2006), no data on the orientation of the quinoline molecules relative to the sorbent surface is given. It is reasonable to assume that even if direct interaction between the framework cation and the lone pair does not occur, the presence of the lone pair may still alter the orientation of the quinoline molecule enough to affect adsorption capacity.

Since it is believed that both naphthalene and DBT are adsorbed with the same orientation (lying flat on the sorbent surface), the difference in capacity between the two may be explained by size difference. The pores in the zeolite can accommodate more of the much smaller naphthalene molecule.

The trend in increasing adsorption capacity in the calorimeter does not follow that of the equilibrium adsorption experiments. In the equilibrium experiments, the capacity for NaY increases in the order DBT < Naph < Quin, which is the same order of decreasing critical diameter. Also, all adsorbed amounts calculated from flow experiments are lower than the

equilibrium adsorbed amounts. It is possible that within the calorimeter equilibrium is not reached, and the orientation of the sorbate molecules is an important factor in determining the adsorbed amount. It appears as though the orientation of the quinoline molecule slows the adsorption rate, however it does not determine the equilibrium amount adsorbed. It would be interesting to repeat flow adsorption experiments for quinoline on NaY and allow the adsorption to continue for a longer period of time to determine whether it is possible for the amount adsorbed to approach the equilibrium capacity.

Amounts adsorbed determined using the breakthrough curve show good agreement with those determined using the new calculation method. Although the amounts determined using the breakthrough curve are within 5-15% of those calculated using the new method, the variability within those calculations are greater than with the new method (Table 7).

5.6 Adsorption on NiY Zeolite

The results for adsorption on NiY zeolite are presented in

Table 14 and Figure 17.

Table 14. Adsorption results on NiY zeolite

Sorbate	$-\Delta H_{\text{Ads}}$		Amount Adsorbed (mmol/g)		
	J/g	kJ/mol	Experimental	Isotherm	Breakthrough
DBT	31.2	33.2	0.94	1.00	0.98
Quinoline	60.9	97.3	0.63	0.87	0.59
Naphthalene	30.3	24.2	1.25	1.23	-

Experiments carried out at 21.8 mM Sorbate in n-C₁₆ at 30°C and 4.00 mL/h

No breakthrough results are available for naphthalene adsorption on NiY.

Amounts adsorbed in the ‘Experimental’ column are calculated using the new method developed in this work. The ‘Isotherm’ column presents the equilibrium amounts adsorbed for a solution concentration of 21.8 mM using the Langmuir isotherms developed in Section 5.4. Finally, the ‘Breakthrough’ column presents adsorbed amounts calculated from the breakthrough curves.

The heats of adsorption on NiY decrease in the order quinoline>DBT>naphthalene. This is the same trend exhibited in adsorption on NaY zeolite, except the magnitude of the heat values is greater on NiY. This implies that the d-electrons of the nickel ion do indeed increase the strength of the adsorption.

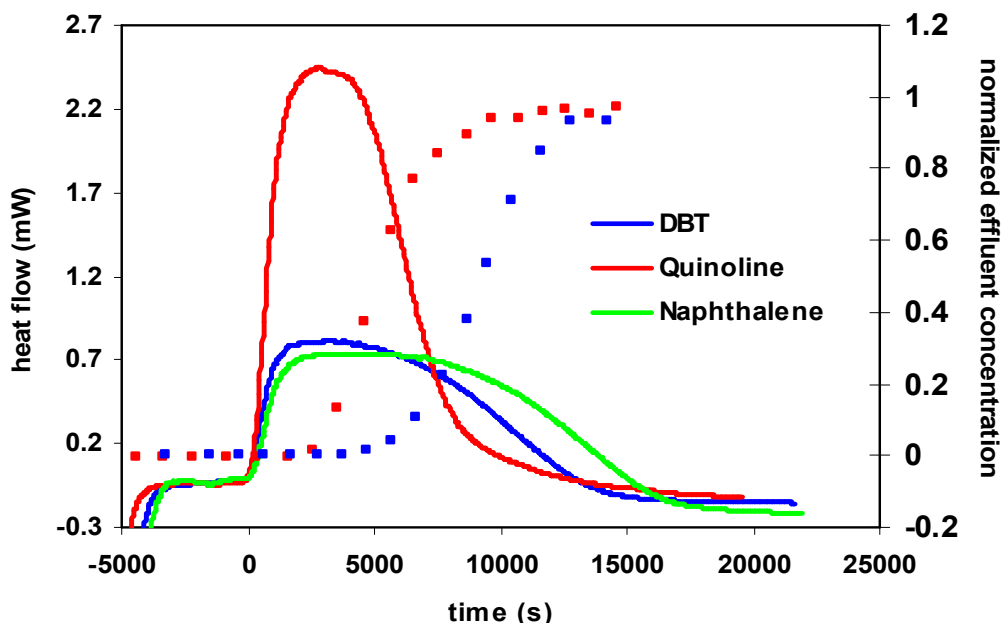


Figure 17. Adsorption results on NiY zeolite

The trend in decreasing adsorption capacity is naphthalene>DBT>quinoline. This is the same trend exhibited in equilibrium adsorption experiments on NiY. In the case of NaY, it was proposed that the trend of increasing adsorption capacities was different between flow experiments and equilibrium experiments because of a slowed rate of quinoline adsorption. However, in the case of NiY, quinoline has the lowest adsorbed amount in both cases. Alterations in the framework structure of NiY have been noted, resulting in lower surface area, and by extension pore volume. If the quinoline molecule stands on edge on the zeolite surface as proposed, then it is possible that the reduced pore size in NiY prevents some quinoline molecules from adsorbing, regardless of the amount of time provided for adsorption.

This is also the same trend of decreasing adsorption capacities exhibited in adsorption on NaY zeolite, except the capacities are much lower. It was hypothesized that exchanging the Na⁺ ions with Ni²⁺ ions would increase adsorption capacity. Nickel ions are smaller than sodium ions (Table 9) and each nickel ion replaces two sodium ions. In this work, each NaY unit cell contained 33 cations compared to only 18 in NiY (Table 9). The pore volume in NiY should thus be larger than NaY. Assuming a pore filling mechanism, the larger pore space would likely increase capacity. An alternative argument would contend that the lower concentration of Ni²⁺ ions in NiY would result in fewer adsorption sites than on NaY. Thus, assuming direct

interaction between the ions and the sorbate molecules, the capacity of NiY should be reduced from NaY. Previous work however has found NiY to have higher capacity than NaY for refractory thiophenic sulphur compounds. Work by this group has found that the capacity for benzothiophene in n-octane was 1.69 and 1.80 mmol/g on NaY and NiY, respectively (Jiang and Ng, 2006). Hernandez-Maldonado et al. (2004a) also found NiY to be a promising sorbent for desulfurization based on its high capacity for sulfur removal from diesel fuels.

It seems that the ionic concentration in NiY sorbent is insufficient to explain adsorption capacity trends, and thus another explanation must be found. Both XRD and BET results in this work indicate that the ion exchange process decreases both the crystallinity and surface area of the zeolite. It appears that this disruption of the zeolite structure decreases the adsorption capacity, which may explain the difference between our results and those in the literature. The reason for the disruption of the structure, however, is currently unknown. The ion exchange procedure employed in this work is similar to those used in the literature. A summary of procedures used by other groups is given in Table 15.

The first thing to note in Table 15 is that a significant variety of ion exchange techniques are employed. In addition to the type of nickel salt, different compositions of ion exchange suspensions are used, and ion exchange is carried out at different temperatures and for different lengths of time. It would seem then that, at least within reasonable limits, the degree of ion exchange is rather insensitive to the parameters of the exchange process. In general then, there is little to suggest that our ion exchange process should disrupt the structure of the zeolite to a greater degree than for other groups.

The pH of the solution is said to play an important role in the ion exchange. Hernandez-Maldonado et al (2004a), for example, maintained their solutions at a pH of around 6 in order to prevent nickel hydrolysis. Many of the exchange procedures in the literature made no mention of pH, and thus it is not known whether the pH was controlled, and if so, at what level it was maintained. In this work, the pH of the ion exchange suspension was maintained at a value above 4. It is possible that side reactions may occur at these lower pH values, affecting the structure of the resulting zeolite. More work should be done studying the effect of ion exchange pH on the properties of the zeolite.

Table 15. Summary of NiY preparation procedures found in literature

REF	Zeolite	Salt	C (M)	Volume (L)	M _z ^a (g)	# IX ^b	t (h) ^c	T (°C)
This Work	NaY	Ni(NO ₃) ₂	0.1	0.1	3	3	12	80
Creaser, 1992	NaY	Ni(NO ₃) ₂	0.1	1	50	2	24	-
Creaser, 1992	NaY	Ni(NO ₃) ₂	0.1	1	50	1	24	-
Creaser, 1992	NaY	Ni(NO ₃) ₂	0.01	0.5	15.7	1	24	-
Nkosi et al., 1997	NaY	NiCl ₂	0.2	0.15	20	1	24	rt
Nkosi et al., 1997	NaY	Ni(NH ₃) ₆ Cl ₂	0.2	0.15	20	1	24	rt
Nkosi et al., 1997	NaY	NiSO ₄	0.2	0.15	20	1	24	rt
Nkosi et al., 1997	NaY	Ni(NO ₃) ₂	0.2	0.15	20	1	24	rt
Nkosi et al., 1997	NaY	NiAc	0.2	0.15	20	1	24	rt
Hernandez-Maldonado et al., 2004a	NaY	NiCl ₂	-	-	-	1	48	rt
Hernandez-Maldonado et al., 2004a	NaY	NiCl ₂	-	-	-	1	48	135
Hernandez-Maldonado et al., 2004a	NaY	NiCl ₂	SSIE ^d	-	-	-	-	-
Velu et al., 2003	NH ₄ Y	Ni(NO ₃) ₂	0.1	5x	-	1	24	80
Sano et al., 1987	NaY	Ni(NO ₃) ₂	0.1	-	-	-	-	110
Sano et al., 1987	NaY	Ni(NO ₃) ₂	0.1	-	-	-	-	110
Podrebarac et al., 1996	NaY	Ni(NO ₃) ₂	-	-	-	1	-	rt
Coughlan et al., 1991	NaY	Ni(NO ₃) ₂	<0.1	0.4	100	1	24	-
Coughlan et al., 1991	KY	Ni(NO ₃) ₂	<0.1	0.4	100	1	24	-
Coughlan et al., 1991	LiY	Ni(NO ₃) ₂	<0.1	0.4	100	1	24	-
Coughlan et al., 1991	RbNaY	Ni(NO ₃) ₂	<0.1	0.4	100	1	24	-
Coughlan et al., 1991	CsNaY	Ni(NO ₃) ₂	<0.1	0.4	100	1	24	-
Dooryhee et al., 1991	NaY	NiCl ₂	0.005	1	0.5	1	-	-
Olson, 1968	Nat ^e	NiCl ₂ , NiAc	1	-	-	1	1440	90

^aM_z = zeolite mass^b# IX = number of ion exchanges^ct = length of each ion exchange^dSolid State Ion Exchange^eNatural faujasite

Preliminary results indicate that although the Ni-exchanged Y zeolites exhibit a higher strength of adsorption, they exhibit a decreased capacity and no discernible change in sulfur selectivity. These factors indicate that NiY would be unsuitable as a desulfurization sorbent relative to NaY, due to a decreased desulfurization ability (capacity, selectivity), and due to the higher heats of adsorption, regeneration would be more difficult as well.

Adsorbed amounts calculated using the new method show good agreement with those predicted from the equilibrium adsorption isotherms, indicating that equilibrium is likely reached within

the calorimeter. It appears that although diffusion of sorbate molecules into the micropores of NiY is inhibited by deformation of the crystalline structure, the exterior surface remains easily accessible such that equilibrium is reached relatively quickly.

Amounts adsorbed determined using the breakthrough curve show good agreement with those determined using the new calculation method. Although the amounts determined using the breakthrough curve are within 5% of those calculated using the new method, the variability within those calculations are greater than with the new method (Table 7).

5.7 Adsorption on CsY Zeolite

Adsorption results on CsY zeolite are presented in Table 16 and Figure 18.

Table 16. Adsorption results on CsY zeolite

Sorbate	$-\Delta H_{\text{Ads}}$		Amount Adsorbed (mmol/g)		
	J/g	kJ/mol	Experimental	Isotherm	Breakthrough
DBT	9.0	25.0	0.36	1.00	0.25
Quinoline	18.1	44.8	0.40	0.86	0.34
Naphthalene	22.1	26.0	0.85	1.06	-

Experiments carried out at 21.8 mM Sorbate in n-C₁₆ at 30°C and 4.00mL/h

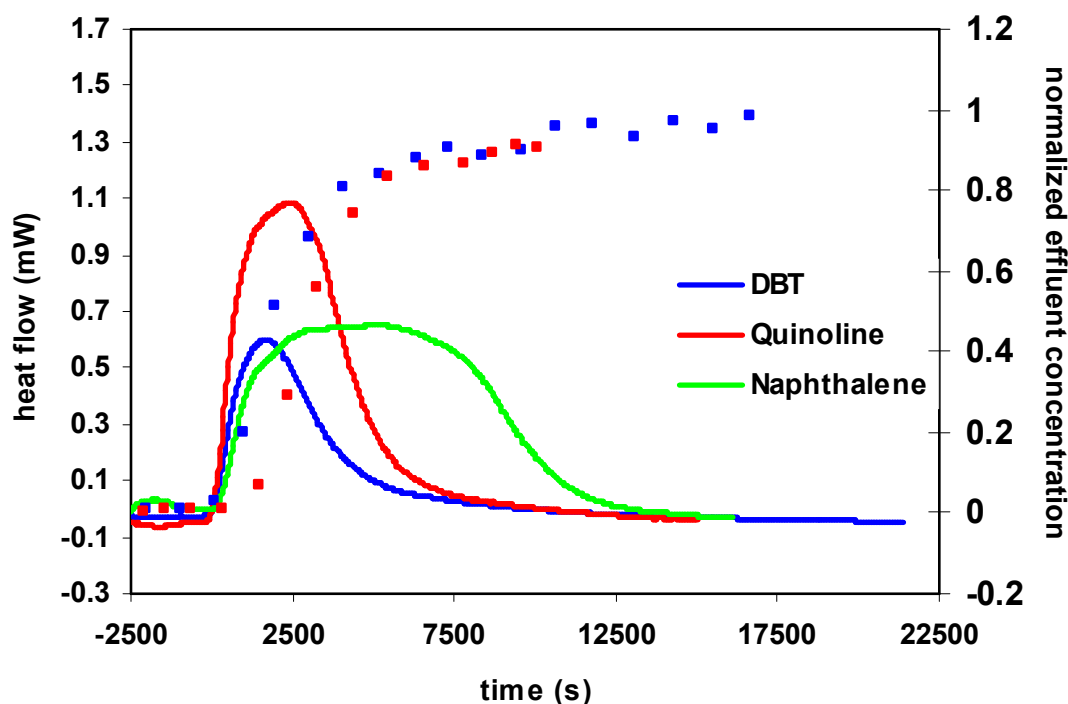


Figure 18. Adsorption results on CsY zeolite

Once again no breakthrough data is available for naphthalene adsorption.

Amounts adsorbed in the 'Experimental' column are calculated using the new method developed in this work. The 'Isotherm' column presents the equilibrium amounts adsorbed for a solution concentration of 21.8 mM using the Langmuir isotherms developed in Section 5.4. Finally, the 'Breakthrough' column presents adsorbed amounts calculated from the breakthrough curves.

The capacity for all three sorbates is substantially reduced from both NiY and NaY zeolites. The adsorption capacities on the three zeolites decrease in the same order as the surface area: CsY<NiY<NaY (Table 9). The crystallinity of the zeolites is also reduced after the ion exchange process. It is likely that these factors are the reason for the decrease in adsorption capacity.

The equilibrium adsorbed amounts on CsY are similar to those on NiY. The low adsorbed amounts obtained in flow conditions relative to equilibrium experiments is likely due to diffusion resistance within the pores of the zeolite. The reduced adsorption rate results in a longer time to reach equilibrium, and lower adsorbed amounts obtained in calorimeter experiments. The greater degree of structural disruption in CsY relative to NiY, as evidenced by the decreased surface area of CsY, would likely result in a slower rate of diffusion within the pores, and ultimately a lower measured adsorbed amount obtained from calorimeter experiments.

Amounts adsorbed determined using the breakthrough curve show moderately good agreement with those determined using the new calculation method, but with more variability (Table 7).

It should be noted that an extremely high quinoline capacity for CsY relative to NiY was obtained from equilibrium adsorption experiments (Table 11). This high amount was not expected, since the more basic CsY zeolite was expected to have the lowest affinity for the basic quinoline molecule. This high equilibrium value is believed to be the results of experimental error. The correlation coefficient for the quinoline/CsY isotherm was only 0.39, compared with values greater than 0.99 for all other combinations studied. More data is required before conclusions regarding quinoline adsorption on CsY may be drawn.

It is also interesting to note that the trend of increasing adsorption capacity is different for CsY than for NaY and NiY zeolites. In the case of CsY, this trend is DBT<Quin<Naph. In order to

explain this trend, it is useful to use naphthalene as the basis for comparison. As discussed previously, it is believed that the capacity of the zeolites for quinoline is less than the similarly sized naphthalene molecule because of the orientation of the adsorbed molecule (naphthalene lying flat of the sorbent surface, while quinoline lies on edge due to the lone pair of electrons). On NiY and NaY zeolites, orientation appeared to be a more important factor than size, since even the much larger DBT molecule was adsorbed in larger quantities than quinoline. In the case of CsY however it appears that size is an important factor in adsorption capacities. Due to the decreased crystalline structure of the CsY, it is likely that the pore size distribution is also altered. Smaller pore openings would restrict entry into the pores, and be most pronounced on the largest sorbate molecule, DBT.

The heats of adsorption on CsY increase in the order $DBT < Naph < Quin$. Once again the heat of adsorption for quinoline is substantially higher than both DBT and naphthalene, likely due to attraction between the framework cation and the lone pair on the quinoline molecule. The heat of adsorption of naphthalene is higher than DBT on CsY, which is different than the case for NaY and NiY. The hypothesis for using CsY as a sorbent is that the increased basicity of the Cs cation would increase selectivity for the more acidic sorbate molecules (DBT and naphthalene). No pronounced effect was observed in the heat of adsorption of quinoline over the other two sorbates. This result likely occurs because the heat of adsorption of quinoline was so much greater than the heat of adsorption of DBT and naphthalene that the minor effect of the basicity of the cation was not noticeable. In comparing adsorption of DBT and naphthalene, which have had much more similar heats of adsorption on NaY and NiY zeolites, it is likely that the change in basicity would have a more noticeable effect. That is believed to be the reason why the heat of adsorption on CsY is higher for the more acidic naphthalene than DBT.

The heat of adsorption of quinoline is substantially lower on CsY than on either NaY or NiY, however. This is likely the result of the increasing basicity of the CsY zeolite compared with NaY and NiY.

Two observations must be addressed regarding the adsorption of quinoline and DBT on CsY. It can be seen in Figure 18 that in neither case is a defined plateau reached in the heat flow curve. Additionally, it appears the breakthrough occurs before the peak heat flow value is reached. Both of these phenomena raise questions about the reliability of the calculations based on these sets of data. Since the capacity of CsY for DBT and quinoline is so much lower than that of NaY and NiY, saturation of the sorbent occurs much more quickly. It is believed that altering

experimental parameters such as feed flow rate and feed concentration may reduce the rate of adsorption such that a defined plateau in the heat flow curve is obtained. A plateau is expected to be obtained in the heat flow curve when the rate of adsorption is limited by the rate at which sorbate molecules are fed to the sorbent. This feed rate, when held constant, is expected to generate a constant heat flow (i.e., a plateau in the heat flow curve). More work is required to verify this hypothesis, and to verify the experimental data in Table 16.

5.8 Elucidation of Adsorption Mechanisms

Examination of adsorption data yields clues into adsorption mechanisms on the zeolites studied. A large amount of insight can be gained, for example, by relating the equilibrium adsorption capacity to the surface area of the sorbent (Table 9). This data is presented in Figure 19.

Figure 19 shows that DBT and naphthalene, equilibrium sorption capacity appears to be a function of surface area. Quinoline adsorption does not appear to follow this trend. The equilibrium isotherm for quinoline on CsY however was determined to be unreliable (Figure 14) due to significant scatter within the data. If the data point for quinoline/C16 adsorption on CsY ($429 \text{ m}^2/\text{g}$, 1.22 mmol/g – enlarged in figure for clarity) is removed, the data appear to agree with that of the other sorbents.

The slope of each line of best fit is the amount adsorbed expressed in mmol/m^2 of sorbent. Since all sorbents show relatively good agreement with this trend, it can be inferred that adsorption occurs in all cases by direct interaction between the sorbate molecule and the sorbent surface. Adsorption via a pore filling mechanism, or some other relatively weak physical force, could occur in multiple layers on the surface of the sorbent, and this straight line relationship would not likely be observed.

The slope of the data series increased in the order $\text{DBT} < \text{Naphthalene} < \text{Quinoline}$. If a reliable equilibrium capacity for quinoline/C16 on CsY were obtained, it would be expected to be lower than the existing value of 1.22 mmol/g , and thus the slope for quinoline in Figure 19 would be expected to increase.

The slope for DBT is the lowest because DBT is the largest molecule, and would thus be expected to take up the most surface area on the sorbent upon adsorption. Naphthalene and quinoline molecules are nearly the same size, although the slope of the quinoline series is much higher, indicating that more quinoline is adsorbed per m^2 of sorbent surface. This is likely due to differences in orientation of the molecules on the sorbent surface. Due to interaction between

the sorbent cation and the aromatic rings of the naphthalene molecule, it lies flat on the sorbent surface. It is believed that quinoline adsorption is due to interaction between the framework cation and the lone pair on the nitrogen atom in quinoline, resulting in the quinoline molecule standing on end on the sorbent surface. Although slowing the rate of quinoline adsorption in flow experiments, this ‘end on’ orientation would allow more quinoline molecules to adsorb per unit surface area at equilibrium, resulting in the greater slope for quinoline than naphthalene.

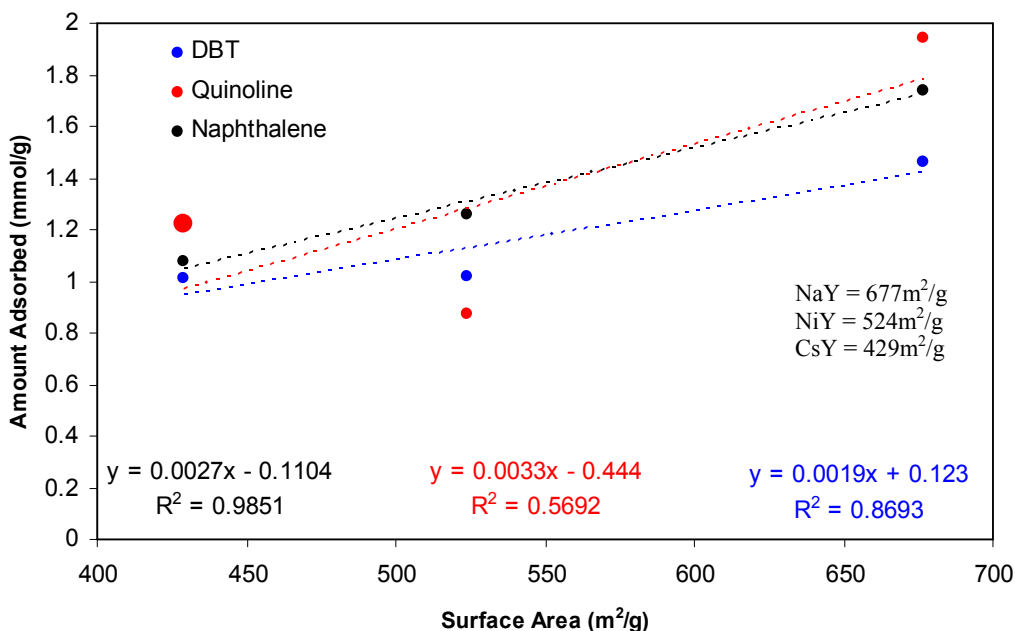


Figure 19. Relationship between surface area and equilibrium sorption capacity

5.9 Competitive Adsorption Experiments

Competitive adsorption experiments were conducted on each of the three zeolites. From these experiments selectivity for DBT was calculated, and comparisons between sorbents drawn. A summary of all competitive adsorption results is presented in Table 17. Amounts adsorbed are calculated based on breakthrough curve data.

Table 17. Summary of competitive adsorption results

	Heat (J/g)	Amount Adsorbed (mmol/g)				Selectivity		
		DBT	Quin	Naph	Total	DBT	Quin	Naph
NaY	52.6	0.45	0.62	0.40	1.47	1	0.73	1.11
NiY	36.7	0.23	0.30	0.22	0.75	1	0.75	1.04
CsY	14.3	0.12	0.24	0.11	0.47	1	0.49	1.04

* Selectivity is defined as the ratio of the number of moles of DBT adsorbed relative to the number of moles of the species in question adsorbed

Competitive adsorption results on NaY are shown in Figure 20.

On NaY zeolite, breakthrough of all three sorbates occurs nearly simultaneously. After breakthrough, DBT and naphthalene reach saturation much more quickly than quinoline, indicating that quinoline is preferentially adsorbed. Before reaching saturation, the effluent concentration of naphthalene remains slightly higher than that of DBT, indicating a slight preference for adsorption of the sulfur containing species over the aromatic naphthalene. Concentration differences between the compounds after saturation are attributed to GC calibration error, since solutions were carefully prepared with equimolar concentrations of the three sorbates.

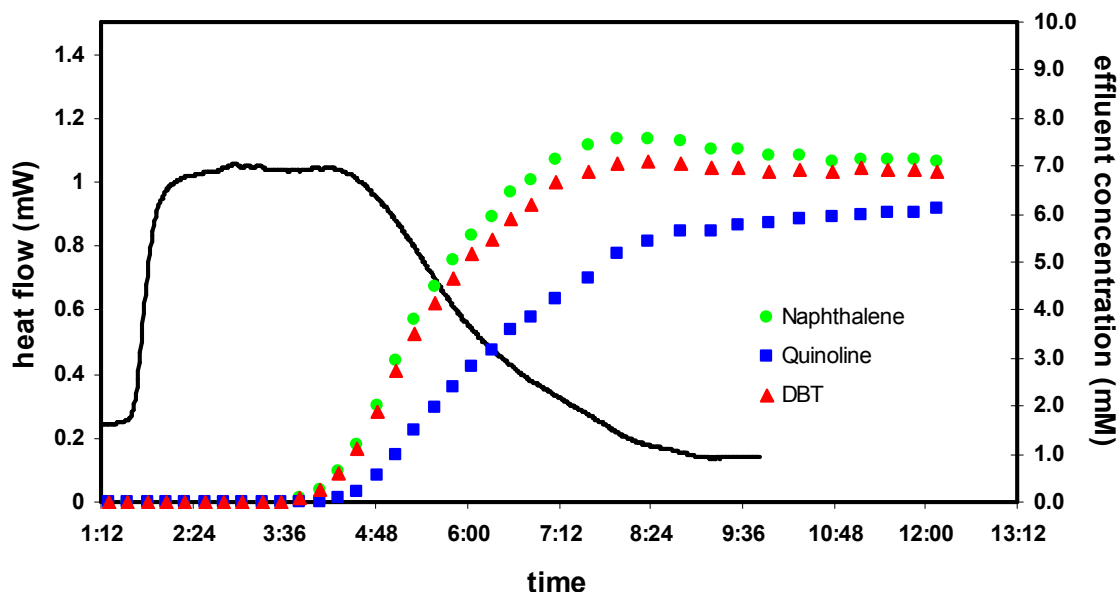


Figure 20. Competitive adsorption results on NaY zeolite

The effluent concentration of both naphthalene and DBT reach levels greater than their feed concentration, and subsequently decrease to the feed concentration. This is likely due to displacement of these molecules by the more strongly adsorbed quinoline. The same phenomenon has been observed in competitive adsorption on activated carbon and activated alumina using the same sorbate molecules in model fuel (Kim et al., 2006). It is noted that the magnitude of this peak is greater for naphthalene than for DBT. This implies that naphthalene is more easily displaced than DBT, further supporting the theory that DBT adsorption is slightly preferred to naphthalene adsorption on NaY zeolite.

Selectivity values on NaY (Table 17) support these qualitative observations. Analysis of selectivity shows that it decreases in the order Naph>DBT>Quin. This is the same order as was predicted based on increasing heats of adsorption.

Adsorption on NiY zeolite is presented in Figure 21. The adsorption process on NiY zeolite is similar to that on NaY zeolite. The total adsorption capacity is reduced compared to NaY, as was observed in the single sorbate experiments. Comparison of heats of adsorption in this case is meaningless, since instantaneous heat flow is the result of a much more complex process involving displacement of both solvent and sorbate molecules by other sorbates.

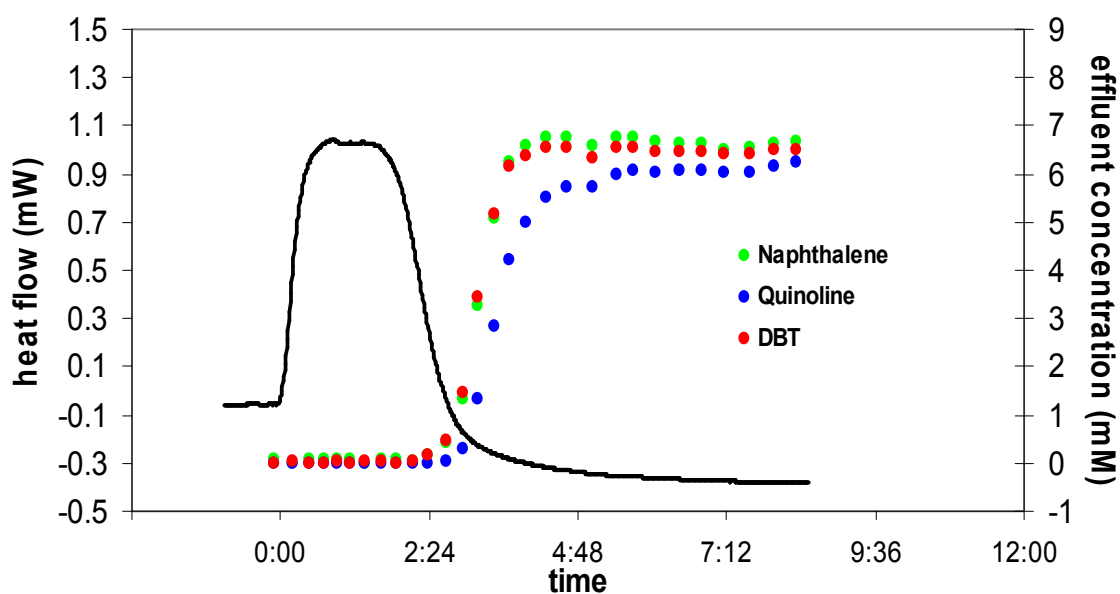


Figure 21. Competitive adsorption results on NiY zeolite

The selectivity towards both quinoline and naphthalene are not significantly altered from that of NaY (Table 17). Examination of the breakthrough curve shows that displacement of DBT and naphthalene does not occur to the extent that it does on NaY zeolite. A small amount of displacement of naphthalene is observed (exhibited by effluent concentration exceeding feed concentration), but almost no displacement of DBT. This is likely due to the increasing strength of interaction between the aromatic rings and the transition metal, which has the ability to back donate d-electron density (Hernandez-Maldonado and Yang, 2004c), making displacement by quinoline molecules more difficult.

Again, as with NaY, selectivity decreases in the order Naph>DBT>Quin. Likewise, as with NaY, this is the same order as was predicted based on increasing heats of adsorption.

Adsorption on CsY zeolite is shown in Figure 22. The observations made during competitive adsorption on CsY zeolite are not surprising, given the results of the single sorbate experiments. First, the total adsorption capacity is reduced compared with that on NaY and NiY zeolites, as was observed previously. Second, naphthalene and DBT break through first, followed by quinoline.

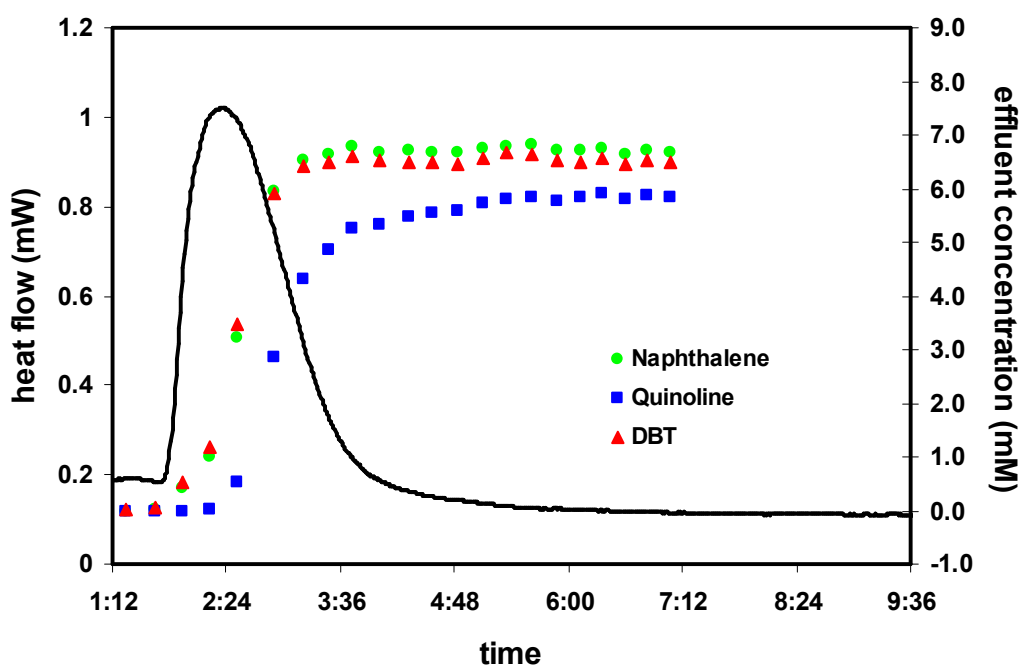


Figure 22. Competitive adsorption results on CsY zeolite

One difference between single sorbate and competitive adsorption experiments is that our competitive adsorption experiments indicate that DBT adsorption is slightly preferred over naphthalene, based on calculated selectivity. In our single sorbate experiments, we observed a slightly higher heat of adsorption for naphthalene than DBT on CsY, indicating we should expect naphthalene adsorption to be slightly preferred.

As mentioned earlier, this may be attributable to our GC calibration. It appears that after saturation the concentration of naphthalene is slightly higher than that of DBT. Since the

solutions were prepared with equimolar concentrations of the sorbates, this difference is likely due to GC calibration. This would have an effect on our amount adsorbed calculations since even though no adsorption is occurring (due to saturation) our GC calibration indicates a slightly higher effluent naphthalene concentration manifesting itself in our calculations as a lower amount of naphthalene adsorbed. This could alter the calculated order of increasing selectivity if the amounts of DBT and naphthalene adsorbed are similar, which is true in this case.

Another observation supports the initial hypothesis that naphthalene adsorption is preferred over DBT adsorption on CsY despite what selectivity calculations show. Between breakthrough and saturation the concentration of DBT is slightly higher than naphthalene, supporting our observation that naphthalene adsorption is slightly preferred over DBT on CsY zeolite, even though our selectivity measurement suggests otherwise. The significance of these observations is not certain, and may be within the limits of experimental error.

Finally, it appears that selectivity for quinoline is increased when using CsY zeolite which was contrary to our predictions. The reason for this is not yet clear although the low amounts adsorbed may present at least a partial explanation. Since the quantities involved are lower than with the other sorbents, small differences in our amounts adsorbed calculations (in absolute terms) would lead to large differences in the relative terms used to calculate selectivity.

5.10 Adsorption Kinetics

In an interesting extension of the new calculation method the effluent concentration as a function of time can be calculated based on the heat flow curve. This results in a sort of duplicate breakthrough curve which, coupled with the breakthrough curve obtained from calorimeter effluent samples, can give interesting insight into the adsorption process. This technique also introduces the potential to calculate kinetic data such as rate constants from the heat flow curve.

Calculation of the effluent concentration is basically the reverse of the calculation of the heat per mole adsorbed (Equation 19). The effluent concentration at any point in time is calculated as:

$$C_{\text{effluent}} (mM) = 3600 \frac{Q(mW)}{\Delta H_{\text{ads}} (kJ / mol) \cdot F (mL / h)} \quad (24)$$

This calculation relies on the assumption that differential heat of adsorption is not a function of coverage. This assumption may not be valid, particularly at high surface coverage. This exercise is presented in order to illus

An example of the data obtained from such a calculation is shown in Figure 23.

The heat flow curve was that measured during the experiment in the calorimeter. The theoretical breakthrough curve is determined using the heat flow curve and equation 24. The measured breakthrough curve is that obtained through analysis of calorimeter effluent samples.

The initial plateau in the theoretical breakthrough curve is simply due to the presence of the different solutions used in the calorimeter. Equation 25 was used indiscriminately, regardless of the fact that the feed concentration was not always 21.8 mmol/g. Before adsorption begins, feed is pure solvent, and thus no sorbate is being fed to the calorimeter. Equation 25 assumes that even during this initial phase, 21.8 mmol/L is being fed, and therefore must be being adsorbed since no sorbate is measured exiting the calorimeter.

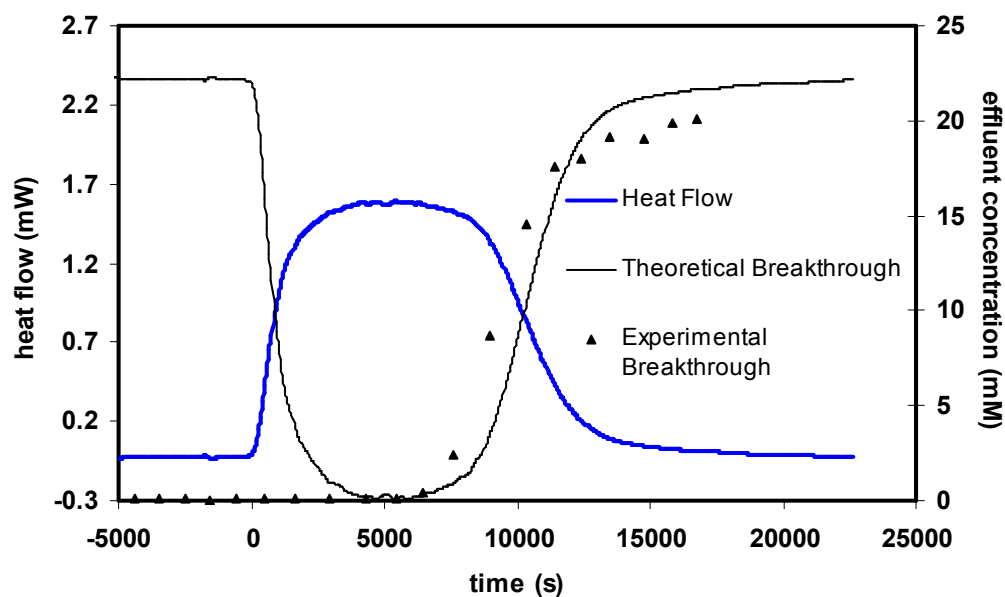


Figure 23. Adsorption kinetics curve for quinoline adsorption on NaY, using equation (24)

Ideally, the theoretical and actual breakthrough curves would overlap exactly. In Figure 23 the measured breakthrough occurs roughly 20 minutes before the theoretical breakthrough. This is likely due to mixing in the calorimeter. The bulk of the calorimeter system is narrow tubing

which is roughly analogous to a plug flow reactor (PFR), however the cell in which adsorption occurs would more accurately be described as a continuous stirred tank reactor (CSTR) as illustrated in Figure 24.

At low turnover frequencies, a CSTR can be assumed to be a completely mixed system. Due to the large volume of the cell relative to the flow rate, this may be assumed to be true. Sorbate molecules passing over the zeolite bed mix in the reservoir-type zone in the cell and exit before they would be expected to if the entire system behaved like a PFR.

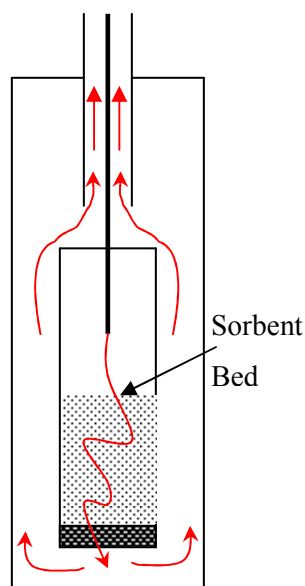


Figure 24. Schematic representation of calorimeter cell

Figure 25 and Figure 26 show the same calculations performed on the heat flow curves for NiY and CsY.

Both figures are similar to Figure 23, in that the measured breakthrough curve is about 20 minutes ahead of the theoretical breakthrough curves. Although not conclusive, the fact that the difference between the measured and theoretical curves is roughly 20 minutes in all cases supports the CSTR analogy. Since the flow rates and volume of the mixing zone are constant, the expected time difference between the curves is expected to be constant as well and independent of the sorbent present.

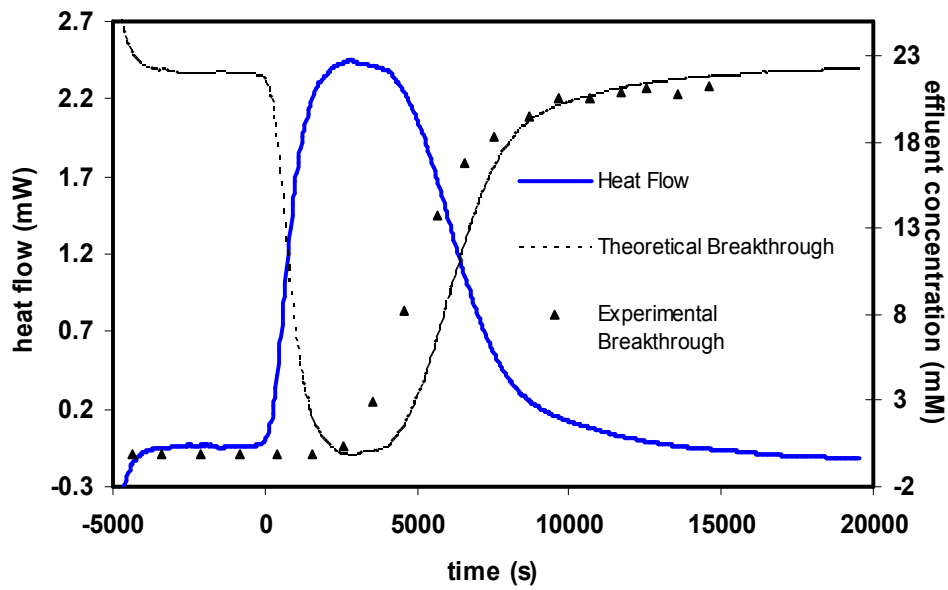


Figure 25. Adsorption kinetics curve for quinoline adsorption on NiY, using equation (24)

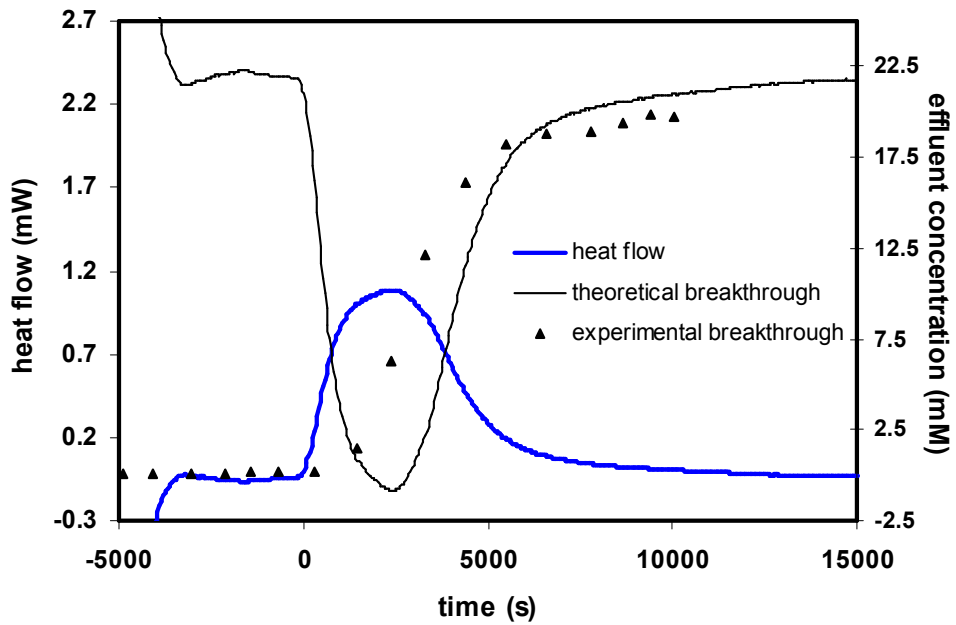


Figure 26. Adsorption kinetics curve for quinoline adsorption on CsY, using equation (24)

It may also be possible to calculate the adsorption rate based on the heat flow curve. Assuming that differential heat is independent of coverage, then

$$r(\text{mmol}/s) = Q(\text{mW}) \cdot \Delta H(\text{kJ}/\text{mol}) \cdot \left(\frac{10^3 \text{ mmol}}{\text{mol}} \right) \left(\frac{\text{mJ}}{10^6 \text{ kJ}} \right) \left(\frac{\text{mJ}}{\text{mW} \cdot s} \right) \quad (25)$$

With this rate data it may be possible to obtain relevant kinetic parameters such as rate constants. As discussed previously, for the adsorption reaction



The rate law is

$$-\frac{d[S]}{dt} = r = k_a[S]C - k_d[A-S] \quad (27)$$

Where :

k_a = adsorption rate constant

k_d = desorption rate constant

C = feed concentration

The amount adsorbed can be related by

$$\begin{aligned} [A-S] &= q \\ [S] &= q_m - q \end{aligned} \quad (28)$$

Where :

q = amount adsorbed (mmol/g)

q_m = adsorption capacity (mmol/g)

Substituting (29) into (28), we obtain

$$r = k_a C(q_m - q) - k_d q \quad (29)$$

Finally, rearranging (30) gives

$$r = k_a C q_m - q(k_a C + k_d) \quad (30)$$

From equation (31) a plot of r vs q should yield a straight line with a slope of $k_a C + k_d$ and an intercept of $k_a \cdot C \cdot q_e$. Thus, a plot of the rate of adsorption versus the amount adsorbed may be used to calculate the rate constants, provided the equilibrium adsorption capacity is known.

At the current stage in this research, these calculations are not feasible. Both the rate of adsorption and the adsorbed amount cannot be calculated from the heat flow curve, because the values would not be independent. To perform these calculations, it would be necessary to use the rate calculated from the heat flow curve, and the adsorbed amount calculated from another source, such as the breakthrough curve. Aside from the fact that breakthrough curves obtained to date have been unreliable, the shift discussed earlier in this section would present additional error. Modelling work to describe diffusion within the calorimeter would likely result in the breakthrough curve being put in a location more representative of where it should lie relative to the heat flow curve.

This technique may be extremely useful if it is developed to determine reliable, accurate rate constants. If developed in conjunction with the ability to accurately perform experiments at elevated temperatures, it may be possible to determine the actual heat of adsorption rather than the heat of displacement, via the Arrhenius Equation (Brazeau and Lipscomb, 2000):

$$\ln(k) = \ln(A) - \Delta H / RT \quad (31)$$

Where :

k = rate constant

A = pre-exponential factor

R = ideal gas constant

T = temperature(K)

$\Delta H = \Delta H_{ads}$ for adsorption

If rate constants are determined at different temperatures, T_1 and T_2 , then the heat of adsorption may be calculated by

$$\Delta H = R \cdot \ln\left(\frac{k_1}{k_2}\right) \left(\frac{1}{T_2} - \frac{1}{T_1}\right)^{-1} \quad (32)$$

Significant work is required before this method can be tested and implemented.

5.11 Comparison of Sorbents

Our work has studied three main adsorption parameters for assessment of the desulfurization ability of the various sorbents. In addition, significant work has been done developing a new technique for the measurement of the heat of adsorption. All work has been presented herein, although it is useful to provide a summary of the adsorption results in a qualitative fashion in order to comparatively assess the three sorbents studied and conclude which is the superior sorbent for desulfurization of our model diesel fuel. A summary of these parameters are presented including a ranking from 1 (best) to 3 (worst) in Table 18. A lower score indicates a more preferred sorbent.

Table 18. Relative ranking of sorbents studied

Sorbent	Heat of Adsorption	Sulfur Capacity	Quinoline Selectivity	Naphthalene Selectivity	Availability	Total Score
NaY	3	1	2	2	1	9
NiY	2	2	1	3	2	10
CsY	1	3	3	3	2	12

An explanation of some of the rankings in the table is warranted. The second column ranks the heats of adsorption of the sorbents, as determined in J/g-sorbent in competitive experiments. The reason for this is that this number represents the total heat evolved per unit mass of sorbent during adsorption, and therefore the theoretical energy required per unit mass of sorbent for regeneration in a competitive environment, such as in actual diesel fuel. Since the highest heat per gram of sorbent was for competitive adsorption on NaY zeolite, it would be the most expensive sorbent to regenerate, and thus receives the worst ranking, a 3. CsY on the other hand, evolved the lowest amount of heat during competitive experiments, and would thus be the least expensive to regenerate.

The third column simply lists the sorbents in order of decreasing sulfur capacity in single component experiments. Single component experiments were chosen for comparison rather than competitive experiments because amounts adsorbed in competitive experiments necessarily depend on both capacity and selectivity. The purpose of this analysis is to independently assess each parameter, so single component experiments were used. NaY had the highest capacity for DBT, while CsY had the lowest.

The fourth and fifth columns rank the sorbents in order of decreasing selectivity of sulfur over quinoline and naphthalene, respectively.

Finally the fifth column assess the availability of each sorbent. NaY was chosen as the most available, since it can simply be purchased in usable form. NiY and CsY were equally available, since they involved modifying the purchased NaY.

The final column is simply the sum of the five criteria for comparison of the sorbents. A lower score represents a superior sorbent. The minimum possible value in this table is 5, whereas the maximum was 20. In our work, the best sorbent was found to be NaY, with a value of 9. The sorbents, in order of decreasing suitability for desulfurization, are NaY>NiY>CsY.

These results are the conclusion of preliminary work. Further work with these three sorbents may alter their relative rankings. If, for example, the reason for the decreased surface area of our modified Y-zeolites is determined and corrected, new modified Y-zeolites may have a higher sulfur removal capacity and thus make them preferred over NaY, as has been suggested in the literature.

As well, further work studying different sorbents, or even different sorbent/sorbate systems, will allow Table 18 to be expanded to provide a more thorough analysis.

Long term goals would likely involve scale-up and commercialization of a desulfurization adsorption column. In such a case, more factors will have to be included such as the cost of providing sufficient adsorbent, and possibly safety concerns with preparation, transportation and use of the adsorbents.

6 Conclusions

1. Calorimetric adsorption experiments indicate a reliable technique for simultaneous determination of heats of displacement and adsorption amounts has been developed. Although opportunity exists to improve upon the technique and the utility of the results obtained therein, this work represents significant progress in the field of liquid phase flow calorimetry which, to our knowledge, has not been previously presented in the literature.
2. It appears that within our experimental range of 6mM to 43.5 mM, the feed concentration has little or no effect on the molar heat of adsorption in our calorimeter experiments. These results are considered preliminary, however, and must be verified.
3. There is little difference in selectivity between the modified Y-type zeolites. In general, selectivity decreases in the order Naph>DBT>Quin. This suggests that aromatics are adsorbed least strongly, followed by the sulfur species. The nitrogen-containing species are preferentially adsorbed by a large margin. The only deviation from this trend occurs on CsY zeolite, where there is evidence that naphthalene adsorption is slightly preferred to that of DBT. These findings indicate that sulfur removal from diesel fuel would be difficult with these sorbents since, due to the preference for quinoline adsorption and the high concentration of competitively adsorbed aromatics, sulphur adsorption would likely be inefficient.
4. In general, adsorption capacity of the sorbents increases in the order CsY<NiY<NaY. The decreased capacity of the modified zeolites appears to be the result of disruption of the crystalline structure due to the modification processes employed.
5. Good qualitative agreement was found between relative heats of displacement and selectivity. Since our procedure measured heat of displacement and not heat of adsorption, it is difficult to establish a quantitative relationship between the parameters, but qualitative analysis suggests that as heat of displacement increases relative to a particular compound, so too does selectivity relative to that compound.
6. In terms of desulfurization capability, our results indicate that the sorbents, in decreasing order of suitability, are NaY>NiY>CsY. On the basis of this work, NaY is the preferred desulfurization sorbent since it represents the highest capacity for sulfur removal coupled with moderate heats of displacement, allowing for easier and more economical sorbent regeneration. These results differ from those in the literature suggesting an increased

removal capacity for NiY over NaY. This discrepancy is likely due to degradation of the crystalline structure of our zeolites during modification, a phenomenon not observed by other research groups.

7. Variability in adsorbed amounts based on breakthrough curve calculations may be attributable to slight differences in particle size distribution. This variability manifests itself from differences in diffusion limitation when the rate of adsorption is small, making it impossible to resolve the difference with current instrumentation.
8. Equilibrium is not necessarily reached in the calorimeter. Flow adsorption results show that on NiY zeolite equilibrium is reached, however on NaY and CsY it is not. Therefore, equilibrium adsorption experiments cannot, in general, be used to predict adsorbed amounts during flow adsorption experiments. Adsorbed amount calculations via an independent method, such as the new method proposed in this work, are required to verify that equilibrium is reached.

7 Recommendations

1. Additional characterization should be conducted to further understand the mechanisms, thermodynamics and kinetics of the adsorption systems studied. Of immediate importance is obtaining more detailed structural information, including pore size distribution. This data could broaden knowledge in this area extensively. Experiments to determine spatial orientation of adsorbed molecules relative to sorbent surface would allow for potential verification of theories put forward in this work.
2. Flow adsorption calorimetric studies examining different sorbate molecules could also illuminate possible adsorption mechanisms. Adsorption of thiophenic molecules of different sizes, such as benzothiophene (BT) and 4,6-dimethyldibenzothiophene (DMDBT) would allow for verification of the theory of size exclusion reducing selectivity of CsY for DBT. Further, adsorption of structurally similar molecules with different heteroatoms (if any) such as DBT, fluorene and carbazole would control several variables not controlled in our current work. These sorbate molecules would have comparable sizes and physical adsorption characteristics, and vary only in adsorption properties related to the sulfur or nitrogen atom.
3. Competitive adsorption experiments should be conducted with varying sorbate concentrations in order to produce a more representative model diesel fuel. For example, the capacity of NaY for a 900ppm DBT/C₁₆ solution may be significantly altered in the presence of 20 wt% aromatic (such as naphthalene) as would be encountered in actual fuel.
4. Adsorption of an actual diesel fuel should be studied using flow calorimetry. This is not one of the primary goals of our work, since the heat flow curve generated from such a complex mixture would be effectively meaningless. This work is important nonetheless, as it allows assessment of the applicability of predictions made based on calorimetry work to sulphur removal in actual diesel fuel
5. Verification of the proposed method of calculating the heat of adsorption and amount adsorbed is recommended. Experiments with immediate urgency include repeating previous experiments (i.e. DBT/C₁₆ adsorption on NaY) with varying flow rates and feed concentrations. Our method assumes that changing these values (within reasonable

limits) should not affect the obtained heat of adsorption results, and this critical assumption should be verified.

6. Modeling work should be commenced in order to utilize the data currently being obtained in our calorimeter experiments. The thermodynamic and kinetic data are currently not being utilized to their full potential. Modeling work would maximize the utility of our results as well as increase our understanding of the data being obtained and its applications.
7. An additional class of sorbate molecules which may be studied is oxygenated molecules. Previous work by Yang et al has shown that oxygenate adsorption is preferred even to that of nitrogen containing compounds. These molecules are not of large concern for practical desulfurization purposes; however, since oxygenates are generally fuel additives and therefore are not necessarily present during the desulfurization stage of fuel processing.
8. Examine adsorption on different sorbents to assess their potential for desulfurization. Much promise has been shown in adsorption on Cu(I)-Y zeolite. Other transition metal or alkali earth metal exchanged Y zeolites may alter sulfur selectivity and heats of adsorption in a favourable manner.
9. Provided the theory regarding the spatial orientation of quinoline on Y-type zeolites is correct, new sorbents may be designed to exploit this phenomenon to increase sulfur selectivity. Due to the suspected difference in orientation between the nitrogen containing species and the sulfur containing and aromatic, alterations in pore structure may exclude nitrogen adsorption, or at least force the nitrogen containing molecules to 'lie flat' and form complexes between the cation and their π -electrons, rather than forming a strong bond with the lone pair.
10. Experimentation with sorbent preparation techniques may improve the adsorption process. For example, ion exchange can be conducted in the liquid and vapour phases, as well as the solid state. It has been shown that solid state ion exchange (SSIE) for Ni produces 100% exchange of Na^+ ions. Increasing the degree of ion exchange would allow more complete exploitation of different properties of different cations. Also, results show that deformation of the zeolite structure occurs in our work to a greater degree than in the

work of other groups. Examination of preparation procedures employed in our group to address this challenge could possibly increase the capacity of sorbents used in our work.

11. The possibility of calcining sorbents in-situ should be examined. Since exposure to the atmosphere leads to moisture adsorption and in some cases (such as with Cu(I)-Y zeolite) auto-reduction of the framework cations, in situ calcination is required. Work herein has been carried out to carefully minimize the exposure time of the sorbents however exposure to the atmosphere could not be completely eliminated. A provided experimental configuration to allow in-situ calcinations is proposed in Appendix C, however it is merely conceptual and a significant amount of development would be required to implement it.
12. Additional process development should focus on temperature control in the calorimeter. Previous work has found that baseline shifts occur at high temperatures due to insufficient feed temperature control. Installation of temperature control to the feed solution on both the sample and reference sides of the calorimeter should eliminate this issue.
13. Once adequate temperature control is achieved, experiments should commence studying the effect of temperature on adsorption. The heats of adsorption and sulphur selectivity as a function of temperature should be studied in addition to adsorbed amounts.

8 References

- Baird, C., *Environmental Chemistry, 2ed*, W.H. Freeman, **1999**, New York
- Brazeau, B.J., Lipscomb, J.D., *Kinetics and Activation Thermodynamics of Methane Monooxygenase Compound Q Formation and Reaction with Substrates*, *Biochemistry* 29, **2000**, 13503-13515
- Breck, D.W., Acara, N.A., US Patent No. 3,216,789, **1965**
- Calero, S., Dubbeldam, D., Krishna, R., Smit, B., Vlugt, T.J.H., Denayer, J.F.M., Martens, J.A., Maesen, T.L.M., *Understanding the Role of Sodium during Adsorption: A Force Field for Alkanes in Sodium Exchanged Faujasites*, *Journal of the American Chemical Society* 126, **2004**, 11377-11386
- Chica, A., Corma, A., Domine, M.E., *Catalytic Oxidative Desulfurization (ODS) of Diesel Fuel on a Continuous Fixed-Bed Reactor*, *Journal of Catalysis* 242, **2006**, 299-308
- Coughlan, B., Keane, M.A., *The Effects of the Environment on the Growth of Nickel Metal Particles Supported on a Range of Y Zeolites Prepared by Ion Exchange and Impregnation*, *Zeolites* 11, **1991**, 2-11
- Corma, A., Fornes, V., Rey, F., *Quinoline as a Probe Molecule for Determination of External Bronsted and Lewis Acidity in Zeolites*, *Zeolites* 13, **1993**, 56-59
- Cooper, C.D., *Air Pollution Control: A Design Approach, 3ed*, Waveland Press **2002**, Prospect Heights, Ill.
- Creaser, D.C., *Ethylene Dimerization Kinetics : Kinetics And Selectivity for 1-Butene*, M.A.Sc. Thesis, **1992**, University of Waterloo
- Dooryhee, E., Catlow, C.R.A., Couves, J.W., Maddox, P.J., Thomas, J.M., Greaves, G.N., Steel, A.T., Townsend, R.P., *A Study of Cation Environment and Movement During Dehydration and Reduction of Nickel-Exchanged Zeolite Y by X-Ray Absorption and Diffraction*, *Journal of Physical Chemistry* 95, **1991**, 5414-4521

- Flanigen, E.M., *Zeolites and Molecular Sieves: An Historical Perspective* in Introduction to Zeolite Science and Practice 2ed. Ed. Van Bekkum, H., Flanigen, E.M., Jacobs, P.A., Jansen, J.C., Elsevier, **2001**, 11-36
- Gao, J., Wang, S., Jiang, Z., Lu, H., Yang, X., Jing, F., Li, C., *Deep Desulfurization from Fuel Oil via Selective Oxidation Using an Amphiphilic Peroxotungsten Catalyst Assembled in Emulsion Droplets*, Journal of Molecular Catalysis A: Chemical 258, **2006**, 261-266
- Groszek, A.J., *Flow Adsorption Microcalorimetry*, Thermochemica Acta 312, **1998**, 133-143
- Groszek, A.J., Lalik, E., Haber, J., *Heats of Displacement of Hydrogen from Palladium by Noble Gases*, Applied Surface Science, 252, **2005**, 654-659
- Haji, S., Erkey, C., *Removal of Dibenzothiophene from Model Diesel by Adsorption on Carbon Aerogels for Fuel Cell Applications*, Industrial Engineering and Chemistry Research 42, **2003**, 6933-6937
- Harai, T., Shiraishi, Y., Komasaawa, I., *Desulfurization Process for Dibenzothiophenes from Light Oil by Photochemical Reaction and Liquid-Liquid Extraction*, Industrial Engineering and Chemistry Research 35, **1996**, 586-589
- Harai, T., Shiraishi, Y., Komasaawa, I., *Effect of Photosensitizer and Hydrogen Peroxide on Desulfurization of Light Oil by Photochemical Reaction and Liquid-Liquid Extraction*, Industrial Engineering and Chemistry Research 36, **1997**, 530-533
- Harrison, R.M., Perry, R., *Handbook of Air Pollution Analysis, 2ed*, Chapman and Hall, **1986**, London
- Hernandez-Maldonado, A.J., Yang, R.T., *Desulfurization of Liquid Fuels by Adsorption via π -Complexation with Cu(I)-Y and Ag-Y Zeolites*, Industrial Engineering and Chemistry Research 42, **2003a**, 123-129
- Hernandez-Maldonado, A.J., Yang, R.T., *Desulfurization of Commercial Liquid Fuels by Selective Adsorption via π -Complexation with Cu(I)-Y Zeolite*, Industrial Engineering and Chemistry Research 42, **2003b**, 3103-3110

Hernandez-Maldonado, A.J., Yang, R.T., *Desulfurization of Diesel Fuels via π -Complexation with Nickel(II)-Exchanged X- and Y-Zeolites*, Industrial and Engineering Chemistry Research 43, **2004a**, 1081-1089

Hernandez-Maldonado, A.J., Stamatis, S.D., Yang, R.T., He, A.Z., Cannella, W., *New Sorbents for Desulfurization of Diesel Fuels via π -Complexation: Layered Beds and Regeneration*, Industrial and Engineering Chemistry Research 43, **2004b**, 769-776

Hernandez-Maldonado, A.J., Yang, R.T., *Desulfurization of Transportation Fuels by Adsorption*, Catalysis Reviews 46(2), **2004c**, 111-150

Hernandez-Maldonado, A.J., Yang, R.T., *New Sorbents for Desulfurization of Diesel Fuels via π -Complexation*, AIChE Journal 50(4), **2004d**, 791-801

Hernandez-Maldonado, A.J., Yang, F.H., Qi, G., Yang, R.T., *Desulfurization of Transportation Fuels by π -Complexation Sorbents Cu(I)-, Ni(II)-, and Zn(II)-Zeolites*, Applied Catalysis B: Environmental 56, **2005**, 111-126

Hines, A.L., Maddox, R.N., *Mass Transfer: Fundamentals and Applications*, Prentice-Hall, **1985**, Upper Saddle River, NJ

Ho, T.C., *Deep HDS of Diesel Fuel: Chemistry and Catalysis*, Catalysis Today 98, **2004**, 3-18

Ho, Y.S., *Selection of Optimum Sorption Isotherm*, Carbon 42, **2004b**, 2115-2116

Hughley, C.A., Rodgers, R.P., Marshall, A.G., Walters, C.C., Qian, K., Mankiewicz, P., *Acidic and Neutral Polar NSO Compounds in Smackover Oils of Different Thermal Maturity Revealed by Electrospray High Field Fourier Transform Ion Cyclotron Resonance Mass Spectrometry*, Organic Geochemistry 35, **2004**, 863-880

Huntley, D.R., Mullins, D.R., Wingeier, M.P., *Desulfurization of Thiophenic Compounds by Ni(III): Adsorption and Reactions of Thiophene, 3-Methylthiophene, and 2,5-Dimethylthiophene*, Journal of Physical Chemistry 100, **1996**, 19620-19627

Jansen, J.C., *The Preparation of Oxide Molecular Sieves in Introduction to Zeolite Science and Practice 2ed.* Ed. Van Bekkum, H., Flanigen, E.M., Jacobs, P.A., Jansen, J.C., Elsevier, **2001**, 175-227

Jayaraman, A., Yang, F.H., Yang, R.T., *Effects of Nitrogen Compounds and Polyaromatic Hydrocarbons on Desulfurization of Liquid Fuels by Adsorption via π -Complexation with Cu(I)Y Zeolite*, Energy & Fuels 20, **2006**, 909-914

Jayne, D., Zhang, Y., Haji, S., Erkey, C., *Dynamics of Removal of Organosulfur Compounds from Diesel by Adsorption on Carbon Aerogels for Fuel Cell Applications*, International Journal of Hydrogen Energy 30, **2005**, 1287-1293

Jiang, M., Ng, F.T.T., Rahman, A., Patel, V., *Flow Calorimetric and Thermal Gravimetric Study of Adsorption of Thiophenic Sulfur Compounds on NaY Zeolite*, Thermochemica Acta 434, **2005**, 27-36

Jiang, M., Ng, F.T.T., *Adsorption of Benzothiophene on Y Zeolites Investigated by Infrared Spectroscopy and Flow Calorimetry*, Catalysis Today 116, **2006**, 530-536

Kim, J.H., Ma, X., Zhou, A., Song, C., *Ultra-Deep Desulfurization and Denitrogenation of Diesel Fuel by Selective Adsorption Over Three Different Adsorbents: A Study on Adsorptive Selectivity and Mechanism*, Catalysis Today 111, **2006**, 74-83

Koltai, T., Macaud, M., Milenkovic, A., Schulz, E., Lemaire, M., Vrinat, M., *Hydrodesulfurization of Diesel Feeds by Association of a Catalytic Process and a Separation Process Using Charge-Transfer Complexes*, Catalysis Letters 3-4, **2002**, 143-148

Kresge, C.T., Leonowicz, M.E., Roth, W.J., Vartuli, J.C., Beck, J.S., *Ordered Mesoporous Molecular Sieves Synthesized by a Liquid-Crystal Template Mechanism*, Nature 359, **1992**, 710-712

Laborde-Boutet, C., Joly, G., Nicolaos, A., Thomas, A., Magnoux, P., *Selectivity of Thiophene/Toluene Competitive Adsorptions onto Zeolites. Influence of the Alkali Metal Cation in FAU(Y)*, Industrial Engineering and Chemistry Research 45, **2006**, 8111-8116

Larrubia, M.A., Gutierrez-Alejandre, A., Ramirez, J., Busca, G., *A FT-IR Study of the Adsorption of Indole, Carbazole, Benzothiophene, Dibenzothiophene, and 4,6-Dibenzothiophene Over Solid Adsorbents and Catalysts*, Applied Catalysis A: General 224, **2002**, 167-178

Lagerge, S., Zajac, J., Partyka, S., Groszek, A.J., *Comparative Study on the Adsorption of Cyanide Gold Complexes onto Different Carbonaceous Samples: Measurement of the*

Reversibility of the Process and Assessment of the Active Surface Sites Inferred by Flow Calorimetry, Langmuir 15, **1999**, 4803-4811

Le Parlouer, P., Mathonat, C., *Development of a New Thermographic and Calorimetric Technique for the Determination of Energetics, Thermodynamics and Kinetics of Hydrogen Storage in Various Materials*, Publication Date Unknown, Accessed online 11 Dec 2007, http://www.setaram.com/files/documents/article_WHTC07.pdf

Li, S.M., Barrie, L.A., Toom, D., *Seasonal Variations of Methanesulfonate, Non-Sea-Salt Sulfate, and Sulfur Dioxide at Three Sites in Canada*, Journal of Geophysical Research 101, **1996**, 4165-4174

Li, W., Xing, J., Xiong, X., Huang, J., Liu, H., *Feasibility Study on the Integration of Adsorption/Bioregeneration of π -Complexation Adsorbent for Desulfurization*, Industrial Engineering and Chemistry Research 45, **2006**, 2845-2849

Li, Y., Yang, F.H., Qi, G., Yang, R.T., *Effects of Oxygenates and Moisture on Adsorptive Desulfurization of Liquid Fuels with Cu(I)Y Zeolite*, Catalysis Today 116, **2006**, 512-518

Liang, F., Lu, M., Birch, M.E., Keener, T.C., Liu, Z., *Determination of Polycyclic Aromatic Sulfur Heterocycles in Diesel Particulate Matter and Diesel Fuel by Gas Chromatography With Atomic Emission Detection*, Journal of Chromatography A 1114, **2006**, 145-153

Liao, H., Adams, P.J., Ching, S.H., Seinfeld, J.H., Mickley, L.J., Jacob, D.J., *Interactions Between Tropospheric Chemistry and Aerosols in a Unified General Circulation Model*, Journal of Geophysical Research 108, **2003**, 4001-4024

Liu, B.S., Xu, D.F., Chu, J.X., Liu, W., Au, C.T., *Deep Desulfurization by the Adsorption Process of Fluid Catalytic Cracking (FCC) Diesel Over Mesoporous Al-MCM-41 Materials*, Energy & Fuels 21, **2007**, 250-255

Luo, M.F., Xing, J.M., Gou, Z.X., Li, S., Liu, H.Z., Chen, J.Y., *Desulfurization of Dibenzothiophene by Lyophilized Cells of Pseudomonas delafieldii R-8 in the Presence of Dodecane*, Biochemical Engineering Journal 13, **2000**, 1-6

- Ma, L., Yang, R.T., *Selective Adsorption of Sulfur Compounds: Isotherms, Heats and Relationship Between Adsorption from Vapour and Liquid Solution*, , Industrial Engineering and Chemistry Research 46, **2007a**, 2760-2768
- Ma, L., Yang, R.T., *Heats of Adsorption from Liquid Solutions and from Pure Vapor Phase: Adsorption of Thiophenic Compounds on NaY and 13X Zeolite*, , Industrial Engineering and Chemistry Research 46, **2007b**, 4874-4882
- Ma, X., Sakanishi, K., Mochida, I., *Hydrodesulfurization Reactivities of Various Sulfur Compounds in Diesel Fuel*, Industrial Engineering and Chemistry Research 33, **1994**, 218-222
- Ma, X., Sakanishi, K., Isoda, T., Mochida, I., *Quantum Chemical Calculation on the Desulfurization Reactivities of Heterocyclic Sulfur Compounds*, Energy & Fuels 9, **1995**, 33-37
- Ma, X., Sun, L., Song, C., *A New Approach to Deep Desulfurization of Gasoline Diesel Fuel and Jet Fuel by Selective Adsorption for Ultra-Clean Fuels and for Fuel Cell Applications*, Catalysis Today 77, **2002**, 107-116
- Macaud, M., Milenkovic, A., Schulz, E., Lemaire, M., Vrinat, M., *Hydrodesulfurization of Alkyldibenzothiophenes: Evidence of Highly Unreactive Aromatic Sulfur Compounds*, Journal of Catalysis 193, **2000**, 255-263
- Macaud, M., Seignon, M., Favre-Reguillon, A., Lemaire, M., Schulz, E., Vrinat, M., *Novel Methodology Toward Deep Desulfurization of Diesel Feed Based on the Selective Elimination of Nitrogen Compounds*, Industrial Engineering and Chemistry Research 43, **2004**, 7843-7849
- Maesen, T., Marcus, B., *The Zeolite Scene – An Overview* in Introduction to Zeolite Science and Practice 2ed. Ed. Van Bekkum, H., Flanigen, E.M., Jacobs, P.A., Jansen, J.C., Elsevier, **2001**, 1-9
- Mathonat, C., Majer, V., Mather, A.E., Grolier, J-P. E., *Use of Flow Calorimetry for Determining Enthalpies of Absorption and the Solubility of CO₂ in Aqueous Monoethanolamine Solutions*, Industrial Engineering and Chemistry Research 37, **1998**, 4136-4141
- Milenkovic, A., Schulz, E., Meille, V., Loffreda, D., Forissier, M., Vrinat, M., Sautet, P., Lemaire, M., *Selective Elimination of Alkyldibenzothiophenes from Gas Oil by Formation of Insoluble Charge-Transfer Complexes*, Energy & Fuels 13, **1999**, 881-887

Milenkovic, A., Loffreda, D., Schulz, E., Chermette, H., Lemaire, M., Sautet, P., *Charge Transfer Complexes Between Tetrinitrofluorenone and Polyaromatic Compounds from Gasoil: A Combined DFT and Experimental Study*, Physical Chemistry Chemical Physics 6, **2004**, 1169-1180

Milton, R.M., US Patent No. 2,882,243, **1959a**

Milton, R.M., US Patent No. 2,882,244, **1959b**

Ng, F.T.T., Rahman, A., Ohasi, T., Jiang, M., *A Study of the Adsorption of Thiophenic Sulfur Compounds Using Flow Calorimetry*, Applied Catalysis B: Environmental 56, **2005**, 127-136

Nkosi, B., Ng, F.T.T., Rempel, G.L., *The Oligomerization of 1-Butene Using NaY Zeolite Ion-Exchanged With Different Nickel Precursor Salts*, Applied Catalysis A: General 151, **1997**, 153-166

Oldfield, C., Pogrebinsky, O., Simmonds, J., Olson, E.S., Kulpa, C.F., *Elucidation of the Metabolic Pathway for Dibenzothiophene Desulfurization by Rhodococcus sp. Strain IGTS8 (ATCC 53968)*, Microbiology 143, **1997**, 2961-2973

Olson, D.H., *Crystal Structure of the Zeolite Nickel Faujasite*, Journal of Physical Chemistry 78, **1968**, 4366-4373

Oxtoby, D.W., Gillis, H.P., Nachtrieb, N.H., *Principles of Modern Chemistry 4ed.*, Saunders College Publishing, **1999**

Podrebarac, G.G., Ng, F.T.T., Rempel, G.L., *The Effect of Butadiene and Reaction Conditions on the Dimerization of 1-Butene Over NiY Zeolite*, Applied Catalysis A: General 147, **1996**, 159-173

Reid, N., Misra, P.K., Bloxam, R., Yap, D., Rao, S.T., Civerlo, K., Brankov, E., Vet, R.J., *Do We Understand Trends in Atmospheric Sulfur Species?*, Journal of the Air and Waste Management Association 51, **2001**, 1561-1567

Richards, F.J., *A Flexible Growth Function for Empirical Use*, Journal of Experimental Botany 10, **1959**, 290-300

- Sampanthar, J.T., Xiao, H., Dou, J., Nah, T.Y., Rong, X., Kwan, W.P., *A Novel Oxidative Desulfurization Process to Remove Refractory Sulfur Compounds from Diesel Fuel*, Applied Catalysis B: Environmental 63, **2006**, 85-93
- Sano, M., Maruo, T., Yamatera, H., Suzuki, M., Saito, Y., *EXAFS Studies on the Origin of Highly Catalytic Activity in Nickel Y Zeolite*, Journal of the American Chemical Society 109, **1987**, 52-55
- Sano, Y., Sugahara, K., Choi, K.H., Korai, Y., Mochida, I., *Two-Step Adsorption Process for Deep Desulfurization of Diesel Oil*, Fuel 84, **2005**, 903-910
- Schnoor, J.L., *Environmental Modeling: Fate and Transport of Pollutants in Water, Air and Soil*, J. Wiley and Sons, **1996**, New York
- Shiraishi, Y., Hirai, T., Komasaawa, I., *A Deep Desulfurization Process for Light Oil by Photochemical Reaction in an Organic Two-Phase Liquid-Liquid Extraction System*, Industrial Engineering and Chemistry Research 37, **1998**, 203-211
- Shiraishi, Y., Hirai, T., Komasaawa, I., *Identification of Desulfurization Products in the Photochemical Desulfurization Process for Benzothiophenes and Dibenzothiophenes from Light Oil Using an Organic Two-Phase Extraction System*, Industrial Engineering and Chemistry Research 38, **1999a**, 3300-3309
- Shiraishi, Y., Hara, H., Hirai, T., Komasaawa, W., *A Deep Desulfurization Process for Light Oil by Photosensitized Oxidation Using a Triplet Photosensitizer and Hydrogen Peroxide in an Oil/Water Two-Phase Liquid-Liquid Extraction System*, Industrial Engineering and Chemistry Research 38, **1999b**, 1589-1595
- Seinfeld, J.H., *Air Pollution: A Half Century of Progress*, AIChE Journal 50(6), **2004**, 1096-1108
- Shackelford, J.F., *Introduction to Materials Science for Engineers, 6ed*, Pearson Education Inc, **2005**, Upper Saddle River, NJ
- Smith, J.M., Van Ness, H.C., Abbott, M.M., *Introduction to Chemical Engineering Thermodynamics, 6ed.*, McGraw Hill, **2001**, New York
- Smith, S.J., Pitcher, H., Wigley, T.M.L., *Future Sulfur Dioxide Emissions*, Climatic Change 73(3), **2005**, 267-318

Song, C., Ma, X., Schmitz, A.D., Schobert, H.H., *Shape Selective Isopropylation of Naphthalene Over Mordenite Catalysts: Computational Analysis Using MOPAC*, Applied Catalysis A: General 182, **1999**, 175-181

Song, C., *Fuel Processing for Low-Temperature and High Temperature Fuel Cells – Challenges, and Opportunities for Sustainable Development in the 21st Century*, Catalysis Today 77, **2002**, 17-49

Song, C., *An Overview of New Design Approaches to Deep Desulfurization for Ultra-Clean Gasoline, Diesel Fuel and Jet Fuel*, Catalysis Today 86, **2003a**, 211-263

Stern, D.L., *Global Sulfur Emissions from 1850-2000*, Chemosphere 58, **2005**, 163-175

Takahashi, A., Yang, F.H., Yang, R.T., *New Sorbents for Desulfurization by π -Complexation: Thiophene/Benzene Adsorption*, Industrial Engineering and Chemistry Research 41, **2002**, 2487-2496

Teravainen, M.J., Pakarinen, J.M.H., Wickstrom, K., Vainiotalo, P., *Comparison of the Composition of Russian and North Sea Crude Oils and Their Eight Distillation Fractions Studied by Negative-Ion Electrospray Ionization Fourier Transform Ion Cyclotron Resonance Mass Spectrometry: The Effect of Suppression*, Energy & Fuels 21, **2007**, 266-273

Turnes Palomino, G., Bordiga, S., Zecchina, A., Marra, G.L., Lamberti, C., *XRD, XAS, and IR Characterization of Copper-Exchanged Y Zeolite*, Journal of Physical Chemistry B 104, **2000**, 8641-8651

Van Afferden, M., Tappe, D., Beyer, M., Truper, H.G., Klein, J., *Biochemical Mechanisms for the Desulfurization of Coal-Relevant Organic Sulfur Compounds*, Fuel 72, **1993**, 1635-1643

Van Koningsveld, H., *How to Build Zeolites in Introduction to Zeolite Science and Practice 2ed.* Ed. Van Bekkum, H., Flanigen, E.M., Jacobs, P.A., Jansen, J.C., Elsevier, **2001**, 69-174

Velu, S., Ma, X., Song, C., *Selective Adsorption for Removing Sulfur from Jet Fuel Over Zeolite Based Sorbents*, Industrial Engineering and Chemistry Research 42, **2003**, 5293-5304

Wang, Y., Yang, F.H., Yang, R.T., Heinzl, J.M., Nickens, A.D., *Desulfurization of High-Sulfur Jet Fuel by π -Complexation with Copper and Palladium Halide Sorbents*, Industrial Engineering and Chemistry Research 45, **2006**, 7649-7655

- Warneck, P., *Chemistry of the Natural Atmosphere, 2ed*, Academic Press, **2000**, San Diego
- Weitkamp, J., *Zeolites and Catalysis*, Solid State Ionics 131, **2000**, 175-188
- Wu, C.N., Tsai, T.S., Liao, C.N., Chao, K.J., *Controlling Pore Size Distributions of MCM-41 by Direct Synthesis*, Microporous Materials 7, **1996**, 173-185
- Xue, M., Chitrakar, R., Sakane, K., Hirotsu, T., Ooi, K., Yoshimura, Y., Feng, Q., Sumida, N., *Selective Adsorption of Thiophene and 1-Benzothiophene on Metal-Ion-Exchanged Zeolites in Organic Medium*, Journal of Colloid and Interface Science 285, **2005**, 487-492
- Yang, L., Wang, Y., Huang, D., Luo, G., Dai, Y., *Preparation of High Performance Adsorbents by Functionalizing Mesoporous Silica Spheres for Selective Adsorption of Organosulfur Compounds*, Industrial and Engineering Chemistry Research 46, **2007**, 579-583
- Yang, F.H., Hernandez-Maldonado, A.J., Yang, R.T., *Selective Adsorption of Organosulfur Compounds from Transportation Fuels by π -Complexation*, Separation Science and Technology 39(8), **2004a**, 1717-1732
- Yang, R.T., Takahashi, A., Yang, F.H., *New Sorbents for Desulfurization of Liquid Fuels by π -Complexation*, Industrial Engineering and Chemistry Research 40, **2001**, 6326-6329
- Yang, R.T., *Adsorbents: Fundamentals and Applications*, John Wiley and Sons, Inc, **2003**, Hoboken, NJ.
- Zhang, S., Zhang, Q., Zhang, Z.C., *Extractive Desulfurization and Denitrogenation of Fuels Using Ionic Liquids*, Industrial Engineering and Chemistry Research 43, **2004**, 614-622
- Zhou, A., Ma, X., Song, C., *Liquid-Phase Adsorption of Multi-Ring Thiophenic Sulfur Compounds on Carbon Materials with Different Surface Properties*, Journal of Physical Chemistry B 110, **2006**, 4699-47

9 Appendix A – Calibration Curves

9.1 Perkin Elmer GC

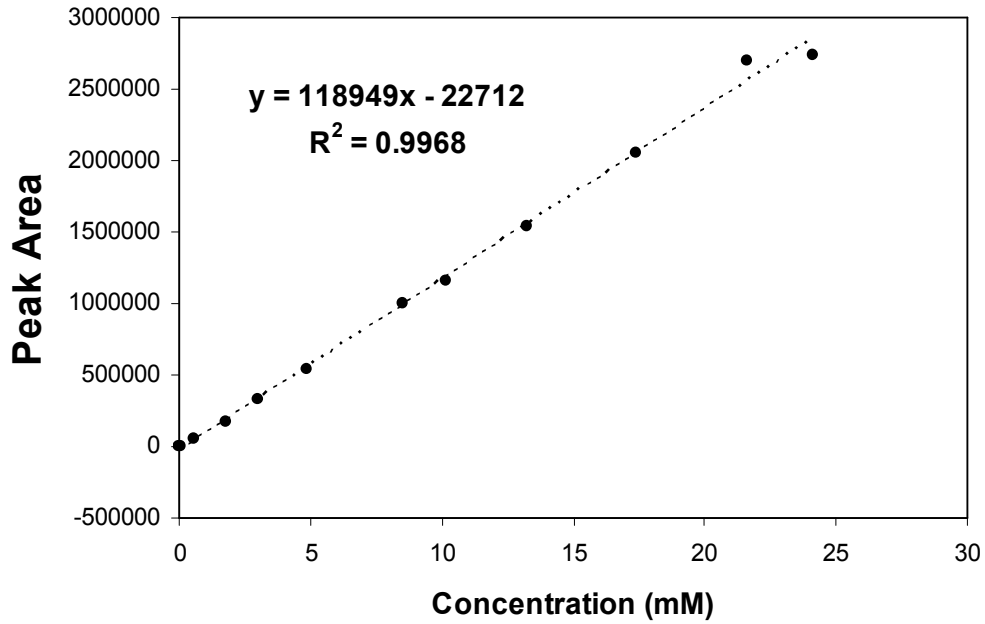


Figure 27. Sample calibration curve for DBT/C16 in Perkin Elmer GC

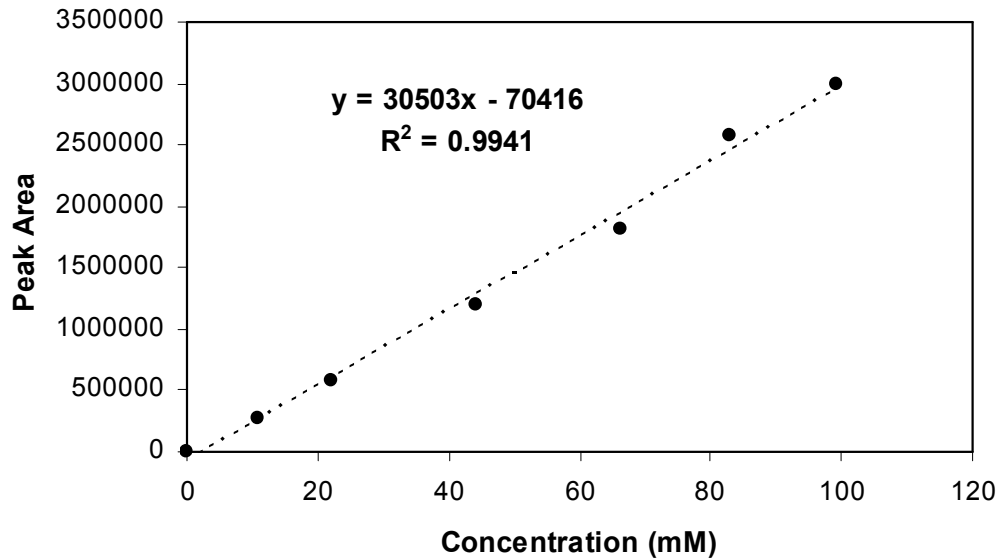


Figure 28. Sample calibration curve for quinoline/C16 on Perkin Elmer GC

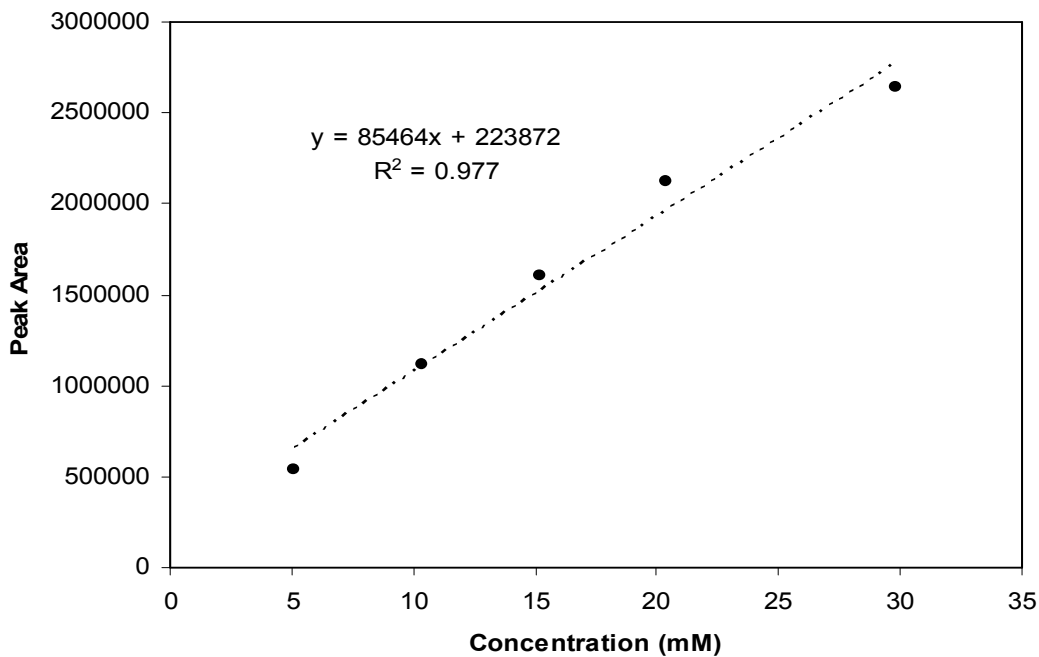


Figure 29. Sample calibration curve for naphthalene/C16 on Perkin Elmer GC

9.2 Varian GC

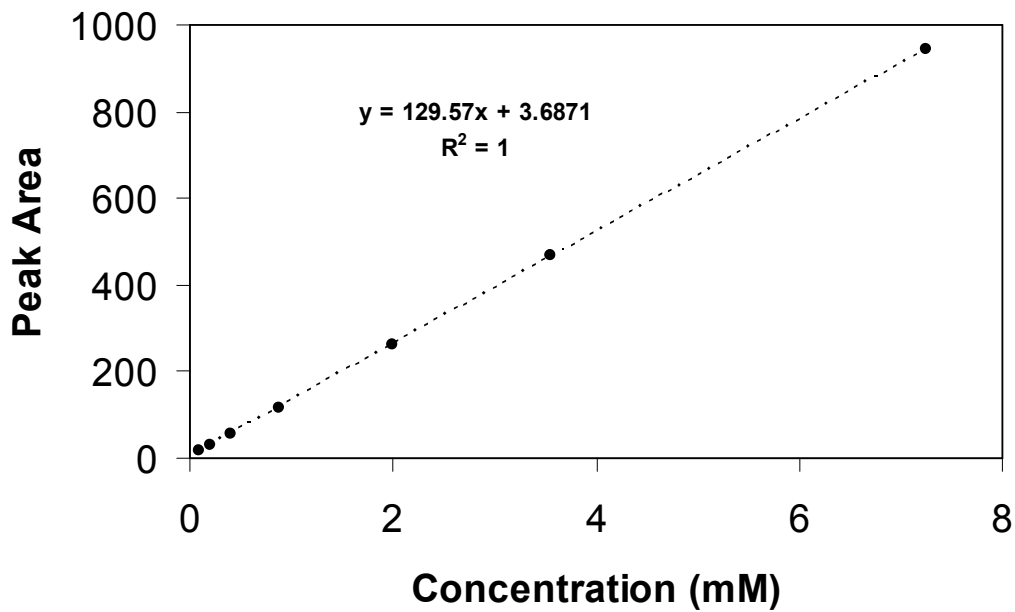


Figure 30. Calibration curve for DBT/C16 in the Varian GC

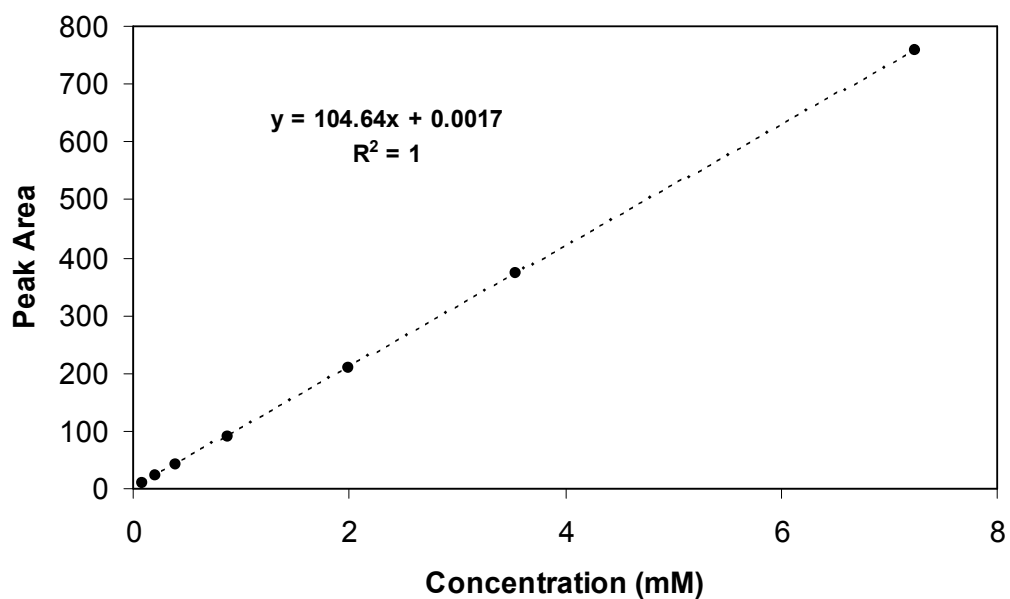


Figure 31. Calibration curve for naphthalene/C16 in the Varian GC

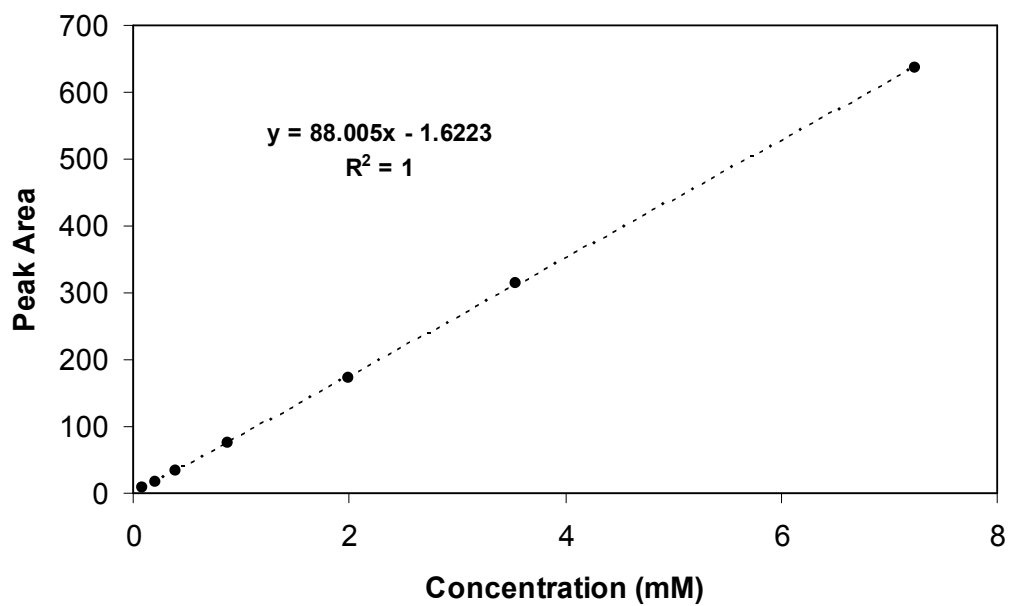


Figure 32. Calibration curve for quinoline/C16 in the Varian GC

10 Appendix B – Sample Calculations

Unit Cell Composition

Zeolite unit cells are composed of Al, Si, O, Na and in certain cases an additional cation (Cs, Ni in this work). The number of O atoms in a unit cell is taken to be constant at 384. Data was obtained giving the composition of the different zeolite samples.

For example, the composition of our NiY sample was found to be 8.26 wt% Al, 24.8 wt% Si, 1.87 wt% Na and 5.59 wt% Ni, with the balance assumed to be oxygen. Therefore, the sample contained $100-8.26-24.8-1.87-5.59=59.48$ wt% O.

To calculate the mass of a unit cell, we use

$$M_{U.C.} = \left(\frac{384 \text{ O atoms}}{U.C.} \right) \left(\frac{\text{atom}}{6.02 \times 10^{23}} \right) \left(\frac{16 \text{ g}}{\text{mol O atoms}} \right) \left(\frac{\text{g zeolite}}{0.5948 \text{ g O atoms}} \right) = 17.16 \times 10^{-21} \text{ g / U.C.}$$

The number of Ni atoms in that unit cell is then calculated as:

$$N_{Ni} = 17.16 \times 10^{-21} \text{ g / U.C.} \left(6.02 \times 10^{23} \text{ atom / mol} \right) \left(\frac{\text{mol Ni}}{58.69 \text{ g Ni}} \right) \left(\frac{0.0559 \text{ g Ni atoms}}{\text{g zeolite}} \right) = 9.83 \approx 10 \text{ Ni atoms / U.C.}$$

Composition value is rounded to the nearest whole number of atoms per unit cell. The above calculation is repeated for each species in the adsorbent to get its unit cell composition. The entire procedure is then repeated for each sorbent to obtain the values given in Table 9.

Heat of Adsorption

Heat of adsorption is calculated based on the heat flow curve. The baseline heat flow value is taken as the heat flow at the point where the curve begins to rise. In Figure 33 this point is at time 2:07, with a corresponding heat flow value of 0.36623mW. The peak value of the heat flow curve is 2.77978.

Therefore, the relative height of the curve is $2.77978-0.36623=2.41355$ mW. Assuming that this heat flow corresponds to complete adsorption of the quinoline being fed, and with a known flow

rate of 4.00mL/h and a known feed concentration of 21.8mM quinoline, the heat of adsorption is calculated as:

$$= 2.41355mW \left(\frac{mJ}{mW \cdot s} \right) \left(\frac{h}{4.00mL} \right) \left(\frac{L}{21.8mmol} \right) \left(\frac{3600s}{h} \right) \left(\frac{10^3 mL}{L} \right) \left(\frac{kJ}{10^6 mJ} \right) \left(\frac{10^3 mmol}{mol} \right)$$

$$= 99.64kJ / mol$$

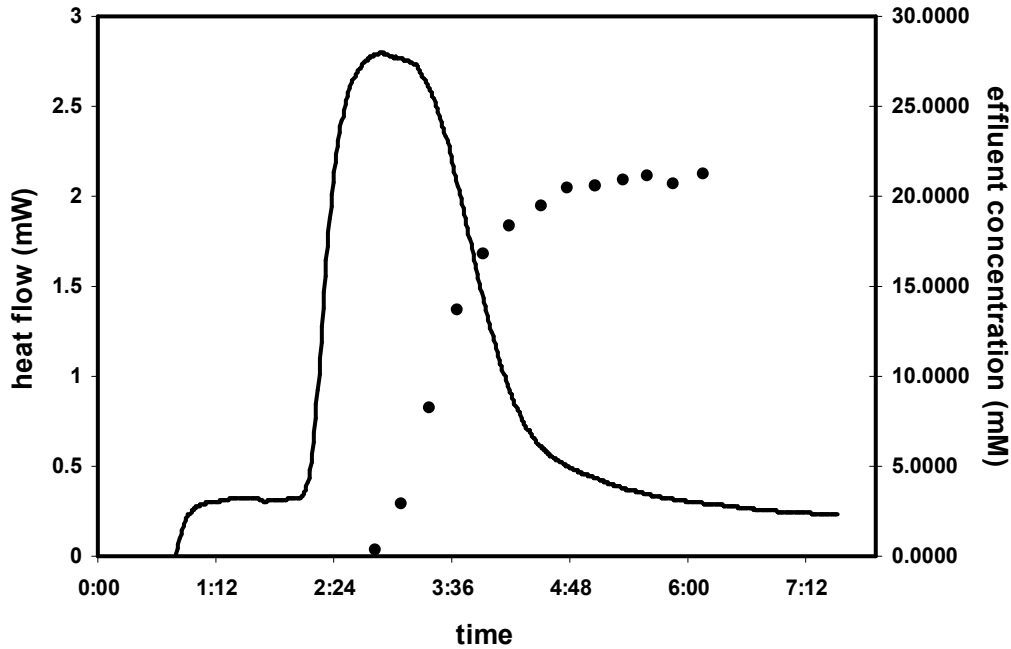


Figure 33. Experiment ID#4 – Quinoline/C16 on NiY

The heat flow curve is integrated using the resident Setsoft software to yield the total energy evolved in joules. In this case, the software calculated a value of 15.1J. Dividing 15.1J by the known zeolite mass (0.2472g), a heat flow of 61.1J/g is obtained.

Finally, to calculate the amount adsorbed, the ratio of the two heats is taken:

$$amount\ adsorbed = \frac{61.1J/g}{99.6kJ/mol} \left(\frac{1000mmol}{mol} \right) \left(\frac{kJ}{1000J} \right) = 0.613mmol / g$$

Breakthrough Curve Time Shift

As discussed previously, the time by which the breakthrough curve should be shifted is calculated as:

$$t_{shift} = t_{bed\ to\ outlet} = t_{valve\ to\ outlet} - t_{valve\ to\ bed}$$

As an example, in RUNID#5, the valve was switched from pure C16 to the quinoline/C16 solution at 1:27:25 pm. The solution was observed to hit the sorbent bed (by the sharp rise in the heat flow curve) at 1:54:57 pm. The difference between the two times is 27:32, or 1652 seconds.

The time it took the pure solvent to travel from the valve to the outlet of the system was determined with a stop watch to be 1:59:42, or 7182s. Thus, the time shift is calculated as:

$$t_{shift} = 7182 - 1652 = 5530s$$

Thus, the time at which each effluent sample is obtained should be shifted by 5530 seconds, or 1:32:10 in order to correspond with the heat flow curve.

11 Appendix C – Proposed Method for In-Situ Calcination

One limitation of our current work is the lack of a capability to calcine sorbents in-situ. Thus, during all experiments, sorbents are exposed to the atmosphere after calcination creating opportunities to adsorb moisture and affect heat of adsorption experiment results. Increased temperature control capabilities obtained by addition of a pre-heater to the calorimeter give rise to potential for in-situ calcination.

This appendix provides a theoretical method for in-situ calcination which has not been tested. It is based on several assumptions which must be verified, and requires the addition of equipment to the current experimental setup.

A general schematic is presented in Figure 34.

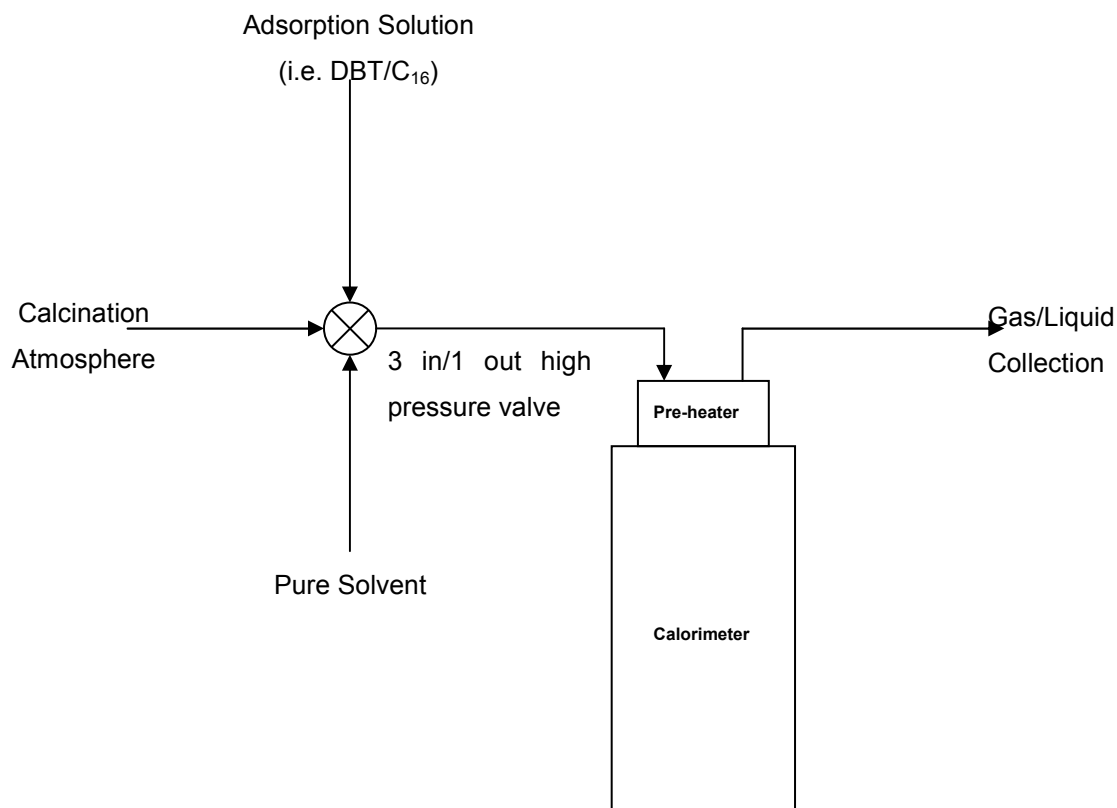


Figure 34. Schematic of in-situ calcinations apparatus

The first step in the new procedure would involve loading uncalcined sorbent into the calorimeter. The calcining atmosphere would then be passed over the bed through a four way valve, and the temperature ramped up to the required temperature for calcining (which may not

exceed 300°C). The calcination atmosphere would be maintained for the prescribed period of time, and the calorimeter would then be cooled to the temperature at which the experiment is to be conducted.

The possibility may exist at this point to increase the gas flow rate and/or to stop preheating the feed gas (if preheating is conducted) in order to accelerate cooling. Once the experiment temperature is attained, the feed would be switched to pure solvent, and experiments carried out as usual.

One major challenge to overcome is the ability to ascertain the sorbent mass. With the new adsorption calculation method (Appendix B), the sorbent mass is not required to determine the heat evolved per mole adsorbed, however the sorbent mass is required to determine the amount adsorbed per gram of sorbent. Two possibilities include describing the mass on a pre-calcined basis, or presenting the amount adsorbed simply in millimoles rather than millimoles per gram of sorbent.

In summary, some of the main points to be addressed in development of this procedure are:

- Verify the ability to calcine sorbents at temperatures of 300°C, and the treatment time and atmosphere required to do so
- Verify whether the reaction vessels used in the calorimeter can be used for gas flow, and if so the maximum pressure which it can support
- Address the ability (or inability) to know the mass of calcined zeolite in the calorimeter
- Determine required time to complete experiment based on temperature control of calorimeter. The length of time required to cool the calorimeter to low temperatures may be such that the amount of gas used, or the amount of time which the calorimeter is dedicated to a single experiment is unacceptable
- Purchase a new valve to allow the required number of feed streams to the calorimeter. The minimum requirement is three feeds (solution, pure solvent and gas) however more may be required if calcinations is carried out in different atmospheres

- Determine the possible requirement for additional temperature control. It may be necessary to pre-heat gases fed to the calorimeter in order to maintain the cell at the required temperature for calcining

The challenges to be addressed are not insignificant however there may be a time in the future when in-situ calcination becomes essential. At such a time this procedure should be examined in detail to determine its feasibility.

12 Appendix D – Breakthrough Curve Data

12.1 DBT/C16 on NaY

Table 19. Breakthrough Data – RUNID#9

t_{samp} (days)	C_{eff} (mmol/L)	t_{shifted} (s)	C_{eff}/C_o
0.024353	0.127168	-3268.9	0.005833
0.038502	0.060532	-2046.4	0.002777
0.053913	0.070001	-714.9	0.003211
0.064654	0.06998	213.0996	0.00321
0.074862	0.084096	1095.1	0.003858
0.087385	0.086255	2177.1	0.003957
0.10051	0.065113	3311.1	0.002987
0.112958	0.062253	4386.6	0.002856
0.1233	0.056072	5280.1	0.002572
0.133682	0.103001	6177.1	0.004725
0.148034	0.383956	7417.1	0.017613
0.163369	1.105581	8742.1	0.050715
0.179023	2.816153	10094.6	0.129181
0.194197	6.080987	11405.6	0.278944
0.207854	10.18939	12585.6	0.467403
0.222628	14.50445	13862.1	0.665342
0.238659	17.41622	15247.1	0.798909
0.252866	18.74987	16474.6	0.860086
0.264671	18.96586	17494.6	0.869993
0.275661	19.55567	18444.1	0.897049

Table 20. Breakthrough Data – RUNID#13

t_{samp} (days)	C_{eff} (mmol/L)	t_{shifted} (s)	C_{eff}/C_o
0.02673	0.544359	2309.5	0.024971
0.043096	0.456893	3723.5	0.020958
0.059468	0.407013	5138	0.01867
0.073235	0.373693	6327.5	0.017142
0.08695	0.391343	7512.5	0.017952
0.103171	0.390272	8914	0.017902
0.118883	0.459611	10271.5	0.021083
0.132488	1.067948	11447	0.048988
0.147014	2.965997	12702	0.136055
0.161806	5.7266	13980	0.262688
0.176053	9.83557	15211	0.451173
0.190347	14.58016	16446	0.668815
0.204271	19.25004	17649	0.883029
0.218889	21.87365	18912	1.003378
0.234699	23.70635	20278	1.087447

12.2 DBT/C16 on NiY

Table 21. Breakthrough Data – RUNID#11

t_{samp} (days)	C_{eff} (mmol/L)	t_{shifted} (s)	C_{eff}/C_o
0.050374	0.103949	-3266.7	0.004768
0.070652	0.076973	-1514.7	0.003531
0.084633	0.06513	-306.7	0.002988
0.095171	0.04684	603.7998	0.002149
0.107318	0.066598	1653.3	0.003055
0.120102	0.04684	2757.8	0.002149
0.131832	0.04684	3771.3	0.002149
0.142278	0.261476	4673.8	0.011994
0.153609	0.892413	5652.8	0.040936
0.16538	2.263588	6669.8	0.103834
0.177301	4.840766	7699.8	0.222053
0.188933	8.315107	8704.8	0.381427
0.197747	11.68931	9466.3	0.536207
0.208777	15.57205	10419.3	0.714314
0.222185	18.42604	11577.8	0.845231
0.236172	20.28635	12786.3	0.930566
0.252608	20.2821	14206.3	0.930372

Table 22. Breakthrough Data – RUNID#12

t_{samp} (days)	C_{eff} (mmol/L)	t_{shifted} (s)	C_{eff}/C_o
0.038387	0.034093	-3299.4	0.001263
0.050777	-0.00342	-2228.9	-0.00013
0.062657	-0.00897	-1202.4	-0.00033
0.075661	-0.03927	-78.900	-0.00145
0.089781	0.001136	1141.1	4.21E-05
0.104382	-0.03373	2402.6	-0.00125
0.12113	0.474564	3849.6	0.017576
0.135887	1.622659	5124.6	0.060098
0.147484	3.442762	6126.6	0.12751
0.160534	6.189759	7254.1	0.22925
0.171396	9.96058	8192.6	0.36891
0.183091	13.66486	9203.1	0.506106
0.195505	17.84497	10275.6	0.660925
0.20727	21.79177	11292.1	0.807103
0.22183	25.16405	12550.1	0.932002
0.236141	26.84036	13786.6	0.994087
0.247825	31.1273	14796.1	1.152863
0.259203	30.81295	15779.1	1.14122
0.268838	30.54801	16611.6	1.131408
0.262941	31.11616	16102.1	1.15245

12.3 DBT/C16 on CsY

Table 23. Breakthrough Data – RUNID#8

t_{samp} (days)	C_{eff} (mmol/L)	t_{shifted} (s)	C_{eff}/C_o
0.032036	0.089937	-3688.1	0.004126
0.0417	0.089751	-2853.1	0.004117
0.051486	0.089126	-2007.6	0.004088
0.062105	0.049682	-1090.1	0.002279
0.071509	0.278851	-277.6	0.012791
0.080971	2.46625	539.8999	0.113131
0.090873	8.173102	1395.4	0.374913
0.100416	12.77815	2219.9	0.586154
0.110948	15.33665	3129.9	0.703516
0.121654	16.77448	4054.9	0.769471
0.131723	17.65949	4924.9	0.810068
0.141903	18.45756	5804.4	0.846677
0.152632	18.33958	6731.4	0.841265
0.163847	18.56226	7700.4	0.85148
0.174756	18.9539	8642.9	0.869445
0.188564	19.12432	9835.9	0.877263
0.205115	18.91312	11265.9	0.867574
0.219542	19.13608	12512.4	0.877802
0.232256	19.42643	13610.9	0.891121
0.244293	19.83262	14650.9	0.909753
0.25751	20.06269	15792.9	0.920307
0.271862	19.81657	17032.9	0.909017
0.28262	20.23584	17962.4	0.92825

Table 24. Breakthrough Data – RUNID#10

t_{samp} (days)	C_{eff} (mmol/L)	t_{shifted} (s)	C_{eff}/C_o
0.049105	0.445121	-2534.3	0.020418
0.063677	0.383063	-1275.3	0.017572
0.075859	0.862811	-222.8	0.039578
0.088631	5.854306	880.6997	0.268546
0.101929	15.46036	2029.7	0.709191
0.115454	20.54277	3198.2	0.942329
0.130459	22.17861	4494.7	1.017367
0.144551	22.80017	5712.2	1.045879
0.158058	23.0601	6879.2	1.057803
0.171976	23.50639	8081.7	1.078275
0.185274	23.4879	9230.7	1.077426

12.4 Quinoline/C16 on NaY

Table 25. Breakthrough Data – RUNID#1

t_{samp} (days)	C_{eff} (mmol/L)	t_{shifted} (s)	C_{eff}/C_o
0.728649	-0.0180	-4893.7	-0.00069
0.744332	-0.0267	-3538.7	-0.00103
0.764575	-0.0385	-1789.7	-0.00148
0.784703	0.0005	-50.7031	1.89E-05
0.798528	0.0219	1143.797	0.000841
0.807602	0.0310	1927.797	0.001193
0.820223	0.0496	3018.297	0.001909
0.838377	0.1489	4586.797	0.005729
0.855275	0.9824	6046.797	0.037786
0.869853	2.9918	7306.297	0.11507
0.881786	6.3455	8337.297	0.244056
0.894679	11.6700	9451.297	0.448847
0.907307	17.1807	10542.3	0.660795
0.918817	21.3929	11536.8	0.822803
0.930831	23.5297	12574.8	0.904989
0.94435	25.9920	13742.8	0.999693
0.959865	25.6552	15083.3	0.98674
0.973713	26.7744	16279.8	1.029784
0.987058	27.0405	17432.8	1.040018
1.001433	28.0194	18674.8	1.077668
1.012162	26.6045	19601.8	1.02325

Table 26. Breakthrough Data – RUNID#2

t_{samp} (days)	C_{eff} (mmol/L)	t_{shifted} (s)	C_{eff}/C_o
0.649697	0.079614	-5700.2	0.003652
0.669147	0.052482	-4019.7	0.002407
0.692318	0.065042	-2017.7	0.002984
0.710819	0.115376	-419.203	0.005292
0.724743	0.034547	783.7968	0.001585
0.743117	0.150246	2371.297	0.006892
0.759477	0.197555	3784.797	0.009062
0.773464	0.221959	4993.297	0.010182
0.789714	1.005665	6397.297	0.046131
0.803609	3.217923	7597.797	0.147611
0.818649	7.662399	8897.297	0.351486
0.833001	11.64386	10137.3	0.534122
0.844315	13.91625	11114.8	0.63836
0.857434	15.70513	12248.3	0.720419
0.872104	17.0725	13515.8	0.783142
0.885796	18.34013	14698.8	0.84129
0.89961	18.90887	15892.3	0.867379
0.912145	19.4494	16975.3	0.892174
0.921867	19.99384	17815.3	0.917149
0.929841	19.93768	18504.3	0.914573
0.937978	20.15171	19207.3	0.924391

12.5 Quinoline/C16 on NiY

Table 27. Breakthrough Data – RUNID#4

t_{samp} (days)	C_{eff} (mmol/L)	t_{shifted} (s)	C_{eff}/C_o
0.037089	-0.13372	-4375.5	-0.00613
0.048657	-0.13714	-3376	-0.00629
0.062963	-0.15255	-2140	-0.007
0.077905	-0.14691	-849	-0.00674
0.092072	-0.10885	374.9995	-0.00499
0.106076	-0.06824	1585	-0.00313
0.11787	0.388555	2604	0.017824
0.1289	2.931857	3557	0.134489
0.14088	8.192149	4592	0.375787
0.153108	13.7106	5648.5	0.628927
0.164034	16.82253	6592.5	0.771676
0.175069	18.32849	7546	0.840756
0.187986	19.48285	8662	0.893709
0.199358	20.48214	9644.5	0.939548
0.211395	20.54264	10684.5	0.942323
0.223171	20.90485	11702	0.958938
0.233021	21.11831	12553	0.96873
0.244612	20.71703	13554.5	0.950323
0.256672	21.20401	14596.5	0.972661

Table 28. Breakthrough Data – RUNID#5

t_{samp} (days)	C_{eff} (mmol/L)	t_{shifted} (s)	C_{eff}/C_o
0.029186	-0.07257	-4375.3	-0.00333
0.040917	-0.09026	-3361.8	-0.00414
0.053301	-0.08562	-2291.8	-0.00393
0.066999	-0.06986	-1108.3	-0.0032
0.079221	-0.06092	-52.300	-0.00279
0.092057	-0.0339	1056.7	-0.00155
0.104979	0.021543	2173.2	0.000988
0.116559	0.705057	3173.7	0.032342
0.128214	3.451425	4180.7	0.158322
0.139719	8.30315	5174.7	0.380878
0.149644	13.02638	6032.2	0.59754
0.162583	16.59011	7150.2	0.761014
0.177705	18.65026	8456.7	0.855516
0.190118	19.10525	9529.2	0.876388
0.201409	18.89167	10504.7	0.86659
0.213799	19.56983	11575.2	0.897698
0.227051	20.94482	12720.2	0.960772
0.241906	21.03729	14003.7	0.965013
0.256611	21.0068	15274.2	0.963615
0.269997	21.24699	16430.7	0.974633
0.282236	21.30323	17488.2	0.977212

12.6 Quinoline/C16 on CsY

Table 29. Breakthrough Data – RUNID#6

t_{samp} (days)	C_{eff} (mmol/L)	t_{shifted} (s)	C_{eff}/C_o
0.016898	0.1070	-4896	0.004907
0.026591	0.1298	-4058.5	0.005955
0.038681	0.1186	-3014	0.005442
0.049375	0.1181	-2090	0.005416
0.057118	0.1359	-1421	0.006236
0.065775	0.1337	-673	0.006131
0.077269	0.1789	320	0.008205
0.090399	1.4547	1454.5	0.06673
0.101348	6.2974	2400.5	0.288872
0.111505	12.1580	3278	0.557707
0.124537	16.1201	4404	0.739456
0.136875	18.1749	5470	0.833709
0.149728	18.7503	6580.5	0.860107
0.163964	18.9343	7810.5	0.868546
0.174016	19.4003	8679	0.889923
0.182315	19.8711	9396	0.91152
0.190127	19.7459	10071	0.905777

Table 30. Breakthrough Data – RUNID#7

t_{samp} (days)	C_{eff} (mmol/L)	t_{shifted} (s)	C_{eff}/C_o
0.020737	0.153311	-4704.3	0.007033
0.033515	0.13901	-3600.3	0.006377
0.045784	0.137214	-2540.3	0.006294
0.057022	0.151601	-1569.3	0.006954
0.070292	0.160168	-422.8	0.007347
0.082734	0.194575	652.2	0.008925
0.091877	1.106582	1442.2	0.050761
0.100899	5.701251	2221.7	0.261525
0.110101	12.74291	3016.7	0.584537
0.126443	18.35595	4428.7	0.842016
0.143191	19.30416	5875.7	0.885512
0.153608	19.7274	6775.7	0.904926
0.163341	20.3874	7616.7	0.935202
0.17708	21.05202	8803.7	0.965689

12.7 Competitive Adsorption on NaY

Table 31. Breakthrough Data – RUNID#21

t_{samp} (days)	t_{shifted} (s)	C_{NAPH} (mmol/g)	C_{QUIN} (mmol/g)	C_{DBT} (mmol/g)
1:52:30	0:21:59	0.0000	0.0000	0.0000
2:08:22	0:37:51	0.0000	0.0000	0.0000
2:26:10	0:55:39	0.0000	0.0000	0.0000
2:41:05	1:10:34	0.0000	0.0000	0.0000
2:56:10	1:25:39	0.0000	0.0000	0.0000
3:11:30	1:40:59	0.0000	0.0000	0.0000
3:26:37	1:56:06	0.0000	0.0000	0.0000
3:41:29	2:10:58	0.0000	0.0000	0.0000
3:56:38	2:26:07	0.0000	0.0000	0.0000
4:11:38	2:41:07	0.0000	0.0000	0.0000
4:26:42	2:56:11	0.0000	0.0000	0.0000
4:41:46	3:11:15	0.0100	0.0000	0.0100
4:56:50	3:26:19	0.0200	0.0000	0.0200
5:11:48	3:41:17	0.0900	0.0000	0.0800
5:26:52	3:56:21	0.2700	0.0100	0.2600
5:41:56	4:11:25	0.6300	0.0700	0.6100
5:56:56	4:26:25	1.2100	0.2300	1.1300
6:12:01	4:41:30	2.0200	0.5400	1.8900
6:27:15	4:56:44	2.9600	0.9900	2.7300
6:42:02	5:11:31	3.8000	1.4800	3.5000
6:57:06	5:26:35	4.4800	1.9700	4.1500
7:12:14	5:41:43	5.0600	2.4100	4.6500
7:27:09	5:56:38	5.5700	2.8400	5.1500
7:42:15	6:11:44	5.9200	3.1700	5.4900
7:57:17	6:26:46	6.4600	3.6000	5.9100
8:12:43	6:42:12	6.6900	3.8400	6.2000
8:27:47	6:57:16	7.1500	4.2400	6.6600
8:53:08	7:22:37	7.4200	4.6400	6.8600
9:17:13	7:46:42	7.5600	5.1500	7.0300
9:40:48	8:10:17	7.5600	5.4200	7.0900
10:05:28	8:34:57	7.5300	5.6300	7.0700
10:32:30	9:01:59	7.3300	5.6500	6.9700
10:52:30	9:21:59	7.3300	5.7900	6.9800
11:14:48	9:44:17	7.2200	5.8100	6.8900
11:40:50	10:10:19	7.2200	5.9000	6.9100
12:04:20	10:33:49	7.1000	5.9200	6.8800
12:30:42	11:00:11	7.1400	6.0000	6.9700
12:50:02	11:19:31	7.1300	6.0300	6.9300
13:12:03	11:41:32	7.1200	6.0300	6.9200
13:31:15	12:00:44	7.0900	6.1000	6.8600

Table 32. Breakthrough Data – RUNID#22

t_{samp} (days)	t_{shifted} (s)	C_{NAPH} (mmol/g)	C_{QUIN} (mmol/g)	C_{DBT} (mmol/g)
1:59:23	0:14:40	0.0000	0.0000	0.0200
2:15:36	0:30:53	0.0000	0.0000	0.0200
2:30:42	0:45:59	0.0000	0.0000	0.0100
2:45:55	1:01:12	0.0000	0.0000	0.0200
3:00:44	1:16:01	0.0000	0.0000	0.0200
3:15:49	1:31:06	0.0000	0.0000	0.0100
3:30:46	1:46:03	0.0000	0.0000	0.0100
3:45:55	2:01:12	0.0000	0.0000	0.0100
4:00:54	2:16:11	0.0000	0.0000	0.0100
4:15:55	2:31:12	0.0000	0.0000	0.0100
4:31:00	2:46:17	0.0000	0.0000	0.0100
4:46:02	3:01:19	0.0100	0.0000	0.0200
5:00:58	3:16:15	0.0300	0.0000	0.0400
5:16:05	3:31:22	0.1400	0.0000	0.1500
5:31:13	3:46:30	0.4700	0.0000	0.4900
5:52:37	4:07:54	1.0700	0.0300	1.0700
6:08:13	4:23:30	1.2100	0.2300	1.1300
6:22:42	4:37:59	2.7300	1.1300	2.6200
6:37:45	4:53:02	3.8300	1.7900	3.6400
6:52:50	5:08:07	4.8700	2.5100	4.5400
7:07:55	5:23:12	6.0000	3.3500	5.6000
7:25:03	5:40:20	6.6000	3.3900	6.1100
7:40:08	5:55:25	7.1500	4.4600	6.5800
7:55:06	6:10:23	7.2500	4.9100	6.6900
8:10:10	6:25:27	7.3500	5.2600	6.8200
8:25:12	6:40:29	7.4100	5.5500	6.8800
8:40:11	6:55:28	7.3500	5.7600	6.9600
9:04:34	7:19:51	7.2100	5.8400	6.8300
9:30:15	7:45:32	7.2400	5.9700	6.8600
9:45:45	8:01:02	7.3200	6.1500	6.9700
10:09:59	8:25:16	7.3200	6.2300	6.9100
10:32:28	8:47:45	7.1600	6.2000	6.8000
10:59:40	9:14:57	7.3000	6.3800	6.8800
11:22:04	9:37:21	7.2000	6.3800	6.8900
11:51:20	10:06:37	7.1900	6.4200	6.8900
12:22:47	10:38:04	7.3100	6.5700	7.0100

12.8 Competitive Adsorption on NiY

Table 33. Breakthrough Data – RUNID#23

t_{samp} (days)	t_{shifted} (s)	C_{NAPH} (mmol/g)	C_{QUIN} (mmol/g)	C_{DBT} (mmol/g)
1:59:23	0:14:40	0.0000	0.0000	0.0200
2:15:36	0:30:53	0.0000	0.0000	0.0200
2:30:42	0:45:59	0.0000	0.0000	0.0100
2:45:55	1:01:12	0.0000	0.0000	0.0200
3:00:44	1:16:01	0.0000	0.0000	0.0200
3:15:49	1:31:06	0.0000	0.0000	0.0100
3:30:46	1:46:03	0.0000	0.0000	0.0100
3:45:55	2:01:12	0.0000	0.0000	0.0100
4:00:54	2:16:11	0.0000	0.0000	0.0100
4:15:55	2:31:12	0.0000	0.0000	0.0100
4:31:00	2:46:17	0.0000	0.0000	0.0100
4:46:02	3:01:19	0.0100	0.0000	0.0200
5:00:58	3:16:15	0.0300	0.0000	0.0400
5:16:05	3:31:22	0.1400	0.0000	0.1500
5:31:13	3:46:30	0.4700	0.0000	0.4900
5:52:37	4:07:54	1.0700	0.0300	1.0700
6:08:13	4:23:30	1.2100	0.2300	1.1300
6:22:42	4:37:59	2.7300	1.1300	2.6200
6:37:45	4:53:02	3.8300	1.7900	3.6400
6:52:50	5:08:07	4.8700	2.5100	4.5400
7:07:55	5:23:12	6.0000	3.3500	5.6000
7:25:03	5:40:20	6.6000	3.3900	6.1100
7:40:08	5:55:25	7.1500	4.4600	6.5800
7:55:06	6:10:23	7.2500	4.9100	6.6900
8:10:10	6:25:27	7.3500	5.2600	6.8200
8:25:12	6:40:29	7.4100	5.5500	6.8800
8:40:11	6:55:28	7.3500	5.7600	6.9600
9:04:34	7:19:51	7.2100	5.8400	6.8300
9:30:15	7:45:32	7.2400	5.9700	6.8600
9:45:45	8:01:02	7.3200	6.1500	6.9700
10:09:59	8:25:16	7.3200	6.2300	6.9100
10:32:28	8:47:45	7.1600	6.2000	6.8000
10:59:40	9:14:57	7.3000	6.3800	6.8800
11:22:04	9:37:21	7.2000	6.3800	6.8900
11:51:20	10:06:37	7.1900	6.4200	6.8900
12:22:47	10:38:04	7.3100	6.5700	7.0100

Table 34. Breakthrough Data – RUNID#24

t_{samp} (days)	t_{shifted} (s)	C_{NAPH} (mmol/g)	C_{QUIN} (mmol/g)	C_{DBT} (mmol/g)
2:33:03	0:21:06	0.0000	0.0000	0.0000
2:47:29	0:35:32	0.0000	0.0000	0.0100
3:03:02	0:51:05	0.0000	0.0000	0.0300
3:23:09	1:11:12	0.0000	0.0000	0.0300
3:42:39	1:30:42	0.0300	0.0000	0.0500
3:59:43	1:47:46	0.4200	0.0000	0.5400
4:17:34	2:05:37	1.0000	0.0100	1.1800
4:32:36	2:20:39	3.2300	0.5400	3.4700
4:54:08	2:42:11	5.9400	2.8500	5.9000
5:17:34	3:05:37	6.5400	4.3000	6.4100
5:32:55	3:20:58	6.6500	4.8400	6.5000
5:48:05	3:36:08	6.7700	5.2400	6.6100
6:03:31	3:51:34	6.6700	5.3400	6.5300
6:23:15	4:11:18	6.7100	5.4900	6.5000
6:38:25	4:26:28	6.6600	5.5300	6.4800
6:54:47	4:42:50	6.6600	5.5900	6.4700
7:10:26	4:58:29	6.7600	5.7400	6.5800
7:25:46	5:13:49	6.7700	5.7900	6.6600
7:40:38	5:28:41	6.8200	5.8500	6.6300
7:56:23	5:44:26	6.7000	5.7700	6.5300
8:12:16	6:00:19	6.7200	5.8300	6.4900
8:26:33	6:14:36	6.7400	5.9000	6.5700
8:40:34	6:28:37	6.6500	5.7900	6.4700
8:55:10	6:43:13	6.7200	5.8900	6.5400
9:09:12	6:57:15	6.6600	5.8400	6.4800

12.9 Competitive Adsorption on CsY

Table 35. Breakthrough Data – RUNID#25

t_{samp} (days)	t_{shifted} (s)	C_{NAPH} (mmol/g)	C_{QUIN} (mmol/g)	C_{DBT} (mmol/g)
1:49:00	0:19:11	0.0100	0.0000	0.0100
2:03:56	0:34:07	0.0000	0.0000	0.0100
2:19:05	0:49:16	0.0000	0.0000	0.0000
2:34:12	1:04:23	0.0100	0.0000	0.0100
2:49:15	1:19:26	0.0500	0.0000	0.0500
3:04:12	1:34:23	0.1900	0.0000	0.2300
3:19:12	1:49:23	0.4600	0.0100	0.5200
3:34:19	2:04:30	1.0000	0.0900	1.1400
3:49:22	2:19:33	2.8000	0.5800	3.0400
4:04:40	2:34:51	5.3500	2.0000	5.4800
4:25:28	2:55:39	6.8800	3.9200	6.8400
4:47:20	3:17:31	7.1800	5.0700	7.0800
5:07:55	3:38:06	7.0900	5.3400	7.0100
5:17:26	3:47:37	7.2200	5.6700	7.0700
5:37:08	4:07:19	7.3000	5.9700	7.1400
6:11:25	4:41:36	7.1600	5.9600	7.0500
6:33:03	5:03:14	7.2400	6.1300	7.0600
7:01:10	5:31:21	7.2500	6.1900	7.1300
7:26:30	5:56:41	7.2400	6.2200	7.0100
7:46:39	6:16:50	7.2900	6.3200	7.0900
8:02:22	6:32:33	7.2900	6.3600	7.0500
8:33:28	7:03:39	7.2100	6.3600	6.9600
8:52:30	7:22:41	7.3500	6.4800	7.1900
9:13:16	7:43:27	7.2600	6.3900	6.9400
9:30:20	8:00:31	7.2600	6.4300	6.9500

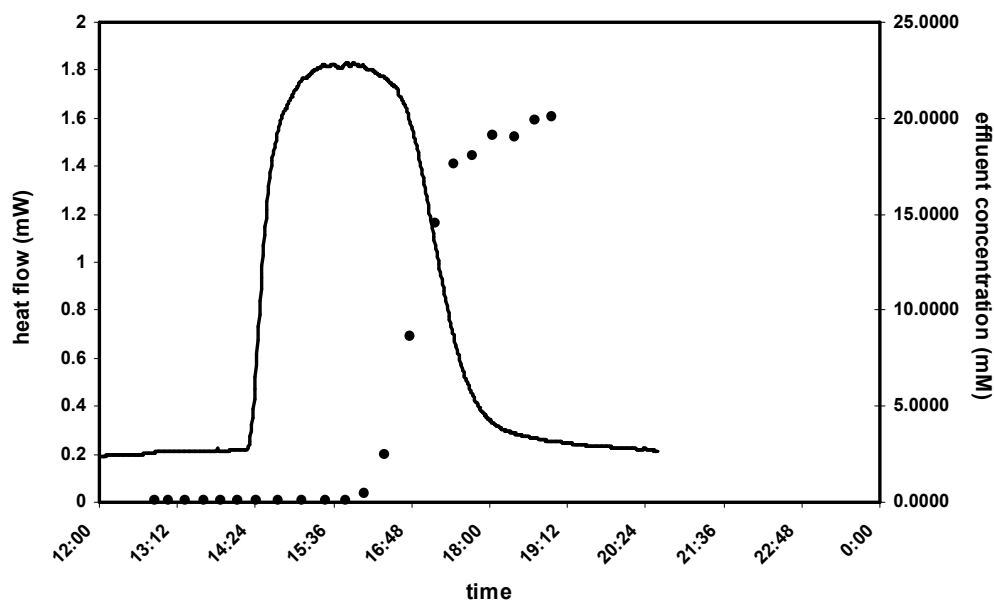
Table 36. Breakthrough Data – RUNID#26

t_{samp} (days)	t_{shifted} (s)	C_{NAPH} (mmol/g)	C_{QUIN} (mmol/g)	C_{DBT} (mmol/g)
2:33:03	0:21:06	0.0000	0.0000	0.0000
2:47:29	0:35:32	0.0000	0.0000	0.0100
3:03:02	0:51:05	0.0000	0.0000	0.0300
3:23:09	1:11:12	0.0000	0.0000	0.0300
3:42:39	1:30:42	0.0300	0.0000	0.0500
3:59:43	1:47:46	0.4200	0.0000	0.5400
4:17:34	2:05:37	1.0000	0.0100	1.1800
4:32:36	2:20:39	3.2300	0.5400	3.4700
4:54:08	2:42:11	5.9400	2.8500	5.9000
5:17:34	3:05:37	6.5400	4.3000	6.4100
5:32:55	3:20:58	6.6500	4.8400	6.5000
5:48:05	3:36:08	6.7700	5.2400	6.6100
6:03:31	3:51:34	6.6700	5.3400	6.5300
6:23:15	4:11:18	6.7100	5.4900	6.5000
6:38:25	4:26:28	6.6600	5.5300	6.4800
6:54:47	4:42:50	6.6600	5.5900	6.4700
7:10:26	4:58:29	6.7600	5.7400	6.5800
7:25:46	5:13:49	6.7700	5.7900	6.6600
7:40:38	5:28:41	6.8200	5.8500	6.6300
7:56:23	5:44:26	6.7000	5.7700	6.5300
8:12:16	6:00:19	6.7200	5.8300	6.4900
8:26:33	6:14:36	6.7400	5.9000	6.5700
8:40:34	6:28:37	6.6500	5.7900	6.4700
8:55:10	6:43:13	6.7200	5.8900	6.5400
9:09:12	6:57:15	6.6600	5.8400	6.4800

13 Appendix E – Calorimeter Experiment Summaries

EXPERIMENTAL DATA SUMMARY

Run ID #	1	Sorbent	NaY
Date	2-Jan-07	Solvent	n-C ₁₆
Temperature (°C)	30	Sorbate	Quinoline
Flow Rate (mL/h)	4.00	Concentration (mmol/L)	21.8
Sorbent Mass (g)	0.2520	Total Heat (J)	15.1582



Heat Flow Calculations

Peak Heat Flow (mW)	1.82351	ΔH (kJ/mol)	65.7
Baseline Heat Flow (mW)	0.23185	ΔH (J/g)	60.2
Corrected Peak (mW)	1.59166	q (mmol/g)	0.92

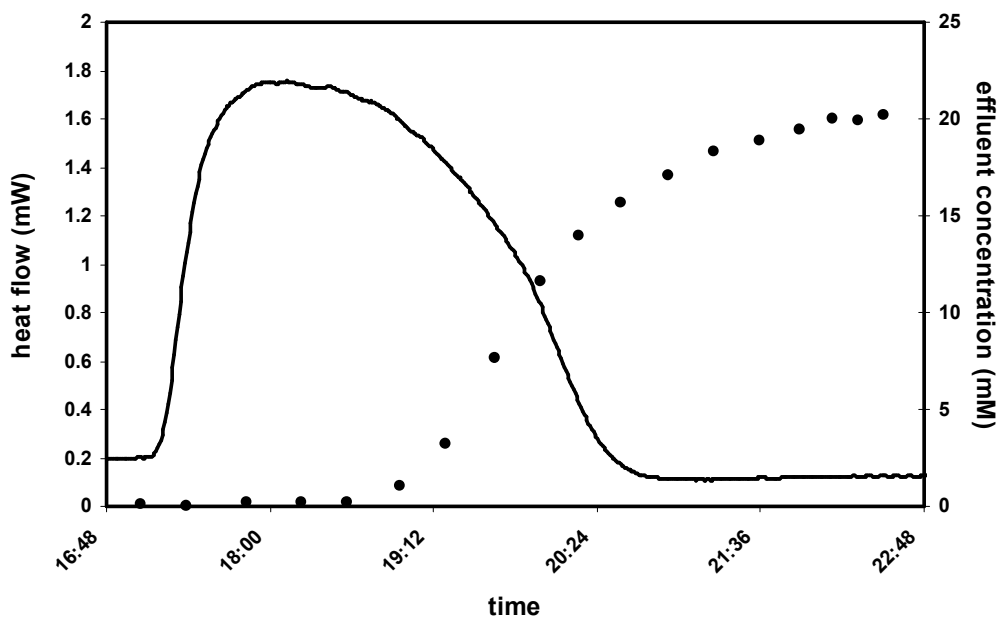
Breakthrough Curve Calculations

(Not used – for comparison purposes only)

Sorbate Fed (mmol)	0.417	ΔH (J/g)	60.2
Sorbate in Effluent (mmol)	0.172	q (mmol/g)	0.97
Amount Adsorbed (mmol)	0.245	ΔH (kJ/mol)	61.9

EXPERIMENTAL DATA SUMMARY

<table style="width: 100%; border-collapse: collapse;"> <tr><td style="border-right: 1px solid black; padding-right: 5px;">Run ID #</td><td style="text-align: center; padding-left: 5px;">2</td></tr> <tr><td style="border-right: 1px solid black; padding-right: 5px;">Date</td><td style="text-align: center; padding-left: 5px;">3-Jan-07</td></tr> <tr><td style="border-right: 1px solid black; padding-right: 5px;">Temperature (°C)</td><td style="text-align: center; padding-left: 5px;">30</td></tr> <tr><td style="border-right: 1px solid black; padding-right: 5px;">Flow Rate (mL/h)</td><td style="text-align: center; padding-left: 5px;">4.00</td></tr> <tr><td style="border-right: 1px solid black; padding-right: 5px;">Sorbent Mass (g)</td><td style="text-align: center; padding-left: 5px;">0.2480</td></tr> </table>	Run ID #	2	Date	3-Jan-07	Temperature (°C)	30	Flow Rate (mL/h)	4.00	Sorbent Mass (g)	0.2480	<table style="width: 100%; border-collapse: collapse;"> <tr><td style="border-right: 1px solid black; padding-right: 5px;">Sorbent</td><td style="text-align: center; padding-left: 5px;">NaY</td></tr> <tr><td style="border-right: 1px solid black; padding-right: 5px;">Solvent</td><td style="text-align: center; padding-left: 5px;">n-C₁₆</td></tr> <tr><td style="border-right: 1px solid black; padding-right: 5px;">Sorbate</td><td style="text-align: center; padding-left: 5px;">Quinoline</td></tr> <tr><td style="border-right: 1px solid black; padding-right: 5px;">Concentration (mmol/L)</td><td style="text-align: center; padding-left: 5px;">21.8</td></tr> <tr><td style="border-right: 1px solid black; padding-right: 5px;">Total Heat (J)</td><td style="text-align: center; padding-left: 5px;">13.5387</td></tr> </table>	Sorbent	NaY	Solvent	n-C ₁₆	Sorbate	Quinoline	Concentration (mmol/L)	21.8	Total Heat (J)	13.5387
Run ID #	2																				
Date	3-Jan-07																				
Temperature (°C)	30																				
Flow Rate (mL/h)	4.00																				
Sorbent Mass (g)	0.2480																				
Sorbent	NaY																				
Solvent	n-C ₁₆																				
Sorbate	Quinoline																				
Concentration (mmol/L)	21.8																				
Total Heat (J)	13.5387																				



Heat Flow Calculations

<table style="width: 100%; border-collapse: collapse;"> <tr><td style="border-right: 1px solid black; padding-right: 5px;">Peak Heat Flow (mW)</td><td style="text-align: center; padding-left: 5px;">1.74667</td></tr> <tr><td style="border-right: 1px solid black; padding-right: 5px;">Baseline Heat Flow (mW)</td><td style="text-align: center; padding-left: 5px;">0.21790</td></tr> <tr><td style="border-right: 1px solid black; padding-right: 5px;">Corrected Peak (mW)</td><td style="text-align: center; padding-left: 5px;">1.52877</td></tr> </table>	Peak Heat Flow (mW)	1.74667	Baseline Heat Flow (mW)	0.21790	Corrected Peak (mW)	1.52877	<table style="width: 100%; border-collapse: collapse;"> <tr><td style="border-right: 1px solid black; padding-right: 5px;">ΔH (kJ/mol)</td><td style="text-align: center; padding-left: 5px;">63.1</td></tr> <tr><td style="border-right: 1px solid black; padding-right: 5px;">ΔH (J/g)</td><td style="text-align: center; padding-left: 5px;">54.6</td></tr> <tr><td style="border-right: 1px solid black; padding-right: 5px;">q (mmol/g)</td><td style="text-align: center; padding-left: 5px;">0.86</td></tr> </table>	ΔH (kJ/mol)	63.1	ΔH (J/g)	54.6	q (mmol/g)	0.86
Peak Heat Flow (mW)	1.74667												
Baseline Heat Flow (mW)	0.21790												
Corrected Peak (mW)	1.52877												
ΔH (kJ/mol)	63.1												
ΔH (J/g)	54.6												
q (mmol/g)	0.86												

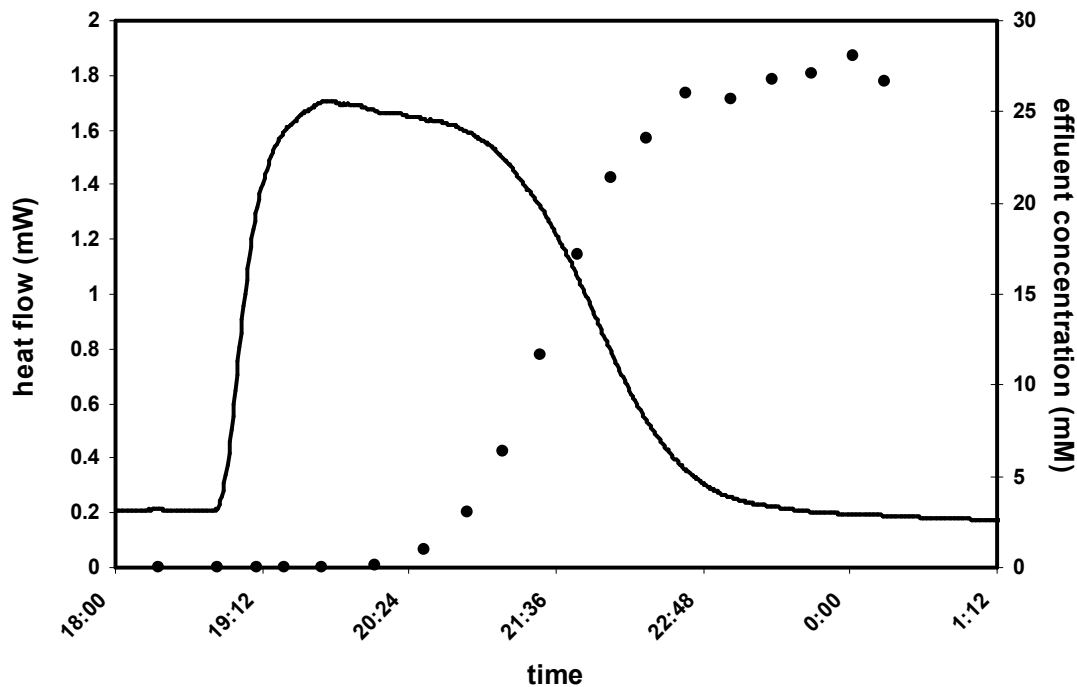
Breakthrough Curve Calculations

(Not used – for comparison purposes only)

<table style="width: 100%; border-collapse: collapse;"> <tr><td style="border-right: 1px solid black; padding-right: 5px;">Sorbate Fed (mmol)</td><td style="text-align: center; padding-left: 5px;">0.474</td></tr> <tr><td style="border-right: 1px solid black; padding-right: 5px;">Sorbate in Effluent (mmol)</td><td style="text-align: center; padding-left: 5px;">0.211</td></tr> <tr><td style="border-right: 1px solid black; padding-right: 5px;">Amount Adsorbed (mmol)</td><td style="text-align: center; padding-left: 5px;">0.263</td></tr> </table>	Sorbate Fed (mmol)	0.474	Sorbate in Effluent (mmol)	0.211	Amount Adsorbed (mmol)	0.263	<table style="width: 100%; border-collapse: collapse;"> <tr><td style="border-right: 1px solid black; padding-right: 5px;">ΔH (J/g)</td><td style="text-align: center; padding-left: 5px;">54.6</td></tr> <tr><td style="border-right: 1px solid black; padding-right: 5px;">q (mmol/g)</td><td style="text-align: center; padding-left: 5px;">1.06</td></tr> <tr><td style="border-right: 1px solid black; padding-right: 5px;">ΔH (kJ/mol)</td><td style="text-align: center; padding-left: 5px;">51.4</td></tr> </table>	ΔH (J/g)	54.6	q (mmol/g)	1.06	ΔH (kJ/mol)	51.4
Sorbate Fed (mmol)	0.474												
Sorbate in Effluent (mmol)	0.211												
Amount Adsorbed (mmol)	0.263												
ΔH (J/g)	54.6												
q (mmol/g)	1.06												
ΔH (kJ/mol)	51.4												

EXPERIMENTAL DATA SUMMARY

Run ID #	3	Sorbent	NaY
Date	5-Jan-07	Solvent	n-C ₁₆
Temperature (°C)	30	Sorbate	Quinoline
Flow Rate (mL/h)	4.00	Concentration (mmol/L)	21.8
Sorbent Mass (g)	0.2512	Total Heat (J)	15.1449



Heat Flow Calculations

Peak Heat Flow (mW)	1.69862	ΔH (kJ/mol)	60.5
Baseline Heat Flow (mW)	0.23387	ΔH (J/g)	60.3
Corrected Peak (mW)	1.46475	q (mmol/g)	1.00

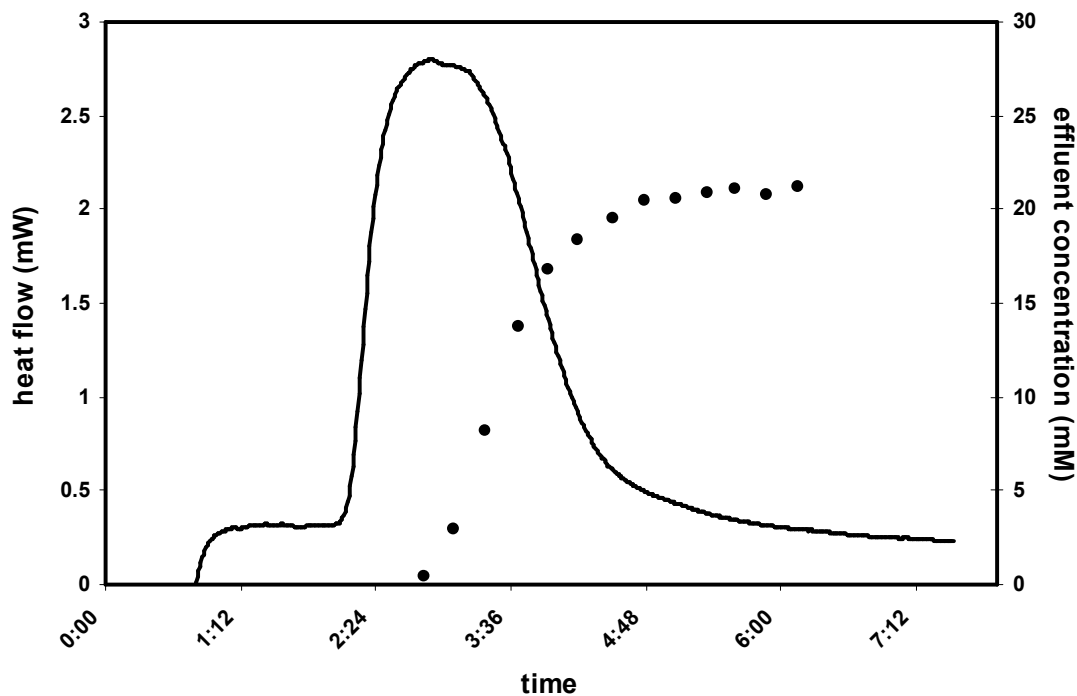
Breakthrough Curve Calculations

(Not used – for comparison purposes only)

Sorbate Fed (mmol)	0.591	ΔH (J/g)	60.3
Sorbate in Effluent (mmol)	0.300	q (mmol/g)	1.16
Amount Adsorbed (mmol)	0.291	ΔH (kJ/mol)	52.0

EXPERIMENTAL DATA SUMMARY

Run ID #	4	Sorbent	NiY
Date	11-Jan-07	Solvent	n-C ₁₆
Temperature (°C)	30	Sorbate	Quinoline
Flow Rate (mL/h)	4.00	Concentration (mmol/L)	21.8
Sorbent Mass (g)	0.2512	Total Heat (J)	15.0851



Heat Flow Calculations

Peak Heat Flow (mW)	2.77507	ΔH (kJ/mol)	101.0
Baseline Heat Flow (mW)	0.32771	ΔH (J/g)	61.0
Corrected Peak (mW)	2.44736	q (mmol/g)	0.60

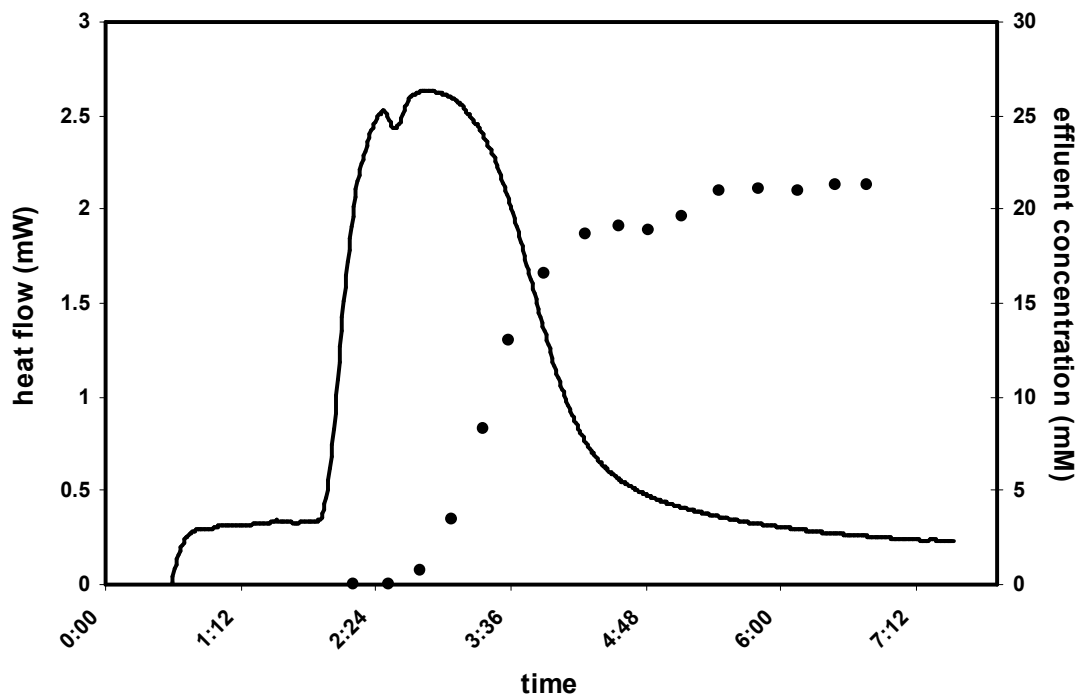
Breakthrough Curve Calculations

(Not used – for comparison purposes only)

Sorbate Fed (mmol)	0.365	ΔH (J/g)	61.0
Sorbate in Effluent (mmol)	0.226	q (mmol/g)	0.56
Amount Adsorbed (mmol)	0.139	ΔH (kJ/mol)	109.0

EXPERIMENTAL DATA SUMMARY

<table style="width: 100%; border-collapse: collapse;"> <tr><td style="border-right: 1px solid black; padding: 2px;">Run ID #</td><td style="padding: 2px;">5</td></tr> <tr><td style="border-right: 1px solid black; padding: 2px;">Date</td><td style="padding: 2px;">12-Jan-07</td></tr> <tr><td style="border-right: 1px solid black; padding: 2px;">Temperature (°C)</td><td style="padding: 2px;">30</td></tr> <tr><td style="border-right: 1px solid black; padding: 2px;">Flow Rate (mL/h)</td><td style="padding: 2px;">4.00</td></tr> <tr><td style="border-right: 1px solid black; padding: 2px;">Sorbent Mass (g)</td><td style="padding: 2px;">0.2518</td></tr> </table>	Run ID #	5	Date	12-Jan-07	Temperature (°C)	30	Flow Rate (mL/h)	4.00	Sorbent Mass (g)	0.2518	<table style="width: 100%; border-collapse: collapse;"> <tr><td style="border-right: 1px solid black; padding: 2px;">Sorbent</td><td style="padding: 2px;">NiY</td></tr> <tr><td style="border-right: 1px solid black; padding: 2px;">Solvent</td><td style="padding: 2px;">n-C₁₆</td></tr> <tr><td style="border-right: 1px solid black; padding: 2px;">Sorbate</td><td style="padding: 2px;">Quinoline</td></tr> <tr><td style="border-right: 1px solid black; padding: 2px;">Concentration (mmol/L)</td><td style="padding: 2px;">21.8</td></tr> <tr><td style="border-right: 1px solid black; padding: 2px;">Total Heat (J)</td><td style="padding: 2px;">15.3057</td></tr> </table>	Sorbent	NiY	Solvent	n-C ₁₆	Sorbate	Quinoline	Concentration (mmol/L)	21.8	Total Heat (J)	15.3057
Run ID #	5																				
Date	12-Jan-07																				
Temperature (°C)	30																				
Flow Rate (mL/h)	4.00																				
Sorbent Mass (g)	0.2518																				
Sorbent	NiY																				
Solvent	n-C ₁₆																				
Sorbate	Quinoline																				
Concentration (mmol/L)	21.8																				
Total Heat (J)	15.3057																				



Heat Flow Calculations

Peak Heat Flow (mW)	2.62385	ΔH (kJ/mol)	93.7
Baseline Heat Flow (mW)	0.35517	ΔH (J/g)	60.8
Corrected Peak (mW)	2.26868	q (mmol/g)	0.65

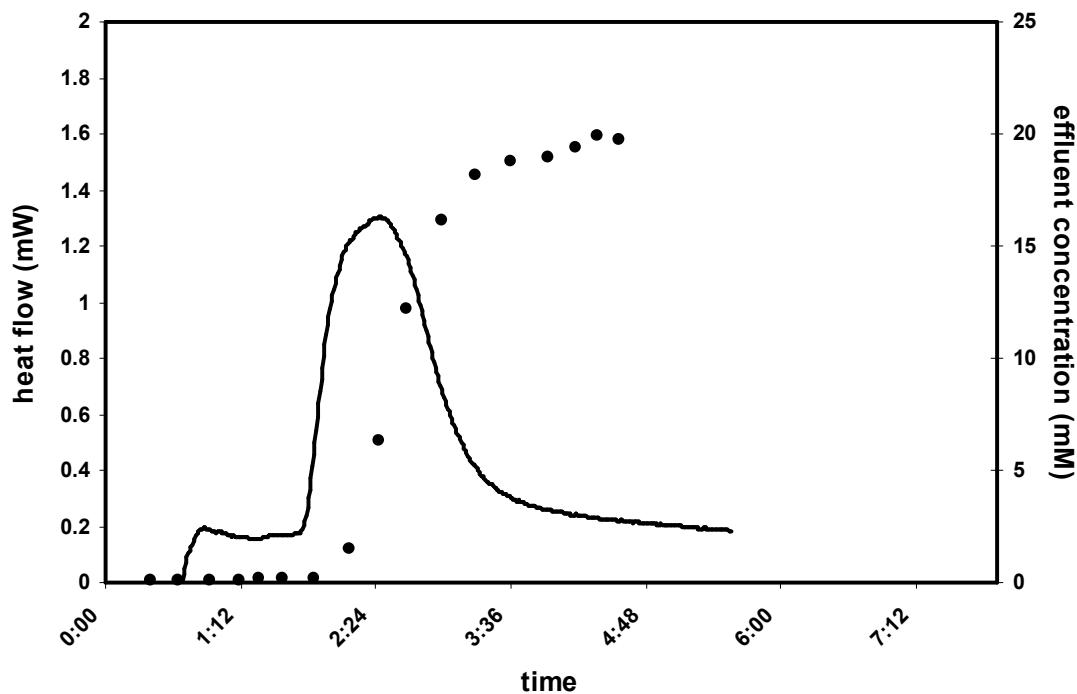
Breakthrough Curve Calculations

(Not used – for comparison purposes only)

Sorbate Fed (mmol)	0.435	ΔH (J/g)	60.8
Sorbate in Effluent (mmol)	0.277	q (mmol/g)	0.62
Amount Adsorbed (mmol)	0.158	ΔH (kJ/mol)	97.3

EXPERIMENTAL DATA SUMMARY

Run ID #	6	Sorbent	CsY
Date	15-Jan-07	Solvent	n-C ₁₆
Temperature (°C)	30	Sorbate	Quinoline
Flow Rate (mL/h)	4.00	Concentration (mmol/L)	21.8
Sorbent Mass (g)	0.2526	Total Heat (J)	4.6674



Heat Flow Calculations

Peak Heat Flow (mW)	1.28863	ΔH (kJ/mol)	44.7
Baseline Heat Flow (mW)	0.20511	ΔH (J/g)	18.5
Corrected Peak (mW)	1.08352	q (mmol/g)	0.41

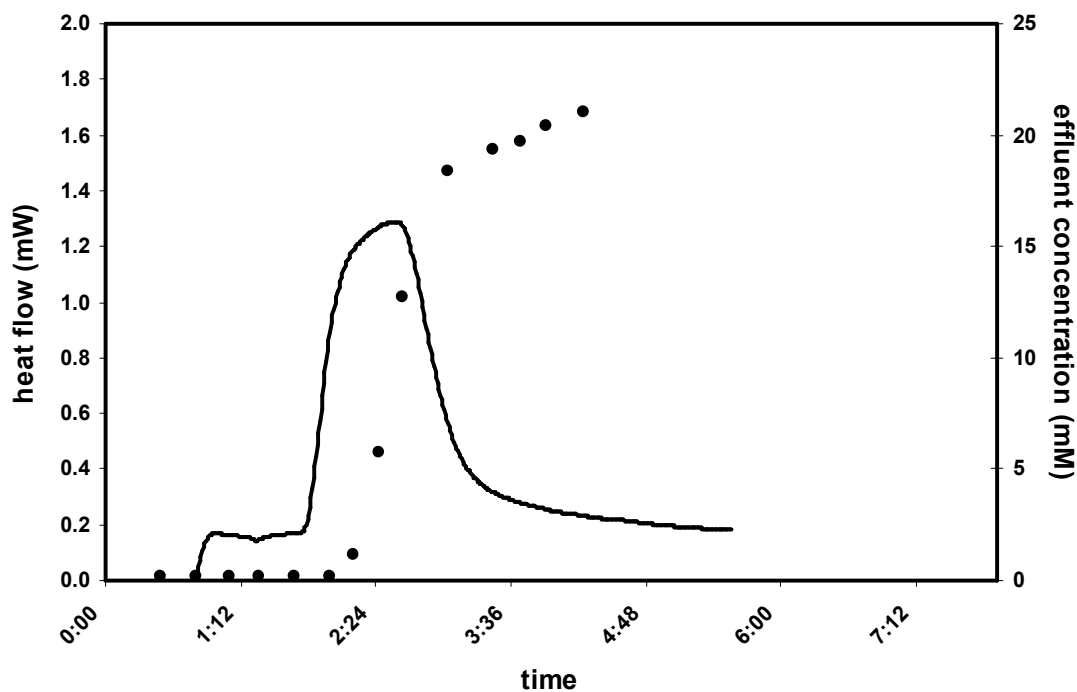
Breakthrough Curve Calculations

(Not used – for comparison purposes only)

Sorbate Fed (mmol)	0.249	ΔH (J/g)	18.5
Sorbate in Effluent (mmol)	0.156	q (mmol/g)	0.37
Amount Adsorbed (mmol)	0.093	ΔH (kJ/mol)	50.4

EXPERIMENTAL DATA SUMMARY

Run ID #	7	Sorbent	CsY
Date	16-Jan-07	Solvent	n-C ₁₆
Temperature (°C)	30	Sorbate	Quinoline
Flow Rate (mL/h)	4.00	Concentration (mmol/L)	21.8
Sorbent Mass (g)	0.2541	Total Heat (J)	4.5006



Heat Flow Calculations

Peak Heat Flow (mW)	1.27349	ΔH (kJ/mol)	44.9
Baseline Heat Flow (mW)	0.18596	ΔH (J/g)	17.7
Corrected Peak (mW)	1.08753	q (mmol/g)	0.39

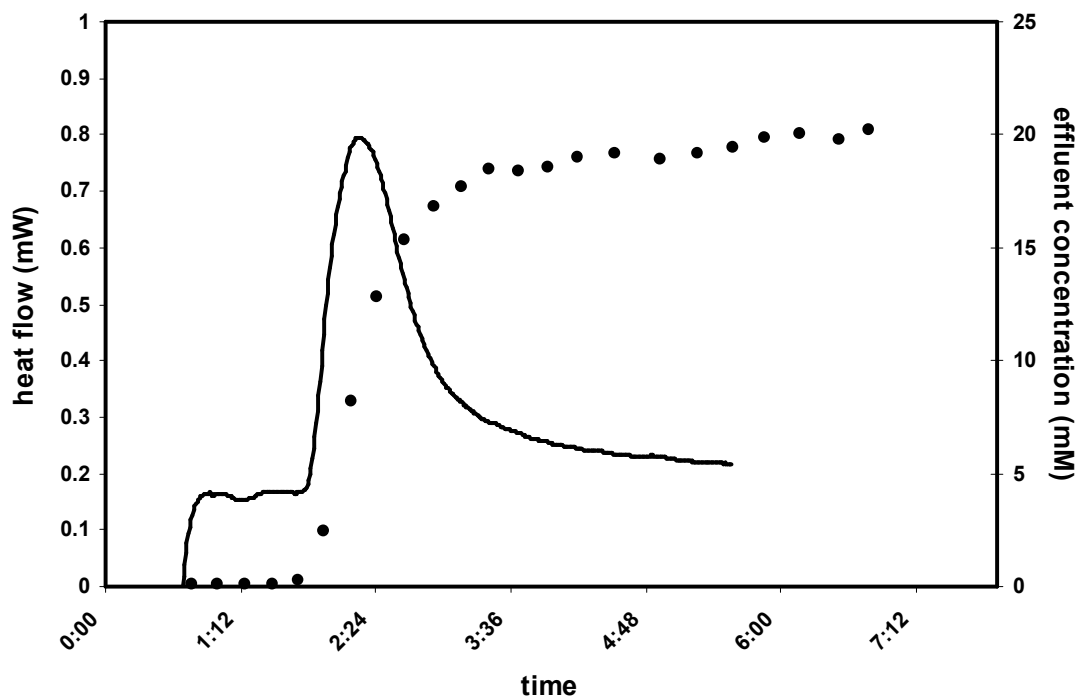
Breakthrough Curve Calculations

(Not used – for comparison purposes only)

Sorbate Fed (mmol)	0.232	ΔH (J/g)	17.7
Sorbate in Effluent (mmol)	0.153	q (mmol/g)	0.31
Amount Adsorbed (mmol)	0.079	ΔH (kJ/mol)	56.8

EXPERIMENTAL DATA SUMMARY

Run ID #	8	Sorbent	CsY
Date	17-Jan-07	Solvent	n-C ₁₆
Temperature (°C)	30	Sorbate	Dibenzothiophene
Flow Rate (mL/h)	4.00	Concentration (mmol/L)	21.8
Sorbent Mass (g)	0.2487	Total Heat (J)	4.4495



Heat Flow Calculations

Peak Heat Flow (mW)	0.78521	ΔH (kJ/mol)	25.6
Baseline Heat Flow (mW)	0.16556	ΔH (J/g)	9.8
Corrected Peak (mW)	0.61965	q (mmol/g)	0.39

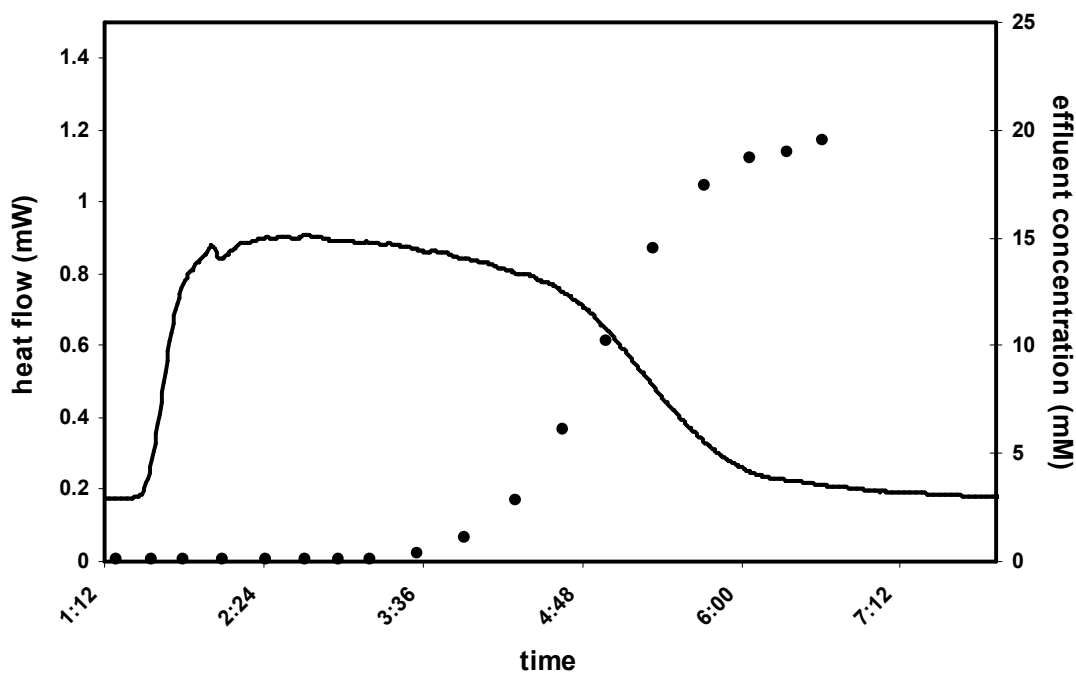
Breakthrough Curve Calculations

(Not used – for comparison purposes only)

Sorbate Fed (mmol)	0.441	ΔH (J/g)	9.8
Sorbate in Effluent (mmol)	0.350	q (mmol/g)	0.37
Amount Adsorbed (mmol)	0.091	ΔH (kJ/mol)	26.8

EXPERIMENTAL DATA SUMMARY

Run ID #	9	Sorbent	NaY
Date	18-Jan-07	Solvent	n-C ₁₆
Temperature (°C)	30	Sorbate	Dibenzothiophene
Flow Rate (mL/h)	4.00	Concentration (mmol/L)	21.8
Sorbent Mass (g)	0.2522	Total Heat (J)	9.0556



Heat Flow Calculations

Peak Heat Flow (mW)	0.90429	ΔH (kJ/mol)	29.5
Baseline Heat Flow (mW)	0.18982	ΔH (J/g)	35.9
Corrected Peak (mW)	0.71447	q (mmol/g)	1.22

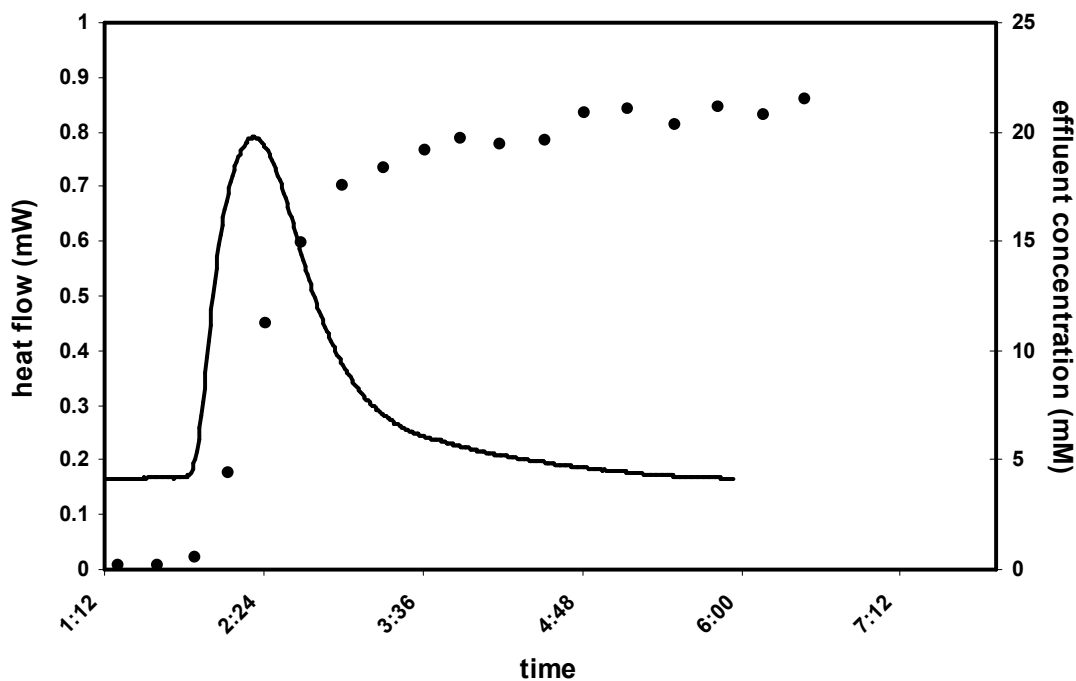
Breakthrough Curve Calculations

(Not used – for comparison purposes only)

Sorbate Fed (mmol)	0.457	ΔH (J/g)	35.9
Sorbate in Effluent (mmol)	0.141	q (mmol/g)	1.25
Amount Adsorbed (mmol)	0.316	ΔH (kJ/mol)	28.7

EXPERIMENTAL DATA SUMMARY

Run ID #	<u>10</u>	Sorbent	<u>CsY</u>
Date	<u>19-Jan-07</u>	Solvent	<u>n-C₁₆</u>
Temperature (°C)	<u>30</u>	Sorbate	<u>Dibenzothiophene</u>
Flow Rate (mL/h)	<u>4.00</u>	Concentration (mmol/L)	<u>21.8</u>
Sorbent Mass (g)	<u>0.2490</u>	Total Heat (J)	<u>2.3157</u>



Heat Flow Calculations

Peak Heat Flow (mW)	<u>0.77784</u>	ΔH (kJ/mol)	<u>24.6</u>
Baseline Heat Flow (mW)	<u>0.18152</u>	ΔH (J/g)	<u>9.3</u>
Corrected Peak (mW)	<u>0.59632</u>	q (mmol/g)	<u>0.38</u>

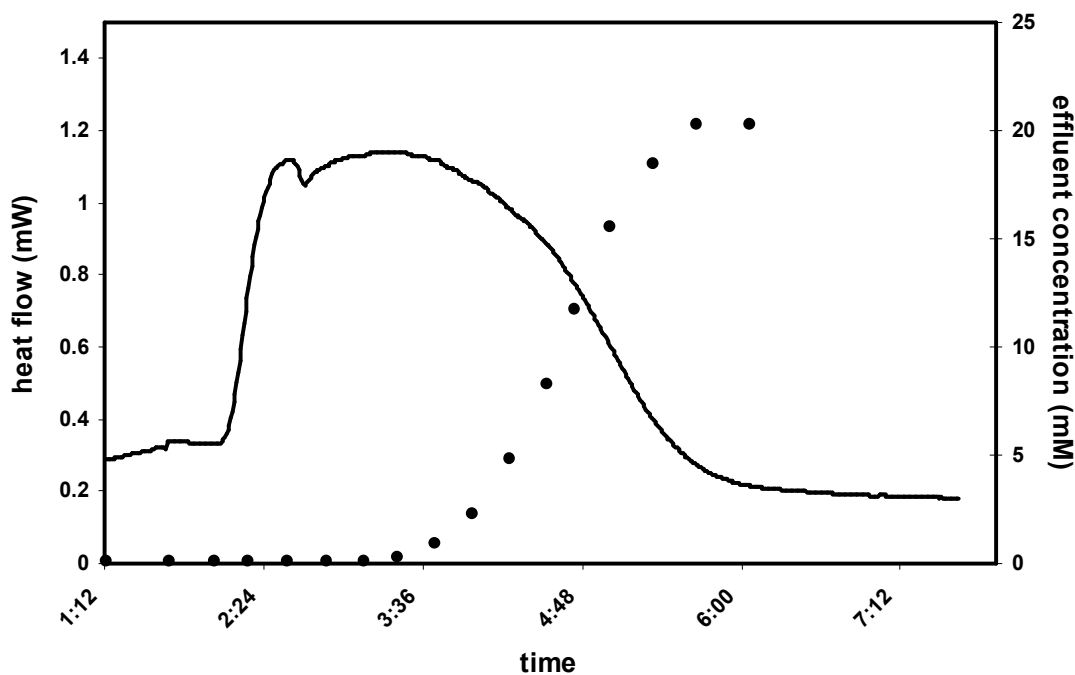
Breakthrough Curve Calculations

(Not used – for comparison purposes only)

Sorbate Fed (mmol)	<u>0.411</u>	ΔH (J/g)	<u>9.3</u>
Sorbate in Effluent (mmol)	<u>0.338</u>	q (mmol/g)	<u>0.29</u>
Amount Adsorbed (mmol)	<u>0.072</u>	ΔH (kJ/mol)	<u>31.7</u>

EXPERIMENTAL DATA SUMMARY

<table style="width: 100%; border-collapse: collapse;"> <tr><td style="border-right: 1px solid black; padding-right: 5px;">Run ID #</td><td style="padding-left: 5px;">11</td></tr> <tr><td style="border-right: 1px solid black; padding-right: 5px;">Date</td><td style="padding-left: 5px;">24-Jan-07</td></tr> <tr><td style="border-right: 1px solid black; padding-right: 5px;">Temperature (°C)</td><td style="padding-left: 5px;">30</td></tr> <tr><td style="border-right: 1px solid black; padding-right: 5px;">Flow Rate (mL/h)</td><td style="padding-left: 5px;">4.00</td></tr> <tr><td style="border-right: 1px solid black; padding-right: 5px;">Sorbent Mass (g)</td><td style="padding-left: 5px;">0.2493</td></tr> </table>	Run ID #	11	Date	24-Jan-07	Temperature (°C)	30	Flow Rate (mL/h)	4.00	Sorbent Mass (g)	0.2493	<table style="width: 100%; border-collapse: collapse;"> <tr><td style="border-right: 1px solid black; padding-right: 5px;">Sorbent</td><td style="padding-left: 5px;">NiY</td></tr> <tr><td style="border-right: 1px solid black; padding-right: 5px;">Solvent</td><td style="padding-left: 5px;">n-C₁₆</td></tr> <tr><td style="border-right: 1px solid black; padding-right: 5px;">Sorbate</td><td style="padding-left: 5px;">Dibenzothiophene</td></tr> <tr><td style="border-right: 1px solid black; padding-right: 5px;">Concentration (mmol/L)</td><td style="padding-left: 5px;">21.8</td></tr> <tr><td style="border-right: 1px solid black; padding-right: 5px;">Total Heat (J)</td><td style="padding-left: 5px;">7.6965</td></tr> </table>	Sorbent	NiY	Solvent	n-C ₁₆	Sorbate	Dibenzothiophene	Concentration (mmol/L)	21.8	Total Heat (J)	7.6965
Run ID #	11																				
Date	24-Jan-07																				
Temperature (°C)	30																				
Flow Rate (mL/h)	4.00																				
Sorbent Mass (g)	0.2493																				
Sorbent	NiY																				
Solvent	n-C ₁₆																				
Sorbate	Dibenzothiophene																				
Concentration (mmol/L)	21.8																				
Total Heat (J)	7.6965																				



Heat Flow Calculations

<table style="width: 100%; border-collapse: collapse;"> <tr><td style="border-right: 1px solid black; padding-right: 5px;">Peak Heat Flow (mW)</td><td style="padding-left: 5px;">1.13591</td></tr> <tr><td style="border-right: 1px solid black; padding-right: 5px;">Baseline Heat Flow (mW)</td><td style="padding-left: 5px;">0.34160</td></tr> <tr><td style="border-right: 1px solid black; padding-right: 5px;">Corrected Peak (mW)</td><td style="padding-left: 5px;">0.79431</td></tr> </table>	Peak Heat Flow (mW)	1.13591	Baseline Heat Flow (mW)	0.34160	Corrected Peak (mW)	0.79431	<table style="width: 100%; border-collapse: collapse;"> <tr><td style="border-right: 1px solid black; padding-right: 5px;">ΔH (kJ/mol)</td><td style="padding-left: 5px;">32.8</td></tr> <tr><td style="border-right: 1px solid black; padding-right: 5px;">ΔH (J/g)</td><td style="padding-left: 5px;">30.9</td></tr> <tr><td style="border-right: 1px solid black; padding-right: 5px;">q (mmol/g)</td><td style="padding-left: 5px;">0.94</td></tr> </table>	ΔH (kJ/mol)	32.8	ΔH (J/g)	30.9	q (mmol/g)	0.94
Peak Heat Flow (mW)	1.13591												
Baseline Heat Flow (mW)	0.34160												
Corrected Peak (mW)	0.79431												
ΔH (kJ/mol)	32.8												
ΔH (J/g)	30.9												
q (mmol/g)	0.94												

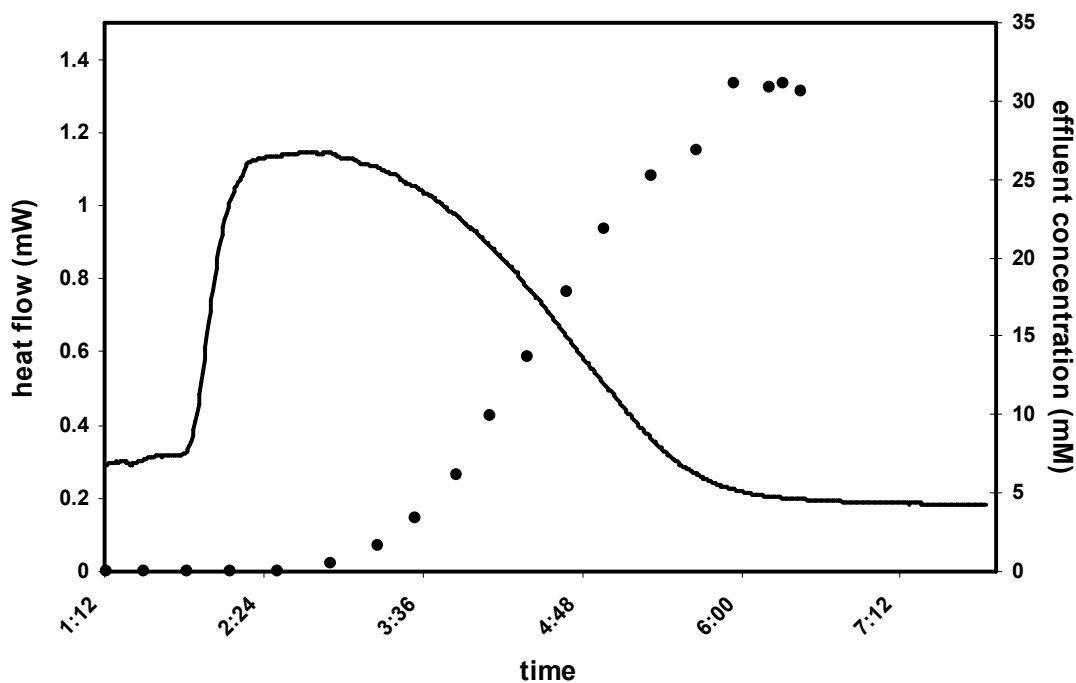
Breakthrough Curve Calculations

(Not used – for comparison purposes only)

<table style="width: 100%; border-collapse: collapse;"> <tr><td style="border-right: 1px solid black; padding-right: 5px;">Sorbate Fed (mmol)</td><td style="padding-left: 5px;">0.358</td></tr> <tr><td style="border-right: 1px solid black; padding-right: 5px;">Sorbate in Effluent (mmol)</td><td style="padding-left: 5px;">0.134</td></tr> <tr><td style="border-right: 1px solid black; padding-right: 5px;">Amount Adsorbed (mmol)</td><td style="padding-left: 5px;">0.224</td></tr> </table>	Sorbate Fed (mmol)	0.358	Sorbate in Effluent (mmol)	0.134	Amount Adsorbed (mmol)	0.224	<table style="width: 100%; border-collapse: collapse;"> <tr><td style="border-right: 1px solid black; padding-right: 5px;">ΔH (J/g)</td><td style="padding-left: 5px;">30.9</td></tr> <tr><td style="border-right: 1px solid black; padding-right: 5px;">q (mmol/g)</td><td style="padding-left: 5px;">0.90</td></tr> <tr><td style="border-right: 1px solid black; padding-right: 5px;">ΔH (kJ/mol)</td><td style="padding-left: 5px;">34.3</td></tr> </table>	ΔH (J/g)	30.9	q (mmol/g)	0.90	ΔH (kJ/mol)	34.3
Sorbate Fed (mmol)	0.358												
Sorbate in Effluent (mmol)	0.134												
Amount Adsorbed (mmol)	0.224												
ΔH (J/g)	30.9												
q (mmol/g)	0.90												
ΔH (kJ/mol)	34.3												

EXPERIMENTAL DATA SUMMARY

Run ID #	<u>12</u>	Sorbent	<u>NiY</u>
Date	<u>25-Jan-07</u>	Solvent	<u>n-C₁₆</u>
Temperature (°C)	<u>30</u>	Sorbate	<u>Dibenzothiophene</u>
Flow Rate (mL/h)	<u>4.00</u>	Concentration (mmol/L)	<u>21.8</u>
Sorbent Mass (g)	<u>0.2493</u>	Total Heat (J)	<u>7.6965</u>



Heat Flow Calculations

Peak Heat Flow (mW)	<u>1.14522</u>	ΔH (kJ/mol)	<u>33.6</u>
Baseline Heat Flow (mW)	<u>0.23221</u>	ΔH (J/g)	<u>31.5</u>
Corrected Peak (mW)	<u>0.81301</u>	q (mmol/g)	<u>0.94</u>

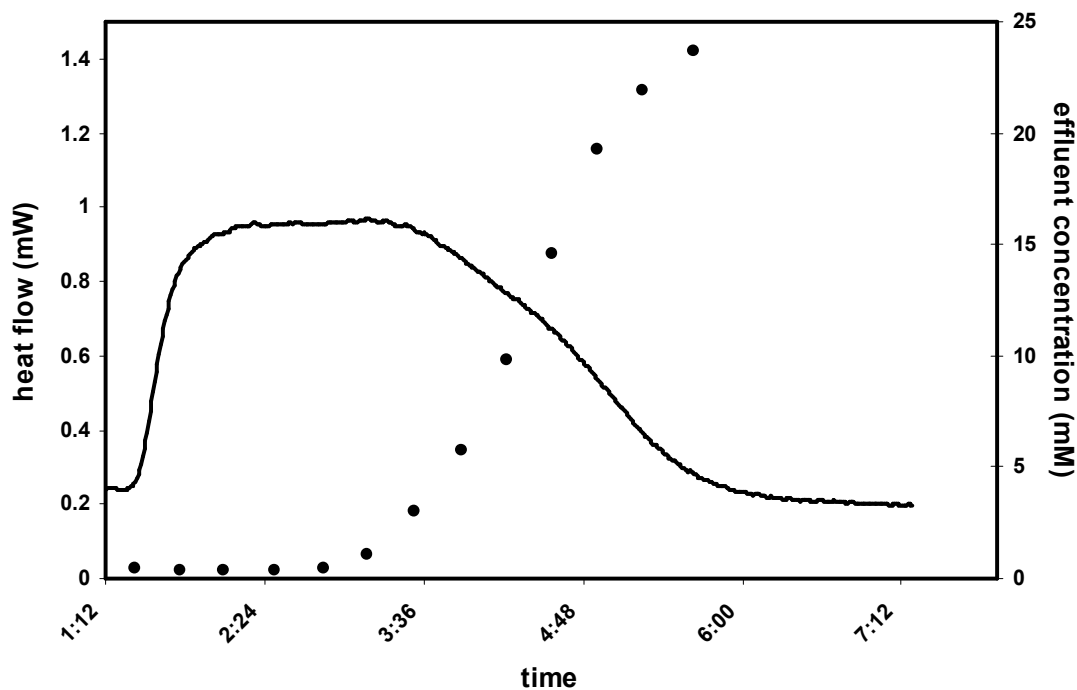
Breakthrough Curve Calculations

(Not used – for comparison purposes only)

Sorbate Fed (mmol)	<u>0.358</u>	ΔH (J/g)	<u>31.5</u>
Sorbate in Effluent (mmol)	<u>0.134</u>	q (mmol/g)	<u>1.07</u>
Amount Adsorbed (mmol)	<u>0.224</u>	ΔH (kJ/mol)	<u>29.5</u>

EXPERIMENTAL DATA SUMMARY

<table style="width: 100%; border-collapse: collapse;"> <tr><td style="border-right: 1px solid black; padding-right: 5px;">Run ID #</td><td style="padding-left: 5px;">13</td></tr> <tr><td style="border-right: 1px solid black; padding-right: 5px;">Date</td><td style="padding-left: 5px;">27-Jan-07</td></tr> <tr><td style="border-right: 1px solid black; padding-right: 5px;">Temperature (°C)</td><td style="padding-left: 5px;">30</td></tr> <tr><td style="border-right: 1px solid black; padding-right: 5px;">Flow Rate (mL/h)</td><td style="padding-left: 5px;">4.00</td></tr> <tr><td style="border-right: 1px solid black; padding-right: 5px;">Sorbent Mass (g)</td><td style="padding-left: 5px;">0.2502</td></tr> </table>	Run ID #	13	Date	27-Jan-07	Temperature (°C)	30	Flow Rate (mL/h)	4.00	Sorbent Mass (g)	0.2502	<table style="width: 100%; border-collapse: collapse;"> <tr><td style="border-right: 1px solid black; padding-right: 5px;">Sorbent</td><td style="padding-left: 5px;">NaY</td></tr> <tr><td style="border-right: 1px solid black; padding-right: 5px;">Solvent</td><td style="padding-left: 5px;">n-C₁₆</td></tr> <tr><td style="border-right: 1px solid black; padding-right: 5px;">Sorbate</td><td style="padding-left: 5px;">Dibenzothiophene</td></tr> <tr><td style="border-right: 1px solid black; padding-right: 5px;">Concentration (mmol/L)</td><td style="padding-left: 5px;">21.8</td></tr> <tr><td style="border-right: 1px solid black; padding-right: 5px;">Total Heat (J)</td><td style="padding-left: 5px;">8.1919</td></tr> </table>	Sorbent	NaY	Solvent	n-C ₁₆	Sorbate	Dibenzothiophene	Concentration (mmol/L)	21.8	Total Heat (J)	8.1919
Run ID #	13																				
Date	27-Jan-07																				
Temperature (°C)	30																				
Flow Rate (mL/h)	4.00																				
Sorbent Mass (g)	0.2502																				
Sorbent	NaY																				
Solvent	n-C ₁₆																				
Sorbate	Dibenzothiophene																				
Concentration (mmol/L)	21.8																				
Total Heat (J)	8.1919																				



Heat Flow Calculations

Peak Heat Flow (mW)	0.96248	ΔH (kJ/mol)	29.6
Baseline Heat Flow (mW)	0.24642	ΔH (J/g)	32.7
Corrected Peak (mW)	0.71606	q (mmol/g)	1.11

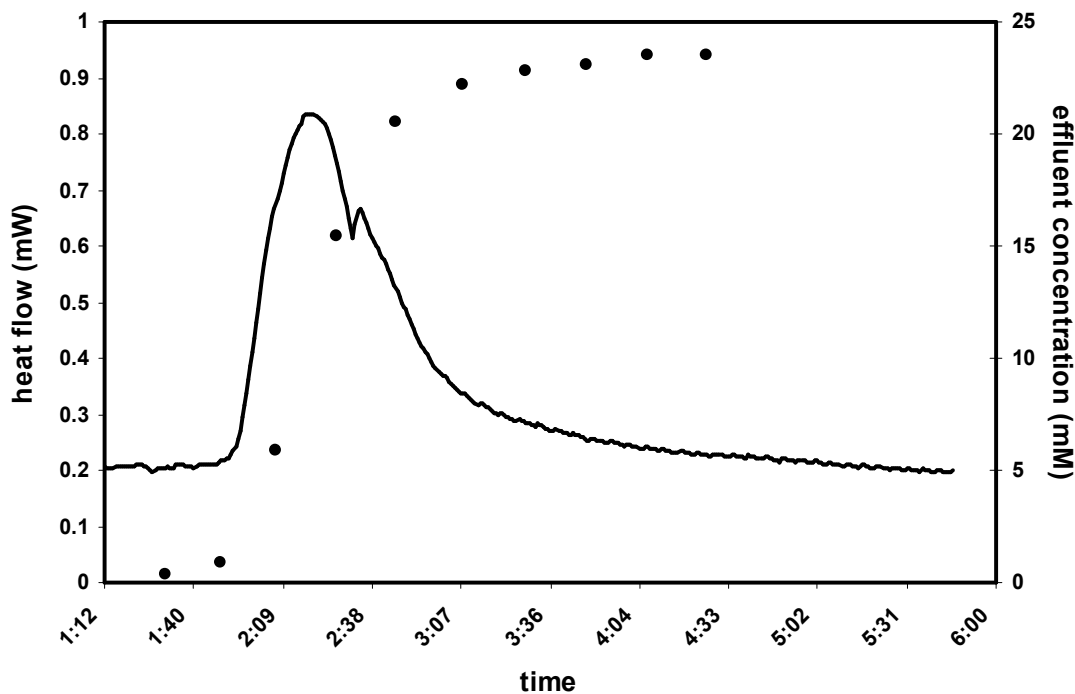
Breakthrough Curve Calculations

(Not used – for comparison purposes only)

Sorbate Fed (mmol)	0.382	ΔH (J/g)	32.7
Sorbate in Effluent (mmol)	0.146	q (mmol/g)	0.94
Amount Adsorbed (mmol)	0.236	ΔH (kJ/mol)	34.7

EXPERIMENTAL DATA SUMMARY

Run ID #	<u>14</u>	Sorbent	<u>CsY</u>
Date	<u>30-Jan-07</u>	Solvent	<u>n-C₁₆</u>
Temperature (°C)	<u>30</u>	Sorbate	<u>Dibenzothiophene</u>
Flow Rate (mL/h)	<u>4.00</u>	Concentration (mmol/L)	<u>21.8</u>
Sorbent Mass (g)	<u>0.2519</u>	Total Heat (J)	<u>1.9965</u>



Heat Flow Calculations

Peak Heat Flow (mW)	<u>0.82561</u>	ΔH (kJ/mol)	<u>24.9</u>
Baseline Heat Flow (mW)	<u>0.22286</u>	ΔH (J/g)	<u>7.9</u>
Corrected Peak (mW)	<u>0.60275</u>	q (mmol/g)	<u>0.32</u>

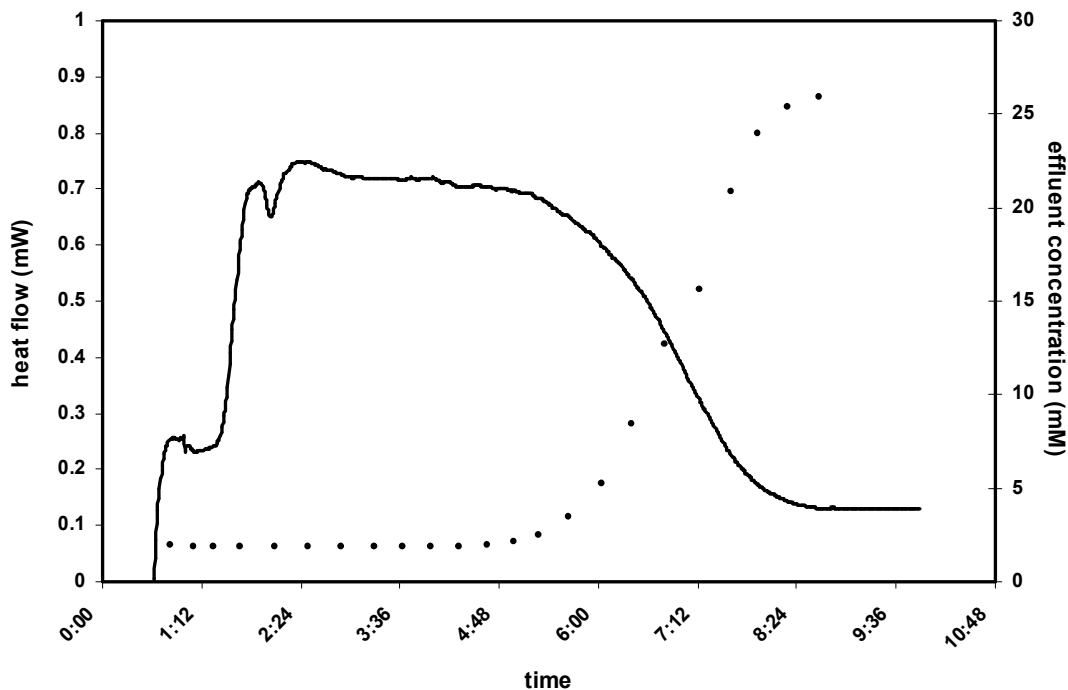
Breakthrough Curve Calculations

(Not used – for comparison purposes only)

Sorbate Fed (mmol)	<u>0.234</u>	ΔH (J/g)	<u>7.9</u>
Sorbate in Effluent (mmol)	<u>0.209</u>	q (mmol/g)	<u>0.10</u>
Amount Adsorbed (mmol)	<u>0.225</u>	ΔH (kJ/mol)	<u>80.7</u>

EXPERIMENTAL DATA SUMMARY

Run ID #	<u>15</u>	Sorbent	<u>NaY</u>
Date	<u>1-Feb-07</u>	Solvent	<u>n-C₁₆</u>
Temperature (°C)	<u>30</u>	Sorbate	<u>Naphthalene</u>
Flow Rate (mL/h)	<u>4.00</u>	Concentration (mmol/L)	<u>21.8</u>
Sorbent Mass (g)	<u>0.2495</u>	Total Heat (J)	<u>9.6556</u>



Heat Flow Calculations

Peak Heat Flow (mW)	<u>0.74811</u>	ΔH (kJ/mol)	<u>20.9</u>
Baseline Heat Flow (mW)	<u>0.24237</u>	ΔH (J/g)	<u>38.7</u>
Corrected Peak (mW)	<u>0.50574</u>	q (mmol/g)	<u>1.85</u>

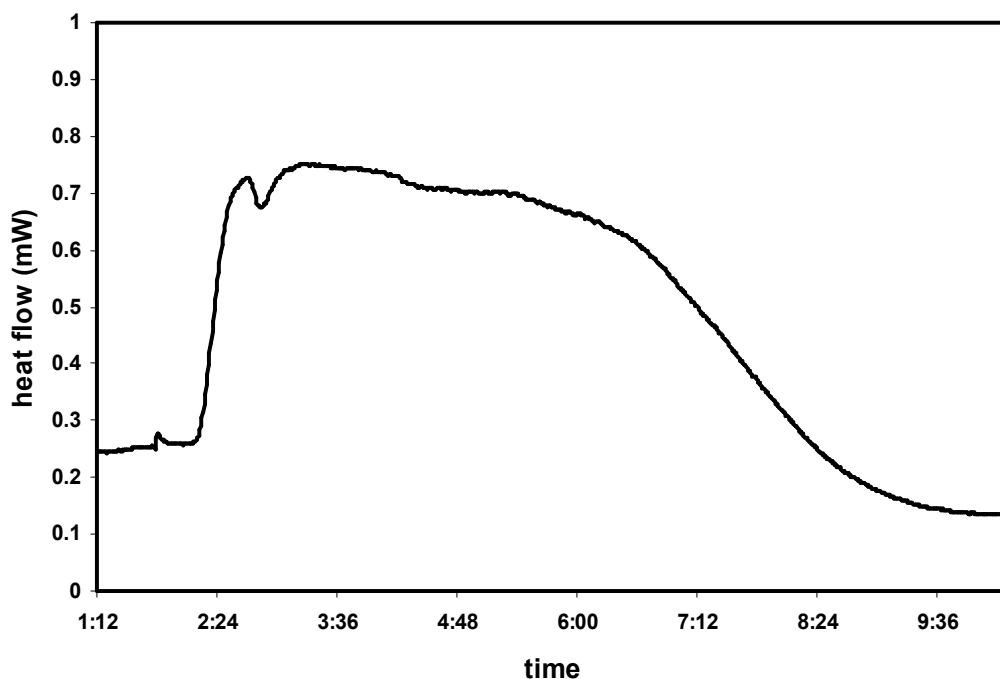
Breakthrough Curve Calculations

(Not used – for comparison purposes only)

Sorbate Fed (mmol)	<u>0.234</u>	ΔH (J/g)	<u>38.7</u>
Sorbate in Effluent (mmol)	<u>0.209</u>	q (mmol/g)	<u>1.77</u>
Amount Adsorbed (mmol)	<u>0.225</u>	ΔH (kJ/mol)	<u>21.9</u>

EXPERIMENTAL DATA SUMMARY

Run ID #	<u>16</u>	Sorbent	<u>NaY</u>
Date	<u>3-Feb-07</u>	Solvent	<u>n-C₁₆</u>
Temperature (°C)	<u>30</u>	Sorbate	<u>Naphthalene</u>
Flow Rate (mL/h)	<u>4.00</u>	Concentration (mmol/L)	<u>21.8</u>
Sorbent Mass (g)	<u>0.2427</u>	Total Heat (J)	<u>9.1636</u>



Heat Flow Calculations

Peak Heat Flow (mW)	<u>0.75039</u>	ΔH (kJ/mol)	<u>20.3</u>
Baseline Heat Flow (mW)	<u>0.25937</u>	ΔH (J/g)	<u>37.8</u>
Corrected Peak (mW)	<u>0.49102</u>	q (mmol/g)	<u>1.86</u>

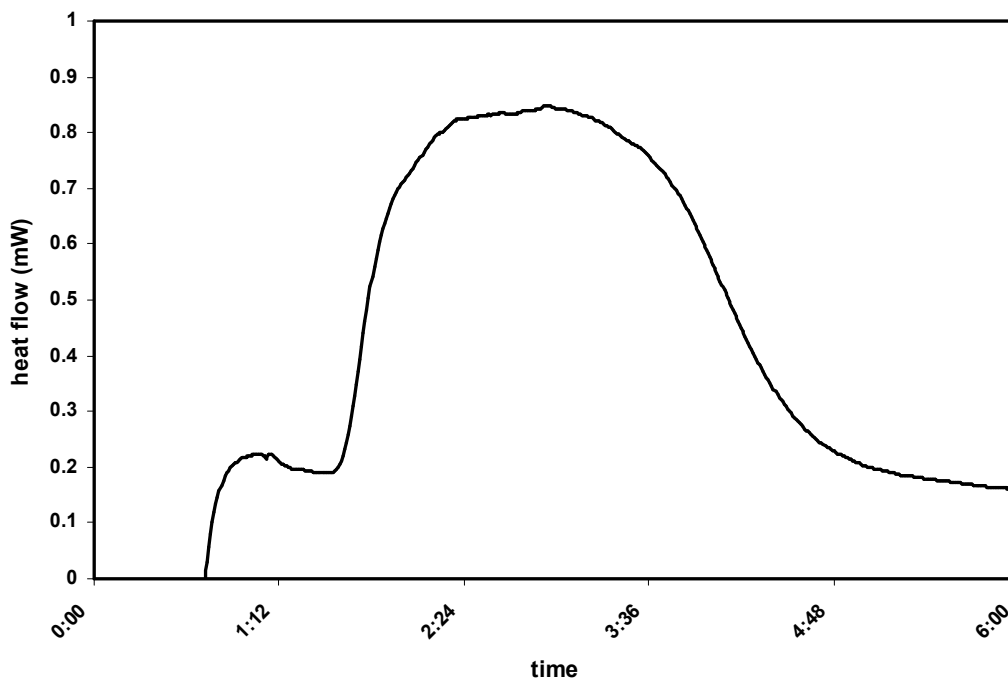
Breakthrough Curve Calculations

(Not used – for comparison purposes only)

Sorbate Fed (mmol)	<u>-</u>	ΔH (J/g)	<u>37.8</u>
Sorbate in Effluent (mmol)	<u>-</u>	q (mmol/g)	<u>-</u>
Amount Adsorbed (mmol)	<u>-</u>	ΔH (kJ/mol)	<u>-</u>

EXPERIMENTAL DATA SUMMARY

<table style="width: 100%; border-collapse: collapse;"> <tr><td style="border-right: 1px solid black; padding-right: 5px;">Run ID #</td><td style="padding-left: 5px;">17</td></tr> <tr><td style="border-right: 1px solid black; padding-right: 5px;">Date</td><td style="padding-left: 5px;">5-Feb-07</td></tr> <tr><td style="border-right: 1px solid black; padding-right: 5px;">Temperature (°C)</td><td style="padding-left: 5px;">30</td></tr> <tr><td style="border-right: 1px solid black; padding-right: 5px;">Flow Rate (mL/h)</td><td style="padding-left: 5px;">4.00</td></tr> <tr><td style="border-right: 1px solid black; padding-right: 5px;">Sorbent Mass (g)</td><td style="padding-left: 5px;">0.2518</td></tr> </table>	Run ID #	17	Date	5-Feb-07	Temperature (°C)	30	Flow Rate (mL/h)	4.00	Sorbent Mass (g)	0.2518	<table style="width: 100%; border-collapse: collapse;"> <tr><td style="border-right: 1px solid black; padding-right: 5px;">Sorbent</td><td style="padding-left: 5px;">CsY</td></tr> <tr><td style="border-right: 1px solid black; padding-right: 5px;">Solvent</td><td style="padding-left: 5px;">n-C₁₆</td></tr> <tr><td style="border-right: 1px solid black; padding-right: 5px;">Sorbate</td><td style="padding-left: 5px;">Naphthalene</td></tr> <tr><td style="border-right: 1px solid black; padding-right: 5px;">Concentration (mmol/L)</td><td style="padding-left: 5px;">21.8</td></tr> <tr><td style="border-right: 1px solid black; padding-right: 5px;">Total Heat (J)</td><td style="padding-left: 5px;">5.4433</td></tr> </table>	Sorbent	CsY	Solvent	n-C ₁₆	Sorbate	Naphthalene	Concentration (mmol/L)	21.8	Total Heat (J)	5.4433
Run ID #	17																				
Date	5-Feb-07																				
Temperature (°C)	30																				
Flow Rate (mL/h)	4.00																				
Sorbent Mass (g)	0.2518																				
Sorbent	CsY																				
Solvent	n-C ₁₆																				
Sorbate	Naphthalene																				
Concentration (mmol/L)	21.8																				
Total Heat (J)	5.4433																				



Heat Flow Calculations

Peak Heat Flow (mW)	0.84333	ΔH (kJ/mol)	27.1
Baseline Heat Flow (mW)	0.18698	ΔH (J/g)	21.6
Corrected Peak (mW)	0.65635	q (mmol/g)	0.80

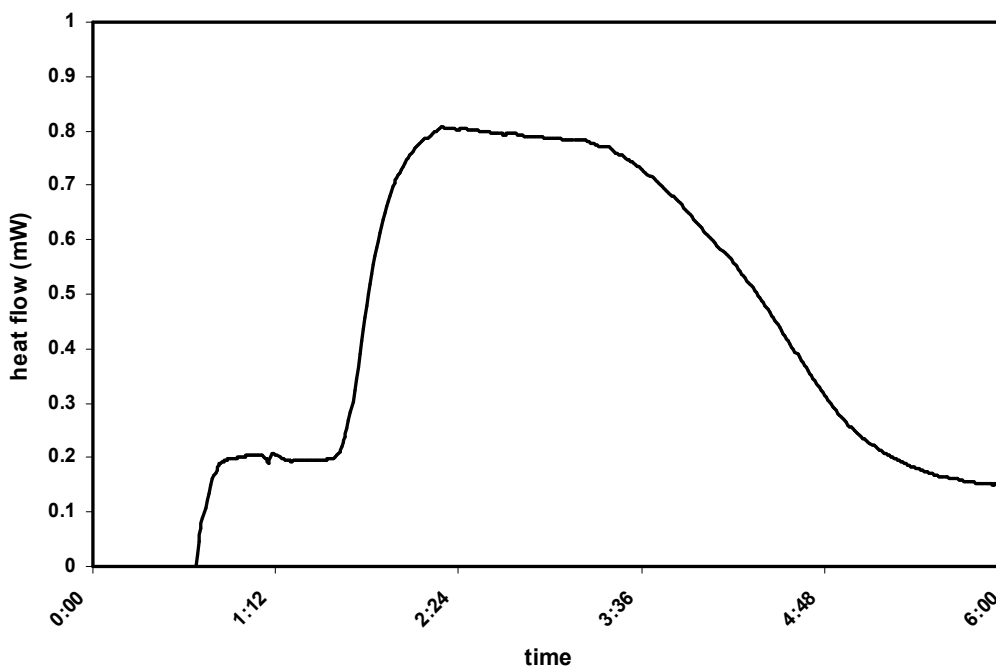
Breakthrough Curve Calculations

(Not used – for comparison purposes only)

Sorbate Fed (mmol)	-	ΔH (J/g)	37.8
Sorbate in Effluent (mmol)	-	q (mmol/g)	-
Amount Adsorbed (mmol)	-	ΔH (kJ/mol)	-

EXPERIMENTAL DATA SUMMARY

Run ID #	<u>18</u>	Sorbent	<u>CsY</u>
Date	<u>7-Feb-07</u>	Solvent	<u>n-C₁₆</u>
Temperature (°C)	<u>30</u>	Sorbate	<u>Naphthalene</u>
Flow Rate (mL/h)	<u>4.00</u>	Concentration (mmol/L)	<u>21.8</u>
Sorbent Mass (g)	<u>0.2525</u>	Total Heat (J)	<u>5.7064</u>



Heat Flow Calculations

Peak Heat Flow (mW)	<u>0.80269</u>	ΔH (kJ/mol)	<u>25.0</u>
Baseline Heat Flow (mW)	<u>0.19624</u>	ΔH (J/g)	<u>22.6</u>
Corrected Peak (mW)	<u>0.60645</u>	q (mmol/g)	<u>0.90</u>

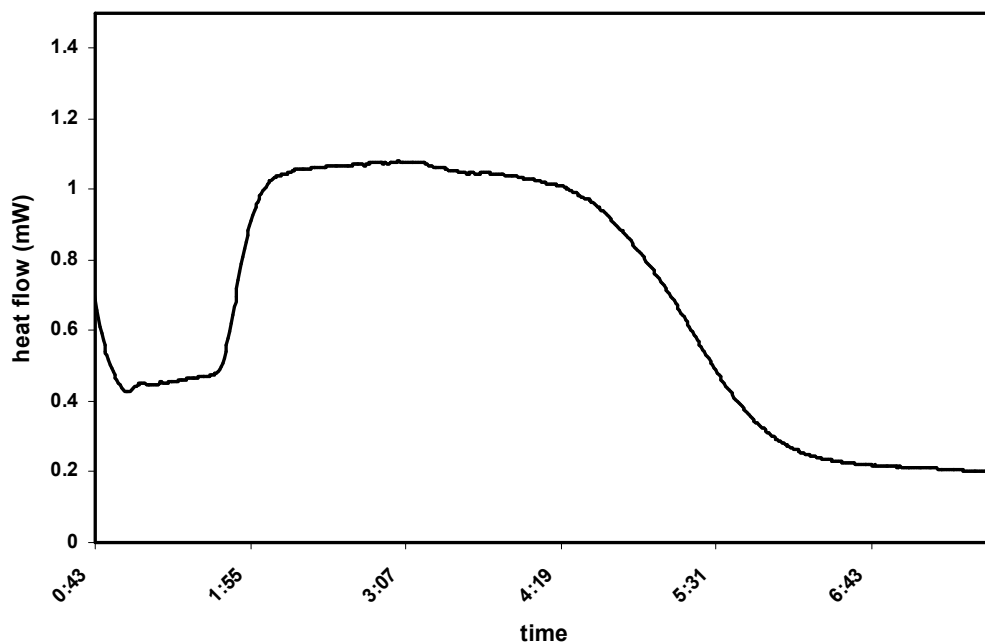
Breakthrough Curve Calculations

(Not used – for comparison purposes only)

Sorbate Fed (mmol)	<u>-</u>	ΔH (J/g)	<u>22.6</u>
Sorbate in Effluent (mmol)	<u>-</u>	q (mmol/g)	<u>-</u>
Amount Adsorbed (mmol)	<u>-</u>	ΔH (kJ/mol)	<u>-</u>

EXPERIMENTAL DATA SUMMARY

Run ID #	19	Sorbent	NiY
Date	8-Feb-07	Solvent	n-C ₁₆
Temperature (°C)	30	Sorbate	Naphthalene
Flow Rate (mL/h)	4.00	Concentration (mmol/L)	21.8
Sorbent Mass (g)	0.2545	Total Heat (J)	8.0773



Heat Flow Calculations

Peak Heat Flow (mW)	1.07805	ΔH (kJ/mol)	24.8
Baseline Heat Flow (mW)	0.47613	ΔH (J/g)	31.7
Corrected Peak (mW)	0.60192	q (mmol/g)	1.28

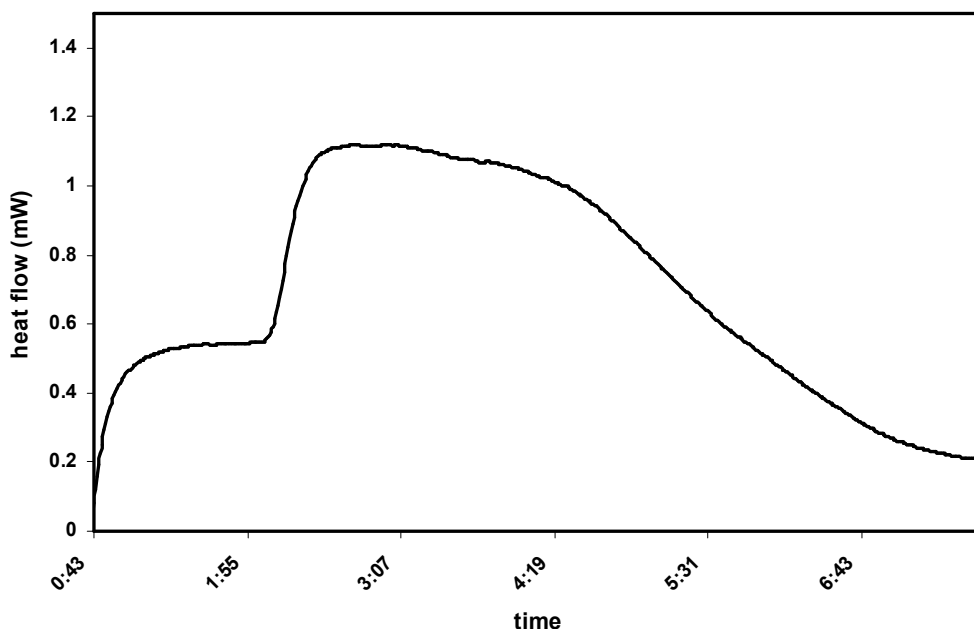
Breakthrough Curve Calculations

(Not used – for comparison purposes only)

Sorbate Fed (mmol)	-	ΔH (J/g)	31.7
Sorbate in Effluent (mmol)	-	q (mmol/g)	-
Amount Adsorbed (mmol)	-	ΔH (kJ/mol)	-

EXPERIMENTAL DATA SUMMARY

Run ID #	<u>20</u>	Sorbent	<u>NiY</u>
Date	<u>13-Feb-07</u>	Solvent	<u>n-C₁₆</u>
Temperature (°C)	<u>30</u>	Sorbate	<u>Naphthalene</u>
Flow Rate (mL/h)	<u>4.00</u>	Concentration (mmol/L)	<u>21.8</u>
Sorbent Mass (g)	<u>0.2550</u>	Total Heat (J)	<u>7.3823</u>



Heat Flow Calculations

Peak Heat Flow (mW)	<u>1.11840</u>	ΔH (kJ/mol)	<u>23.5</u>
Baseline Heat Flow (mW)	<u>0.54802</u>	ΔH (J/g)	<u>29.0</u>
Corrected Peak (mW)	<u>0.57038</u>	q (mmol/g)	<u>1.23</u>

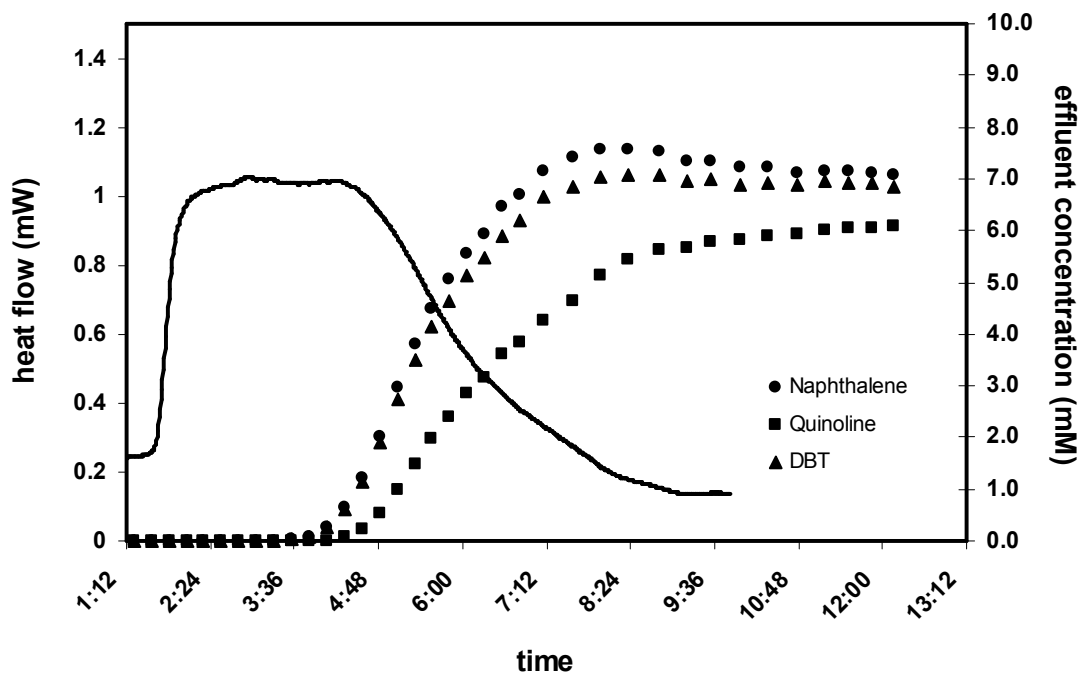
Breakthrough Curve Calculations

(Not used – for comparison purposes only)

Sorbate Fed (mmol)	<u>-</u>	ΔH (J/g)	<u>29.0</u>
Sorbate in Effluent (mmol)	<u>-</u>	q (mmol/g)	<u>-</u>
Amount Adsorbed (mmol)	<u>-</u>	ΔH (kJ/mol)	<u>-</u>

EXPERIMENTAL DATA SUMMARY

Run ID #	21	Sorbent	NaY
Date	27-Mar-07	Solvent	n-C ₁₆
Temperature (°C)	30	Sorbate	DBT/Quin/Naph
Flow Rate (mL/h)	4.00	Concentration (mmol/L)	7.25 / 7.25 / 7.25
Sorbent Mass (g)	0.2500	Total Heat (J/g)	49.58

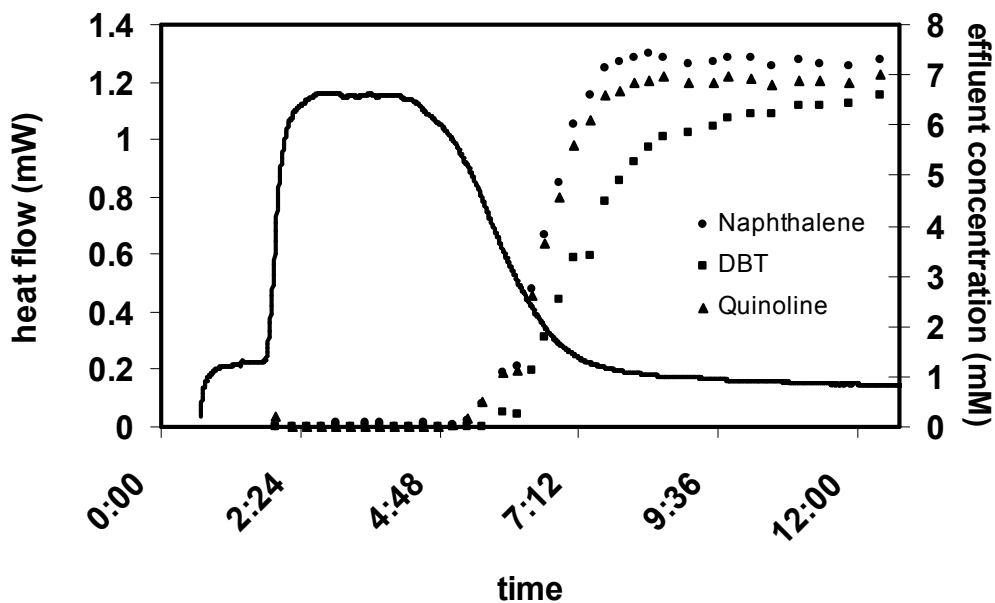


Breakthrough Curve Calculations

	Naph	Quin	DBT
Sorbate Fed (mmol)	<u>0.310</u>	<u>0.310</u>	<u>0.310</u>
Sorbate Out (mmol)	<u>0.202</u>	<u>0.141</u>	<u>0.191</u>
Amount Adsorbed (mmol)	<u>0.108</u>	<u>0.169</u>	<u>0.119</u>
Amount Adsorbed (mmol/g)	<u>0.43</u>	<u>0.68</u>	<u>0.48</u>

EXPERIMENTAL DATA SUMMARY

Run ID #	22	Sorbent	NaY
Date	28-Mar-07	Solvent	n-C ₁₆
Temperature (°C)	30	Sorbate	DBT/Quin/Naph
Flow Rate (mL/h)	4.00	Concentration (mmol/L)	7.25 / 7.25 / 7.25
Sorbent Mass (g)	0.2525	Total Heat (J/g)	55.62

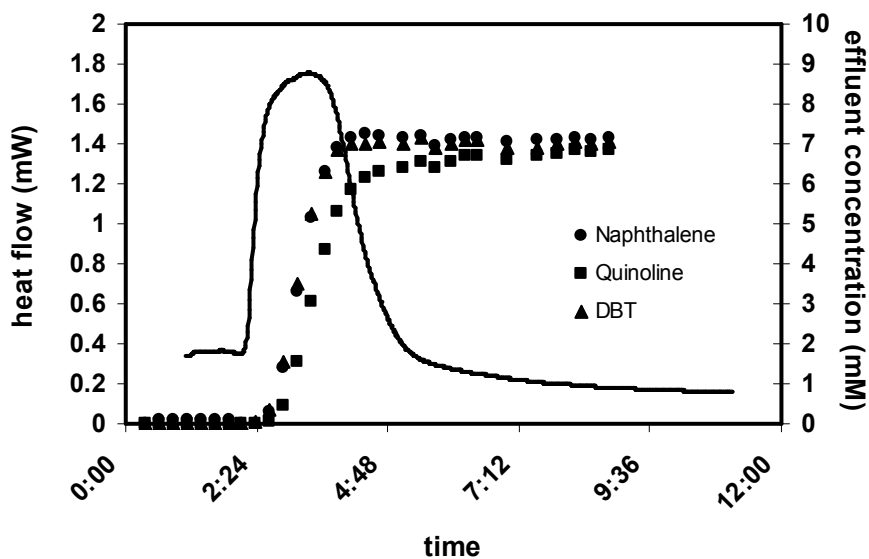


Breakthrough Curve Calculations

	Naph	Quin	DBT
Sorbate Fed (mmol)	0.275	0.275	0.275
Sorbate Out (mmol)	0.178	0.137	0.169
Amount Adsorbed (mmol)	0.097	0.138	0.106
Amount Adsorbed (mmol/g)	0.38	0.55	0.42

EXPERIMENTAL DATA SUMMARY

Run ID #	23	Sorbent	NiY
Date	3-Apr-07	Solvent	n-C ₁₆
Temperature (°C)	30	Sorbate	DBT/Quin/Naph
Flow Rate (mL/h)	4.00	Concentration (mmol/L)	7.25 / 7.25 / 7.25
Sorbent Mass (g)	0.2524	Total Heat (J/g)	38.51

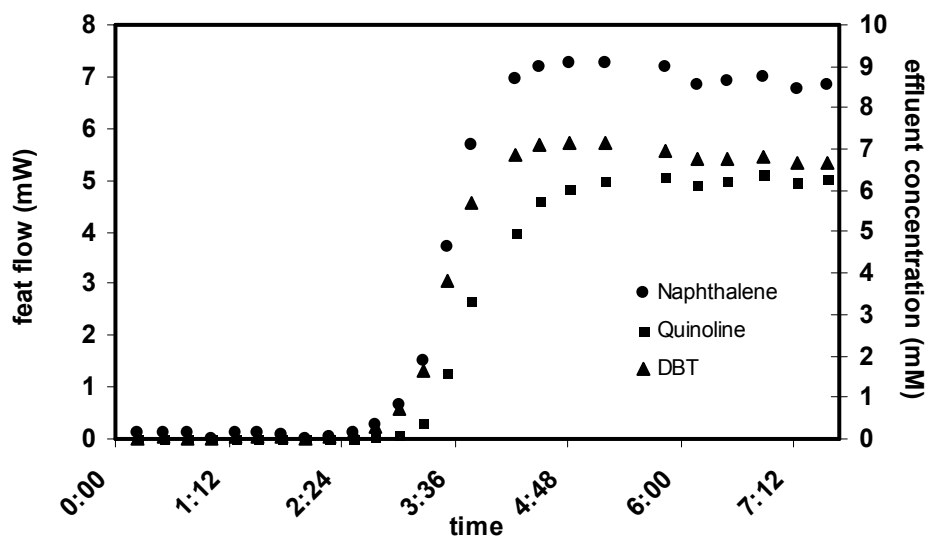


Breakthrough Curve Calculations

	Naph	Quin	DBT
Sorbate Fed (mmol)	<u>0.220</u>	<u>0.220</u>	<u>0.220</u>
Sorbate Out (mmol)	<u>0.165</u>	<u>0.145</u>	<u>0.163</u>
Amount Adsorbed (mmol)	<u>0.055</u>	<u>0.075</u>	<u>0.057</u>
Amount Adsorbed (mmol/g)	<u>0.20</u>	<u>0.28</u>	<u>0.21</u>

EXPERIMENTAL DATA SUMMARY

Run ID #	24	Sorbent	NiY
Date	11-Apr-07	Solvent	n-C ₁₆
Temperature (°C)	30	Sorbate	DBT/Quin/Naph
Flow Rate (mL/h)	4.00	Concentration (mmol/L)	7.25 / 7.25 / 7.25
Sorbent Mass (g)	0.2516	Total Heat (J/g)	-



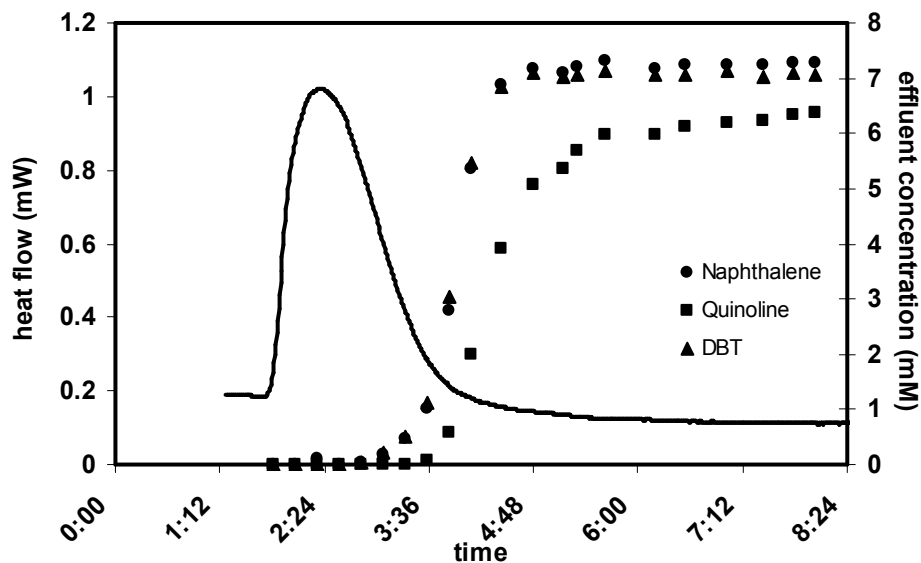
Breakthrough Curve Calculations

	Naph	Quin	DBT
Sorbate Fed (mmol)	<u>0.177</u>	<u>0.177</u>	<u>0.177</u>
Sorbate Out (mmol)	<u>0.119</u>	<u>0.097</u>	<u>0.117</u>
Amount Adsorbed (mmol)	<u>0.058</u>	<u>0.080</u>	<u>0.060</u>
Amount Adsorbed (mmol/g)	<u>0.23</u>	<u>0.32</u>	<u>0.24</u>

NOTE: No heat flow curve is available for this experiment due to a software malfunction

EXPERIMENTAL DATA SUMMARY

Run ID #	25	Sorbent	CsY
Date	16-Apr-07	Solvent	n-C ₁₆
Temperature (°C)	30	Sorbate	DBT/Quin/Naph
Flow Rate (mL/h)	4.00	Concentration (mmol/L)	7.25 / 7.25 / 7.25
Sorbent Mass (g)	0.2501	Total Heat (J/g)	14.35

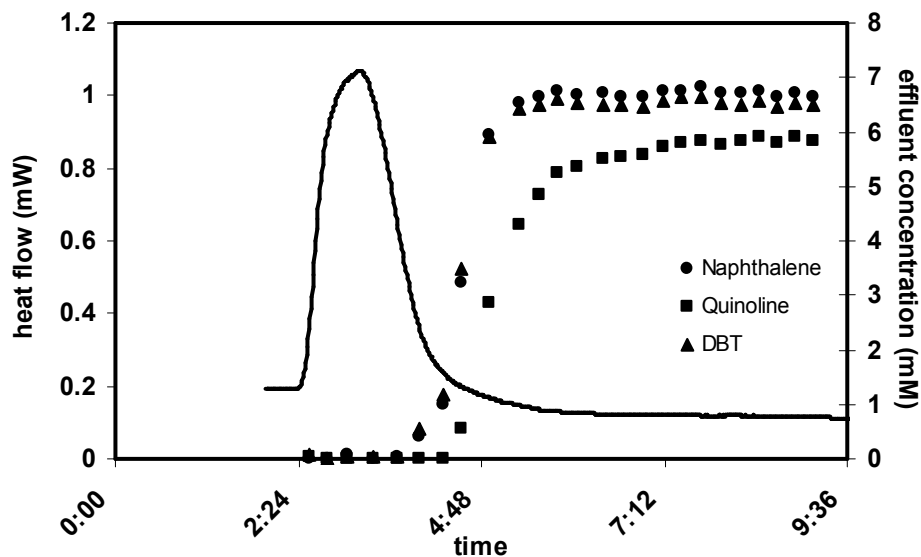


Breakthrough Curve Calculations

	Naph	Quin	DBT
Sorbate Fed (mmol)	0.176	0.176	0.176
Sorbate Out (mmol)	0.169	0.132	0.165
Amount Adsorbed (mmol)	0.007	0.044	0.011
Amount Adsorbed (mmol/g)	0.09	0.23	0.10

EXPERIMENTAL DATA SUMMARY

Run ID #	26	Sorbent	CsY
Date	18-Apr-07	Solvent	n-C ₁₆
Temperature (°C)	30	Sorbate	DBT/Quin/Naph
Flow Rate (mL/h)	4.00	Concentration (mmol/L)	7.25 / 7.25 / 7.25
Sorbent Mass (g)	0.2517	Total Heat (J/g)	14.19

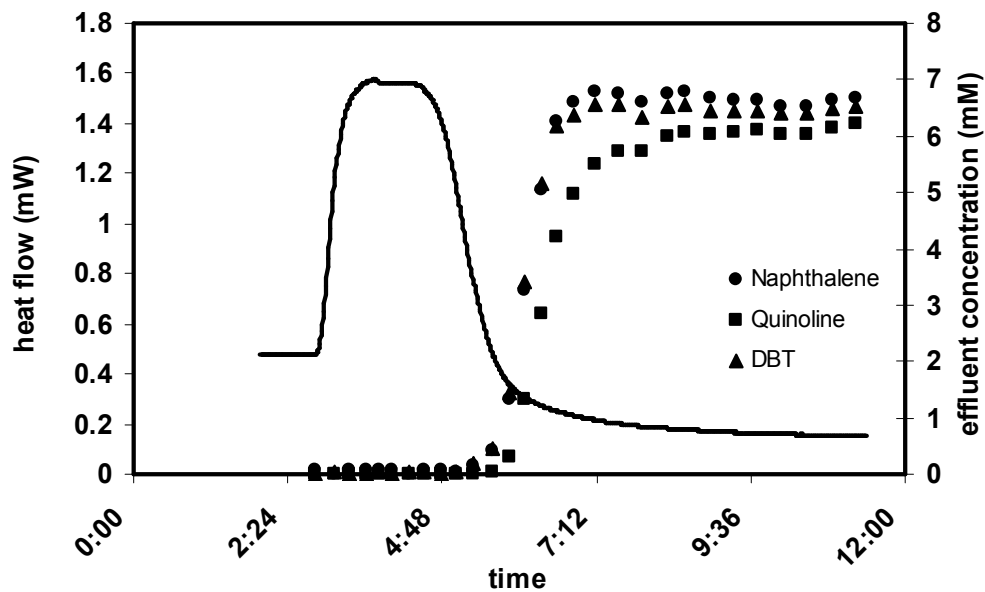


Breakthrough Curve Calculations

	Naph	Quin	DBT
Sorbate Fed (mmol)	0.141	0.141	0.141
Sorbate Out (mmol)	0.125	0.096	0.123
Amount Adsorbed (mmol)	0.016	0.045	0.018
Amount Adsorbed (mmol/g)	0.13	0.24	0.13

EXPERIMENTAL DATA SUMMARY

Run ID #	27	Sorbent	NiY
Date	20-Apr-07	Solvent	n-C ₁₆
Temperature (°C)	30	Sorbate	DBT/Quin/Naph
Flow Rate (mL/h)	4.00	Concentration (mmol/L)	7.25 / 7.25 / 7.25
Sorbent Mass (g)	0.2511	Total Heat (J/g)	34.99

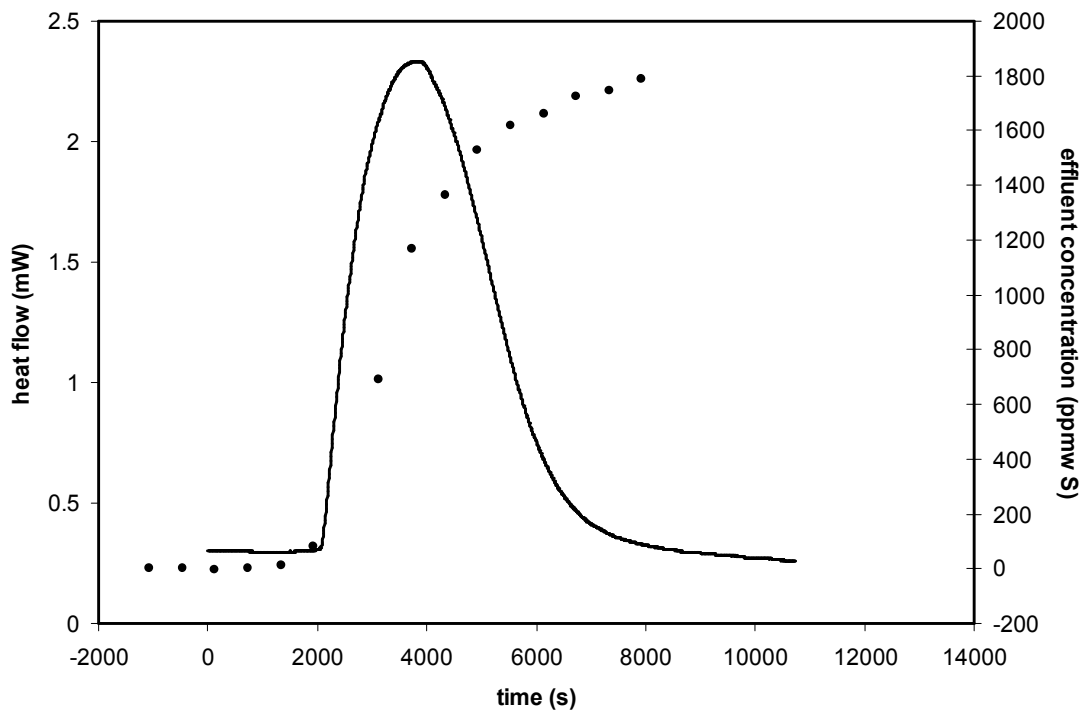


Breakthrough Curve Calculations

	Naph	Quin	DBT
Sorbate Fed (mmol)	<u>0.193</u>	<u>0.193</u>	<u>0.193</u>
Sorbate Out (mmol)	<u>0.138</u>	<u>0.116</u>	<u>0.135</u>
Amount Adsorbed (mmol)	<u>0.055</u>	<u>0.077</u>	<u>0.058</u>
Amount Adsorbed (mmol/g)	<u>0.22</u>	<u>0.31</u>	<u>0.23</u>

EXPERIMENTAL DATA SUMMARY

Run ID #	28	Sorbent	NaY
Date	20-Jun-05	Solvent	n-C ₁₆
Temperature (°C)	30	Sorbate	DBT
Flow Rate (mL/h)	7.6	Concentration (ppmw S)	1800
Sorbent Mass (g)	0.2511	Total Heat (J)	-



Heat Flow Calculations

Peak Heat Flow (mW)	-
Baseline Heat Flow (mW)	-
Corrected Peak (mW)	-
ΔH (kJ/mol)	-
ΔH (J/g)	-
q (mmol/g)	-

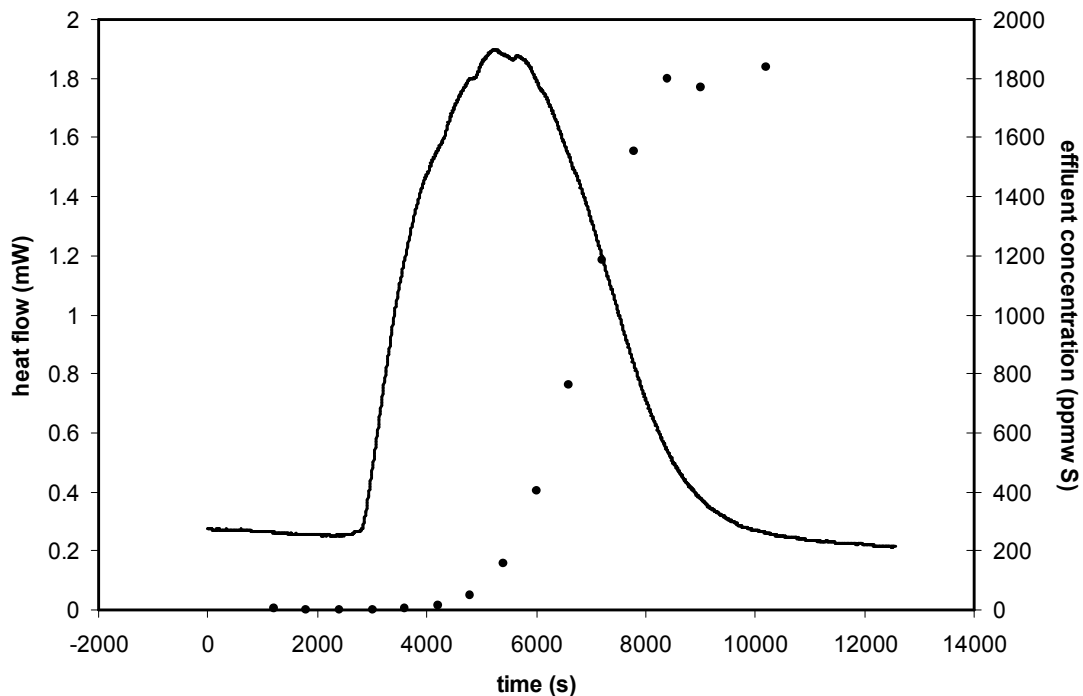
Breakthrough Curve Calculations

(Not used – for comparison purposes only)

Sorbate Fed (mmol)	-
Sorbate in Effluent (mmol)	-
Amount Adsorbed (mmol)	-
ΔH (J/g)	23.24
q (mmol/g)	0.90
ΔH (kJ/mol)	25.86

EXPERIMENTAL DATA SUMMARY

Run ID #	29	Sorbent	NaY
Date	22-Jun-05	Solvent	n-C ₁₆
Temperature (°C)	30	Sorbate	DBT
Flow Rate (mL/h)	5.8	Concentration (ppmw S)	1800
Sorbent Mass (g)	0.2441	Total Heat (J)	-



Heat Flow Calculations

Peak Heat Flow (mW)	-	ΔH (kJ/mol)	-
Baseline Heat Flow (mW)	-	ΔH (J/g)	-
Corrected Peak (mW)	-	q (mmol/g)	-

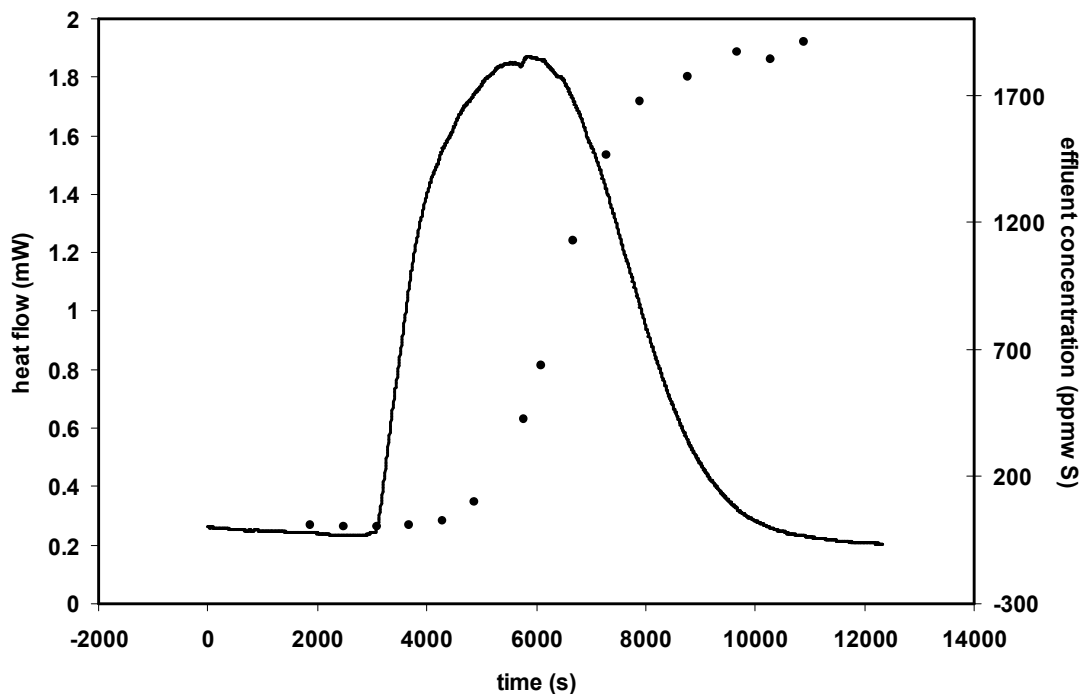
Breakthrough Curve Calculations

(Not used – for comparison purposes only)

Sorbate Fed (mmol)	-	ΔH (J/g)	26.12
Sorbate in Effluent (mmol)	-	q (mmol/g)	1.04
Amount Adsorbed (mmol)	-	ΔH (kJ/mol)	25.03

EXPERIMENTAL DATA SUMMARY

Run ID #	30	Sorbent	NaY
Date	23-Jun-05	Solvent	n-C ₁₆
Temperature (°C)	30	Sorbate	DBT
Flow Rate (mL/h)	5.9	Concentration (ppmw S)	1800
Sorbent Mass (g)	0.2520	Total Heat (J)	-



Heat Flow Calculations

Peak Heat Flow (mW)	-	ΔH (kJ/mol)	-
Baseline Heat Flow (mW)	-	ΔH (J/g)	-
Corrected Peak (mW)	-	q (mmol/g)	-

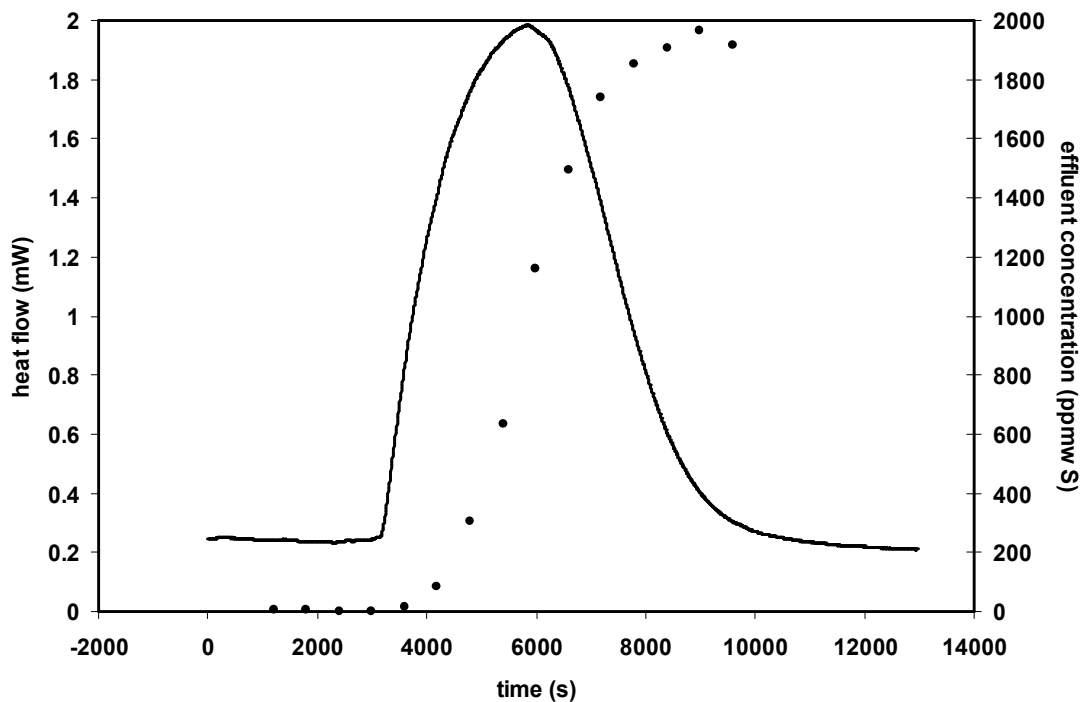
Breakthrough Curve Calculations

(Not used – for comparison purposes only)

Sorbate Fed (mmol)	-	ΔH (J/g)	26.84
Sorbate in Effluent (mmol)	-	q (mmol/g)	1.33
Amount Adsorbed (mmol)	-	ΔH (kJ/mol)	20.17

EXPERIMENTAL DATA SUMMARY

Run ID #	31	Sorbent	NaY
Date	24-Jun-05	Solvent	n-C ₁₆
Temperature (°C)	30	Sorbate	DBT
Flow Rate (mL/h)	6.0	Concentration (ppmw S)	1800
Sorbent Mass (g)	0.2495	Total Heat (J)	-



Heat Flow Calculations

Peak Heat Flow (mW)	-	ΔH (kJ/mol)	-
Baseline Heat Flow (mW)	-	ΔH (J/g)	-
Corrected Peak (mW)	-	q (mmol/g)	-

Breakthrough Curve Calculations

(Not used – for comparison purposes only)

Sorbate Fed (mmol)	-	ΔH (J/g)	26.15
Sorbate in Effluent (mmol)	-	q (mmol/g)	1.03
Amount Adsorbed (mmol)	-	ΔH (kJ/mol)	25.36

14 Appendix F – Equilibrium Isotherm Calculation Data

14.1 DBT Experiments

Table 37. Raw Data for DBT/C₁₆ Isotherm on NaY Zeolite

C_{sol} mmol/L	C_{sol} ppm	M_{sol} g	n_{sol} mmol	C_e mmol/L	n_e mmol	M_z g	q mmol/g	C_e/q_e
0.52	21.5	9.9982	0.00673	0.03	0.000388	0.048	0.132037	0.227208
1	41.4	9.9984	0.01293	0.11	0.001423	0.0479	0.240329	0.457707
2.33	96.5	9.999	0.03014	0.29	0.003751	0.0476	0.554371	0.523116
3.27	135.4	10.0002	0.04230	0.58	0.007503	0.0463	0.751624	0.771663
5.29	219.0	9.998	0.06842	1.44	0.018625	0.0468	1.064017	1.353362
10.18	421.4	9.9972	0.13166	5.8	0.075011	0.0468	1.210395	4.791824
15.96	660.7	10.0033	0.20654	10.84	0.140279	0.0471	1.406737	7.705777
21.34	883.4	9.9987	0.27603	16.14	0.20877	0.0463	1.452735	11.11008
31.66	1310.6	10.0008	0.40961	26.54	0.343365	0.0468	1.415401	18.75088

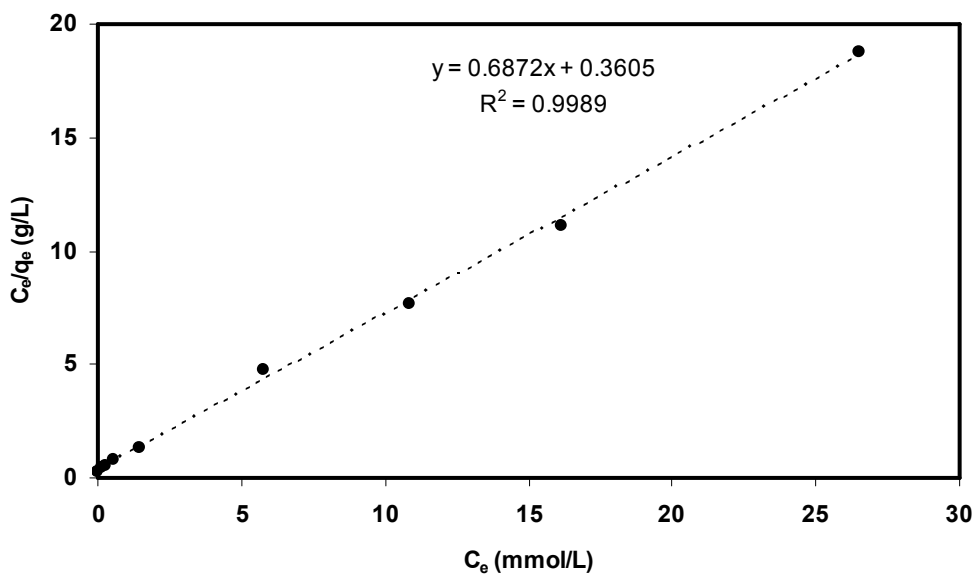


Figure 35. Linear isotherm for DBT adsorption on NaY zeolite

Table 38. Raw Data for DBT/C₁₆ Isotherm on NiY Zeolite

C_{sol} mmol/L	C_{sol} ppm	M_{sol} g	n_{sol} mmol	C_e mmol/L	n_e mmol	M_z g	q mmol/g	C_e/q_e
0.52	21.5	10.0029	0.00673	0.04	0.000518	0.0492	0.126247	0.316838
1.01	41.8	10.002	0.01307	0.06	0.000776	0.0497	0.247329	0.242592
2.39	98.9	10.0013	0.03092	0.37	0.004787	0.0504	0.518559	0.713516
3.15	130.4	10.001	0.04075	0.75	0.009703	0.0494	0.628562	1.193199
5.23	216.5	10.0033	0.06768	2.13	0.027564	0.0501	0.800733	2.660062
10.52	435.5	9.9976	0.13606	7.07	0.09144	0.0491	0.90877	7.779748
15.64	647.5	10.0009	0.20235	11.84	0.153183	0.0492	0.999259	11.84878
20.93	866.4	10	0.27076	17.22	0.222768	0.0482	0.995743	17.29361
25.9	1072.2	9.9997	0.33505	21.95	0.28395	0.0512	0.998009	21.99378

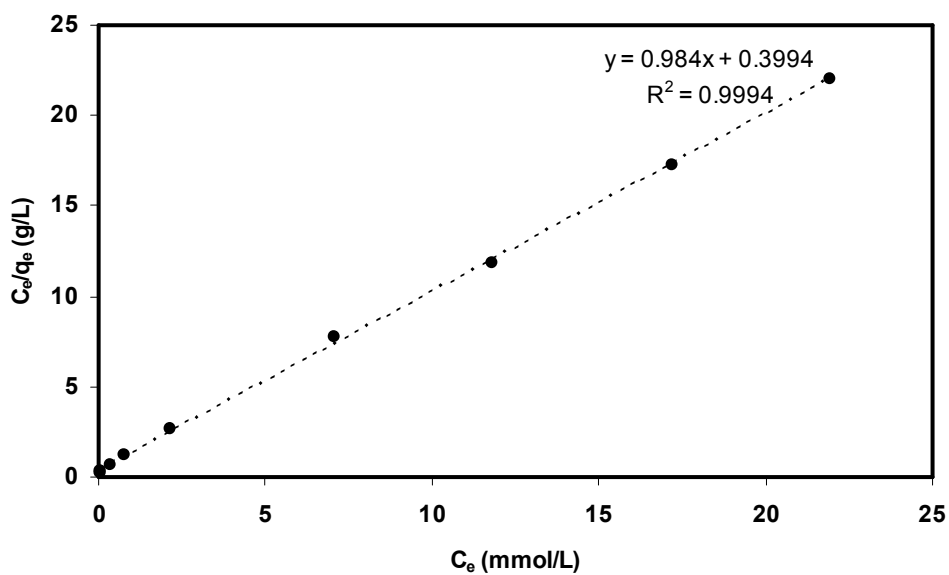


Figure 36. Linear isotherm for DBT adsorption on NiY zeolite

Table 39. Raw Data for DBT/C₁₆ Isotherm on CsY Zeolite

C_{sol} mmol/L	C_{sol} ppm	M_{sol} g	n_{sol} mmol	C_e mmol/L	n_e mmol	M_z g	q mmol/g	C_e/q_e
0.53	9.6	10.0019	0.00686	0.0100	0.000129	0.0541	0.124368	0.080406
1.02	18.5	10.0001	0.0132	0.0200	0.000259	0.0533	0.242716	0.082401
2.38	43.1	9.9994	0.03079	0.1600	0.00207	0.0528	0.543893	0.294175
3.23	58.5	10.0019	0.04179	0.2300	0.002976	0.0532	0.729647	0.315221
5.15	93.3	10.0046	0.06665	1.6500	0.021355	0.0523	0.866137	1.90501
10.59	191.8	9.9973	0.13696	6.8800	0.08898	0.0528	0.908747	7.57086
31.82	576.3	10.0003	0.41166	27.61	0.357191	0.0540	1.008607	27.3744

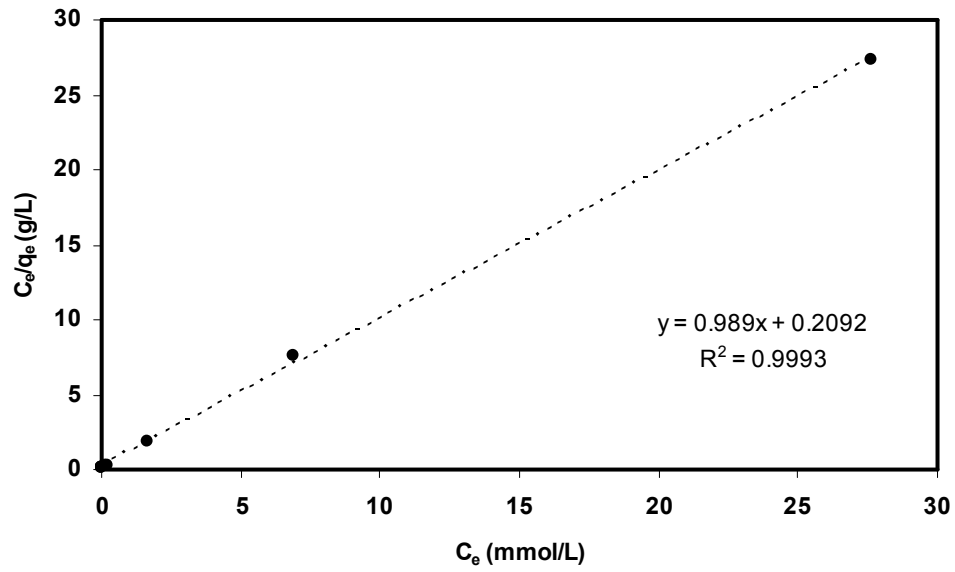


Figure 37. Linear isotherm for DBT adsorption on CsY zeolite

14.2 Quinoline Adsorption Experiments

Table 40. Raw Data for Quinoline/C₁₆ Isotherm on NaY Zeolite

C_{sol} mmol/L	C_{sol} ppm	M_{sol} g	n_{sol} mmol	C_e mmol/L	n_e mmol	M_z g	q mmol/g	C_e/q_e
0.53	9.6	9.998	0.00686	0	0	0.043	0.159419	0
1.11	20.1	10.0021	0.01436	0	0	0.0421	0.341156	0
1.74	31.5	10.0016	0.02251	0.06	0.000776	0.0524	0.414828	0.144638
3.01	54.5	9.9965	0.03893	0.16	0.002069	0.0475	0.775925	0.206206
3.18	57.6	9.9982	0.04113	0.13	0.001681	0.0435	0.906886	0.143348
3.12	56.5	10.001	0.04037	0.06	0.000776	0.0439	0.901822	0.066532
4.32	78.2	10.0019	0.0559	0.26	0.003364	0.0501	1.048555	0.24796
10.53	190.7	9.9973	0.13619	3.63	0.046947	0.0442	2.018971	1.797946
21.51	389.6	9.9998	0.27826	14.52	0.187836	0.0462	1.957253	7.41856
26.84	486.1	10.0032	0.34733	19.85	0.256874	0.0465	1.945287	10.20415
32.33	585.5	10.0003	0.41825	25.66	0.331963	0.0451	1.913299	13.41139

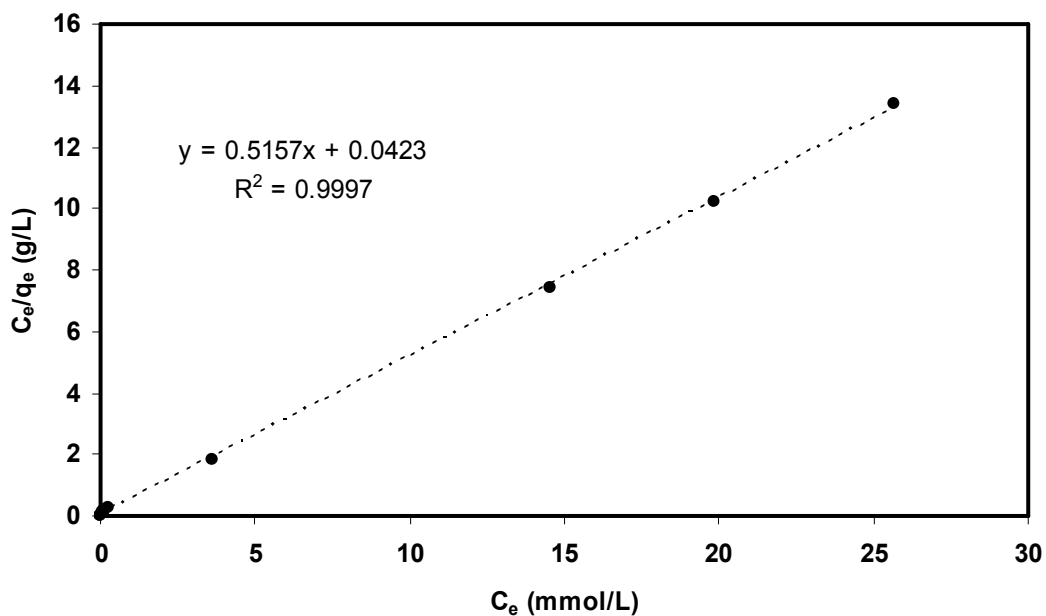


Figure 38. Linear isotherm for quinoline adsorption on NaY zeolite

Table 41. Raw Data for Quinoline/C₁₆ Isotherm on NiY Zeolite

C_{sol} mmol/L	C_{sol} ppm	M_{sol} g	n_{sol} mmol	C_e mmol/L	n_e mmol	M_z g	q mmol/g	C_e/q_e
0.41	7.4	10.0021	0.005305	0	0	0.0465	0.114089	0
0.56	10.1	9.9976	0.007243	0	0	0.0489	0.148114	0
0.96	17.4	9.9976	0.012416	0	0	0.0517	0.240158	0
1.11	20.1	9.9981	0.014357	0.02	0.000259	0.0496	0.284238	0.070363
1.74	31.5	10.0011	0.022512	0.01	0.000129	0.0515	0.434617	0.023009
3.02	54.7	9.9987	0.039063	0.47	0.006079	0.0501	0.658365	0.71389
4.3	77.9	9.9979	0.055616	1.52	0.01966	0.0496	0.724924	2.096772
5.2	94.2	9.9993	0.067266	2.37	0.030658	0.0489	0.748631	3.16578
9.09	164.6	10.0005	0.1176	5.89	0.0762	0.0513	0.807002	7.298615
14.09	255.2	10.004	0.18235	10.47	0.1355	0.052	0.900947	11.6211
18.16	328.9	10.0039	0.23502	14.61	0.189078	0.0509	0.902611	16.18638
28.07	508.4	10.0013	0.363178	24.77	0.320482	0.0499	0.855639	28.94914

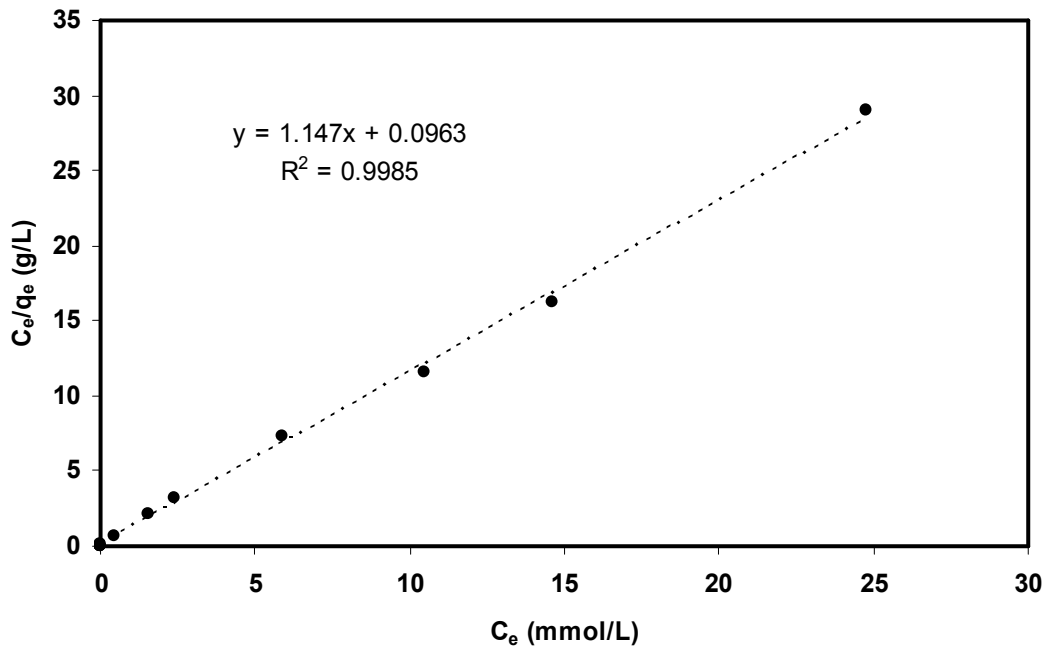


Figure 39. Linear isotherm for quinoline adsorption on NiY zeolite

Table 42. Raw Data for Quinoline/C₁₆ Isotherm on CsY Zeolite

C_{sol} mmol/L	C_{sol} ppm	M_{sol} g	n_{sol} mmol	C_e mmol/L	n_e mmol	M_z g	q mmol/g	C_e/q_e
0.41	7.4	9.9977	0.005303	0	0	0.0516	0.102767	0
0.96	17.4	10	0.012419	0.64	0.008279	0.0498	0.083127	7.69908
1.74	31.5	10.0036	0.022518	0.74	0.009577	0.0516	0.2508	2.950561
3.02	54.7	9.9984	0.039062	2.38	0.030784	0.05	0.165562	14.37527
4.29	77.7	10.0008	0.055502	3.79	0.049034	0.0498	0.129896	29.17718
4.3	77.9	10.0005	0.05563	2.38	0.030791	0.0508	0.488967	4.867402
9.09	164.6	10.0037	0.117637	5.68	0.073507	0.0501	0.880842	6.448378
14.09	255.2	9.9971	0.182224	11.6	0.150021	0.0503	0.640215	18.11891
18.16	328.9	10.0005	0.234941	15.85	0.205056	0.052	0.574713	27.57899
28.07	508.4	10.0005	0.363149	23.67	0.306225	0.0501	1.136206	20.83249

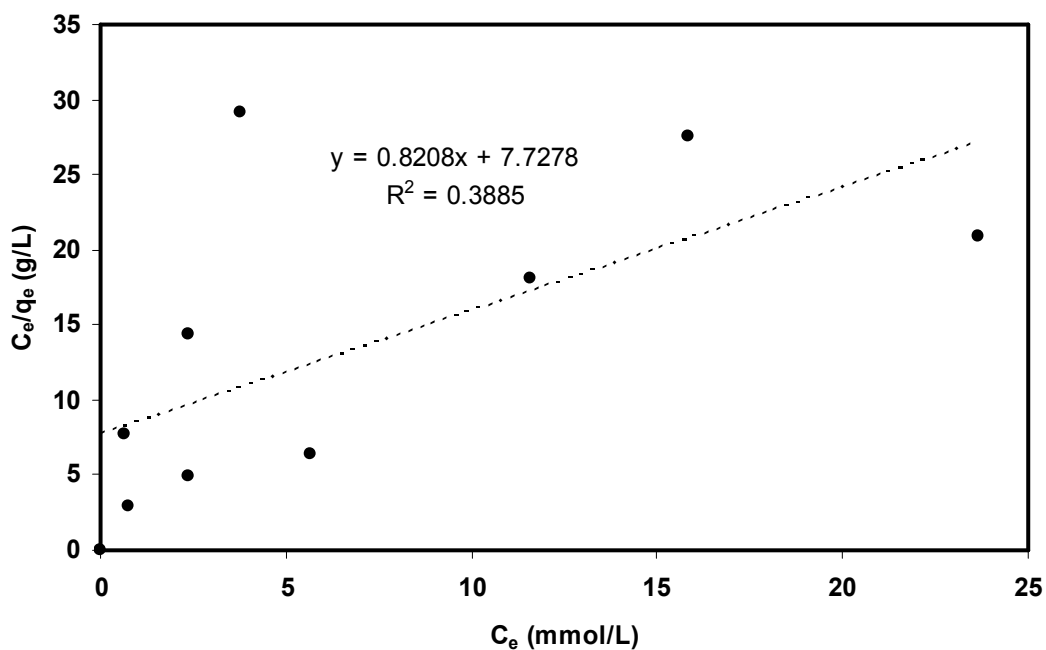


Figure 40. Linear isotherm for quinoline adsorption on CsY zeolite

14.3 Naphthalene Adsorption Experiments

Table 43. Raw Data for Naphthalene/C₁₆ Isotherm on NaY Zeolite

C_{sol} mmol/L	C_{sol} ppm	M_{sol} g	n_{sol} mmol	C_e mmol/L	n_e mmol	M_z g	q mmol/g	C_e/q_e
0.39	7.1	10.0033	0.00504	0.04	0.000518	0.0443	0.102242	0.39123
0.98	17.7	10.0027	0.01268	0.08	0.001035	0.0446	0.261123	0.306369
1.86	33.7	10.0039	0.0240	0.23	0.002977	0.0449	0.46982	0.48955
2.9	52.5	10.0012	0.03752	0.45	0.005822	0.0471	0.673004	0.668644
4.9	88.7	10.0002	0.0633	1.2	0.015524	0.046	1.040574	1.153209
9.81	177.7	9.9996	0.12690	4.6	0.059506	0.0466	1.446289	3.180555
14.81	268.2	9.9985	0.19156	8.88	0.11486	0.0463	1.656643	5.360236
19.58	354.6	10.0028	0.25336	13.55	0.17534	0.047	1.660204	8.161646
29.5	534.3	10.0013	0.38167	23.92	0.309484	0.0458	1.576325	15.17454

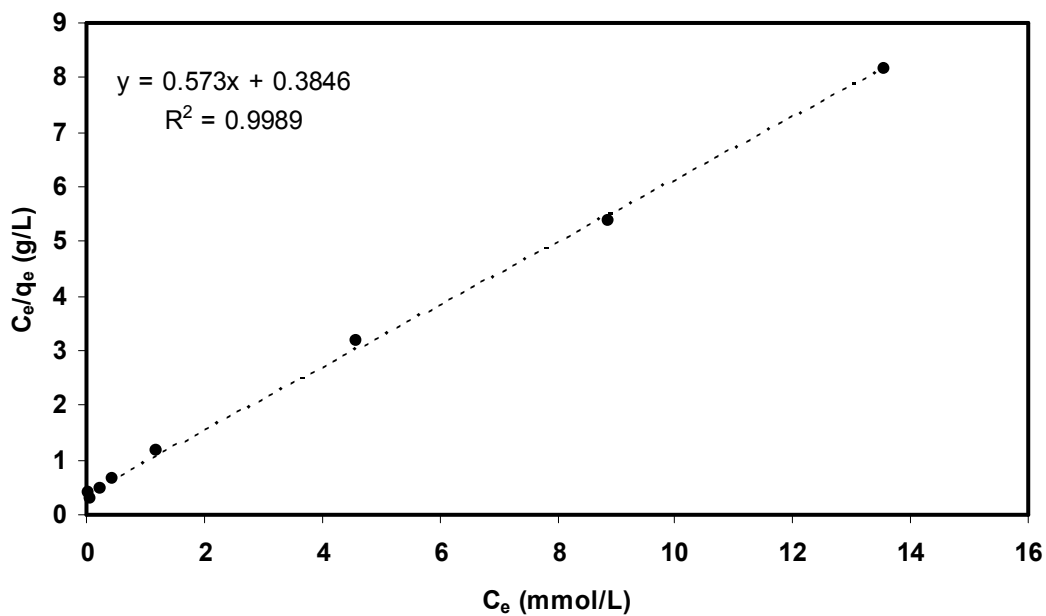


Figure 41. Linear isotherm for naphthalene adsorption on NaY Zeolite

Table 44. Raw Data for Naphthalene/C₁₆ Isotherm on NiY Zeolite

C_{sol} mmol/L	C_{sol} ppm	M_{sol} g	n_{sol} mmol	C_e mmol/L	n_e mmol	M_z g	q mmol/g	C_e/q_e
0.39	7.1	10.0049	0.00504775	0.02	0.000259	0.0527	0.090871	0.220093
0.93	16.8	10.0006	0.01203177	0.08	0.001035	0.0512	0.214781	0.372473
1.82	33.0	10.0023	0.023550047	0.26	0.003364	0.049	0.411954	0.631138
2.82	51.1	9.9974	0.036471757	0.55	0.007113	0.0498	0.589528	0.93295
4.76	86.2	10.0021	0.061591198	1.68	0.021738	0.0491	0.811673	2.0698
9.52	172.4	10.0027	0.123189785	5.48	0.070912	0.0497	1.051872	5.209761
14.57	263.9	10.0037	0.188556157	10.03	0.129802	0.0504	1.165753	8.603882
19.26	348.8	9.9977	0.249101814	14.44	0.186762	0.0519	1.201158	12.02173
24.01	434.9	9.999	0.31057696	19.38	0.250686	0.0486	1.232315	15.7265

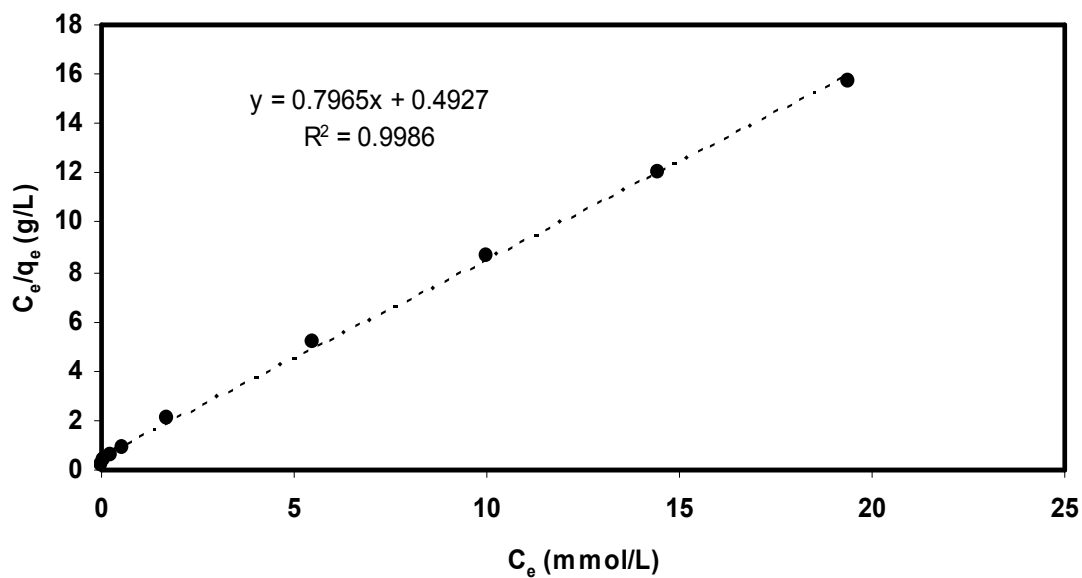


Figure 42. Linear isotherm for naphthalene adsorption on NiY zeolite

Table 45. Raw Data for Naphthalene/C₁₆ Isotherm on CsY Zeolite

C_{sol} mmol/L	C_{sol} ppm	M_{sol} g	n_{sol} mmol	C_e mmol/L	n_e mmol	M_z g	q mmol/g	C_e/q_e
0.39	7.1	9.9972	0.00504	0.0300	0.000388	0.0528	0.088179	0.340215
0.93	16.8	10.0025	0.01203	0.1000	0.001294	0.0526	0.204184	0.489755
1.82	33.0	9.9976	0.02354	0.2800	0.003621	0.0541	0.368163	0.760533
2.82	51.1	9.9979	0.03647	0.4500	0.00582	0.0507	0.604602	0.744291
4.76	86.2	9.9975	0.06156	1.2200	0.015779	0.0529	0.865485	1.409614
9.52	172.4	9.9999	0.12316	5.2300	0.067658	0.0522	1.063171	4.919248
14.57	263.9	10.0030	0.18854	10.2800	0.133028	0.0525	1.057423	9.721748
19.26	348.8	9.9980	0.24911	14.8900	0.192588	0.0522	1.082791	13.7515
24.01	434.9	10.0009	0.31064	19.7100	0.255004	0.0533	1.04376	18.88364
29.5	534.3	9.9978	0.38155	24.99	0.323215	0.0532	1.096453	22.79168

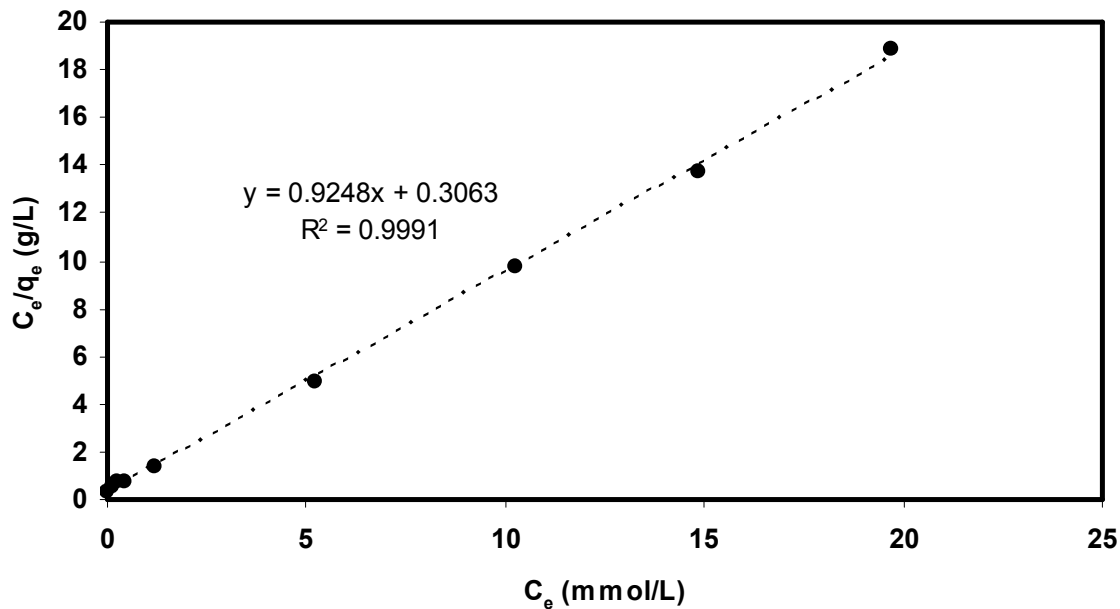


Figure 43. Linear isotherm for naphthalene adsorption on CsY zeolite